



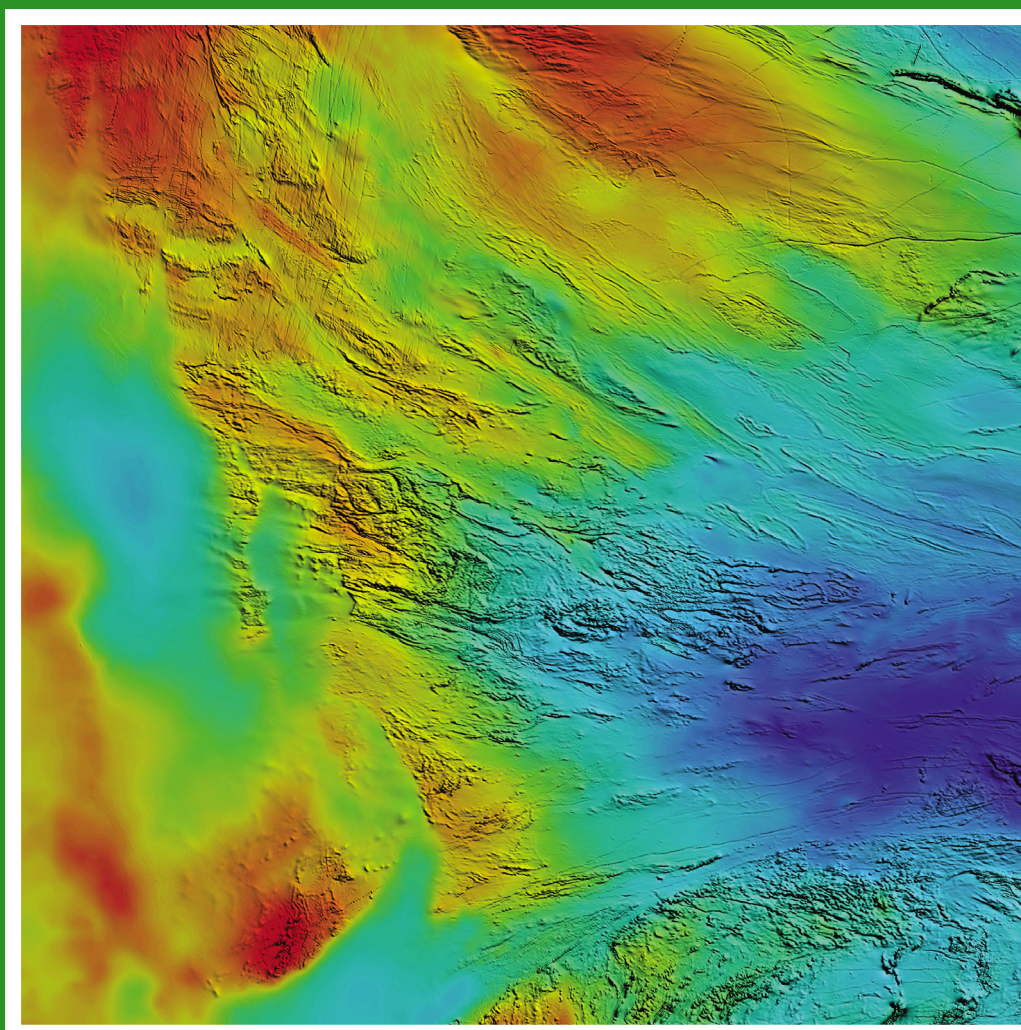
Government of
Western Australia

Department of
Mines and Petroleum

**REPORT
123**

3D ARCHITECTURE, STRUCTURAL EVOLUTION, AND MINERAL PROSPECTIVITY OF THE GASCOYNE PROVINCE

by ARA Aitken, A Joly, MC Dentith,
SP Johnson, AM Thorne, and IM Tyler



Geological Survey of Western Australia



Government of **Western Australia**
Department of **Mines and Petroleum**

REPORT 123

3D ARCHITECTURE, STRUCTURAL EVOLUTION, AND MINERAL PROSPECTIVITY OF THE GASCOYNE PROVINCE

by

ARA Aitken¹, A Joly¹, MC Dentith¹, SP Johnson, AM Thorne, and IM Tyler

**1 Centre for Exploration Targeting, The University of Western Australia, 35 Stirling
Highway, Crawley, Perth WA 6009**

Perth 2014



**Geological Survey of
Western Australia**

MINISTER FOR MINES AND PETROLEUM
Hon. Bill Marmion MLA

DIRECTOR GENERAL, DEPARTMENT OF MINES AND PETROLEUM
Richard Sellers

EXECUTIVE DIRECTOR, GEOLOGICAL SURVEY OF WESTERN AUSTRALIA
Rick Rogerson

REFERENCE

The recommended reference for this publication is:

Aitken, ARA, Joly, A, Dentith, MC, Johnson, SP, Thorne AM and Tyler, IM 2014, 3D architecture, structural evolution, and mineral prospectivity of the Gascoyne Province: Geological Survey of Western Australia, Report 123, 94p.

National Library of Australia Cataloguing-in-Publication entry:

Author: Aitken, A. R. A., author.
Title: 3D architecture, structural evolution, and mineral prospectivity of the Gascoyne province / by ARA Aitken, A Joly, MC Dentith, SP Johnson, AM Thorne, IM Tyler.
ISBN: 9781741685176 (ebook)
Subjects: Geology--Western Australia--Gascoyne Region.
Mines and mineral resources--Western Australia--Gascoyne Region.
Other Authors/Contributors: Joly, A., author.
Dentith, Mike, author.
Johnson, S. P., author.
Thorne, A. M., author.
Tyler, I. M., author.
Geological Survey of Western Australia
Series: Report (Geological Survey of Western Australia) ; 123.
Dewey Decimal Classification: 559.413

ISSN 0508-4741

Grid references in this publication refer to the Geocentric Datum of Australia 1994 (GDA94). Locations mentioned in the text are referenced using Map Grid Australia (MGA) coordinates, Zone 50. All locations are quoted to at least the nearest 100 m.

Copy editor: SR White

Cartography: M Prause

Desktop publishing: RL Hitchings

Printed by Images on Paper, Perth, Western Australia

Disclaimer

This product was produced using information from various sources. The Department of Mines and Petroleum (DMP) and the State cannot guarantee the accuracy, currency or completeness of the information. DMP and the State accept no responsibility and disclaim all liability for any loss, damage or costs incurred as a result of any use of or reliance whether wholly or in part upon the information provided in this publication or incorporated into it by reference.

Published 2014 by Geological Survey of Western Australia

This Report is published in digital format (PDF), as part of a digital dataset on CD, and is available online at <www.dmp.wa.gov.au/GSWApublications>.

Further details of geological publications and maps produced by the Geological Survey of Western Australia are available from:

Information Centre
Department of Mines and Petroleum
100 Plain Street
EAST PERTH WESTERN AUSTRALIA 6004
Telephone: +61 8 9222 3459 Facsimile: +61 8 9222 3444
www.dmp.wa.gov.au/GSWApublications

Cover photograph: Composite geophysical image of the Gascoyne region generated by draping Bouguer gravity data over greyscale total magnetic intensity data.

Contents

Abstract	1
Introduction	2
Geology of the Gascoyne Province and its adjacent terranes	2
Components of the West Australian Craton	2
Paleoproterozoic continent assembly	6
Paleoproterozoic to Neoproterozoic intraplate evolution	6
Capricorn Orogeny (1820–1770 Ma)	7
Mangaroon Orogeny (1680–1620 Ma)	7
Mutherbukin Tectonic Event (1385–1170 Ma)	7
Edmundian Orogeny (1030–955 Ma)	7
Mundine Well Dolerite Suite (c. 755 Ma), Mulka Tectonic Event (c. 570 Ma), and formation of the Carnarvon Basin	8
Structural interpretation of geology and geophysics	8
Methods and implementation	8
Geological information	8
Domain definition and characterization	8
Event definition and characterization	8
Interpretational confidence estimation	9
Results	9
Narryer Terrane and Yarlwarweelor Gneiss Complex	9
Errabiddy Shear Zone	12
Paradise Zone	12
Mooloo Zone	12
Mutherbukin Zone	12
Limejuice Zone	17
Mangaroon Zone	17
Boora Boora Zone	21
Crustal structure	21
Density and magnetic susceptibility measurements	21
Yilgarn Craton	21
Halfway Gneiss	21
Dalgaringa and Bertibubba Supersuites	21
Moorarie Supersuite	21
Durlacher Supersuite	23
Thirty Three Supersuite	23
Camel Hills Metamorphics	23
Moogie Metamorphics	23
Leake Spring Metamorphics	23
Pooranoo Metamorphics	23
Edmund Group and Narimbunna Dolerite Suite	23
Mundine Well Dolerite Suite	24
Summary of petrophysical data	24
2D combined gravity and magnetic modelling	24
Profile 1	24
Profile 2	27
Profile 3	29
Profile 4	31
Profile 5	33
Summary of forward modelling results	35
Prospectivity analysis: rationale and methodology	35
The mineral systems approach	35
GIS-based automated prospectivity analysis	36
Definition of fuzzy logic (knowledge-based GIS-driven prospectivity model)	36
Application to the Gascoyne Province	36
Mineral deposits and occurrences in the Gascoyne Province	37
Selection of commodity types for prospectivity analysis	37
Igneous and metamorphic-related REE mineral systems (carbonatite, pegmatite, veins)	38
Results of igneous and metamorphic-related REE prospectivity analysis	38
Orogenic and intrusive gold mineral system	38
Results of gold prospectivity analysis	40
Surficial uranium mineral system	44
Results of surficial uranium prospectivity analysis	44
Porphyry base metal mineral system	46
Results of PBM prospectivity analysis	46

Granite-hosted tin–tungsten mineral system	48
Results of granite-hosted tin–tungsten prospectivity analysis	49
Discussion	49
Tectonic summary	49
Inward-stepping intraplate orogenesis	52
Lower-crustal structure of the Gascoyne Province	52
Crustal structure and mineral prospectivity	52
Conclusions	53
Appendix 1: Geophysical analysis methods*	54
Figures 1.1 – 1.5 Project-wide analysis of geological and geophysical confidence factors	
Appendix 2: Fuzzy-logic mineral prospectivity*	61
Tables 2.1 – 2.5 Input parameters and geological rationale for predictor maps	
Figures 2.1 – 2.67 Predictor maps for source, pathways, and physical and chemical traps	
References	89

Figures

1. Geological overview of the western Capricorn Orogen, including the Narryer Terrane	3
2. Map of the tectonic zones of the western Capricorn Orogen overlain on geophysical imagery	4
3. Data richness map of the western Capricorn Orogen	10
4. Structural interpretation of the Narryer Terrane	11
5. Structural interpretation of the Errabiddy Shear Zone	13
6. Structural interpretation of the Paradise Zone	14
7. Structural interpretation of the Mooloo Zone	15
8. Structural interpretation of the Mutherbukin Zone	16
9. Structural interpretation of the Limejuice Zone	18
10. Structural interpretation of the Mangaroon Zone	19
11. Structural interpretation of the Boora Boora Zone	20
12. Petrophysical data from the western Capricorn Orogen	22
13. Combined gravity and magnetic model along Profile 1	25
14. Combined gravity and magnetic model along Profile 2	28
15. Combined gravity and magnetic model along Profile 3	30
16. Combined gravity and magnetic model along Profile 4	32
17. Combined gravity and magnetic model along Profile 5	34
18. Multi-stage fuzzy inference network used for combining fuzzy REE predictor maps	39
19. Fuzzy prospectivity model and zone of high fuzzy value for magmatic REE prospectivity analysis	40
20. Multi-stage fuzzy inference network used for combining fuzzy gold predictor maps	41
21. Fuzzy prospectivity model and zone of high fuzzy value for intrusion-related gold prospectivity analysis	42
22. Fuzzy prospectivity model, disregarding granite, and zone of high fuzzy value for the orogenic gold prospectivity analysis	43
23. Model for formation of carnotite deposits in calcretized channels	43
24. Multi-stage fuzzy inference network used for combining fuzzy surficial uranium predictor maps	44
25. Fuzzy prospectivity model and zone of high fuzzy value for the surficial uranium prospectivity analysis	45
26. Fuzzy prospectivity model and zone of high fuzzy value for the surficial uranium prospectivity analysis, MOUNT PHILLIPS map sheet area	45
27. Schematic diagram showing model for genesis of PBM deposits	46
28. Multi-stage fuzzy inference network used for combining fuzzy PBM predictor maps	47
29. Fuzzy prospectivity model and zone of high fuzzy value for the PBM prospectivity analysis	48
30. Multi-stage fuzzy inference network used for combining fuzzy Sn–W predictor maps	49
31. Fuzzy prospectivity model and zone of high fuzzy value for the Sn–W prospectivity analysis	50
32. Structural overview of the Gascoyne Province, with faults coloured according to activation history	51

Table

1. Summarized structural evolution of the Gascoyne Province	10
---	----

* Appendices, including PDFs, tables in MS Excel (spreadsheet) format and spatially located GIS data used to construct predictor and prospectivity maps, are provided on USB (inside back cover of printed Report) or as compressed files that can be downloaded from <www.dmp.wa.gov.au/GSWApublications>.

3D architecture, structural evolution, and mineral prospectivity of the Gascoyne Province

by

ARA Aitken¹, A Joly¹, MC Dentith¹, SP Johnson, AM Thorne, and IM Tyler

Abstract

Understanding of the geology of the Gascoyne Province has advanced significantly in recent years following intensive study by the Geological Survey of Western Australia. Building on this database, an interpretation of regional gravity and magnetic data has been undertaken emphasising geological structure. Working on individual structural domains, structures have been attributed to discrete events and then assigned to one of eight tectonic events known to have affected the province. These provide an improved regional tectonic framework and characterize the extent of tectonic activity during different events. Combined gravity and magnetic modelling of a series of cross sections allows the subsurface structure of the area to be constrained. Domain-bounding structures at the surface extend to mantle depths, and in several cases there are significant Moho offsets. These structures are boundaries to variations in lower-crustal character. Crustal-scale structure is characterized by primarily south-dipping structures as imaged in seismic reflection studies.

Using this improved structural understanding of the Gascoyne Province, regional prospectivity analysis has been undertaken using a mineral systems approach. We use a knowledge-based approach, with inputs determined by spatial mapping of geological proxies for favourable components of the mineral system. These are combined within a fuzzy-logic framework, with subjectively assigned weightings based on expert knowledge. Mineral systems considered are: 1) igneous and metamorphic-related rare earth elements (REE), 2) orogenic and intrusive gold, 3) surficial uranium, 4) porphyry base metal, 5) granite-related tin–tungsten (Sn–W).

The resulting maps show the spatial variations in geological characteristics considered favourable for each mineral system, and hence are indicators of relative variations in prospectivity. The results for the REE analysis indicate that much of the province has quite high prospectivity, with prospectivity concentrated in the central parts. The areas most prospective for gold are concentrated around major crustal boundaries, of which the Limejuice Zone is particularly prospective. Surficial uranium shows highest prospectivity around Mount Phillips region, but with isolated regions of increased prospectivity across the whole province. The analysis for porphyry base metals shows broad zones of moderate prospectivity across much of the area, with slight focusing around major crustal structures, but few areas of high prospectivity. Occurrences of Sn–W mineralization cluster at the margins of the Mutherbukin Zone, but the analysis suggests that a large part of the province is equally prospective for these commodities. Prospectivity for the REE, gold and Sn–W deposit types is strongest in the central regions of the province, perhaps reflecting the influence of a greater degree of intraplate reworking.

KEYWORDS: crustal structure, geophysical interpretation, structural terranes, structural evolution, GIS, mineral prospectivity

¹ Centre for Exploration Targeting, The University of Western Australia, 35 Stirling Highway, Crawley, Perth WA 6009

Introduction

The Capricorn Orogen of Western Australia is a ~1000 km long, 500 km wide region of variably deformed meta-igneous, metasedimentary and low metamorphic grade sedimentary rocks located between the Pilbara and Yilgarn Cratons (Fig. 1). The orogen records the punctuated Paleoproterozoic assembly of the West Australian Craton, and nearly two billion years of subsequent intraplate reworking (Cawood and Tyler, 2004; Sheppard *et al.*, 2010a,b; Johnson *et al.*, 2011a). The core of the orogen is occupied by granitic and medium- to high-grade metamorphic rocks of the Gascoyne Province, and all these elements are overlain by numerous, variably deformed, low-grade metasedimentary rocks. Over the past decade and a half, on-going field mapping combined with whole rock and accessory phase geochemical, geochronological, and isotope analyses (Sheppard *et al.*, 2007; Johnson *et al.*, 2011b,c), have provided a rigorous, temporal, tectonomagmatic evolution for the Gascoyne Province. The results of a recent vibroseis-source, deep-crustal seismic transect through the Capricorn Orogen yielded a detailed view of the deep-crustal structure of the orogen (Johnson *et al.*, 2011a, 2013), providing a new spatial framework on which the tectonomagmatic history can be placed. These datasets allow an opportunity to assess the prospectivity of the Gascoyne Province within this new architectural framework.

Funded by the Western Australian Government's Exploration Incentive Scheme, the Centre for Exploration Targeting (CET; www.cet.edu.au) at The University of Western Australia has undertaken a study of the prospectivity of the Gascoyne Province. In this work the structural evolution of the province and the geometry of major features are interpreted, with an emphasis on delineating deep-penetrating fault zones considered to be likely conduits for hydrothermal fluids and magmas, which are important elements of many mineral systems. This study is based on joint interpretation of geological and geophysical data, and modelling of existing regional gravity and aeromagnetic data constrained by near-surface geological data, a petrophysical database, and deep seismic reflection data.

Using these products and other Geological Survey of Western Australia (GSWA) data (e.g. whole rock major and trace element geochemistry), a multi-commodity regional prospectivity analysis is undertaken. This includes:

- translation of the 4D controls on mineralization into the framework of the mineral systems approach (MSA; Knox-Robinson and Wyborn, 1997; McCuaig and Hronsky, 2000; Hronsky and Groves, 2008)
- implementation of Geographic Information Systems (GIS)-based conceptual prospectivity modelling for six different types of commodities including: rare earth element (REE)-pegmatite and carbonatite; orogenic and intrusive gold; surficial uranium; porphyry base metal (PBM); and granite-hosted tin–tungsten (Sn–W).

Geology of the Gascoyne Province and its adjacent terranes

The geology of the Gascoyne Province includes a ~300 m.y. period of continental assembly during the early Paleoproterozoic, during which two Archean terranes and one Archean to Paleoproterozoic terrane were amalgamated to form the West Australian Craton (Johnson *et al.*, 2011b). This was followed by intermittent tectonism in an intraplate setting, extending from the late Paleoproterozoic to the latest Neoproterozoic. These events have led to diverse geology across the province, which can be subdivided into a number of zones (Fig. 2), each with different geological character (Sheppard *et al.*, 2010b).

Components of the West Australian Craton

Each of the three main tectonic components of the West Australian Craton in the Capricorn Orogen — the Narryer Terrane of the Yilgarn Craton, the Glenburgh Terrane and the Pilbara Craton — preserves a separate and distinct tectonomagmatic history.

The Narryer Terrane preserves the oldest (c. 4400 Ma or older) known zircons on Earth (Froude *et al.*, 1983; Compston and Pidgeon, 1986; Wilde *et al.*, 2001; Kemp *et al.*, 2010), as well as relicts of the oldest crust in Australia — the c. 3730 Ma Manfred Complex (Kinny *et al.*, 1988; Myers, 1988). The terrane was constructed during several tectonomagmatic episodes between c. 3730 and 3100 Ma (Myers, 1988), followed by the deposition of supracrustal sequences (e.g. Jack Hills) (Spaggiari, 2007; Rasmussen *et al.*, 2010), and the subsequent intrusion of Neoproterozoic granites between c. 2750 and 2620 Ma (Cassidy *et al.*, 2006; Spaggiari, 2007). The 2750–2620 Ma magmatic event was accompanied by major deformation, which was responsible for the development of the main northeast–southwest structural grain of the terrane (Spaggiari, 2007). However, along the northern and northeastern margin of the terrane, subsequent structural and metamorphic reworking and extensive granite emplacement took place during the 1820–1770 Ma Capricorn Orogeny (Sheppard *et al.*, 2003) — the strongly reworked parts are known as the Yarlalweelor Gneiss Complex.

The Pilbara Craton is composed of numerous geologically distinct terranes, the oldest of which is the East Pilbara Terrane, which preserves a history including the development of granite–greenstone basement between c. 3700 and 2830 Ma (Van Kranendonk *et al.*, 2007; Thorne *et al.*, 2011). The terrane was constructed through a series of mantle plume events and accreted with other terranes, including the Scholl, Karratha and Regal Terranes, during the c. 3070 Ma Prinsep Orogeny (Van Kranendonk *et al.*, 2007).

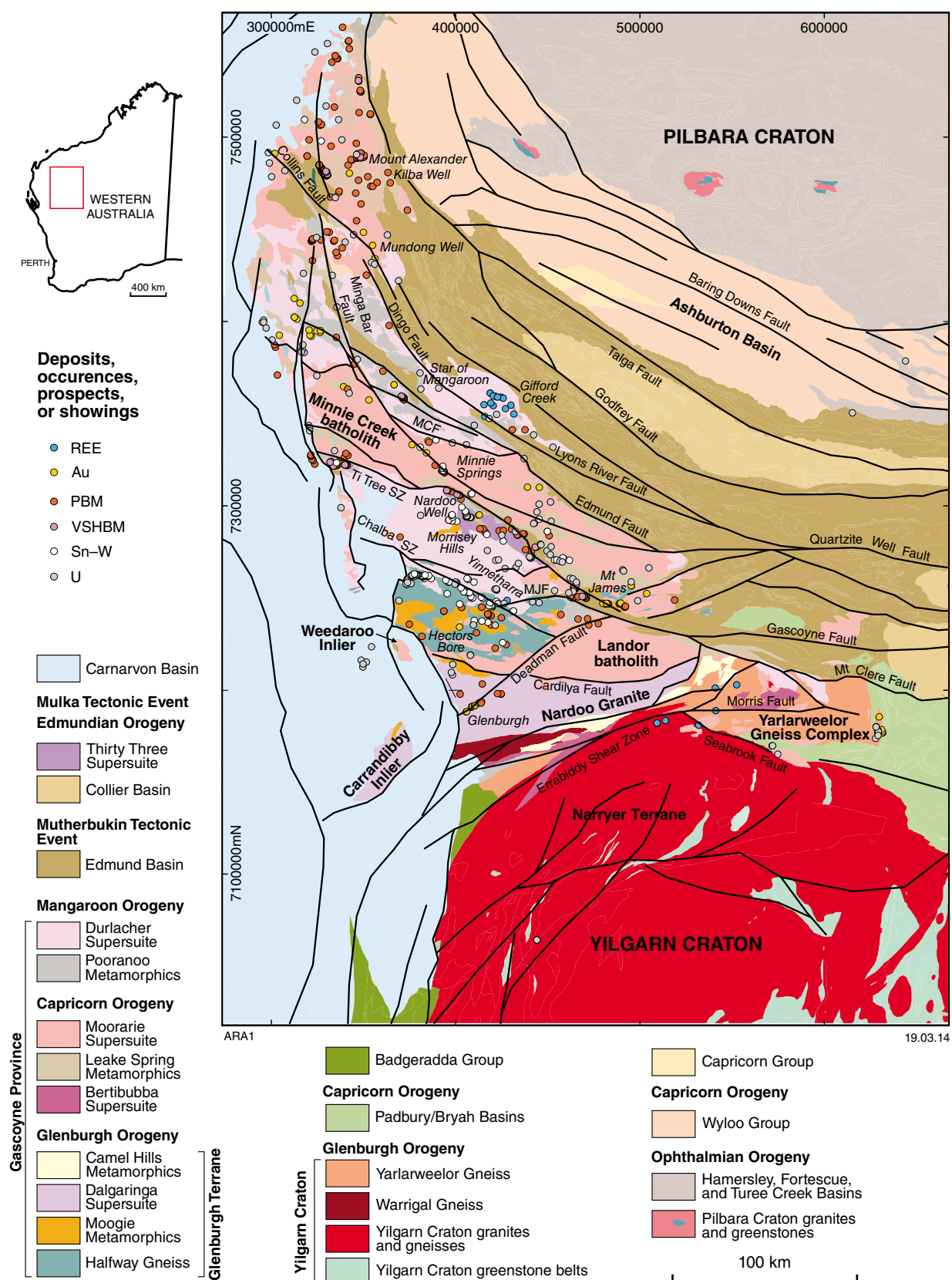


Figure 1. Geological overview of the western Capricorn Orogen, including the Narryer Terrane, after GSWA (2012). MJF – Mount James Fault, MCF – Minnie Creek Fault. Italicized names are significant sites of mineralization. Inset shows location (red rectangle) in Western Australia

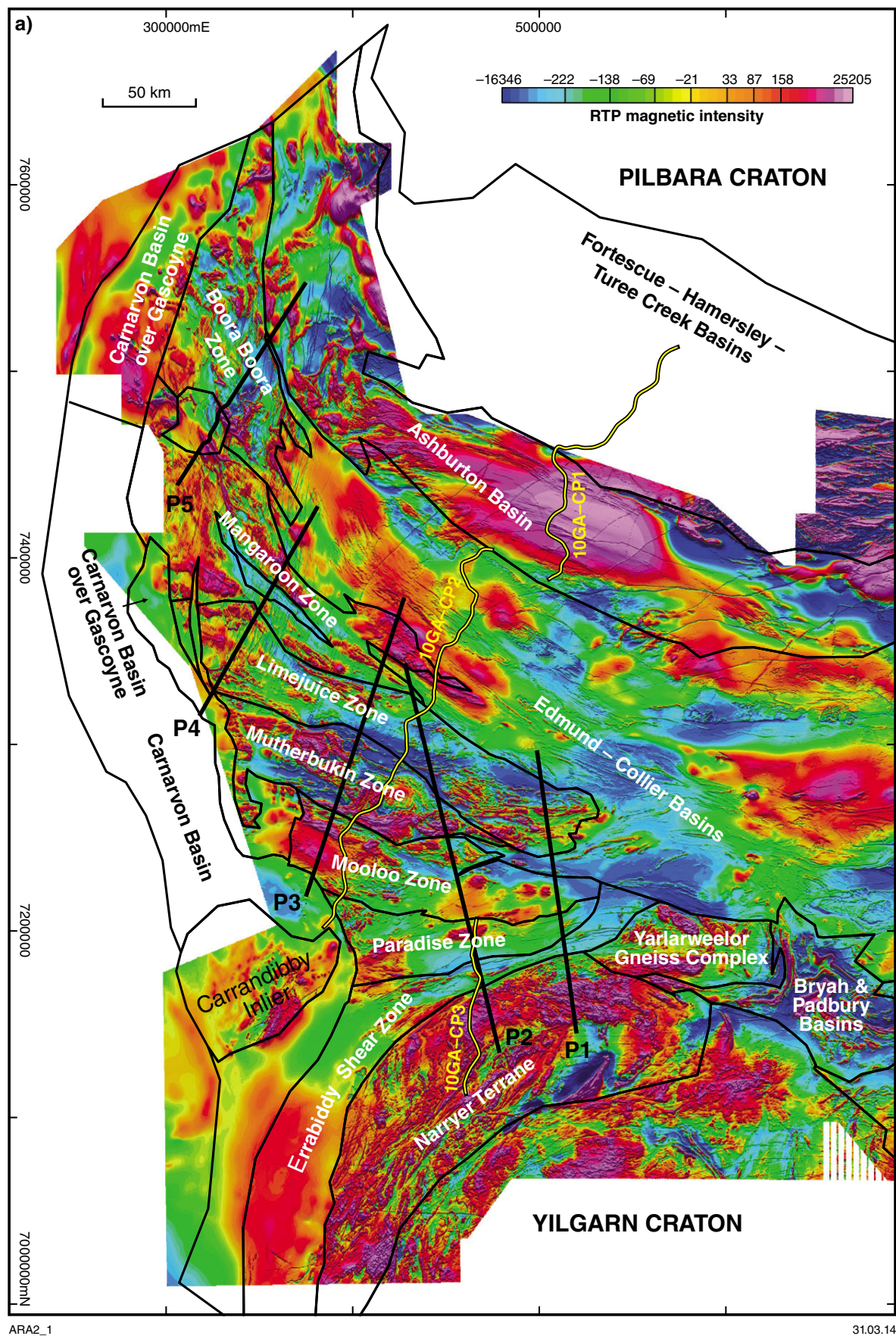
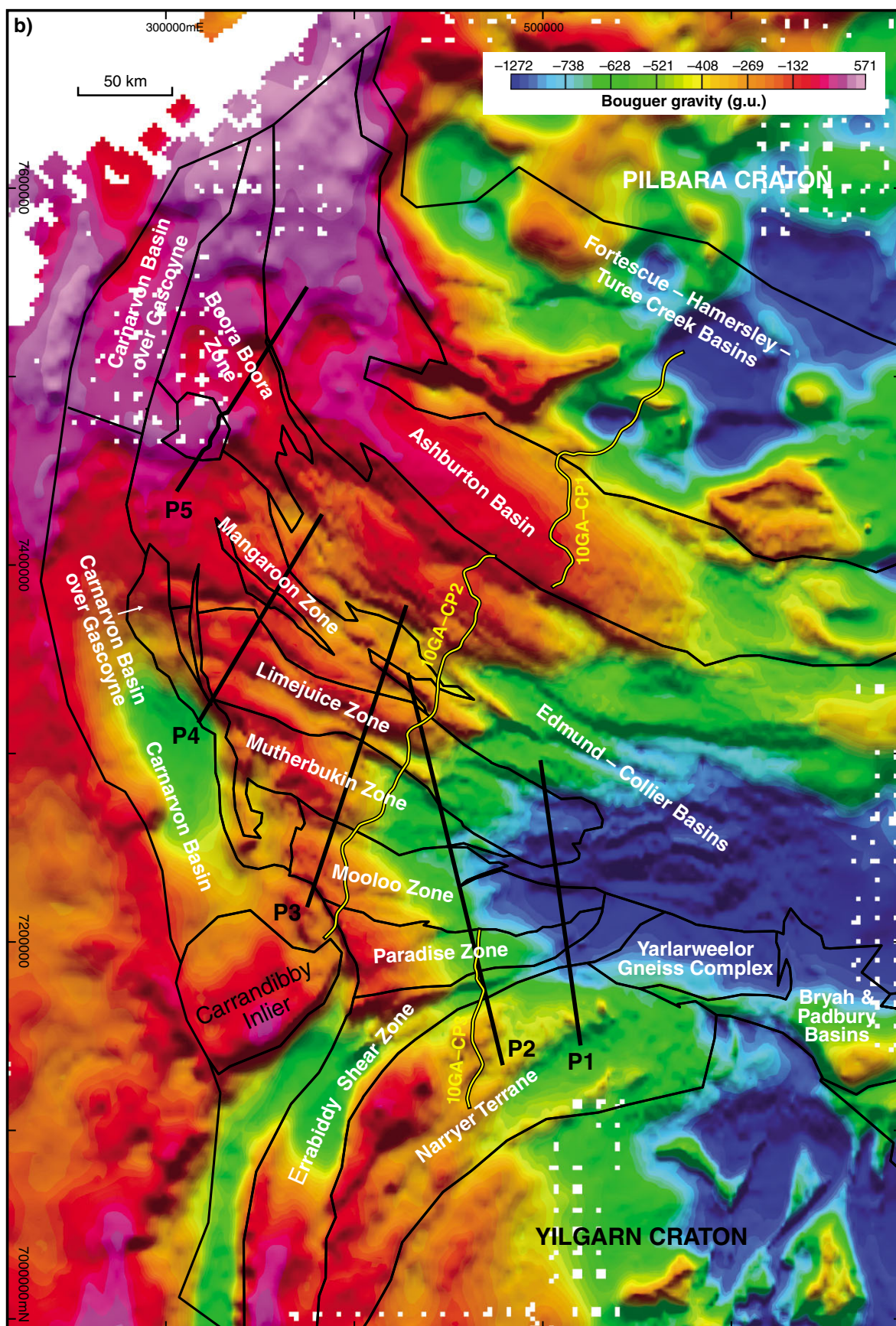


Figure 2. Map of the tectonic zones of the western Capricorn Orogen overlain on: a) RTP magnetic field; b) (facing) Bouguer gravity. Combined magnetic/gravity profile locations (P1 to P5) are indicated in black, and deep-crustal seismic reflection lines are indicated in grey



ARA2_2

31.03.14

Following cratonization at c. 2830 Ma (Van Kranendonk et al., 2007), the craton was subject to extension and continental rifting that included deposition of a thick sequence of siliciclastic sedimentary and volcanic rocks — the 2775–2450 Ma Fortescue and Hamersley Groups — within and along the craton's southern margin (Blake, 1993, 2001; Thorne and Trendall, 2001; Blake et al., 2004; Thorne et al., 2011). Along the southern margin, this succession is ~10 km thick and records the development of a rift to passive margin, and finally to an active margin (Blake and Barley, 1992; Blake, 1993, 2001; Thorne and Trendall, 2001; Blake et al., 2004; Thorne et al., 2011).

The Archean to Paleoproterozoic Glenburgh Terrane comprises a series of heterogeneous granitic gneisses — the Halfway Gneiss — dated to between c. 2555 and 2430 Ma (Johnson et al., 2010; Johnson et al., 2011d). These rocks are overlain by an unknown thickness of siliciclastic metasedimentary rocks — the Moogie Metamorphics — deposited sometime between c. 2240 and 2125 Ma (Johnson et al., 2010; Johnson et al., 2011d). Along the southern margin of this terrane, the gneisses and metasedimentary rocks are intruded by an extensive c. 2000 Ma granite batholith — the Dalgaringa Supersuite — which is interpreted to have formed in a continental margin arc, leading up to the final suturing of the West Australian Craton (Sheppard et al., 2004; Johnson et al., 2011b). The isotopic evolution of all these rocks implies that the Glenburgh Terrane is exotic to both the Pilbara and Yilgarn Cratons and represents an exotic microcontinent sutured within the Capricorn Orogen (Johnson et al., 2011d).

Paleoproterozoic continent assembly

Recent work indicates that the three principal components of the West Australia Craton — the Pilbara Craton, the Glenburgh Terrane and the Yilgarn Craton — were amalgamated during two distinct and discrete Paleoproterozoic tectonic events (Occhipinti et al., 2004; Johnson et al., 2011b). First, the Pilbara Craton and the Glenburgh Terrane were sutured during the 2215–2145 Ma Ophthalmian Orogeny. This orogeny is associated with prominent folding of the rocks of the Pilbara Craton, including the low-grade metasedimentary rocks along the southern Pilbara margin, in which several generations of folding are recognized (Tyler and Thorne, 1990; Thorne and Seymour, 1991; Martin and Morris, 2010; Thorne et al., 2011). However, any Ophthalmian-age structures in the Glenburgh Terrane have been rendered unrecognizable due to successive structural and magmatic reworking (Sheppard et al., 2010a). Deposition of the upper part of the Turee Creek Group and the entire lower Wyloo Group along the southern Pilbara margin, took place in a retro-foreland basin setting (Martin and Morris, 2010), while contemporaneous deposition of the Moogie Metamorphics in the Gascoyne Province took place in a pro-foreland basin (Johnson et al., 2011b). However, the polarity of subduction during the Ophthalmian Orogeny is uncertain.

Collision of the combined Pilbara–Glenburgh terrane with the Yilgarn Craton and suturing of the West Australian Craton occurred during the 2005–1950 Ma Glenburgh Orogeny (Occhipinti et al., 2004; Johnson et al., 2011c). Ocean basin closure and subduction magmatism is recorded by the 2002–1975 Ma Dalgaringa Supersuite (Fig. 1). This suite of granitic rocks and gneisses have chemical and isotopic signatures characteristic of modern-day Andean-type magmas (Sheppard et al., 2004) and record the evolution of a continental margin arc, the Dalgaringa Arc, along the southern margin of the Glenburgh Terrane (Sheppard et al., 2004; Johnson et al., 2010). The majority of magmatic activity took place during the 2005–1985 Ma period, although abundant inherited zircons in the gneisses suggest that arc magmatism began as early as c. 2080 Ma (Johnson et al., 2011b). These gneisses were deformed (D_{1g}) at high-pressure and temperature (Johnson et al., 2010, 2011b) possibly reflecting construction of the arc in the middle crust. This deformation event is most prominent in rocks of the Dalgaringa Supersuite in the western part of the Paradise Zone (Occhipinti et al., 2004; Johnson et al., 2010, 2011b). Following this tectonometamorphism, relatively undeformed stocks and plutons of arc-related granite (the Nardoo Granite) were emplaced between c. 1980 and 1970 Ma (Occhipinti et al., 2004). Metasedimentary rocks, the Quartpot Pelite and Petter Calc-silicate of the Camel Hills Metamorphics, were deposited at the same time as the Dalgaringa Supersuite, possibly in a forearc setting (Johnson et al., 2011b).

Crustal thickening, metamorphism, and deformation associated with the collision of the Yilgarn Craton and the combined Pilbara – Glenburgh Terrane took place during the 1965–1950 Ma D_{2g} event of the Glenburgh Orogeny (Johnson et al., 2010, 2011b). Tectonism was accompanied by the intrusion of granitic stocks and dykes of the 1961–1945 Ma Bertibubba Supersuite (Fig. 1), which are the first common magmatic element across the suture zone, indicating that the Yilgarn Craton and Glenburgh Terrane were amalgamated at this time. Deformation and metamorphism associated with the collision are best preserved in rocks of the Halfway Gneiss, Moogie Metamorphics, and Camel Hills Metamorphics in the Mooloo and Errabiddy Shear Zones (Occhipinti et al., 2004; Johnson et al., 2010, 2011b). Rocks of the Dalgaringa Supersuite appear to have been little affected by the D_{2g} event as they may only record a history of uplift from mid-crustal to upper-crustal depths during the collision (Johnson et al., 2011b).

Paleoproterozoic to Neoproterozoic intraplate evolution

Following the amalgamation of the West Australian Craton during the 2005–1950 Ma Glenburgh Orogeny, the evolution of the Gascoyne Province records a long history of intraplate tectonic activity. At least five major tectonic events affected the province from the Paleoproterozoic to Neoproterozoic (Table 1).

Capricorn Orogeny (1820–1770 Ma)

Of all the intraplate reworking events to affect the Gascoyne Province, the 1820–1770 Ma Capricorn Orogeny has the largest footprint. There is evidence for Capricorn Orogeny deformation, metamorphic mineral assemblages, and granitic magmatism across the Gascoyne Province, as well as adjacent tectonic units, such as the Ashburton Basin and Yarlweelor Gneiss Complex (Fig. 1). The orogeny is characterized by extensive deformation at low to intermediate metamorphic grades, and it was accompanied by the intrusion of voluminous, felsic magmatic stocks and plutons of the 1820–1775 Ma Moorarie Supersuite, which includes the Minnie Creek batholith in the Limejuice Zone (Fig. 1). Sedimentation is recorded across the orogen with the deposition of the 1830–1800 Ma upper Wyloo and Capricorn Groups in the Ashburton Basin (Thorne and Seymour, 1991), and the 1840–1810 Ma Leake Spring Metamorphics in the Gascoyne Province (Sheppard et al., 2010b).

The oldest event, D_{1n} , is recorded in the southernmost part of the province in the Yarlweelor Gneiss Complex (YGC; Fig. 1), Errabiddy Shear Zone, and Mooloo Zone, and is characterized by upright isoclinal folds and an intense foliation (Sheppard et al., 2010b). Metamorphism during this event peaked within the upper amphibolite facies in the YGC, but was generally of greenschist facies grade elsewhere (Johnson et al., 2011a). Age constraints derived from the Moorarie Supersuite indicate that this event occurred between c. 1820 and 1810 Ma. The second event, D_{2n} , is the main event in the central part of the province (the Mutherbukin and Limejuice Zones), and was synchronous with the intrusion of the Minnie Creek batholith (1808–1786 Ma), which occupies most of the Limejuice Zone (Fig. 1). Structures preserved from this event include a strong gneissosity within rafts of Leake Spring Metamorphics (Fig. 1), as well as gneissic fabrics within the granites of the Moorarie Supersuite (Sheppard et al., 2010b). A third event (D_{3n}) is only recognized in the Limejuice Zone, and is characterized by the folding of D_{2n} gneissic fabrics about upright, close to tight folds of variable orientation (Sheppard et al., 2010b).

Mangaroon Orogeny (1680–1620 Ma)

The 1680–1620 Ma Mangaroon Orogeny encompasses complex deformation, metamorphism, magmatism, and sedimentation (Sheppard et al., 2005; Sheppard et al., 2010b). In outcrop, structures and metamorphic assemblages associated with this event are confined to the Mangaroon Zone, although sedimentation and granite magmatism took place across the entire province (Fig. 1).

Sedimentation mostly took place prior to tectonic activity, between c. 1760 and 1680 Ma, with the deposition of siliciclastic fluvial and shallow marine sediments, the Pooranoo Metamorphics, across the entire province (Fig. 1). In the Mangaroon Zone, deeper water turbiditic rocks may have been deposited during the earliest stages of orogenesis at c. 1680 Ma (Sheppard et al., 2005). Deformation and medium- to high-grade metamorphism, including granite magmatism and in situ melting of

the turbiditic metasedimentary rocks of the Pooranoo Metamorphics (D_{1m}), took place in the Mangaroon Zone between c. 1680 and 1677 Ma (Sheppard et al., 2005; Sheppard et al., 2010b). Wholesale retrogression of these high-grade fabrics and large-scale, southeast-trending upright folds are attributed to D_{2m} , dated at between c. 1677 and 1659 Ma.

Following deformation and metamorphism in the Mangaroon Zone, voluminous megacrystic K-feldspar-phryic monzogranites were passively emplaced across the province from the Boora Boora Zone in the north to the Mooloo Zone in the south (Fig. 1). Granite emplacement occurred between c. 1670 and 1650 Ma, although at c. 1620 Ma, minor stocks of granite were emplaced in the Yarlweelor Gneiss Complex (Sheppard et al., 2010b).

Mutherbukin Tectonic Event (1385–1170 Ma)

Following the Mangaroon Orogeny, fine-grained siliciclastic and carbonate sedimentary rocks were deposited in the Edmund Basin some time between c. 1620 and 1465 Ma (Martin and Thorne, 2004; Martin et al., 2008). The sediments were deposited under fluvial to deep-marine conditions in a series of southwesterly dipping half grabens, and covered much of the Gascoyne Province (Cutten et al., 2011). At c. 1465 Ma, the basin was intruded by voluminous mafic sills of the Narimbunna Dolerite.

The 1385–1170 Ma Mutherbukin Tectonic Event is a poorly defined tectonothermal event, known primarily from the Mutherbukin Zone of the Gascoyne Province, although hydrothermal alteration and transpressional faulting has affected rocks of the Edmund Basin (Johnson et al., 2011c). In the Gascoyne Province, the event is characterized by a strong, steeply dipping schistosity within earlier metasedimentary rocks, and a well-developed foliation or gneissic banding within the granitic rocks. Although the recognition of different-aged fabrics is difficult in the field, U–Th–Pb SHRIMP phosphate geochronology has resolved two episodes of medium-grade metamorphism. The first (D_{1u}) is dated between c. 1280 and 1250 Ma, and the second (D_{2u}) between c. 1250 and 1170 Ma. U–Th–Pb SHRIMP phosphate dating of hydrothermally altered sedimentary rocks of the Edmund Basin suggests that the D_{1u} event may be as old as c. 1385 Ma (Johnson et al., 2011c).

Following the Mutherbukin Tectonic Event, a ~2 km thick sequence of siliciclastic fluvial to deep marine sediments (Martin and Thorne, 2004; Martin et al., 2008) were deposited in the Collier Basin between c. 1170 and 1070 Ma.

Edmundian Orogeny (1030–955 Ma)

The Edmundian Orogeny is characterized by widespread folding and low-grade metamorphism of sedimentary rocks within the Edmund and Collier Basins (Martin and Thorne, 2004; Cutten et al., 2011). The influence

of the Edmundian Orogeny on basement rocks of the Gascoyne Province is less clear, but reworking is recorded in a narrow corridor along the northern margin of the Mutherbukin Zone (Fig. 1). In this zone, rocks of the 1840–1810 Ma Leake Spring Metamorphics and 1760–1680 Ma Pooranoo Metamorphics were metamorphosed at medium grade and intruded by leucocratic granitic rocks of the 995–940 Ma Thirty Three Supersuite (Sheppard et al., 2007; Sheppard et al., 2010b).

U–Th–Pb SHRIMP phosphate geochronology has resolved three episodes of medium-grade metamorphism (Sheppard et al., 2007; Sheppard et al., 2010b). The first, D_{1e} , is recognized only from inclusion trails within garnet porphyroblasts but is dated at c. 1025 Ma (Sheppard et al., 2007). The second, D_{2e} , is characterized by a pervasive foliation that includes garnet and staurolite porphyroblasts, and has been dated at between c. 1025 and 995 Ma (Sheppard et al., 2007). The final event, D_{3e} , is characterized by kilometre-scale, east-southeasterly trending upright folding of the D_{2e} foliation and retrogression of M_{2e} assemblages at greenschist facies (Sheppard et al., 2007), and is constrained to between c. 995 and 954 Ma, the younger age defined by the oldest crosscutting undeformed pegmatite of the Thirty Three Supersuite.

Mundine Well Dolerite Suite (c. 755 Ma), Mulka Tectonic Event (c. 570 Ma), and formation of the Carnarvon Basin

The c. 755 Ma Mundine Well Dolerite Suite provides a critical constraint on post-Edmundian deformation. These dykes are prominent in aeromagnetic and photo mosaic images as north-northeasterly trending features and are concentrated in the northwestern part of the Gascoyne Province, although they are observed throughout.

In several locations, these dykes are displaced by southeast-trending faults of the c. 570 Ma Mulka Tectonic Event, most notably on the Chalba and Ti Tree shear zones (Fig. 1). Deformation is concentrated in narrow zones around the major shear zones, and the overall displacements are universally dextral and on the order of tens of metres (Sheppard et al., 2010b). However, cumulative fault movements across the across the Ti Tree and Chalba Shear Zones are significant at ~9 and ~35 km, respectively (Sheppard et al., 2010b). $^{40}\text{Ar}/^{39}\text{Ar}$ dating of one of these shear zones has provided an age of 570 ± 10 Ma (Bodorkos and Wingate, 2007).

The final event to have significantly affected the Gascoyne Province is the formation of the Carnarvon Basin to the west. The oldest sedimentary rocks adjacent to the Gascoyne Province are Devonian. These are in unconformable contact with basement rocks of the province. They are overlain in turn by Lower Carboniferous and Upper Carboniferous – Permian sedimentary rocks. Movements during the mid-Carboniferous tilted the Devonian rocks, which are in turn unconformably overlain by Carboniferous to Neogene sedimentary rocks (Hocking et al., 1983).

Structural interpretation of geology and geophysics

Methods and implementation

This study used domain-based structural interpretation of aeromagnetic data (e.g. Aitken and Betts, 2009) to obtain a better understanding of the large-scale structural architecture and tectonic evolution of the region. Structures in this interpretation were defined primarily by their expression in reduced-to-pole (RTP) aeromagnetic data, its first vertical derivative, and its tilt derivative. Bouguer gravity data was also used for delineating the larger structures. Geological information was influential in locating structures and essential for the interpretation of their meaning.

Geological information

The interpretation drew upon several sources of geological information. Foremost amongst these are geological maps of the region provided by GSWA. Recent 1:100 000 scale mapping, including interpreted solid geology in areas lacking outcrop, covers most of the study area and this was supplemented by 1:500 000 scale mapping elsewhere. In addition to these maps, the GSWA WAROX database of structural measurements was used to provide structural constraint on the strike, dip, and type of foliations, trend and plunge of fold axes, etc. A particular use of these data was to help differentiate primary structures from secondary structures in the aeromagnetic interpretation. A limited series of crustal-scale seismic reflection and MT lines provided key constraints on the 3D geometry of the major faults in the area, and these were incorporated into the interpretation where applicable.

Domain definition and characterization

The method used calls for structurally distinct domains to be identified, within which a common structural evolution is likely. Based on geological differences, the Gascoyne Province has already been subdivided into several tectonic zones (Fig. 2), each of which preserves a different history and different characteristics. These zones are bounded by major shear zones, which typically show activity late in the evolution of the province, but in most cases with a probable earlier history. These zones are sufficient for the purposes of the geophysical interpretation.

Event definition and characterization

Each domain was structurally interpreted on an individual basis, using a method akin to form-surface mapping in structural geology. A key aim was to define magnetic form lines for early structures. Later generations of structure could then be inferred from the deformation of these.

Additional indications of structure included increased or reduced magnetization associated with shear zones, and also intrusive and sedimentary contacts and dykes.

From this mapping, a local sequence of deformation events was identified within each domain. Throughout this Report, deformational event identifiers (D_1 , D_2 , etc.) indicate the event in that particular zone only. These were linked to the stratigraphy and the regional tectonic event (e.g. Glenburgh Orogeny) on the basis of local overprinting relationships with mapped and inferred geology (Table 1). The stratigraphic position of deformation is poorly constrained in many places due to a lack of local outcrop, and less detailed and less certain stratigraphy in the regions not recently mapped. The local deformation events were assigned to tectonic events based on their stratigraphic position, and correlations in deformation style or orientation with deformation events identified in field mapping. Assigning structures to tectonic events is somewhat hampered by the lack of major lithological packages between events, and the fact that isotopic dates rarely sample the individual localities that best constrain an overprinting relationship. For that reason, many deformation events are attributed to two events (e.g. Mutherbukin/Edmundian, late Glenburgh or early Capricorn).

Interpretational confidence estimation

As part of this work we prepared a map of the data richness, considered a proxy for interpretational confidence, throughout the Gascoyne Province. Following Aitken et al. (2013a), this method differentiates areas of relative data richness from areas of relative data poverty. In essence, this approach provides a map of the opportunity presented to the interpreter to make a correct and well constrained interpretation, although it cannot account for interpreter biases and experience. Therefore, it is a map of the reliability of the structural interpretation, which feeds into understanding the reliability of the prospectivity analyses that are partly based on it.

The analysis includes measures to quantify: 1) the local (within 10 km) abundance of outcrop, the scale of mapping at that outcrop, and the relevance of the geology to the interpretation; 2) the strength of gradients in both RTP aeromagnetic data and Bouguer gravity data, and the influence of structural complexity in these images; 3) the influence of imperfect gravity data distribution. These measures are combined using a weighted sum, in which the weights are selected to best match the interpreter's perception of uncertainty. Further details are available in Appendix 1.

The resulting image (Fig. 3) shows generally moderate to high data richness within the Gascoyne Province, where outcrop is generally good, and where the area is mostly mapped at 1:100 000 scale, and gravity and magnetic fields are well sampled and have relatively high-amplitude signals. Data richness is lower for the Errabiddy Shear Zone, and the eastern Paradise and Mooloo Zones

(Fig. 2 cf. Fig. 3), which are dominated by low-amplitude magnetic anomalies, and have few outcrops. The Narryer Terrane has moderate data richness because the strength of the potential field data offsets the lack of outcrop. Similarly, the Boora Boora Zone has moderate data richness despite poor geological control. The Edmund and Collier Basins generally have low data richness, as outcrop is quite sparse and the basins provide a thick mask of generally non-magnetic sedimentary rocks that inhibit the definition of basement-derived anomalies.

Results

Narryer Terrane and Yarlalweelor Gneiss Complex

These zones represent the margins of the Yilgarn Craton that have been reworked during the later tectonic events in the Gascoyne Province (Fig. 4). The Yarlalweelor Gneiss Complex is distinct from the Narryer Terrane, in that it carries a much greater degree of Paleoproterozoic reworking.

The first fabric recognized is a linear magnetic fabric (D_1), preserved in small, rootless, isoclinal F_2 folds. D_2 is the dominant north-trending tectonic fabric in the Narryer Terrane. These deformation events are well constrained by their relationships with Archean granitic rocks. Small, magnetic granites (e.g. A in Fig. 4) truncate S_1 layering and are aligned with, but do not deform, S_2 . These are interpreted to indicate intrusion in the early stages of D_2 , and one of these has been dated at 2636 ± 7 Ma (Nelson, 1996) (Table 1). S_2 foliations are truncated by the large granitic intrusion in the north of the Narryer Terrane (B in Fig. 4). This granite has been dated at 2615 ± 2 Ma (Nelson, 1999).

The next deformation event, D_3 , is characterized by northeast-oriented fabrics and folds, which are strongly developed within the YGC. This event is also observed within the Narryer Terrane, where it is associated with faulting, and the re-orientation and deformation of D_2 structural fabrics. In the YGC, this event overprints the 1965–1945 Ma Bertibubba Supersuite and is aligned with the 1820–1775 Ma Moorarie Supersuite, indicating that it represents either the latest stages of the Glenburgh Orogeny, or the earlier stages of the Capricorn Orogeny. This aeromagnetic fabric is interpreted to correlate with the D_{1n} fabric identified in the YGC from field mapping. In outcrop this event is defined by upright, close to isoclinal folds (Sheppard et al., 2010b). Geochronological constraints on this event place it at 1813–1800 Ma.

The D_3 foliation is subsequently deformed within an east-southeasterly trending corridor, bounded by the Morris Fault to the north and a parallel fault ~40 km to the south (F_1 , Fig. 4). At this scale, this deformation (D_4) is primarily fault-dominated, although a large-scale fold is interpreted with the Seabrook Fault as an axial planar structure. This event deforms the Moorarie Supersuite, but not the 1680–1620 Ma Durlacher Supersuite, indicating a Capricorn Orogeny age.

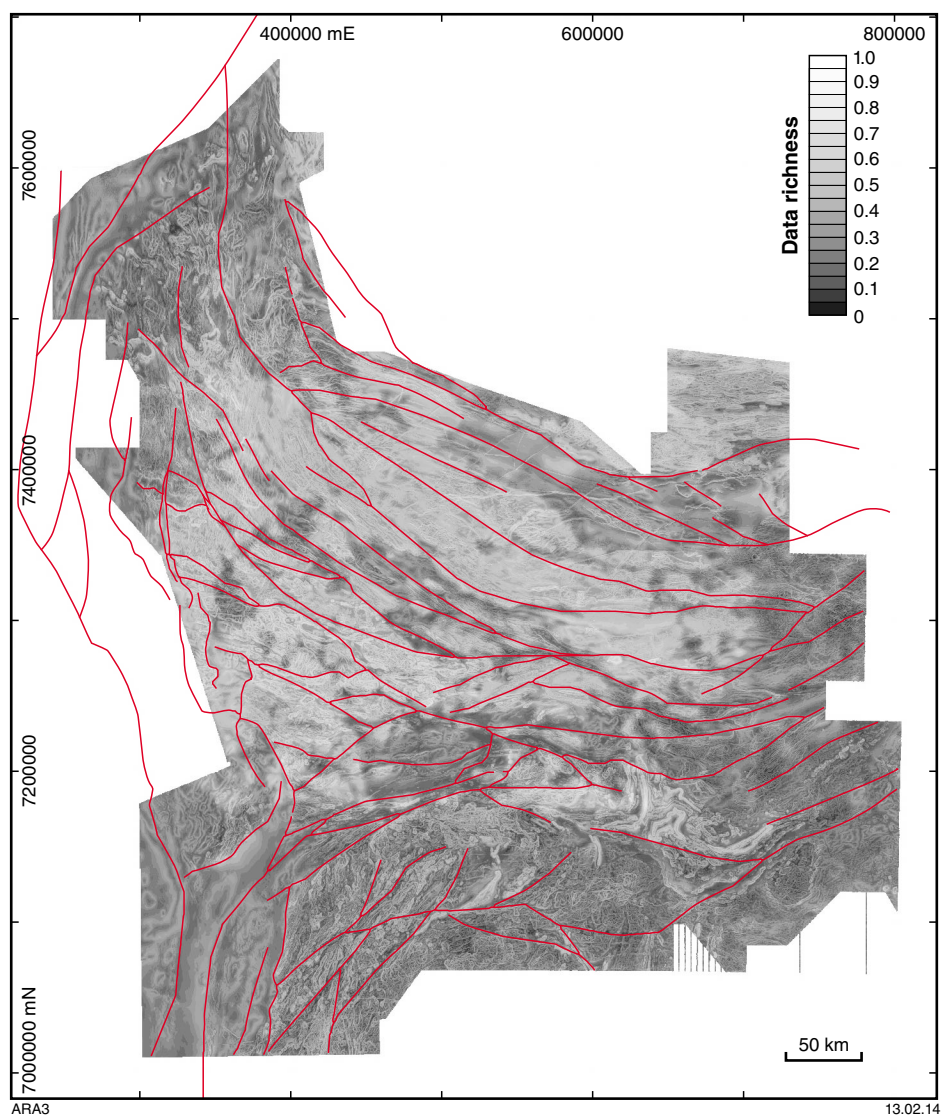


Figure 3. Data richness map of the western Capricorn Orogen, considered a proxy for interpretational confidence. Analysis is based on geology, magnetic, and gravity data. See Appendix 1 for the individual components. Crustal-scale faults are shown in red. Most of the region shows moderate to high data richness, but with much lower values in some key areas (e.g. Errabiddy Shear Zone; see Fig. 2)

Table 1. Summarized structural evolution of the Gascoyne Province

Zone	Tectonic event							
	Pre-2.0 Ga	Glenburgh Orogeny (2005–1950 Ma)	Capricorn Orogeny (1820–1770 Ma)	Mangaroon Orogeny (1680–1620 Ma)	Mutherbukin Tectonic Event (1385–1170 Ma)/Edmundian Orogeny (1030–955 Ma)	Mundine Well Dolerite Suite (c. 755 Ma)	Mulka Tectonic Event (c. 570 Ma)	Phanerozoic events
Narryer/YGC	D ₁ , D ₂	–	D ₃ , D ₄	–	–	–	–	–
Errabiddy	–	D ₁ ?	D ₁ ? D ₂	–	–	–	–	–
Paradise	–	D ₁ , D ₂	D ₃	–	–	–	D ₄	D ₅
Mooloo	D ₁ ?	D ₂	D ₂ ? D ₃	–	D ₄	–	D ₅	–
Mutherbukin	–	–	–	D ₁	D ₂ (M), D ₃ (E)	D ₄	D ₅	–
Limejuice	–	–	D ₁ , D ₂	–	D ₃	–	–	D ₄
Mangaroon	–	–	–	D ₁ , D ₂	D ₃	–	–	D ₄
Boora Boora	–	–	D ₁ , D ₂	D ₃	D ₄	–	–	–

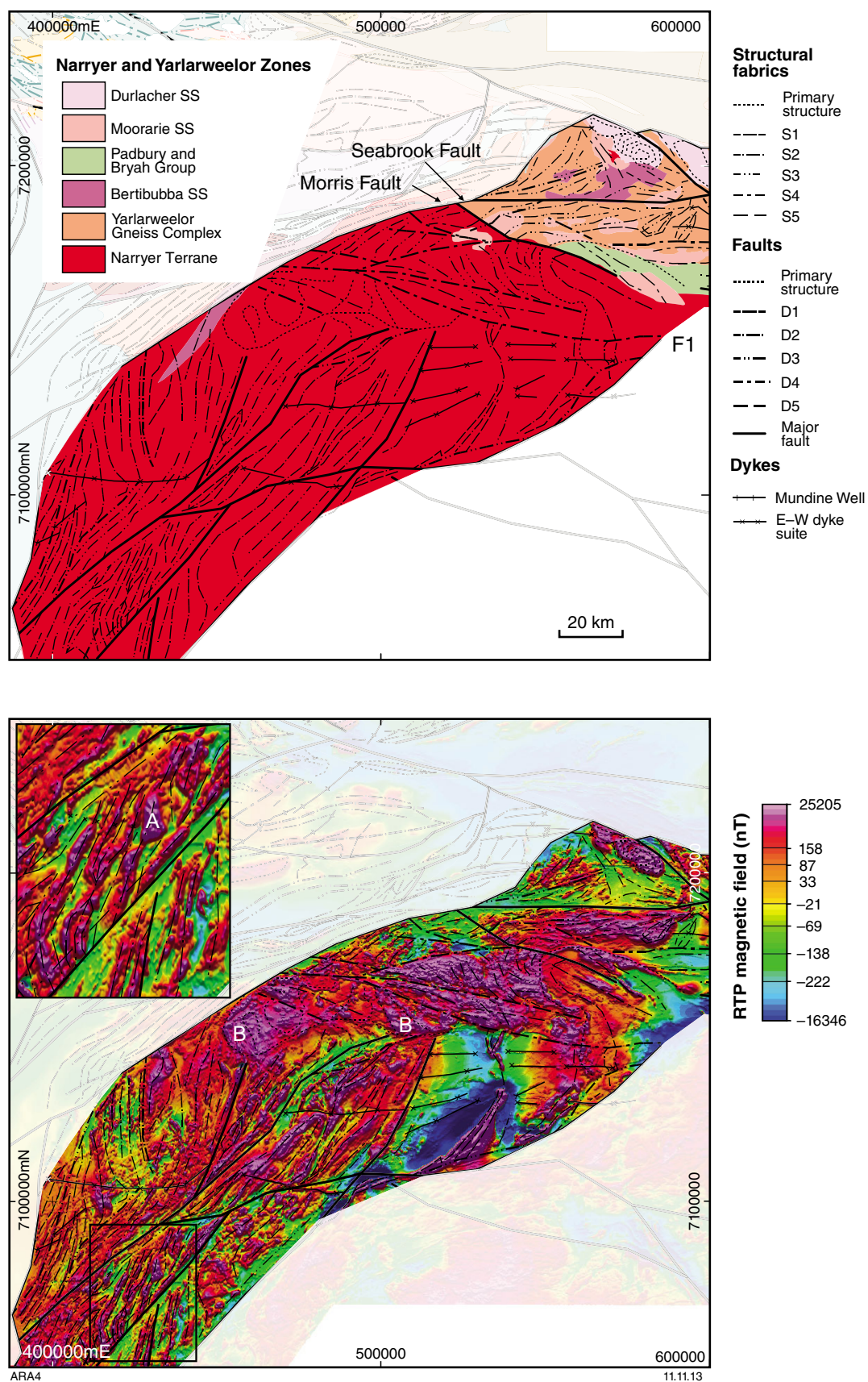


Figure 4. Structural interpretation of the Narryer Terrane overlain on: a) geology; b) RTP magnetic field. Structural events are relevant only to this zone. Inset is magnified two times. SS – Supersuite

Errabiddy Shear Zone

The Errabiddy Shear Zone is the 5–20 km wide zone of sheared rocks that demarcates the transition between the Yilgarn Craton and the Glenburgh Terrane (Fig. 5). At the surface, it represents the suture between these terranes, although it has been significantly reactivated in later events. It is characterized by reduced magnetization and reduced density relative to the neighbouring zones. Our interpretation recognizes just two fabrics within the shear zone. The first (S_1) is identified in all units except the Erong Granite of the 1820–1775 Ma Moorarie Supersuite (E) and is defined by a low-amplitude magnetic fabric. Overprinting relationships between S_1 and the 1965–1945 Ma Bertibubba Supersuite and Erong Granite suggest that S_1 is either late-Glenburgh or early Capricorn Orogeny age (Table 1). S_1 was isoclinally folded during D_2 , producing S_2 , which is the main tectonic fabric within the Errabiddy Shear Zone. S_2 is observed within the Erong Granite, indicating a maximum age for the Capricorn Orogeny. Field mapping has identified a series of upright, close to isoclinal D_{1n} (Capricorn Orogeny) folds within the Errabiddy Shear Zone. These folds plunge either east-northeast to northeast or west-southwest to southwest, and S_2 is interpreted to represent this event. Both D_1 and D_2 are postdated by fault that are interpreted to have exploited the shear zone during later tectonic events. An easterly trending dyke swarm, likely late Mesoproterozoic in age, also cuts S_1 and S_2 .

Paradise Zone

The Paradise Zone lies to the north of the Errabiddy Shear Zone, and is dominated by granitic rocks of the Dalgaringa Supersuite (Fig. 6). Several deformation events are interpreted for this zone. The earliest (D_1) is defined by tight folding of magnetic foliations within 2005–1970 Ma Dalgaringa Supersuite rocks in the southwest Paradise Zone. The axial traces of these folds are part of a more widespread event (D_2), which is observed throughout the western Paradise Zone and Carandibby Inlier, but is conspicuously absent from the 1980–1970 Ma Nardoo Granite (A). Features within the Nardoo Granite, and within a small pluton (B) external to the Nardoo Granite, are aligned with this trend, indicating likely control on intrusion, and possibly that intrusion was syn-deformational. Both D_1 and D_2 are constrained to be Glenburgh Orogeny age (Table 1), and may relate to previously identified D_{1g} and D_{2g} events (Sheppard et al., 2010b). Later events (D_3) are fault dominated, and correlate with later activity on the Errabiddy Shear Zone (probably Capricorn Orogeny), the Deadman Fault (probably Mulka Tectonic Event), and the Carnarvon Basin margin (Permian–Carboniferous).

The Carandibby Inlier is interpreted as an extension of the Paradise Zone, and shows magnetic character and deformation similar to that of the southwest Paradise Zone.

Mooloo Zone

The Mooloo Zone represents the Archean to Paleoproterozoic Glenburgh Terrane onto which the

Dalgaringa Arc has been thrust along the shallowly south-dipping Cardilya Fault (Fig. 7). The Cardilya Fault merges with the Errabiddy Shear Zone at depth (Johnson et al., 2011a, 2013), generating a ‘crocodile’ structure, typical of suture zones (Meissner, 1989). The western half of the Mooloo Zone is dominated by the 2555–2430 Ma Halfway Gneiss, while the eastern half is dominated by 1820–1775 Ma Moorarie Supersuite (Fig. 7).

The deformation history of the Mooloo Zone is relatively complicated. The first identified fabric (D_1) is a convoluted magnetic fabric within the Halfway Gneiss, although it is only observed in one locality (A). The D_1 fabric is isoclinally folded around an east-southeast trending axis (L_2/D_2), which defines the dominant tectonic fabric within the Halfway Gneiss. D_2 is not observed in the Moorarie Supersuite, constraining its age to the Glenburgh Orogeny, or perhaps the earliest Capricorn Orogeny (Table 1). Field mapping suggests that both the later Glenburgh Orogeny fabric (D_{2g}) and the earliest Capricorn Orogeny fabric (D_{1n}) are widely observed within the Mooloo Zone.

Post-Moorarie deformation includes a relatively limited array of north-northeasterly trending faults (D_3) that probably pre-date the 1680–1620 Ma Durlacher Supersuite, and are most likely of Capricorn Orogeny age. D_4 involves east-southeast oriented shearing, sub-parallel to the S_2 fabric but penetrating into Moorarie and Durlacher Supersuite rocks. This event is interpreted to represent reactivation of the D_2 architecture, probably during the Mutherbukin Tectonic Event, although the minimum age is not constrained. D_5 represents late activity associated with the Deadman Fault Zone, probably during the Mulka Tectonic Event.

Mutherbukin Zone

The Mutherbukin Zone is characterized by the 1680–1620 Ma Durlacher Supersuite (Fig. 8). Although these rocks are younger than those in the neighbouring Mooloo and Limejuice Zones, deformation is equally complicated, dominantly reflecting the Mutherbukin Tectonic Event and Edmundian Orogeny. The presence of the 995–940 Ma Thirty Three Supersuite within the Mutherbukin Zone allows separation of these orogenic events; a task that is difficult elsewhere.

The earliest identifiable deformation (D_1) in the Mutherbukin Zone is characterized by diversely oriented fabrics within most Durlacher Supersuite granites. In the southwestern part of the Mutherbukin Zone (A), an arcuate area of low magnetic intensity coincides with strongly deformed granitic rocks of the Durlacher Supersuite. These rocks are interpreted to have been deformed at mid-crustal depths in a regional-scale sheath fold (Johnson et al., 2011c). Recent U–Pb SHRIMP zircon geochronology (GSWA, 2011) indicated that the main regional phase of deformation (that is imaged in the aeromagnetic data) took place at c. 1320 Ma, during the early phases of the Mutherbukin Tectonic Event (Table 1).

These foliations are deformed by a more pervasive, broadly east–west trending event (D_2) that post-dates all Durlacher Supersuite intrusions, but does not extend into

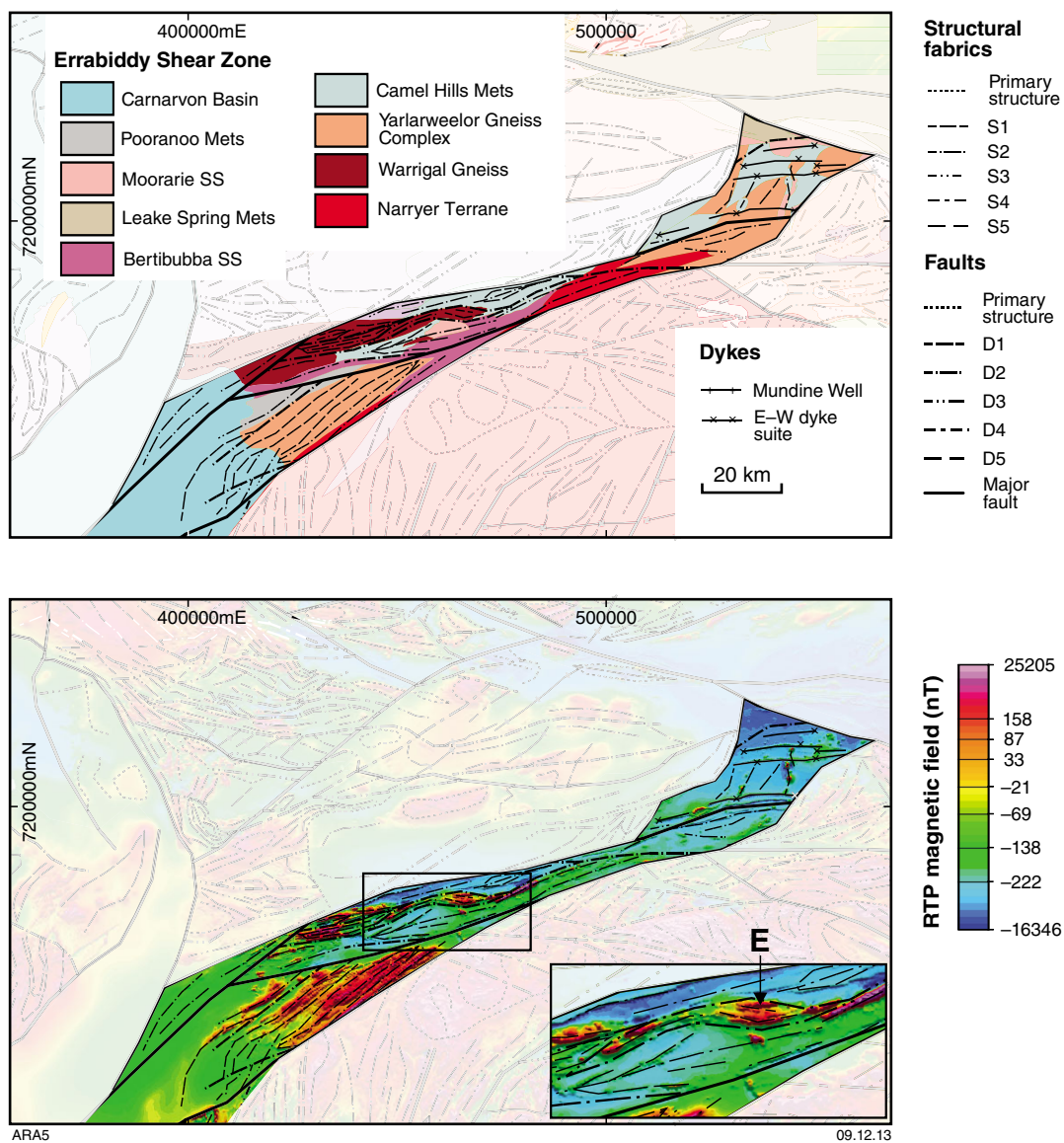


Figure 5. Structural interpretation of the Errabiddy Shear Zone overlain on: a) geology; b) RTP magnetic field. Mets – Metamorphics; other symbology as per Figure 4

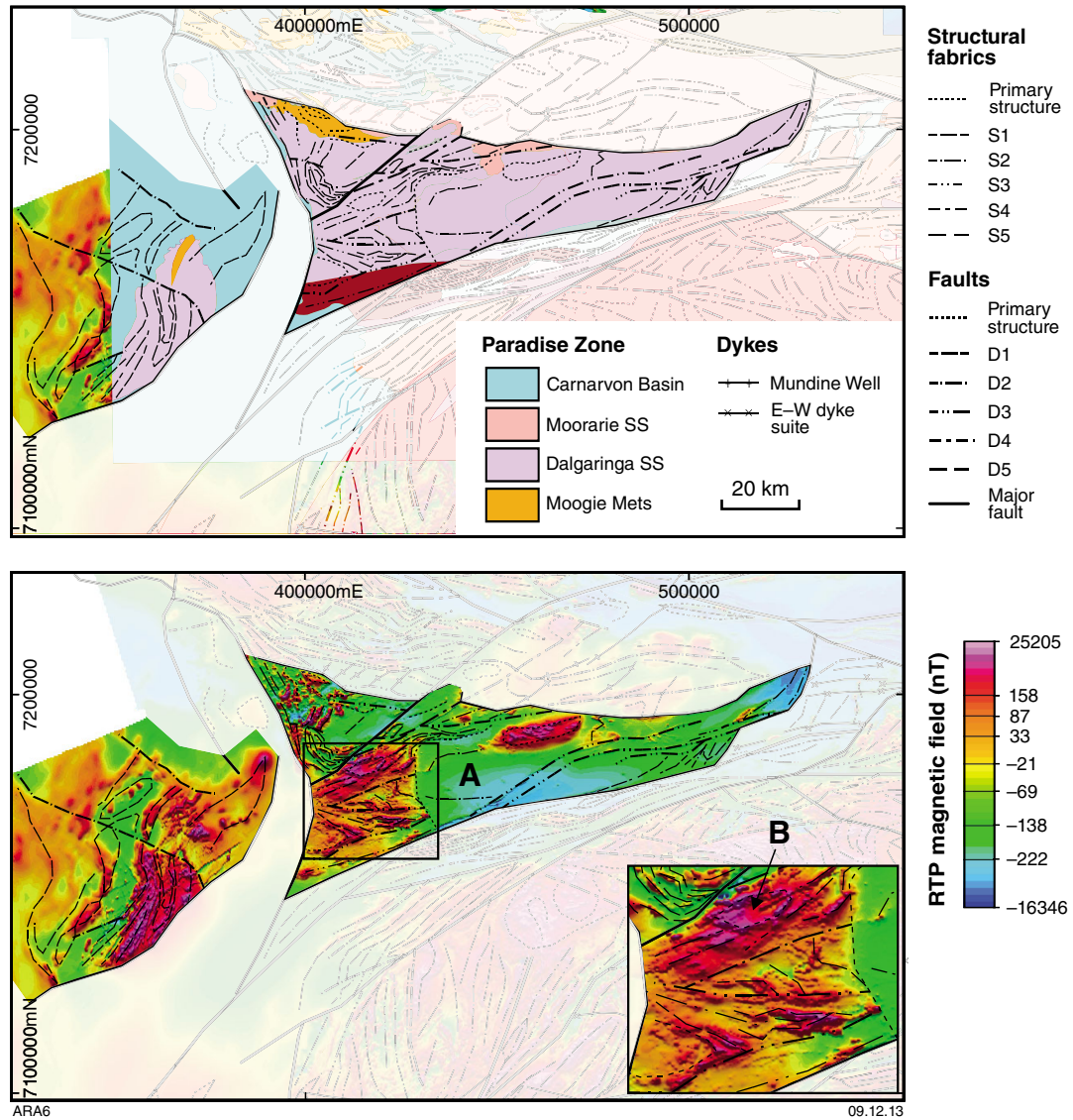


Figure 6. Structural interpretation of the Paradise Zone overlain on: a) geology; b) RTP magnetic field. Symbolry as per Figures 4 and 5

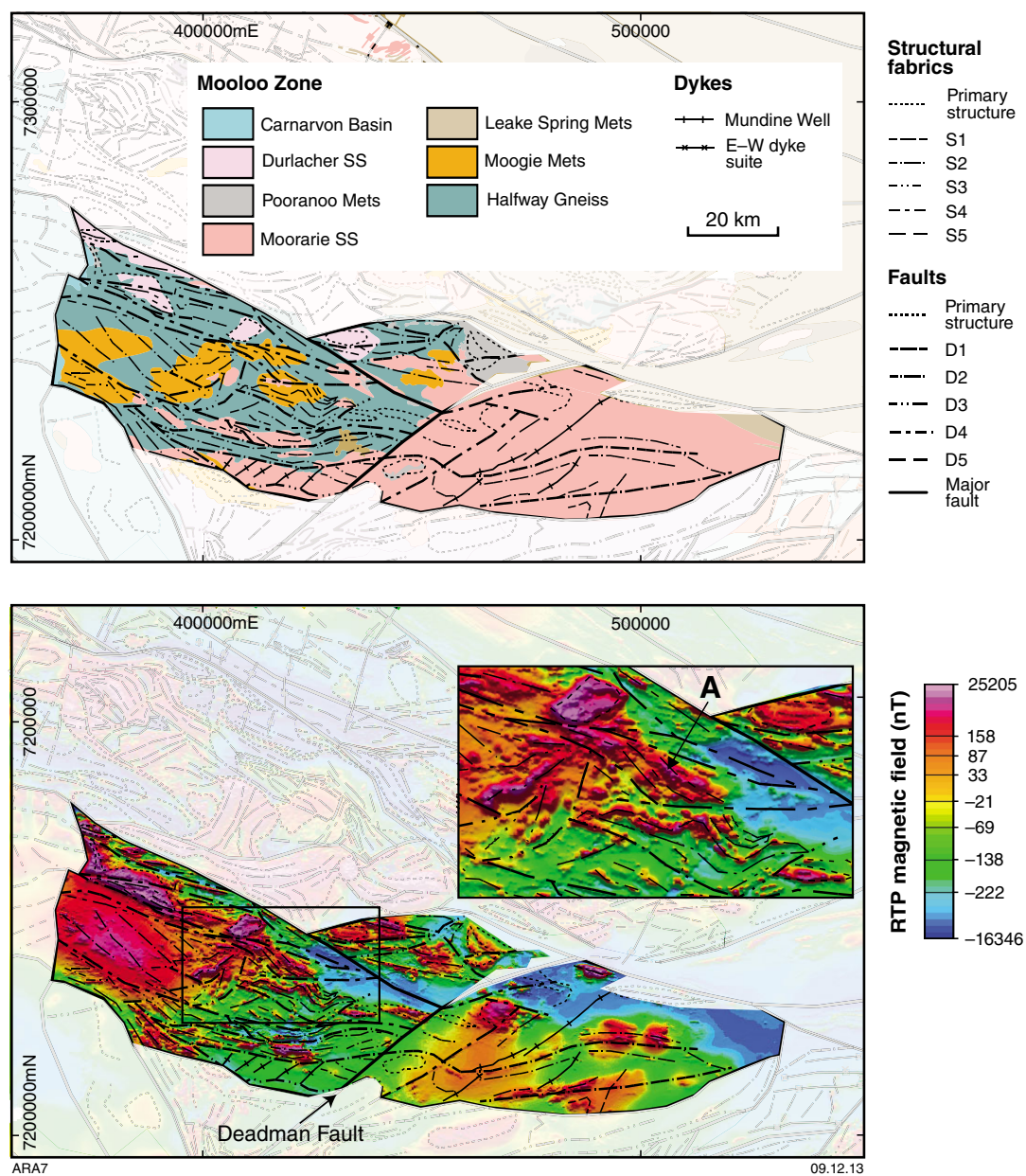


Figure 7. Structural interpretation of the Mooloo Zone overlain on: a) geology; b) RTP magnetic field. Symbolry as per Figures 4 and 5

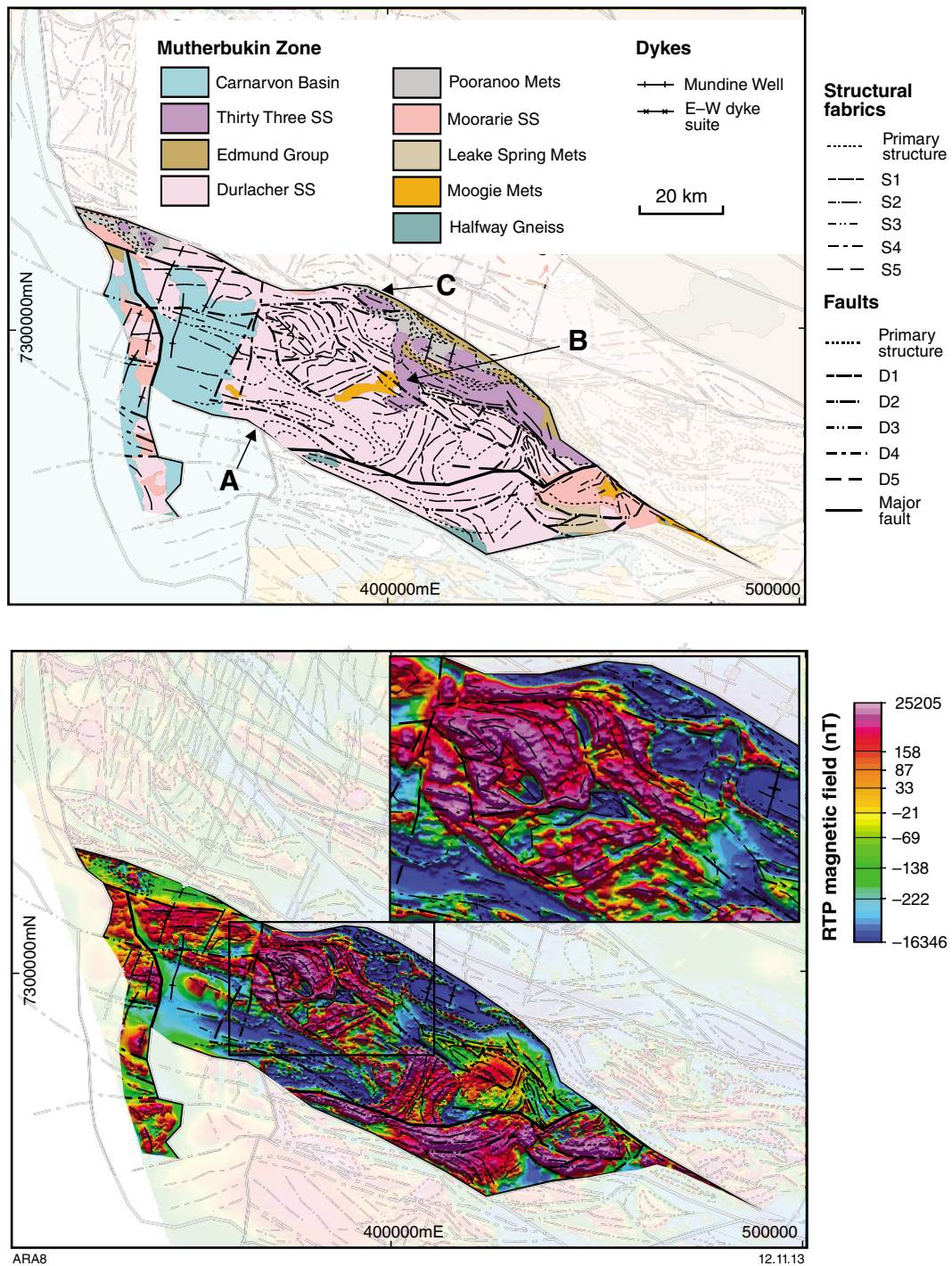


Figure 8. Structural interpretation of the Mutherbukin Zone overlain on: a) geology; b) RTP magnetic field. Symbology as per Figures 4 and 5

the Thirty Three Supersuite. Apparent folding of the Thirty Three Supersuite by this event (B, Fig. 8) is interpreted to represent the intrusion of granitic melt into pre-existing fold structures.

D₃ is limited in extent, affecting only the northern part of the Mutherbukin Zone. This event is characterized by an easterly trending fault that cuts D₂ structures, and which accommodated the emplacement of Thirty Three Supersuite granites within the shear zone (C). This fault may represent reactivation of the Ti Tree shear zone during the Edmundian Orogeny, but the relative age of the fault is poorly constrained. Given that the D₂ event is not observed within the Thirty Three Supersuite, we interpreted it to be Mutherbukin Tectonic Event age, whereas the D₃ event is interpreted to be Edmundian in age.

Away from the Thirty Three Supersuite, it is difficult to assign structures to one orogeny or the other. Geological mapping indicates that both Mutherbukin and Edmundian deformation are associated with relatively high-grade fabrics of similar orientations, although the latest Edmundian Orogeny event is distinct in that it produced recognizable folding at lower metamorphic grade. U–Pb dating on metamorphic monazite and xenotime has proved effective in identifying each event (Johnson et al., 2011c).

D₄ is also limited in extent to a north-northeasterly trending fault that forms the boundary between the Mutherbukin Zone and the Carnarvon Basin. This fault zone is parallel to the c. 755 Ma Mundine Well Dolerite Suite, with which it is interpreted to be coeval, although later reactivation during formation of the Carnarvon Basin is likely. D₅ represents the post-Mundine Well reactivation of the east-southeasterly trend, including the Ti Tree and Chalba shear zones. In the latter case, this is constrained to the Mulka Tectonic Event, at 570 ± 10 Ma, through ⁴⁰Ar/³⁹Ar dating on white micas developed within the shear zone (Bodorkos and Wingate, 2007). The final event to have affected this zone is the formation of the Carnarvon Basin, which has reactivated predominantly north-oriented structures.

Limejuice Zone

The Limejuice Zone is completely dominated by the Minnie Creek batholith, a large, composite batholith of granitic rocks of the 1820–1775 Ma Moorarie Supersuite. Exposures of other rock types are limited, but are sufficient to allow the relative ages of tectonic fabrics to be differentiated (Fig. 9).

The oldest observed deformation is represented by a fabric within the Moorarie Supersuite that is (rarely) isoclinally folded (e.g. A in Fig. 9). This early fabric seems to be confined to magnetic highs (possibly 1840–1810 Ma Leake Spring Metamorphics or early Moorarie Supersuite rocks) that have subsequently been engulfed by later Moorarie Supersuite rocks, or overlain by later Leake Spring Metamorphics. The predominant fabric (S₂/D₂) within the Moorarie Supersuite typically trends east-southeast to southeast, although it too is significantly deformed. D₂ (isoclinal folding) is not developed in all rocks of the Moorarie Supersuite or Leake Spring Metamorphics, suggesting that it is of Capricorn Orogeny

age (Table 1). These fabrics may correlate with the mapped D_{2n} and D_{3n} deformation events, respectively. In the Limejuice Zone, the first is associated with a gneissic fabric (S_{2n}) that is invariably folded around upright close to tight F_{3n} folds.

D₃ is characterized by southeast to easterly oriented faulting and fault-related deformation. This deformation post-dates the 1620–1465 Ma Edmund Group, but predates the c. 755 Ma Mundine Well Dolerite Suite, and is interpreted to represent either the Mutherbukin Tectonic Event or Edmundian Orogeny. D₄ is characterized by northerly oriented structures that postdate the Mundine Well Dolerite Suite and are associated with the opening of the Carnarvon Basin. Several of these can be directly correlated with a package of Devonian-age rocks deposited at the inception of the extension that led to the formation of the Carnarvon Basin.

Mangaroon Zone

The Mangaroon Zone is dominated by the 1680–1620 Ma Durlacher Supersuite and the 1760–1680 Ma Pooranoo Metamorphics, although 1620–1465 Ma Edmund Group and 1820–1775 Ma Moorarie Supersuite rocks are also significant (Fig. 10).

The earliest aeromagnetic fabric (S₁) is only observed in the southeast of the zone. This fabric is characterized by complexly deformed magnetic fabrics that are folded about east-southeasterly trending F₂ axes (A in Fig. 10). These F₂ axes, and an associated fabric where S₁ is not defined, are the earliest expression of the main east-southeast trend of this zone. Both of these events deformed the Pooranoo Metamorphics and the Durlacher Supersuite; however, late Durlacher Supersuite plutons clearly cut these fabrics (B in Fig. 10), pointing to deformation during the Mangaroon Orogeny (Table 1).

Geological mapping indicates that, in the Mangaroon Zone, the Mangaroon Orogeny comprised two discrete deformational/metamorphic events (Sheppard et al., 2005). The first, S_{1m}, is characterized by a regionally extensive gneissic layering or foliation within amphibolite facies Pooranoo Metamorphics. The second is generally observed as a pervasive, east-southeasterly trending foliation that overprints S_{1m}. The mineral assemblages of the later foliation indicate greenschist facies conditions. F_{2m} folds are upright, close to tight, and plunge steeply west-northwest or east-southeast.

Rocks evidencing Mangaroon Orogeny deformation are overlain by the Edmund Group. These are deformed by a third deformation event, characterized by close folding within the Edmund Group, as well as east-southeasterly oriented fault zones within the basement rocks. These fault zones can be distinguished from their D₂ equivalents because they cut all Durlacher Supersuite intrusions, and because they are more linear. This event predates the Mundine Well Dolerite Suite, and is interpreted to relate to either the Mutherbukin or the Edmundian Orogeny. As with the other zones, the final event, D₄, is much younger and is characterized by north-oriented structures that have accommodated extension associated with the formation of the Carnarvon Basin.

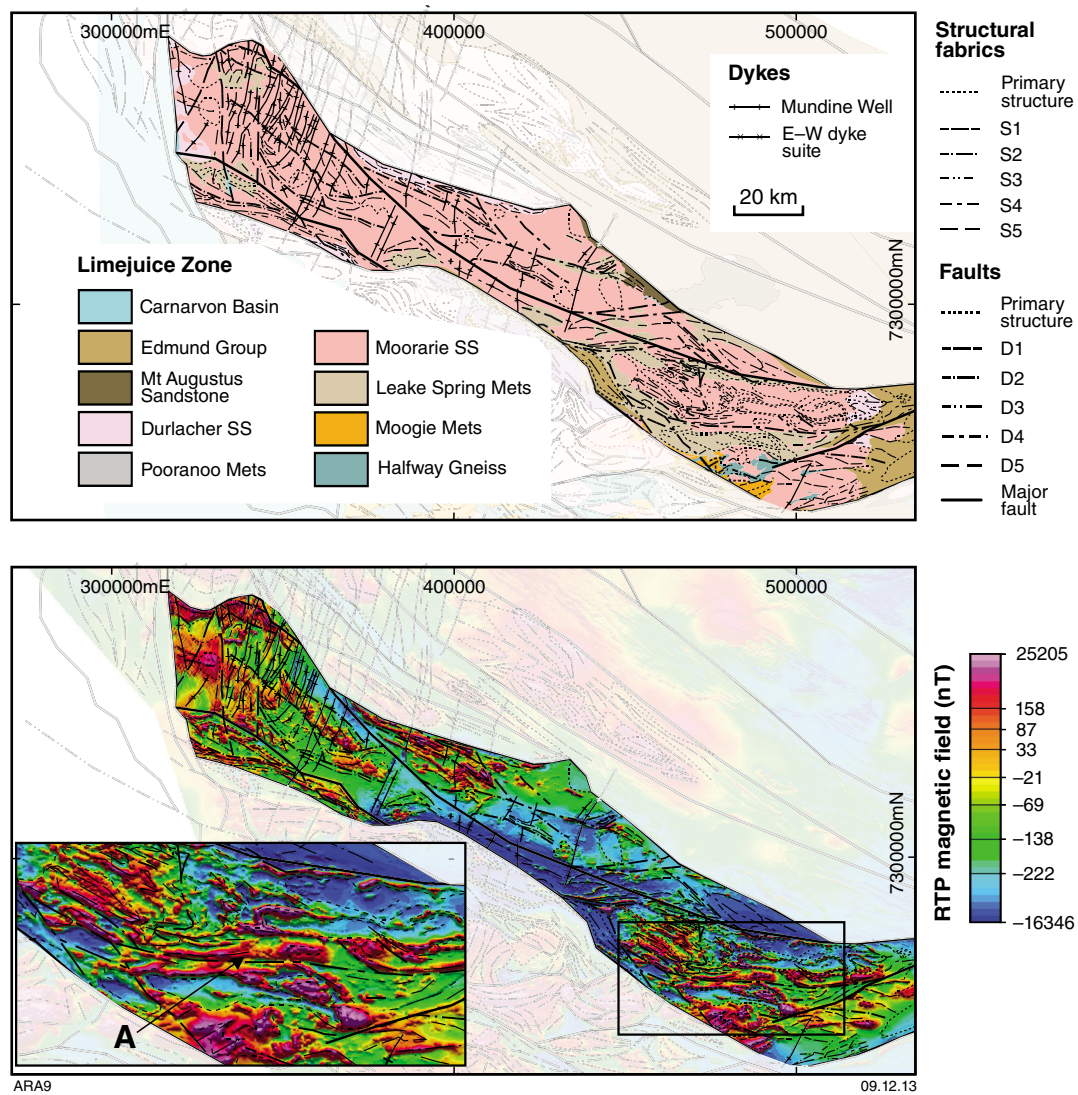


Figure 9. Structural interpretation of the Limejuice Zone overlain on: a) geology; b) RTP magnetic field. Symbology as per Figures 4 and 5

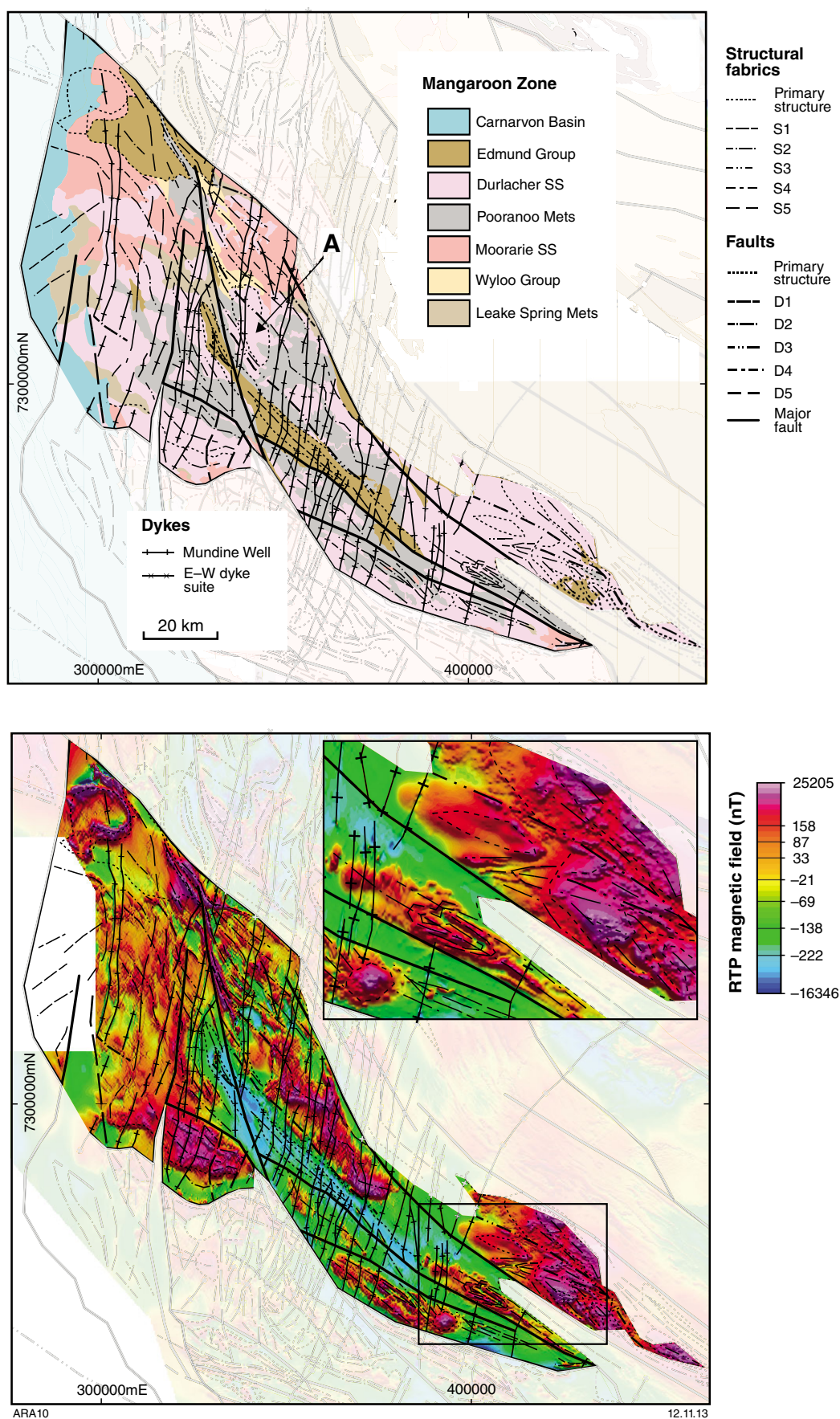


Figure 10. Structural interpretation of the Mangaroon Zone overlain on: a) geology; b) RTP magnetic field. Symbolry as per Figures 4 and 5

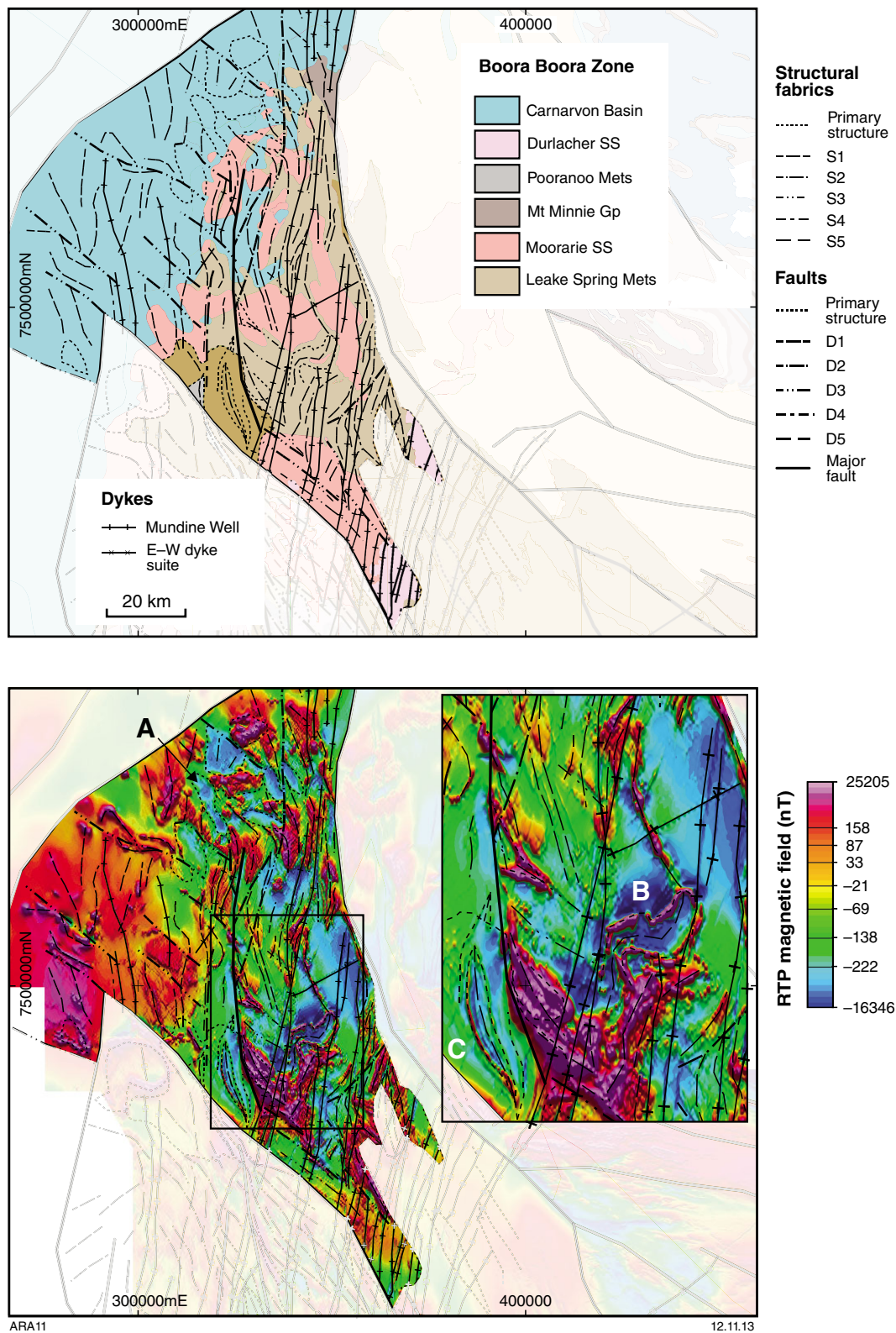


Figure 11. Structural interpretation of the Boora Boora Zone overlain on: a) geology; b) RTP magnetic field. Symbology as per Figures 4 and 5

Boora Boora Zone

The geology of the Boora Boora Zone has not yet been mapped in the same level of detail as the other zones, and is less well understood (Fig. 11). This zone is dominated by the 1820–1775 Ma Moorarie Supersuite, with extensive exposures of the 1840–1810 Ma Leake Spring Metamorphics and more limited exposures of the 1680–1620 Ma Durlacher Supersuite, the 1760–1680 Ma Pooranoo Metamorphics, and the 1620–1465 Ma Edmund Group.

The earliest event interpreted from the aeromagnetic data is a pervasive north-oriented fabric that is observed within both the Moorarie Supersuite and the Leake Spring Metamorphics. This fabric is also cut by younger Moorarie Supersuite intrusions in the far northwest of the Boora Boora Zone (A in Fig. 11), indicating deformation during the Capricorn Orogeny (Table 1). In several examples, the contact between the Leake Spring Metamorphics and the Moorarie Supersuite is quite tightly folded.

Subsequent deformation is defined by east-southeasterly trending shear zones. Rocks affected by these structures are overlain by the Edmund Group, indicating that the structures represent the latest Capricorn Orogeny or Mangaroon Orogeny. The shear zones are closely related in space to the Lyons River and Minga Bar Faults, indicating that both these structures were active at that time. Later northerly oriented faulting and upright folding of the Edmund Group adjacent to the Minga Bar fault (C in Fig. 11) predates the Mundine Well Dolerite Suite, indicating further motion on this fault during the Mutherbukin or Edmundian Orogenies.

Crustal structure

Density and magnetic susceptibility measurements

To constrain properties for gravity and magnetic modelling, measurements of magnetic susceptibility and specific gravity were made on 185 hand specimens from throughout the Capricorn Orogen. These specimens were selected to provide the most representative database of the surface rocks possible; however, the distribution of outcrop may introduce spatial biases into the dataset, and may also lead to preferential sampling of erosion-resistant units. The use of specimens from outcrop also introduces the possibility that weathering may influence the results, which is especially relevant for magnetic susceptibility. The data were primarily collected to provide constraints on the petrophysical properties of units during geophysical modelling, but may also provide additional insight into other aspects of the rocks, such as oxidation states related to hydrothermal alteration. Details on the method and analysis are given in Appendix 2. Where statistical analysis was undertaken, magnetic susceptibility data were analysed using the \log_{10} of the initial readings taken in SI $\times 10^{-5}$ units.

Yilgarn Craton

The oldest rocks considered are those of the Yilgarn Craton, sourced from the Narryer Terrane, the Yarlalweelor Gneiss Complex, and the Errabiddy Shear Zone. Ten samples were analysed.

The specific gravity data for the Yilgarn Craton rocks generated a mean of 2684 kg/m³, a median of 2676 kg/m³, and a standard deviation of 38 kg/m³ (Fig. 12). These are typical for granitic rocks and, given the lithological diversity and deformation history, have very low variability. There is no obvious link between lithology and density; in particular, there is no detectable difference between foliated and nonfoliated samples.

For magnetic susceptibility, the same 10 samples yielded a mean of 1.63×10^{-5} SI units, a median of 1.61, and a standard deviation of 0.44 (Fig. 12). As with specific gravity, there are no discernible links between magnetic susceptibility and either lithologies or tectonic zones.

Halfway Gneiss

The Halfway Gneiss is the basement to the Glenburgh Terrane. A total of nine samples were analysed.

The specific gravity data for the Halfway Gneiss generated a mean of 2702 kg/m³, a median of 2626 kg/m³, and a standard deviation of 162 kg/m³ (Fig. 12). These densities are typical for granitic gneiss, and show significant variability, including a high-density amphibolite sample (3050 kg/m³), and several gneissic monzogranite samples (2560–2630 kg/m³).

For magnetic susceptibility, the same nine samples yielded a mean of 1.37×10^{-5} SI units, a median of 1.31, and a standard deviation of 0.36 (Fig. 12). There are no discernible correlations between lithologies or tectonic zones.

Dalgaringa and Bertibubba Supersuites

The Dalgaringa Supersuite are interpreted as a pre-collisional continental arc. Only three samples were available for analysis, one from the Paradise Well area (S.G. = 2700 kg/m³, susceptibility = 1.36×10^{-5} SI units) and another two from the younger Nardoo Granite (S.G. = 2690–2720 kg/m³, susceptibility = $1.86 - 2.6 \times 10^{-5}$ SI units) (Fig. 12).

The Bertibubba Supersuite are the first rocks common to both sides of the Errabiddy Shear Zone. Two samples were analysed, yielding specific gravity estimates of 2700 and 2750 kg/m³, and magnetic susceptibility measurements of 2.62×10^{-5} and 1.0×10^{-5} SI units (Fig. 12). The sample from the Yarlalweelor gneiss is more magnetic and denser than the example from the Errabiddy Shear Zone.

Moorarie Supersuite

The Moorarie Supersuite is very common and widespread, and samples were sourced from all zones except the Narryer and Paradise Zones. A total of 27 samples were analysed.

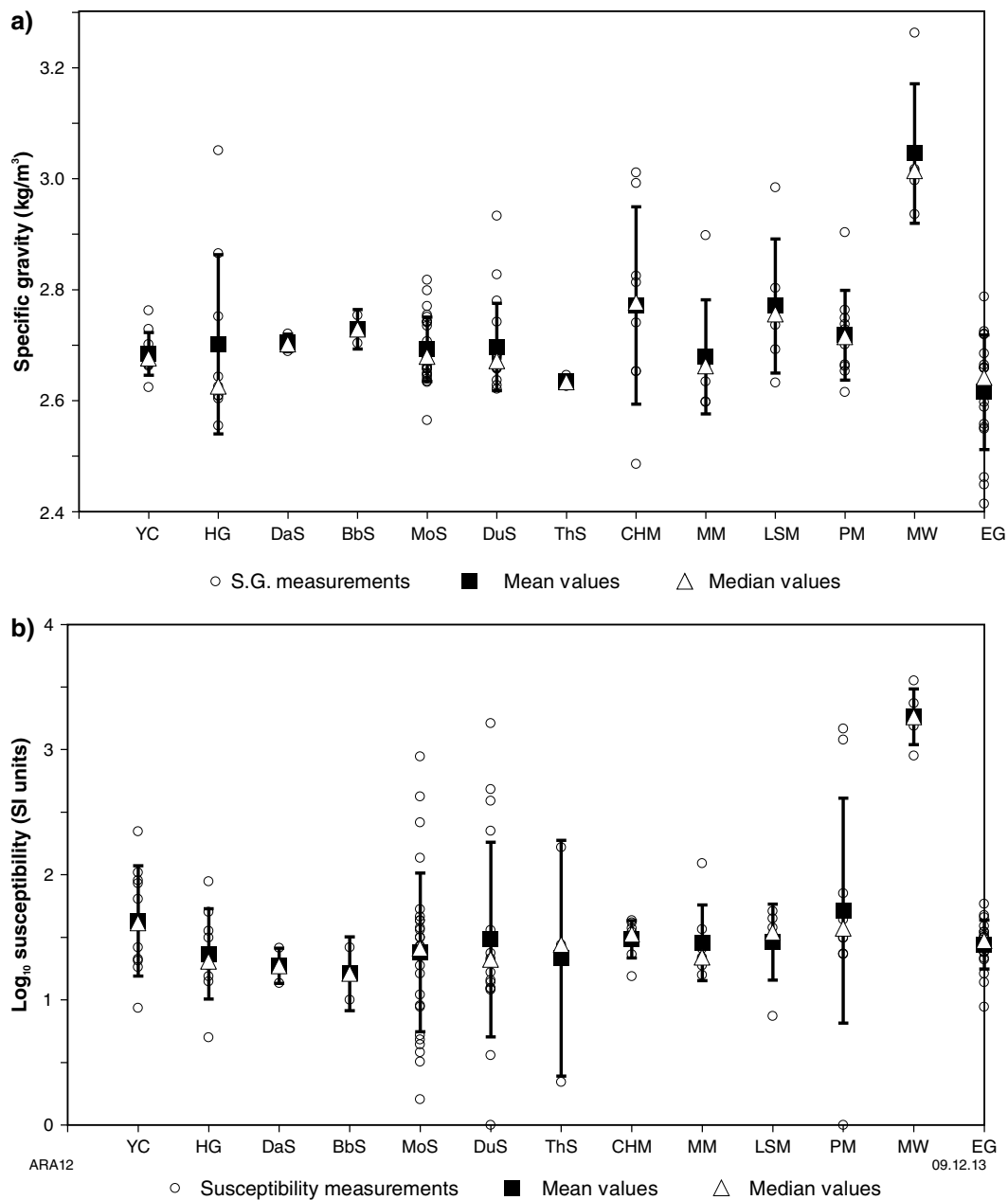


Figure 12. Petrophysical data from the western Capricorn Orogen: a) specific gravity data for the main rock types. Note the relatively tight clustering of the granitic supersuites around 2700 kg/m^3 . Metasedimentary rocks show more variability, but are not distinctive; b) susceptibility data plotted and analysed as log_{10} of the measured susceptibility. As with the gravity data, variability within units is in most cases higher than the differences between them. In contrast with density, the granitic supersuites show more variability in susceptibility than the metasedimentary packages. YC – Yilgarn Craton (granite); HG – Halfway Gneiss; DaS – Dalgaringa Supersuite; BbS – Bertibubba Supersuite; MoS – Moorarie Supersuite; DuS – Durlacher Supersuite; ThS – Thirty Three Supersuite; CHM – Camel Hills Metamorphics; MM – Moogie Metamorphics; LSM – Leake Spring Metamorphics; PM – Pooranoo Metamorphics; MW – Mundine Well Dolerite Suite; EG – Edmund Group (Narimbunna Dolerite not included)

The specific gravity data for the Moorarie Supersuite generated a mean of 2693 kg/m³, a median of 2679 kg/m³, and a standard deviation of 58 kg/m³ (Fig. 12). These are typical for granitic rocks and have low variability, given the high sample diversity. There is no obvious link between lithology and density; however, the Minnie Creek batholith contains several biotite granodiorite samples that are denser than average (~2800 kg/m³).

For magnetic susceptibility, the same samples yielded a mean of 1.38×10^{-5} SI units, a median of 1.41, and a standard deviation of 0.63 (Fig. 12). As with specific gravity, there are few discernible links between magnetic susceptibility and lithology or tectonic zones.

Durlacher Supersuite

Eighteen samples of Durlacher Supersuite rocks were collected from the Yarlarweelor Gneiss Complex, the Mutherbukin Zone, and the Mangaroon Zone. The specific gravity of these samples generated a mean of 2697 kg/m³, a median of 2671 kg/m³, and a standard deviation of 79 kg/m³ (Fig. 12). As with the other suites, these are typical for granitic rocks. Samples from the Yarlarweelor Gneiss Complex and Mutherbukin Zone, which average 2650–2670 kg/m³, are typically less dense than samples from the Mangaroon Zone, with a mean of 2710 kg/m³.

For magnetic susceptibility, these samples yielded a mean of 1.48×10^{-5} SI units, a median of 1.32, and a standard deviation of 0.78 (Fig. 12). There are no discernible correlations with either lithology or tectonic zones.

Thirty Three Supersuite

Three samples of the Thirty Three Supersuite constrained the density to between 2630 and 2650 kg/m³, and magnetic susceptibility to between 2.2 and 165×10^{-5} SI units (Fig. 12).

Camel Hills Metamorphics

The Camel Hills Metamorphics were sampled from the Errabiddy Shear Zone. Eight samples have been analysed from the Quartpot Pelite and the Petter Calc-Silicate units.

The specific gravity data gave an overall mean density of 2772 kg/m³, a median of 2777 kg/m³, and a standard deviation of 178 kg/m³ (Fig. 12). However, there is a distinct difference between the Quartpot Pelite, typically 2500–2800 kg/m³, and the Petter Calc-silicate, typically 2800–3000 kg/m³.

For magnetic susceptibility, the overall mean is 1.48×10^{-5} SI units, the median is 1.52, and the standard deviation is 0.15 (Fig. 12). Unlike specific gravity, there is no discernible difference in magnetic susceptibility between the Quartpot Pelite and Petter Calc-Silicate.

Moogie Metamorphics

Seven samples of the Moogie Metamorphics were mostly obtained from the Mooloo Zone, except for one from the Limejuice Zone. The specific gravity data indicate

a mean of 2679 kg/m³, a median of 2662 kg/m³, and a standard deviation of 103 kg/m³ (Fig. 12). Despite varying compositions, density is quite consistent with just one high-density outlier, a chloritoid schist.

Magnetic susceptibility data indicate a mean of 1.46×10^{-5} SI units, a median of 1.34, and a standard deviation of 0.30 (Fig. 12). There are no discernible correlations of magnetic susceptibility with lithologies or tectonic zones.

Leake Spring Metamorphics

Six samples of the Leake Spring Metamorphics were mostly obtained from the Mutherbukin and Limejuice Zones. The specific gravity data indicate a mean of 2771 kg/m³, a median of 2756 kg/m³, and a standard deviation of 121 kg/m³ (Fig. 12). Garnet and staurolite schists are denser than other lithologies.

Magnetic susceptibility data indicate a mean of 1.46×10^{-5} SI units, a median of 1.34, and a standard deviation of 0.30 (Fig. 12). There are no discernible trends in magnetic susceptibility between lithologies or tectonic zones.

Pooranoo Metamorphics

Ten samples of the Pooranoo Metamorphics were mostly obtained from the Mutherbukin and Mangaroon Zones. The specific gravity data indicate a mean of 2718 kg/m³, a median of 2715 kg/m³, and a standard deviation of 81 kg/m³ (Fig. 12). The quartzite-dominated Mount James subgroup are less dense (mean 2660 kg/m³) than the other samples (mean 2760 kg/m³). There is a general increase in density with metamorphic grade.

Magnetic susceptibility data indicate a mean of 1.71×10^{-5} SI units, a median of 1.57, and a standard deviation of 0.90 (Fig. 12). The Mount James subgroup and most of the other samples show generally low susceptibility (20–70 $\times 10^{-5}$ SI units), but there are two more magnetic samples (1200–1500 $\times 10^{-5}$ SI units).

Edmund Group and Narimbunna Dolerite Suite

Edmund Group samples were sourced from throughout the area, with a total of 18 specimens measured. Overall, these yielded a mean specific gravity of 2615 kg/m³, a median of 2641 kg/m³, and a standard deviation of 103 kg/m³ (Fig. 12). These specific gravities are relatively high for nonmetamorphosed sedimentary rocks, which indicates significant compaction. Within the Edmund Group, there is significant variability; however, due to low population sizes, characteristic densities cannot be inferred for individual formations or lithologies.

For magnetic susceptibility, the same 18 samples yielded a mean of 1.44×10^{-5} SI units, a median of 1.47, and a standard deviation of 0.2 (Fig. 12). All samples show low susceptibility, less than 60×10^{-5} SI units, and there is little variation. As with specific gravity, there are no discernible links between formations or lithologies.

The Narimbunna Dolerite Suite intrudes into the Edmund Group as a series of prominent sills. These sills are petrophysically distinct from the Edmund Group itself, and are visible in both the aeromagnetic and gravity data. Thus, these sills provide the basis for geophysical delineation of structures in the Edmund Basin. Specific gravity measurements ($n = 2$) indicate a density of between 3000 and 3020 kg/m³ for the sills and a magnetic susceptibility of 40–60 $\times 10^{-5}$ SI units.

Mundine Well Dolerite Suite

The Mundine Well Dolerite Suite is a series of north-northeasterly trending dykes that are very prominent in the western part of the Gascoyne Province. Specific gravity data ($n = 5$) indicate a mean density of 3050 kg/m³, of which three samples lie within the range 3000–3020 kg/m³ (Fig. 12). Magnetic susceptibility is relatively high, ranging 900–2300 $\times 10^{-5}$ SI units, although the magnetic response of these dykes is typically a linear low, indicating reverse remanent magnetization (Fig. 12).

Summary of petrophysical data

The petrophysical data provide the basis of the density and susceptibility values used in forward modelling. As is common with petrophysical data, there is significant overlap between the properties of different rock types (Fig. 12), and these properties do not provide a reliable basis for geological discrimination. The densities of the granite suites all cluster quite tightly around 2700 kg/m³ and only the Thirty Three Supersuite is distinctly less dense (2630 kg/m³). Magnetic susceptibility permits greater lithological discrimination and the Yilgarn Craton is typically more magnetic than the Gascoyne Province. Although the mean values of the granitic suites within the Gascoyne Province are all very similar, the Moorarie and Durlacher Supersuites show much greater variability than the other suites, although this may be an artefact of the much larger populations available for these suites. There is no petrophysical basis for geophysical distinction between these two major granite suites.

Metamorphic rocks are not able to be distinguished from the granitic suites on the basis of average density or magnetic susceptibility, but may be slightly more dense overall. They do have characteristically higher variability in density, and typically lower variability in magnetic susceptibility.

The sedimentary rocks of the Edmund Group show consistently low magnetic susceptibility, and relatively high density for sedimentary rocks at ~2600 kg/m³. The Edmund Group are typically less dense and less magnetic than the underlying basement rocks; however, the petrophysical contrast is slight and does not permit clear differentiation from the basement rocks. Hence, there is no major gravity low associated with the Edmund Basin.

The Narimbunna and Mundine Well Dolerite Suites are petrophysically distinct from the other rock types, and from each other. The former is characterized by dense rocks with low susceptibilities (although higher than the

Edmund Group into which they intrude), whereas the latter are similarly dense but are characterized by strong, reverse remanent magnetization (not defined) superimposed upon high magnetic susceptibility.

2D combined gravity and magnetic modelling

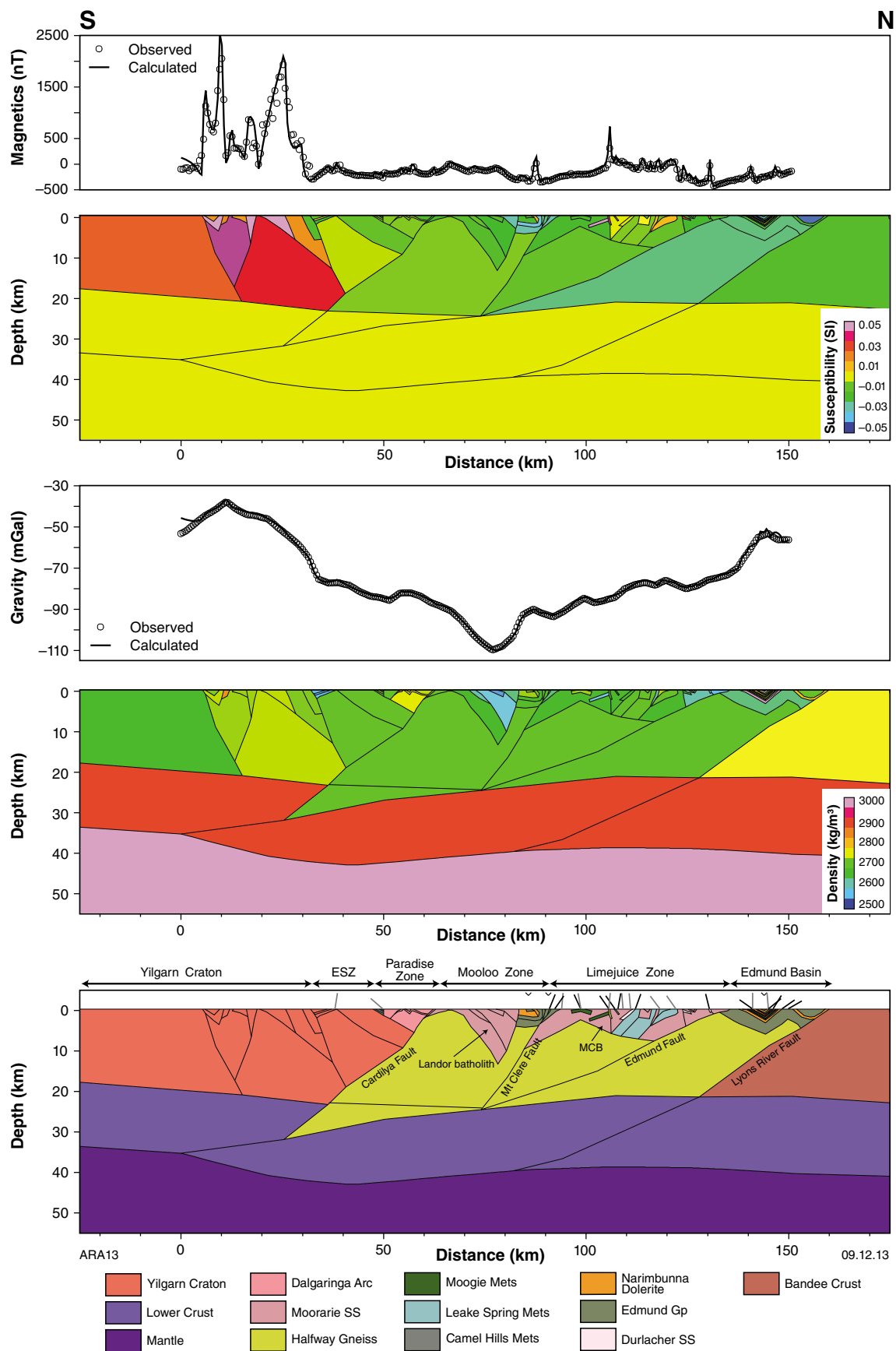
Here, we present the results of five models that cross the Gascoyne Province (Figs 2, 13–17). In combination with the seismic lines and continent-scale analyses, these provide a comprehensive view of crustal structure in the Gascoyne Province. Methods are described in detail in Appendix 1. We do not follow the routes of the recent crustal-scale seismic reflection transects GA10-CP1, GA10-CP2, and GA10-CP3 (Fig. 2), as these have already been considered in some detail (Johnson et al., 2011a, 2013). Those major geotransects revealed many key features of the Gascoyne Province, including the gross structure of the major faults, and differences in the middle to lower crust. These lower-crustal domains — the Carluhunda, Bandee and MacAdam seismic provinces — do not reach the surface, and thus remain somewhat enigmatic. Johnson et al. (2011a, 2013) provided a more comprehensive discussion of the significance of those features. We follow the geometries imaged in those seismic profiles as a starting point for our profiles; however, some reinterpretation is required to satisfy the gravity and magnetic data.

Profile 1

Profile 1 (Fig. 13) crosses the southeastern tip of the Gascoyne Province, and is aimed at extending the seismic understanding of the crustal structure of the Yilgarn Craton – Glenburgh Terrane Suture, and internal structure within the Gascoyne Province.

The Yilgarn Craton (0–30 km) is characterized by highly magnetic and relatively dense crust, with a relatively shallow Moho (~35 km). The northern margin of the Yilgarn Craton, where it has been reworked during post-collisional events, is crossed between 30 and 40 km. This region contains intrusions of the 1820–1775 Ma Moorarie Supersuite, has reduced magnetic susceptibility and density relative to the Yilgarn Craton to the south, and is underlain by thick crust (45 km).

Figure 13. (facing) Combined gravity and magnetic model along Profile 1 (see Figure 2 for location). On all profiles (Figs 13–17), the Moho is sampled from Kennett et al. (2011), and the geometry of major fault zones is initially similar to the structure imaged in the seismic reflection lines (Johnson et al., 2011a, 2013). Tick marks above the geological interpretation indicate the apparent dips from geological data used as structural control on the profile. Black ticks indicate primary structures, grey ticks indicate secondary structures, and upward and downward inflexions indicate the axes of antiforms and synforms, respectively. Well-defined features include a very magnetic and dense Yilgarn Craton; the low-density Lander batholith; the magnetically heterogeneous Minnie Creek batholith (MCB). ESZ – Errabiddy Shear Zone



The Errabiddy Shear Zone (40–50 km) is defined by a shallowly north-dipping structure with low magnetic susceptibility relative to the YGC, but similar density. The Errabiddy Shear Zone overlies the thickest crust on this profile due to structural thickening caused by the interleaving of the Yilgarn Craton with the Glenburgh Terrane. The Paradise Zone lies above this structure, and is predominantly composed of 2005–1970 Ma Dalgaringa Supersuite granitic rocks. These have a moderate magnetic susceptibility and not much internal contrast; however, some folded layering is inferred on the basis of changes in anomaly asymmetry in the magnetic field signal. For density, there is a fundamental difference between the moderate-density ($\sim 2700 \text{ kg/m}^3$) southern part of the Paradise Zone and higher density ($\sim 2750 \text{ kg/m}^3$) northern part. The boundary (at 55 km) is inferred to dip south. This is interpreted to represent the boundary of 1980–1970 Ma Nardoo Granite (in the north) within the Dalgaringa Supersuite, although there is no outcrop with which to constrain this interpretation.

The Cardilya Fault (60 km) separates the Paradise Zone from the Mooloo Zone, and in the seismic profile, this fault is imaged as a moderately south-dipping structure that merges with the Errabiddy Shear Zone at depth, and dictates the crustal geometry of the suture zone. That geometry is supported by this profile, although sensitivity to this structure at depth is low due to low petrophysical contrast. At the surface, the Mooloo Zone is dominated by outcrops of the Moorarie Supersuite, which make up a large batholith — here informally named the Landor batholith — centred around Landor Homestead. This batholith is associated with relatively low-amplitude, long-wavelength magnetic anomalies, and a deep gravity low. The asymmetries of these anomalies indicate a moderately north-dipping intrusion with a total preserved thickness of $\sim 10 \text{ km}$. Its overall architecture indicates that it may have been folded around an upright to steeply south-inclined axial surface, with open geometry. The intrusion has three bands, with a very low density central band (2575 kg/m^3) causing the deep gravity low. The very low density of this intrusion is remarkable, but it is within the confines of the petrophysical data for the Moorarie Supersuite, which has a lower 2σ limit of 2577 kg/m^3 , and a lowest measured value of 2565 kg/m^3 . The basement beneath this granitic intrusion is inferred to be the 2555–2430 Ma Halfway Gneiss, which is more magnetic and denser than the Moorarie Supersuite intrusions.

From 80 to 95 km, outcrop is dominated by 1620–1465 Ma Edmund Group sedimentary rocks, and the c. 1465 Ma Narimbunna Dolerite. These cover the inferred trace of the Mt Clere Fault. The basic geometry is a syncline; however, the geometry of the Edmund Group indicates that significant structural reworking is required on the northern limb of this syncline. Beneath these sedimentary rocks, the Mt Clere Fault separates the Limejuice Zone from the Mooloo Zone. The Mt Clere Fault is interpreted to be a continuation of the Ti Tree Shear Zone, which, in the seismic reflection profile, is interpreted to dip relatively steeply to the south before merging with the listric Edmund Fault at $\sim 20 \text{ km}$ depth (Johnson et al., 2011a, 2013). Here we adopt this steeply south-dipping geometry, although the petrophysical contrast is too low to permit a robust analysis of the geometry of this fault.

The Limejuice Zone (95–135 km) is dominated by the Moorarie Supersuite, with the Minnie Creek batholith comprising the majority of the zone. On profile 1, modelling suggests that the relatively low-density Minnie Creek batholith has a broad anticlinal form, and a thickness of approximately 5 km. In contrast to the Landor batholith, the Minnie Creek batholith contains abundant inclusions of the 1840–1810 Ma Leake Spring Metamorphics. These inclusions are typically more magnetic and denser than the Moorarie Supersuite, and show relatively chaotic structure. Most are verified by surface exposures; however, several buried examples are invoked to satisfy the geophysical data alone, principally the magnetic data. Geological mapping indicates that the Minnie Creek batholith contains many heterogeneities within the Moorarie Supersuite — tonalites, quartz diorites and some metagabbro (Sheppard et al., 2010b) — and it is likely that some of the variability can be explained by these.

The Edmund Basin (135–160 km) is juxtaposed against the Limejuice Zone by the Edmund Fault. On the seismic profile, this structure is interpreted as a shallowly south-dipping listric fault that merges with the Ti Tree Shear Zone (Mt Clere Fault) at approximately 20 km depth (Johnson et al., 2011a, 2013). Modelling on profile 1 indicates that this structure is acceptable; however, petrophysical contrast is again too low to permit a robust geometry for the Edmund Fault. The Edmund Group is preserved in the footwall of this fault where it is significantly folded (e.g. the Cobra Syncline). Here, the geometry of the Edmund Group is constrained primarily by geological observations, and it defines a syncline–anticline pair, reflecting the upright open folding that characterizes the Edmundian Orogeny. Basement beneath the Edmund Group has slightly lower magnetic susceptibility than in the Limejuice Zone, but is otherwise similar, indicating that the buried boundary with the Mangaroon Zone is at the Lyons River Fault (160 km).

According to the seismic interpretations (Johnson et al., 2011a, 2013), the Lyons River Fault dips shallowly south, and penetrates the entire crust. Furthermore, it separates two distinct zones of characteristic reflectivity (termed seismic provinces) and is interpreted to represent the suture zone between the Glenburgh Terrane and the Pilbara Craton. The basement of the Glenburgh Terrane, inferred to be dominated by the Halfway Gneiss, is juxtaposed against the Bandee Seismic Province, crust of unknown provenance that forms the basement to the Ashburton Basin (Johnson et al., 2011a, 2013). In profile 1, the Bandee Seismic Province is inferred to be significantly denser (2770 kg/m^3) and somewhat more magnetic than the Limejuice Zone, to explain long-wavelength gradients in both gravity and magnetic data. This zone of high-density crust is well imaged in a continent-scale gravity model (Aitken et al., 2013b), where it is associated with a 0.5 – 1.5% increase in vertically averaged crustal density over background values. In that model, it extends north from the Lyons River Fault to the Baring Downs Fault, and from 115.7°E to 120.7°E .

Profile 2

Profile 2 (Fig. 14) is in a similar north-south orientation to profile 1, but is located ~50 km to the west. The southern end of the profile runs close to seismic transect 10GA-CP3 and the northern end of the profile crosses seismic transect 10GA-CP2 (Fig. 2). As in profile 1, the part of the profile crossing the Narryer Terrane (0 to 30 km) is characterized by highly magnetized and relatively dense crust with a thickness close to the average for the Yilgarn Craton (~35 km).

The Errabiddy Shear Zone (30–40 km) is projected to dip more steeply north than in profile 1, and is less strongly magnetized than the Narryer Terrane, but more strongly magnetized than the Paradise Zone. In the upper crust, the southern boundary of the Errabiddy Shear Zone comprises the 1965–1945 Ma Bertibubba Supersuite, which causes a distinct gravity low and a magnetic low.

The Paradise Zone (40–70 km) is occupied primarily by low-susceptibility, moderate-density 2005–1970 Ma Dalgaringa Supersuite rocks, although some small inclusions of the 2000–1975 Ma Camel Hills Metamorphics are observed — one flat lying, the other steeply north dipping. The 1980–1970 Ma Nardoo Granite is more magnetic and denser than the rest of the Dalgaringa Supersuite. In the model, the Nardoo Granite is represented as a shallowly south-dipping slab. This slab sits directly above the Cardilya Fault, and defines the geometry of this fault to ~15 km depth.

The deep-crustal structure of the southern part of the profile is interesting because the crust is thick, and yet gravity values are relatively high, and increase gradually to the south from ~95 km (middle Mooloo Zone). This long-wavelength feature is probably not explained by a gradational density increase within the upper crust, which on this profile would require densities in excess of 2800 kg/m³; nor is it easily explained by the geometry of the Moho and a lower crust of regular density (2900 kg/m³). Instead, the observed gravity gradient requires a high-density lower crust. Using the geometry of the MacAdam Seismic Province (Johnson et al., 2011a, 2013) — identified in seismic profile GA10-CP3 as a ~15 km thick zone of weakly reflective lower crust that is distinct from the lower crust elsewhere — a density of 3290 kg/m³ provides a good fit to the data with reasonable upper crust densities. As with the Bandee Seismic Province, this large-scale, high-density province is well imaged in continent-scale gravity models (Aitken et al., 2013b), where it is associated with a 1–1.5% increase in vertically averaged crustal density over background values.

The Mooloo Zone (70–115 km) preserves a simpler structure dominated by the Landor batholith to the south, and the 2555–2430 Ma Halfway Gneiss to the north. The Landor batholith is modelled with a total thickness of ~20 km, although sensitivity to this boundary is low. The profile crosses the Deadman Fault close to its intersection with the Chalba Shear Zone. Both of these features are associated with magnetic lows, possibly indicative of hydrothermal alteration during late-stage activation of these structures. In the model, this low magnetic intensity zone has a basin-like geometry. The Mount James region

is dominated by the Halfway Gneiss, and preserves a strongly magnetized, low-density layer overlying a less strongly magnetized, but higher density ‘core’. These features are interpreted to represent a hanging wall antiform above the shallowly southeast-dipping Mount James Fault.

The profile crosses a small part of the Mutherbuckin Zone (115–140 km). This zone is characterized by the intrusion of 1680–1620 Ma Durlacher Supersuite intrusions into a ~7.5 km thick 1820–1775 Ma Moorarie Supersuite intrusion. The southernmost Durlacher Supersuite intrusion (115–120 km) is folded and is structurally overlain by the 1840–1810 Ma Leake Spring Metamorphics, indicating that the contact between the Leake Spring Metamorphics and the underlying Moorarie Supersuite may have controlled emplacement of the Durlacher Supersuite. This folded sequence is truncated against a steeply south-dipping highly magnetic feature at 120 km. Outcrop evidence suggests that this is the Moorarie Supersuite, although it could potentially be a large buried inclusion of the Leake Spring Metamorphics within the Moorarie intrusion. The north side of this magnetic feature is characterized by alternating short-wavelength magnetic fabrics interpreted to represent folding of magnetically distinct phases within the Moorarie Supersuite (125–135 km).

The northern Durlacher Supersuite intrusion is demarcated by a transition to much lower magnetic intensity, and a gravity low. This gravity low extends southwards, and this is interpreted to indicate that the contact with the lower density Durlacher Supersuite intrusion dips to the south. The Durlacher Supersuite intrusion is inferred to reach ~5 km depth. The Thirty Three Supersuite has intruded into the Durlacher Supersuite, and this very low density granite contributes further to the gravity low. Magnetic modelling suggests a roughly tabular body of granite approximately 1 km thick.

The Ti Tree Shear Zone (140 km) separates the Mutherbuckin Zone from the Limejuice Zone, and on the basis of magnetic and gravity gradients, this fault zone dips steeply to the south. At the surface, the footwall of this fault is occupied by an upright synclinal structure in which the 1760–1680 Ma Pooranoo Metamorphics, 1620–1465 Ma Edmund Group, and c. 1465 Ma Narimbunna Dolerite are folded with a wavelength of 5 km. These units are inferred to overlie a relatively magnetic and relatively dense Durlacher Supersuite pluton, which is similarly folded. In turn, this Durlacher Supersuite is modelled as intruding into the Minnie Creek batholith which must be relatively dense (2750 kg/m³) to explain short-wavelength gravity highs, and is approximately 12 km thick at its deepest point, but thins towards the north. As with profile 1, the Minnie Creek batholith contains many heterogeneities, including a large low-density region (occupied by massive biotite monzogranite), and inclusions of the Leake Spring Metamorphics that generate sharp magnetic highs.

The Minnie Creek batholith is modelled as thrust over the Edmund Group along the Edmund Fault (200 km). The footwall of the Edmund Fault contains the Cobra Syncline, which is preserved between the Edmund Fault and the

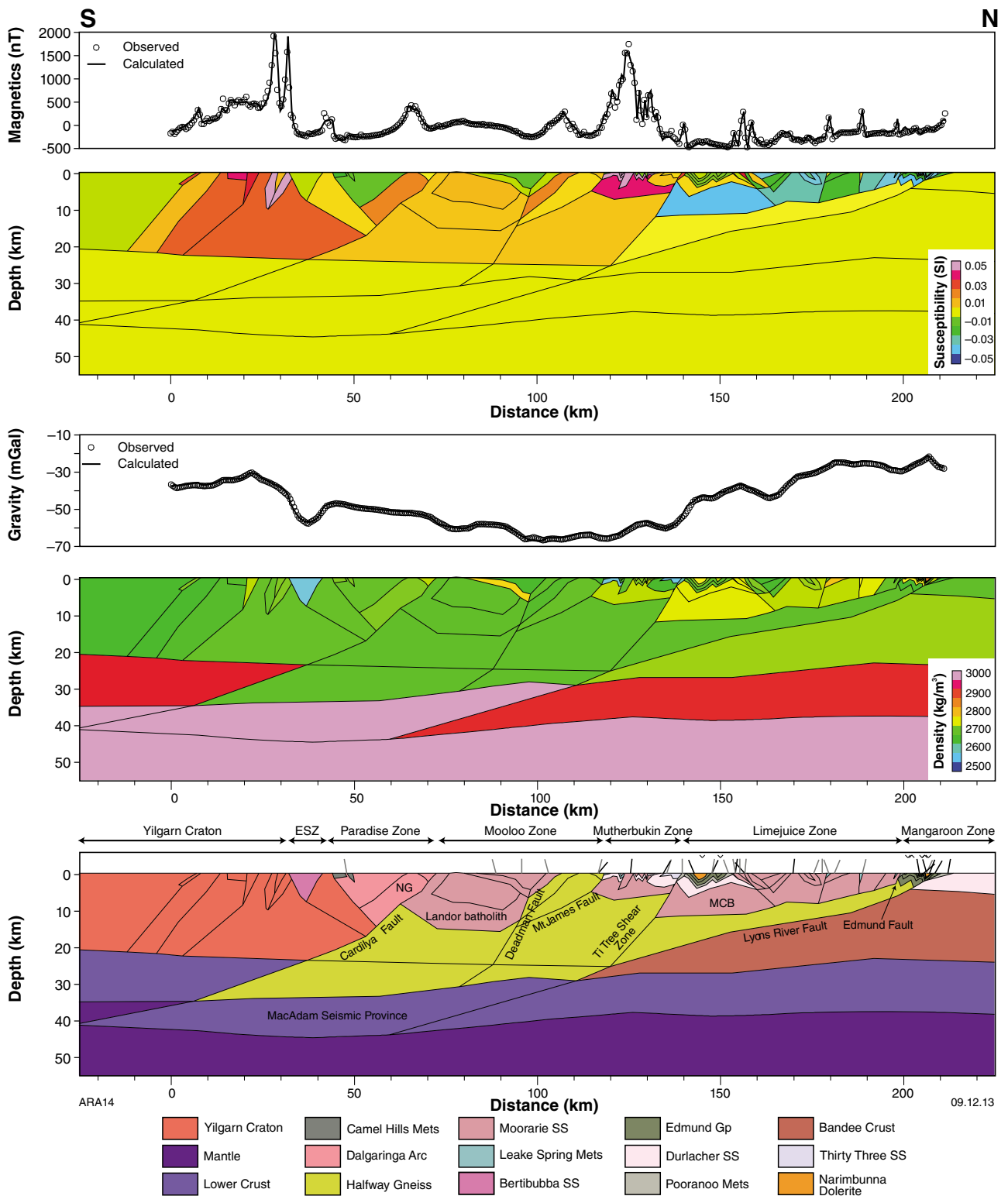


Figure 14. Combined gravity and magnetic model along Profile 2 (see Figure 2 for location). Data sources and symbology as per Figure 13. Well-defined features include: a highly magnetic and dense Yilgarn Craton; the relatively dense and magnetic Nardoo Granite (NG); the very high density MacAdam Seismic Province; very strong magnetization within the Mutherbukin Zone; a dense and magnetically heterogeneous Minnie Creek batholith (MCB); denser basement in the Banded Seismic Province

Lyons River Fault. In detail, the Cobra Syncline comprises a series of synclines and anticlines with a wavelength of 2–3 km. The wavelength of folding reduces (and the amplitude increases) towards the Lyons River Fault.

North of the Lyons River Fault, rocks at the surface are dominated by Durlacher Supersuite intrusions in the Mangaroon Zone. However, the crust in the footwall of the Lyons River Fault is inferred to be denser than the crust in the hanging wall, consistent with the results of profile 1. This contrast contributes significantly to the long-wavelength gravity gradient at the north end of the profile. However, the morphology of the Moho and the top of the lower crust also contribute significantly. This likely represents an extension of the dense Bandee Seismic Province.

Profile 3

Profile 3 (Fig. 15) runs approximately parallel to seismic profile 10GA-CP2 (Johnson et al., 2011a, 2013), and extends from the Carnarvon Basin in the southwest, over the Weedarra Inlier, across the Gascoyne Province, and into the Edmund Basin (Figs 1 and 2).

The base of a reflective sequence at the southern end of 10GA-CP2, interpreted as Carnarvon Basin (Fig. 2), occurs at 0.9 s (TWT) (Johnson et al., 2011a, 2013). Assuming $V_p = 4.5$ km/s, the Carnarvon Basin at the margin of profile 3 is estimated to be ~2 km thick. Fitting the gravity low associated with the marginal basin requires sedimentary rocks with a density of 2550 kg/m³. The geometry of the basin shows a marginal trough with a maximum thickness of 2.7 km, and then a rise towards the surface. Gravity data resolution is insufficient to determine whether the basin dips east or west. Basement rocks of the 2005–1970 Ma Dalgaringa Supersuite are exposed in the Weedarra Inlier several kilometres from the end of the profile, so that the boundary between the Mooloo and Paradise Zones (the Cardilya Fault) lies buried beneath this basin.

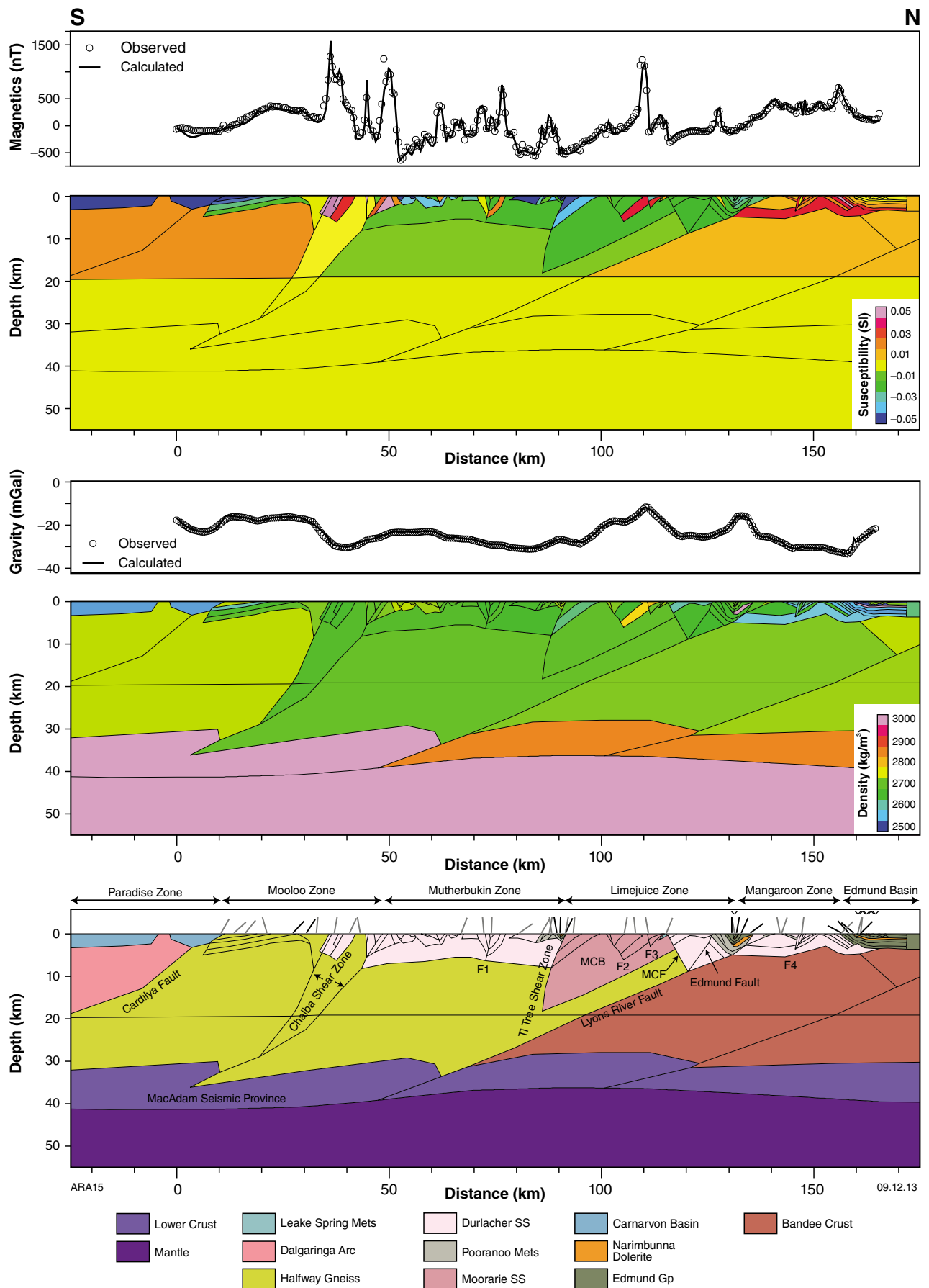
Gascoyne Province basement rocks at the eastern margin of the Carnarvon Basin consist of the 2555–2430 Ma Halfway Gneiss (Mooloo Zone), and at this location the basement is relatively dense (2740 kg/m³) and magnetic (0.02 SI units). This basement is overlain by a series of southwest-dipping layers (Halfway Gneiss) with lower susceptibility and density. The southern edge of the Chalba Shear Zone is encountered at ~30 km, and this fault zone is characterized by reduced magnetic susceptibility and density within the basement rocks (Halfway Gneiss), perhaps indicating shearing and alteration on the Chalba Shear Zone. Within the Chalba Shear Zone, 1680–1620 Ma Durlacher Supersuite granitic rocks cause strong magnetic highs and gravity lows. The example crossed by the profile shows clear asymmetry in both, indicating a southerly dip. The northern edge of the Chalba Shear Zone is encountered at ~50 km, and dips moderately southward. The Chalba Shear Zone is a fundamental boundary, juxtaposing the relatively high-density and high-susceptibility crust of the Mooloo Zone, against the lower density, low-susceptibility crust of the Mutherbukin Zone.

Outcrop within the Mutherbukin Zone is dominated by the Durlacher Supersuite. However there is significant variability within these rocks and this is expressed in the aeromagnetic data, which exhibit many high-amplitude anomalies. The southernmost rocks encountered are highly magnetized, but these give way to the north to a prominent, low-magnetization unit that persists to 60 km. Both of these units are relatively dense (2720–2750 kg/m³). Between 60 and 75 km, the rocks are lower density, but preserve significant magnetic detail. Although some short-wavelength folding is inferred, the geometry imaged for this large Durlacher Supersuite intrusion is chaotic, and likely reflects a combination of polyphase intrusion and faulting processes.

The total thickness of this intrusion is estimated at ~7 km, and it has a concave downwards geometry that is necessary to account for longer wavelength arcuate trends in the aeromagnetic and gravity data. However, the sensitivity of the model to the position of this boundary is low, and thus significantly different geometries could be obtained with small changes in rock properties. Nevertheless, the structure imaged is consistent with the structure imaged in seismic line 10GA-CP2, which shows a concave downwards Durlacher Supersuite intrusion to 2 s TWT, although the degree of concavity is less in profile 3 than in the seismic line. The host rock for this intrusion is inferred to be the Halfway Gneiss.

The profile crosses a relatively large fault zone (F1 in Fig. 15) at around 75 km, which is demarcated in the potential field data by asymmetric magnetic anomalies that indicate features with opposing dips, and a reduction in the gravity field. Our joint aeromagnetic–gravity model indicates that this fault dips steeply south, at least in the uppermost crust, and is associated with a reduction in density from south to north of 30 kg/m³. Within this low-density, low-susceptibility block, there are several short-wavelength magnetic highs. These are correlated with the 1760–1680 Ma Pooranoo Metamorphics, 1620–1465 Ma the Edmund Group, and the c. 1465 Ma Narimbunna Dolerite, which together contribute to an increase in gravity towards the Ti Tree Shear Zone. In both outcrop and the potential field models, fold structures increase in tightness towards the Ti Tree Shear Zone.

The Ti Tree Shear Zone (90 km) is the boundary between the Mutherbukin Zone and the Limejuice Zone, which is principally occupied by the Minnie Creek batholith (Moorarie Supersuite). Again, following the interpretation of the seismic line, we infer a steeply south-dipping structure, although the petrophysical contrast is low at depth, and the geometry of this fault zone is poorly constrained by the potential field data. In this interval, the Minnie Creek batholith is relatively homogenous, but layering within the intrusion dips consistently south at a shallow to moderate angle. The preserved true thickness is estimated to be at least 12 km, possibly more, although due to the dip, the deepest point is at ~18 km depth. This layering is disrupted by a few small faults at 102 km (F2 in Fig. 15) and 110 km (F3 in Fig. 15), and a larger fault (the Minnie Creek Fault) at 115 km.



The Edmund Fault is crossed at 125 km, and as with the other profiles, it is associated with thrusting of basement rocks over the Pooranoo Metamorphics and the Edmund Group. On this profile, these units define a 10 km wide syncline, the geometry of which is well constrained by the geology. The aeromagnetic data, however, show only a slight reduction in field intensity, whereas the gravity data show a strong gravity high that cannot be explained by the exposed geology. We infer a sill of Narimbunna Dolerite emplaced deep within the Edmund Group to explain this anomaly. Interestingly, the gravity data suggest that this sill only exists on the northern limb of the syncline. These units extend to the Lyons River Fault.

As in profiles 1 and 2, the shallowly south-dipping Lyons River Fault separates the relatively low-density Glenburgh Terrane from the relatively high-density Bandee Seismic Province. The Mangaroon Zone to the north is characterized by a low-density, high-susceptibility basement of Durlacher Supersuite. There is significant structure within the Durlacher Supersuite, including at least one fault zone (F4 at 145 km) and a broad antiform, with an axial plane inclined to the north that intersects the surface at ~150 km. Beyond 155 km, the Durlacher Supersuite is overlain by lower magnetic susceptibility Edmund Group sedimentary rocks, including some sills of Narimbunna Dolerite. These sills contribute significantly to a gravity gradient that increases to the north; however, there is a requirement also for denser basement in this region, and for a relatively dense unit (2680 kg/m^3) within the Kiangi Creek Formation.

Due to its proximity to the seismic line 10GA-CP2, the deep crust of this profile is especially well constrained. The Moho geometry shows thick crust in the south and the north, with thinner crust in the central portion. The lower crust south of the Lyons River Fault (i.e. the MacAdam Seismic Province) must be especially dense because, despite thick crust, gravity values are relatively high. The density of this lower crust has been modelled at 3000 kg/m^3 , somewhat less than on profile 2. The Chalba Shear Zone does not penetrate the Moho on the profile, although it may do so farther south, but is inferred to cause an offset at the top of the MacAdam Seismic Province. This is required to explain long-wavelength gradients in the gravity data. North of the Lyons River Fault, the lower crust is less dense (2850 kg/m^3), and is inferred to follow the northward sloping Moho geometry, which explains the northwards reduction in gravity.

Figure 15. (facing) Combined gravity and magnetic model along Profile 3 (see Figure 2 for location). Data sources and symbology as in Figure 13. Well-defined features include: magnetic basement beneath the Carnarvon Basin; southwest-dipping structure within the Mooloo Zone; the broad Chalba Shear Zone; the very high density MacAdam Seismic Province; magnetically heterogeneous Durlacher and Moorarie batholiths; denser basement in the Bandee Seismic Province. MCB – Minnie Creek batholith ; MCF – Minnie Creek Fault

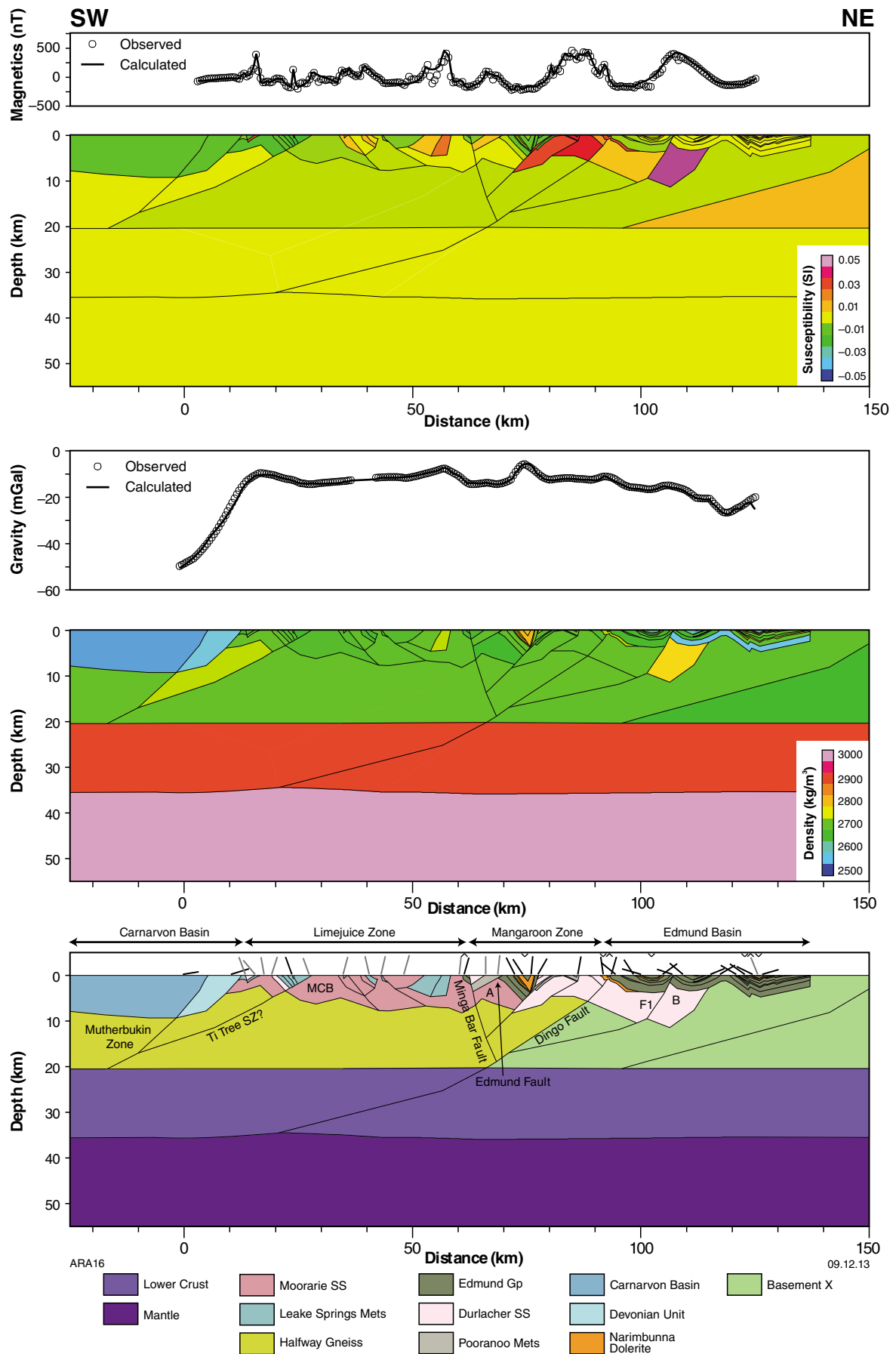
Profile 4

Profile 4 is oriented north-northwest (Figs 2 and 16) and is aimed at understanding the crustal structure of the Limejuice and Mangaroon Zones. The first feature of interest is the Carnarvon Basin, which is much deeper than in profile 3 (up to 10 km thick, assuming a density of 2550 kg/m^3). The gravity signal is the lowest associated with this basin, and hence this is probably the deepest part. To the east (50–60 km), a Devonian sandstone unit outcrops within a fault-bounded block. Assuming similar density to other sedimentary rocks of the Carnarvon Basin, this unit is required by the gravity data to extend to a similar depth as the Carnarvon Basin. Geological data indicate that bedding (short black lines) within these basins dips shallowly to the southwest. A steep-sided deepening of this basin to the southwest is required by the gravity data, perhaps indicating down-to-the-west normal faulting in this area.

The first exposed basement rocks are north of the main branch of the Ti Tree Shear Zone (12 km), and thus belong to the Limejuice Zone. However, they are within a 15 km wide zone of multiple splays. Outcrop is dominated by the 1840–1810 Ma Leake Spring Metamorphics, 1680–1620 Ma Durlacher Supersuite, and 1820–1775 Ma Moorarie Supersuite. Modelling suggests that the structure of this area is defined by an open inclined anticline involving all exposed units. Basement (inferred to be the 2555–2430 Ma Halfway Gneiss) is denser and more magnetic than elsewhere on the profile. The Leake Spring Metamorphics appear to structurally overlie the Moorarie Supersuite, and the Durlacher Supersuite appears to have exploited the contact between these units.

The northern edge of the Ti Tree Shear Zone at ~25 km juxtaposes these rocks against the exposed Minnie Creek batholith. The Minnie Creek batholith extends to ~65 km, and thickens northwards, from approximately 4 km to approximately 7 km thickness. Long-wavelength trends in the potential field data indicate that the base of the intrusion preserves a broadly folded geometry. However, sensitivity to the geometry of this surface is quite low due to the weak petrophysical contrast.

Within the Minnie Creek batholith, there is significant heterogeneity, including several quite large inclusions of the Leake Spring Metamorphics, which are characteristically more magnetic than the Moorarie Supersuite. It is possible that the Minnie Creek batholith extends beyond the Minga Bar Fault. Although there is virtually no exposure of Moorarie Supersuite north of the Minga Bar Fault in this area, a completely buried unit (A on Fig. 16 at 65–75 km) would have susceptibility similar to the adjacent Moorarie Supersuite. Basement to the 1760–1680 Ma Pooranoo Metamorphics was most likely Moorarie Supersuite, and this is the preferred interpretation for this block. An alternative explanation is that the Pooranoo Metamorphics may have been engulfed by the Durlacher Supersuite, which exploited pre-existing layering within the sedimentary rocks.



The Minga Bar Fault (65 km) demarcates the transition to the Mangaroon Zone, which is dominated in outcrop by the Durlacher Supersuite. The Minga Bar Fault Zone itself contains a narrow band of 1620–1465 Ma Edmund Group, which is interpreted to comprise a steeply north-inclined synclinal structure, despite a single strike and dip measurement that indicates south-dipping bedding. The Minga Bar Fault dips steeply, and magnetic and gravity gradients indicate that it probably dips to the north here. Multiscale edges to the southeast of this profile, indicate a steep northerly dip in the northwest changing to a steep southerly dip in the southeast (Goodwin, 2011).

Within the Mangaroon Zone, the Durlacher Supersuite defines a batholith with similar breadth and thickness to the Minnie Creek batholith. The Durlacher Supersuite is typically more magnetic and slightly less dense than the Moorarie Supersuite. The exception is a completely buried example at the northern end of the profile (B on Fig. 16 at 100–110 km), where anomalously dense (2785 kg/m³) and exceptionally strongly magnetized ($\kappa = 0.05$ SI units) material is required.

The Edmund Group overlies these units in several deep synclines. Definition of the geometry of the Edmund Basin is largely driven by surface geology, although the petrophysically distinct c. 1465 Ma Narimbunna Dolerite and minor petrophysical variations within the Edmund Group provide some control on the geometry of these features at depth. The Dingo Fault, an extension of the Lyons River Fault, demarcates the southern boundary of the Edmund Basin proper, and also passes laterally into a set of en echelon faults (Fig. 1), including a related south-dipping normal fault (F1 on Fig. 16 at 105 km) that offsets the basin strata by approximately 3 km.

The deep crust of this profile is less well constrained than for profiles to the east. However, the Moho is evidently very flat in this area, with just a slight ~2 km rise at the southern end (20 km). The regional gravity anomaly is also quite flat indicating that there is no requirement for significant density variation in the deep crust. In particular, there is no requirement that the crust north of the Dingo Fault is denser than that to the south. The nature of this basement is unknown but we infer that it is not the Bandee Seismic Province, as it lacks the defining characteristic of high density. Alternatively, the less dense nature of the modelled basement may reflect uncertainties in the gravity modelling because the location of profile 4 farther from the deep seismic transect means the Moho geometry is less well constrained, and therefore less well known.

Figure 16. (facing) Combined gravity and magnetic model along Profile 4 (see Figure 2 for location). Data sources and symbology as in Figure 13. Well-defined features include: ~10 km thick Carnarvon Basin; an overall flat Moho; a north-tilted, gently folded Minnie Creek batholith; a very magnetic Durlacher Supersuite batholith in the Mangaroon Zone, extending under the Edmund Basin; an unknown basement to the Carnarvon Basin, inferred to be the Mutherbukin Zone. MCB – Minnie Creek batholith, SZ – Shear Zone

Profile 5

Profile 5 (Fig. 17) traverses the Boora Boora Zone (Fig. 2), across an area of reasonable outcrop but only first edition 1:250 000 scale maps are available for geological constraint. Furthermore, gravity data here are spaced at ~10 km. The structure of this profile is relatively uncomplicated. Outcropping rocks belong to the 1820–1775 Ma Moorarie Supersuite, but there is little indication of the rocks into which these intruded. We assume that basement to the south of the Collins Fault, which is linked to the Dingo Fault, is 2555–2430 Ma Halfway Gneiss. As with profile 4, basement to the north of the Collins Fault is unknown, as there is no requirement for high-density Bandee Seismic Province. Within the Moorarie Supersuite there are many inclusions of 1840–1810 Ma Leake Spring Metamorphics (formerly mapped as Morrissey Metamorphics); however, these rocks are also part of the supracrustal succession that overlies the basement rocks. The Leake Spring Metamorphics are characteristically highly magnetized, and are also relatively dense compared with the basement rocks. The upper Wyloo Group, which is similar in age to the Leake Spring Metamorphics, is also present, principally to the north of the Talga Fault, indicating a transition from one basin to another. It is not clear from the imaged structure how these basins relate to each other.

Granitic intrusions of the 1680–1620 Ma Durlacher Supersuite are rare, and restricted to a few small exposures in the south of the profile. Similarly, the 1760–1680 Ma Pooranoo Metamorphics are rarely exposed, although outcrops do exist within the core of the Uaroo anticline (30 km), indicating a thin layer of Pooranoo Metamorphics between the 1620–1465 Ma Edmund Group and the Leake Spring Metamorphics.

The supracrustal succession, including the Edmund Group, defines two major fold structures. The Uaroo structure (15–60 km) is located above the inferred trace of the Collins Fault, and a syncline to the north of the Talga Fault (90–110 km). The former is a broad, open, roughly symmetric fold with an anticlinal axis at ~30 km, and a synclinal axis at ~40 km. The depth to Moorarie Supersuite basement at the synclinal axis is modelled as 11 km. To the north of the Talga Fault, the upper Wyloo Group and the Edmund Group define an asymmetric, south-inclined syncline, with a maximum thickness of ~6 km.

As with profile 4, lower-crustal structure is fairly flat, and little in the way of lower-crustal density variation is required. The sole feature is a slightly thickened upper crust to the north of the Talga Fault, which partially accounts for the gravity low at ~85 km, and the gradual increase in gravity to the north. These anomalies could be fitted adequately with relatively minor variations (± 20 kg/m³) in the densities of the upper-crustal blocks, in which case the crust immediately to the north of the Talga Fault would be less dense than that to the south.

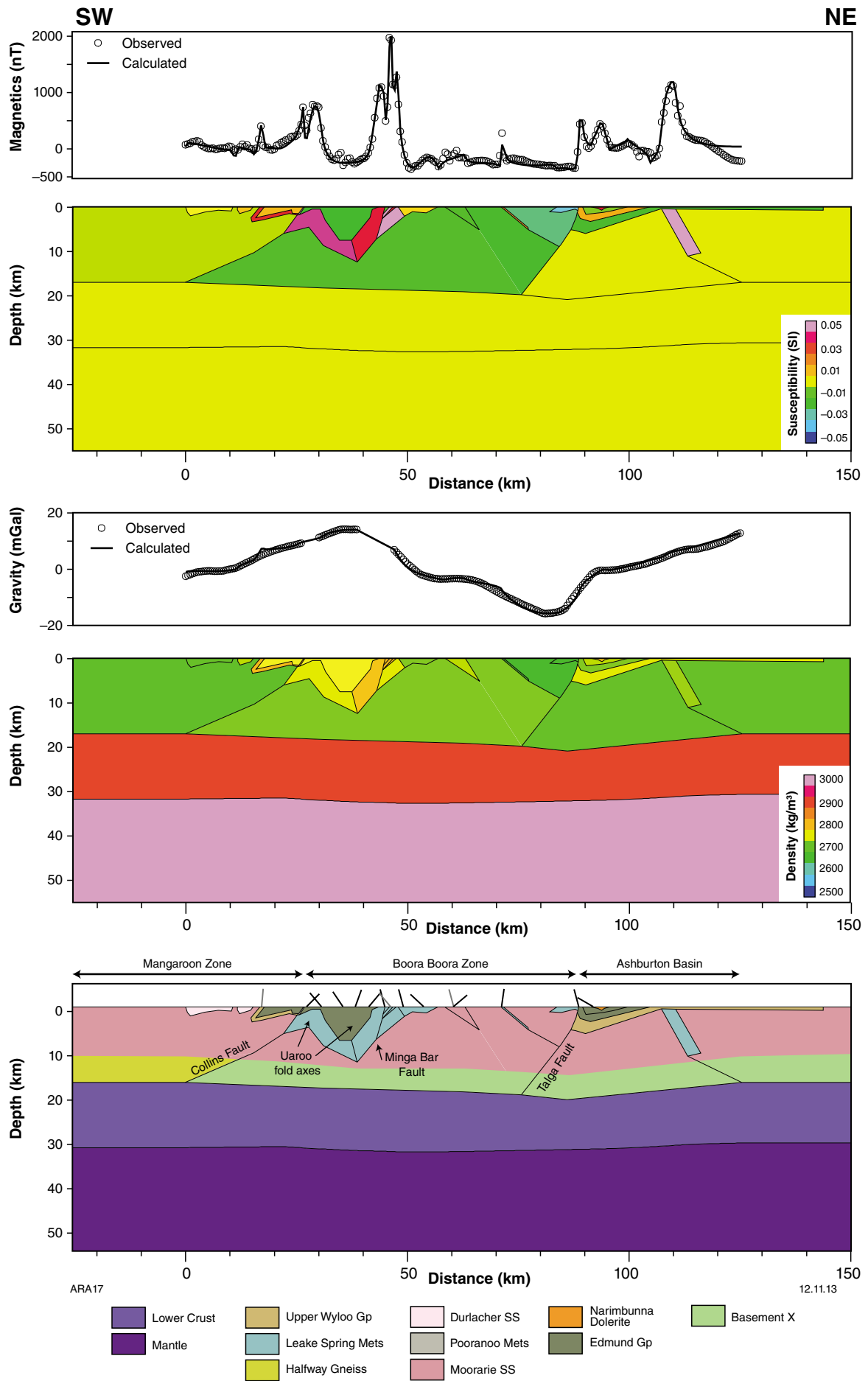


Figure 17. (facing) Combined gravity and magnetic model along Profile 5 (see Figure 2 for location). Data sources and symbology as in Figure 13. Well-defined features include: the Uaroo large-scale fold; a southwest-dipping Ashburton Basin bounded by the Talga Fault; an overall flat Moho; several very magnetic bodies inferred to be Leake Spring Metamorphics

Summary of forward modelling results

The series of profiles across the Gascoyne Province highlight the different character and structure of each major tectonic zone, and also highlight the geometries of major features and the lower-crustal structure of the Gascoyne Province. The predominantly south-dipping, thrust-dominated architecture imaged in the seismic lines is compatible with the gravity and magnetic fields, although the petrophysical contrast between many of the blocks is quite low, and sensitivity is limited. Basement to most of the province is inferred to be the Halfway Gneiss, which shows relatively high variability in its properties. North of the Lyons River Fault, the seismic survey identified that the crust had differing reflective character; this was designated the Bandee Seismic Province (Johnson et al., 2011a, 2013). Here, we show that, for profiles 1 through 3 this zone is also somewhat denser than the basement rocks above the Lyons River Fault. The lower-crustal structure, with the Moho derived from a recent seismic compilation, shows many interesting features, including very dense lower crust in the MacAdam Seismic Province, and significant displacements of the Moho and the top of the lower crust associated with the major fault zones.

The major granitic suites of the province (the Moorarie and Durlacher Supersuites) are shown to consist largely of large batholiths that are ~5 to 10 km thick and have tabular geometries. In each, but especially within the Minnie Creek batholith, quite chaotic magnetic and gravity signals indicate the influence of rafts of metasedimentary material within the granitic rocks, and also the influence of heterogeneities within them. The other granitic suites are relatively rare, although the Dalgaringa Supersuite is preserved in a fault-bounded wedge between the Errabiddy and Cardilya Shear Zones. Within the Dalgaringa Supersuite, the Nardoo Granite is petrophysically distinct.

With the exception of the Edmund Group, which is preserved in several outliers that have a synclinal structure, as well as in the greater Edmund Basin, which is imaged at the northern end of each line, sedimentary and metasedimentary rocks are mostly preserved as either tectonic slivers or as inclusions within later granitic suites. Only in the Boora Boora Zone (profile 5, Fig. 17) are the stratigraphic relationships between the sedimentary units preserved, and we have low confidence here due to the lower resolution of mapping and sparse gravity data.

Prospectivity analysis: rationale and methodology

The mineral systems approach

Prospectivity analyses, in some cases based on empirical spatial relationships between mineral deposits and regional geological features, and in other cases based on geological concepts of ore deposit formation, have long been used for regional exploration targeting (Bonham-Carter, 1994; Carranza, 2008). Prospectivity analysis research has increasingly focused on the mineral systems approach (MSA) (Wyborn et al., 1994; Knox-Robinson and Wyborn, 1997) as a unifying conceptual framework for the development of more effective exploration targeting methods and models (McCuaig et al., 2010; Joly et al., 2012; Joly et al., 2013). This approach to understanding the formation of ore deposits recognizes that they are small expressions of much larger Earth systems that operate on a variety of scales to focus mass and energy flux. The systems approach provides a holistic view of the entire process of mineralization including geodynamic setting, architecture, metal source, fluid flow drivers and pathways, and depositional mechanisms. As a generalized, process-based framework, the approach can be easily adapted to different geological environments and deposit types (Joly et al., 2012).

By breaking down the critical processes that lead to the formation of mineral deposits into definable entities, and by assuming that the probability of occurrence of each of these processes is independent, mineral-systems models can be integrated into a probabilistic framework and a probability of success can be calculated for discovery of potentially economic mineralization in a particular area. This concept has been applied to the development of targeting decision tools (Kreuzer et al., 2008) and prospectivity analysis (Porwal and Kreuzer, 2010; Joly et al., 2012).

A major advantage of the mineral systems approach is that it allows identification and prioritization of the critical components for prospectivity analysis at a variety of scales ranging from craton scale to deposit scale (McCuaig et al., 2010). Moreover, because this approach comprises a series of components that can be theoretically considered conditionally independent, the approach can be readily integrated into a spatial statistical framework for estimating the probability of mineral deposits at any scale. For example, the overall probability of the occurrence of a deposit of the targeted type at a specific scale can be estimated from the individual probabilities of occurrence of the components that are considered critical at that scale. The probabilities for the occurrence of the mineral-systems components can be assigned subjectively based on expert knowledge, or estimated empirically from the distribution of known mineral deposits. This kind of probabilistic approach can be used to demarcate exploration targets at a variety of scales.

GIS-based automated prospectivity analysis

A mineral prospectivity model can be defined as a simplified mathematical function describing the relationship between targeting criteria (represented by predictor maps) and the targeted mineral deposits (Porwal et al., 2003). A variety of linear and nonlinear functions are used to approximate the relationship between exploration criteria and mineral deposits. Based on the type of function used, mineral prospectivity models are classified as linear (e.g. weights-of-evidence, WofE) or nonlinear (e.g. fuzzy, logistic regression, neural networks, neuro-fuzzy, Bayesian network classifiers). They have also been alternatively classified into knowledge driven and data driven, based on whether the model parameters are estimated using conceptual knowledge or empirical data, respectively. WofE is a data-driven approach that uses the theory of conditional probability to quantify the spatial association between a set of predictor maps and a set of known mineral deposits (Agterberg, 1989; Agterberg and Bonham-Carter, 1990; Bonham-Carter and Agterberg, 1990).

Definition of fuzzy logic (knowledge-based GIS-driven prospectivity model)

In this work, we used a fuzzy-logic knowledge-driven approach (Bonham-Carter, 1994), because it provides a convenient way to interpret and transfer expert knowledge into a quantitative spatial analysis using a GIS platform. This kind of analysis establishes the relationship between the spatial exploration datasets and the exploration model and is often employed in regions with few or no known mineral occurrences with which to ‘train’ the exploration datasets. Knowledge-driven techniques are subjective in that the ‘explorer’ determines the relative significance of the exploration datasets and assigns a significance weighting based on the exploration model. However, this subjectivity also lends the technique great flexibility, especially given commonly limited or poorly distributed data.

Knowledge-based prospectivity mapping is achieved by extracting the spatial relationships from geoscientific datasets on the basis of an exploration model, quantifying these spatial relationships and integrating them using mathematical operators chosen by the user. Fuzzy logic is a form of many-valued logic that deals with reasoning that is approximate rather than fixed and exact. Fuzzy-logic variables may have a truth value that ranges arbitrarily in degree between 0 and 1, contrasting with traditional logic theory, where binary sets are either true or false.

The fuzzy-logic overlay method has been used widely in mineral potential assessments. For instance, An et al. (1991) used fuzzy logic to combine geophysical and geological maps for prospectivity analysis of base metal and iron deposits using expert knowledge to define the relative importance of a proxy (fuzzy-membership value or map weight). Bonham-Carter (1994) described examples of using fuzzy-logic overlay for assessing gold potential and landfill suitability. D’Ercole et al. (2000) used a fuzzy-logic approach to make a prospectivity analysis

of Mississippi Valley-type deposits using geochemical, stratigraphic, geophysical, and structural criteria. Knox-Robinson (2000) applied vector algebra in fuzzy modelling, where favourability was expressed as a vector whose direction is defined by ‘fuzzy-membership value’, and magnitude is defined by ‘fuzzified confidence value’, which represents a measure of the modeller’s confidence in a prospectivity value (e.g. accuracy with which it has been mapped). Carranza and Hale (2000) applied fuzzy logic to map gold potential using derivatives of geological maps as inputs. Porwal et al. (2003) incorporated a data-driven approach in fuzzy modelling. A data-driven model uses a piece-wise linear function based on quantified spatial associations between predictor patterns and known mineral deposits for deriving fuzzy-membership values of input predictor maps. In other words, this data-driven approach simulates human reasoning for deriving fuzzy-membership values.

Fuzzy modelling is implemented here in the following steps: 1) generating predictor maps based on geoscience datasets; 2) assigning map weights, class-weights, and confidence factors; 3) estimating fuzzy values for each predictor map; 4) combining the fuzzy predictor maps using an appropriate fuzzy inference network to derive the fuzzy prospectivity map (Joly et al., 2012). A detailed breakdown of the method is given in Appendix 2.

Application to the Gascoyne Province

Knowledge-driven mineral prospectivity mapping is appropriate in frontier or less explored (so-called ‘greenfields’) areas where no, or very few, mineral deposits of the type sought are known. The Gascoyne Province is a greenfields exploration area with only a few known prospects and deposits. Knowledge-driven fuzzy models are therefore the most appropriate for a prospectivity analysis in the area.

In addition to the new interpretations of geophysical data described above, all information relevant to prospectivity analysis of the Gascoyne Province has been extracted from public-domain sources. The extents of mapped geological entities were taken from the Geological Survey of Western Australia (GSWA) interpreted bedrock geological map (GSWA, 2012). All chemical data used in this study are whole rock data extracted from the GSWA state geochemistry database (GSWA, 2011), and Geoscience Australia’s OZCHEM database (Champion et al., 2007). These data were analysed in their logarithm form. Subsequently, threshold values Z_{log} (which corresponds to: $(\log [X] - \text{mean}(\log [X]))/2\sigma(\log [X])$, with $[X]$ = the element content; (Singer and Kousta, 1999)) were used to generate related predictor maps (see Cheng, 2007 for details). Element ratios and contents were interpolated using the inverse distance weight (IDW) algorithm, a spatial autocorrelation technique that defines objects that are close to the point of interest as more influential than those that are more distant. This is especially suitable if the geochemistry sampling collection is unevenly distributed, as is the case in the Gascoyne Province.

ArcGIS software was used to carry out the prospectivity analysis using a 100 m unit cell size according to the overall accuracy of available geophysical, geological, and geochemical data.

Mineral deposits and occurrences in the Gascoyne Province

The Gascoyne Province hosts a variety of mineralization styles including carbonatite-related REEs (e.g. Gifford Creek Ferrocarbonatite Suite, GCFS), rare earth metal pegmatites (e.g. Yinnetharra), base metal deposits (e.g. Mount James, Glenburgh, Star of Mangaroon, Minnie Springs, Mundong Well, Hectors Bore), and tungsten-bearing skarns (e.g. Nardoo Well). The presence of these deposits confirms that ore-forming processes were viable within the province.

Exploration by Newmont and Newcrest since 1974 documents REE mineralization in the area of the Gifford Creek Ferrocarbonatite Suite. The REE mineralization at the Yangibana prospect is hosted in ironstone veins and dykes which are associated with sideritic carbonate-bearing carbonatite dykes and widespread fenitic alteration (Sheppard et al., 2010b; Pirajno and González-Álvarez, 2013). The ironstones outcrop over an area of 500 km² and contain up to 20% Nd₂O₃ and 1600 ppm Eu₂O₃. The prospect has an estimated total resource of about 2.77 Mt, averaging 1.52% REE oxides.

REE pegmatites were discovered in 1945 near Yinnetharra Homestead, where up to 300 t of beryl and 5 t of tantalite–columbite were produced (Witt, 1990). Although the Yinnetharra pegmatites are zoned and renowned for their giant (metre-size) crystals (Hardy, 1992; Trautman, 1992; Sweetapple, 2000), the vast majority of the Yinnetharra pegmatites are barren, containing combinations of only muscovite, biotite, and tourmaline. Locally, however, some pegmatites (e.g. Morrissey Hills, Fig.1) contain rare-element-bearing minerals that were the subject of sporadic, small-scale mining, e.g. mica, beryl, and tantalite–columbite (Carter, 1984; Fetherston, 2004). In the past, there have been several periods of tantalite mining at Arthur River, most recently in 1979–80 during a period of high tantalite prices. At that time, high-grade pods of eluvial tantalite were mined and yielded about 3 t of tantalite concentrates assaying 48.0% Ta₂O₅ and 10% Nb₂O₅ (Equis, 1999).

The Gascoyne Province is considered underexplored as a gold and base metal province due to continued success of gold exploration in the Yilgarn Craton, as well as exploration in the surrounding basins of the Ashburton and Peak Hill districts. At Glenburgh, base metal and gold mineralization, discovered by Helix Resources NL in the 1990s, has a current estimated total resource of 25–30 Mt at 1.3 – 1.6 g/t gold for 1.04 Moz of contained gold (Gascoyne Resources Limited, 2012). Base metal and gold mineralization is hosted within migmatized pelitic gneisses contained within gneissic granitoids of the Dalgaringa Supersuite (Johnson et al., 2011b). At Mount James deposit (Fig. 1), RAB drilling by Gascoyne Resources Limited (2012) identified a broad zone of low-grade gold mineralization, within which individual intercepts such as 14 m at 1.57 g/t Au and 4 m at 8 g/t Au

were returned over a strike extent of 3.6 km that remains open to the west and at depth. Channel sampling of a costean in the area returned 18 m at 2.49 g/t Au. The gold mineralization is situated within the Mt James Fault, a major shear zone that separates altered mafic schist from felsic schists (Gascoyne Resources Limited, 2012).

At Mundong Well (Fig.1), uraniferous and base metal quartz vein mineralization are associated with Cu–Pb sulfides in gneissic rocks of the Moorarie Supersuite. In the Minnie Creek batholith, leucocratic monzogranite hosts copper–tungsten mineralization, interpreted as both porphyry style (Sullivan, 1996) and intrusion-related style (Pirajno et al., 2008). Surface samples at the Mundong Well prospect returned assays of up to 3.6% U, 5.4% Cu, 5.8% Pb, 54 g/t Ag, and 1.8 g/t Au (Ferguson, 1999).

The Star of Mangaroon mine has a history of minor base metal and associated gold production dating back to 1956 (Blockley, 1971; Martin et al., 2005). The Star of Mangaroon mine is not operating at present. Mining from 1956 to 1960 produced 11.61 t of concentrate containing 8.43 t Pb, 0.1418 t Cu, 2923.6 g Ag, and 1524 g Au (Blockley, 1971). Lead mineralization is hosted by strongly sheared metasedimentary rocks of the 1760–1680 Ma Pooranoo Metamorphics, and in weakly sheared biotite-bearing granite of the 1680–1620 Ma Durlacher Supersuite (Martin et al., 2005).

At Hectors Bore, tungsten-rich mineralization is hosted by a marble unit of the Moogie Metamorphics (Hassan, 2006). To date, no drilling has been carried out at Hectors Bore.

At Nardoo Well (Fig.1), Mincor Resources NL (2006) targeted outcropping, high-grade tungsten mineralization associated with the contact between leucocratic granites and pegmatites of the 995–940 Ma Thirty Three Supersuite, and pelitic schists of the Pooranoo Metamorphics. The tungsten is hosted in scheelite, mainly as vesuvianite skarns. Assay results from Mincor Resources NL (2006) include values up to 6.66% WO₃ over 3 metres. Granites of the Moorarie Supersuite in the northern part of the province are associated with tungsten-skarn mineralization (Sullivan, 1996).

Selection of commodity types for prospectivity analysis

The Gascoyne Province has an extended history of magmatism, and structural reworking and reactivation (Tyler and Thorne, 1990; Sheppard et al., 2010). This needs to be taken into account during mineral exploration (Table 1). Associating known mineralization with particular tectonic events and mapping structures active during each event is an important indicator of prospectivity since active structures are more likely to be conduits for mineralizing fluids. Timing of magmatism is also important. Granitic rocks are a source of metal-bearing fluid, and identifying intrusions with similar ages as those known to host mineralization is an important indicator of prospectivity. To a lesser extent, the nature of sedimentary units can also be used to advantage. An example is the presence of chemical and physical property contrasts associated with different lithotypes.

The primary basis for the selection of commodities for the prospectivity analysis was the known endowment (i.e. known mineral deposits and occurrences) of the Gascoyne Province. The known mineral systems in the Gascoyne Province (Sheppard et al., 2010b) are REE, intrusion- and shear-zone related base metal, gold, tungsten, and surficial uranium. The tectonic context of the different events affecting the Gascoyne Province is now reasonably well understood. This permits the addition of various deposit types for analysis based on perceived prospectivity within interpreted geological and tectonic settings.

Based on the above, the following deposit styles were analysed:

- igneous and metamorphic-related REE systems
- orogenic and intrusion-related gold systems
- surficial uranium systems
- porphyry base metal systems
- tin–tungsten systems.

Igneous and metamorphic-related REE mineral systems (carbonatite, pegmatite, veins)

The term ‘rare earth elements’ describes a set of 17 chemical elements, specifically the 15 lanthanides plus scandium and yttrium. Rare earth metals are often concentrated in peralkaline and peraluminous volcanics, granites, granitic pegmatites and veins, as well as in alkaline-ultramafic and carbonatite complexes (Long et al., 2010).

Examples of REE-bearing pegmatites are known in many parts of the world (e.g. Aldan in Russia, Five Miles in Ontario, Ytterby in Sweden) and most commonly occur in, or near, granitic or syenitic bodies (igneous) or in high-grade metamorphic zones (metamorphic) near their contacts with granitic stocks or batholiths. One of the most significant REE pegmatites is the Greenbushes deposit of the Yilgarn Craton (Partington et al., 1995), which occurs within a large pegmatite body of the lithium–cesium–tantalum family hosted within Archean metasedimentary rocks.

REE-bearing veins are widely distributed throughout the world but are relatively rare. They are localized in shear zones, faults, fractures, breccia zones, and diatremes in metasedimentary and metavolcanic rocks, and are commonly, but not invariably, associated with alkalic rock complexes including carbonatites (Sweetapple and Collins, 2002).

Because of their relatively small size, carbonatites are frequently difficult to locate in the field and investigations rely on strong magnetic and radiometric targets or previous reports of their occurrence (Kogarko et al., 1995; Woolley, 1987, 2001). The largest carbonatite-related REE deposit is the Bayan Obo deposit in Inner Mongolia, China, and this represents 70% of the world’s

REE resources. Although the origin of the deposit is still under debate, more than 30 carbonatite dykes occur within 3.5 km of the deposit’s East ore body (Zhongxin et al., 1992).

The Gascoyne Province contains all the ingredients required to form igneous and metamorphic-related REE mineral systems. The presence of the Gifford Creek Ferrocarbonatite Suite prospect highlights the potential for carbonatite-style REE mineralization and the presence of the Yinnetharra deposits shows the potential for pegmatite-style REE mineralization. Factors favourable for the formation of such deposits are:

- granitic or alkaline igneous rocks as a main source of metals
- magma flow focused and locally enhanced by varying compressional/extensional tectonic regimes
- sites where fluids can migrate into dilatational zones of high, fracture-related permeability
- anatectic processes that are required to form REE ore minerals.

Details of the predictor maps used in the prospectivity analysis, along with their geological rationale, are given in Appendix 2. The predictor maps were combined using a four-stage inference network (Fig. 18) to generate the final prospectivity map (Fig. 19).

Results of igneous and metamorphic-related REE prospectivity analysis

The final GIS model map contains 21 main prospective clusters ([α], [β], [χ], [δ], [ε], [ϕ], [γ], [η], [ι], [ϕ], [κ], [λ], [μ], [ν], [σ], [π], [θ], [ρ], [σ], [τ], and [υ], Fig. 19) with a very high fuzzy PRODUCT value varying from 0.35 to 0.37. The occurrences at Yinnetharra [κ] and the Gifford Creek Ferrocarbonatite Suite [β] each fall into the high fuzzy value range of 0.23 to 0.37. The REE occurrences at [υ] occur in areas of high to middle fuzzy PRODUCT value (0.23 – 0.37). The results show other highly prospective areas that have not yet been explored in the Limejuice and Mutherbukin Zones.

Orogenic and intrusive gold mineral system

Groves et al. (1998) proposed the term orogenic gold deposit to include deposits variously defined as mesothermal gold, metamorphic gold, gold-only, lode gold, shear-zone hosted, and structurally controlled gold deposits. Orogenic gold deposits are interpreted by a number of authors as genetically distinct from intrusion-related gold systems (e.g. Lang and Baker, 2001; Hart, 2007), but recent work interprets intrusion-related to be a subclass of orogenic gold deposits on the basis of temporal, spatial, and genetic similarities (Hagemann and Cassidy, written comm., 2013). For this analysis, we attempt to develop a single prospectivity model that incorporates the two types of gold system.

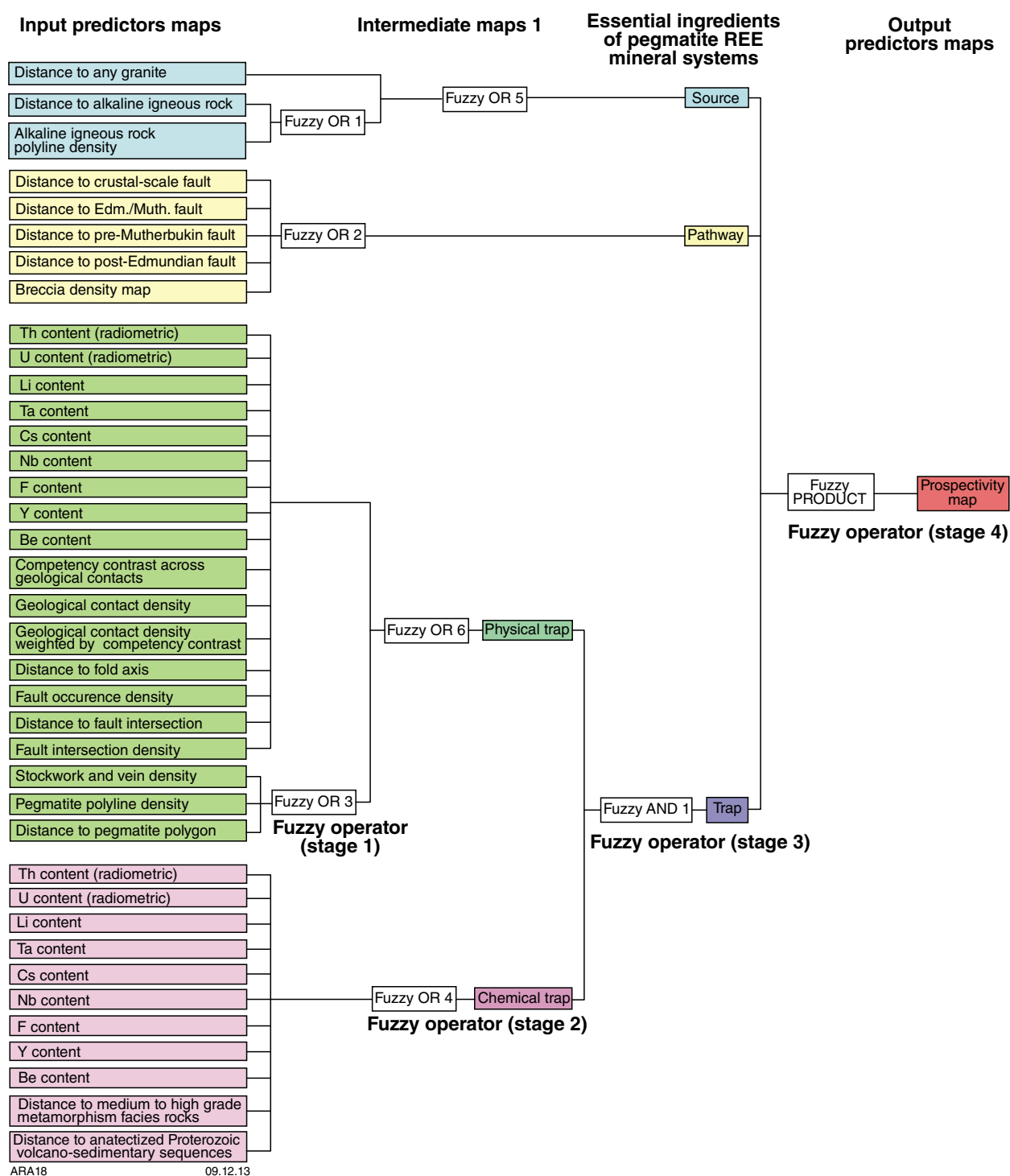


Figure 18. Multi-stage fuzzy inference network used for combining fuzzy REE predictor maps

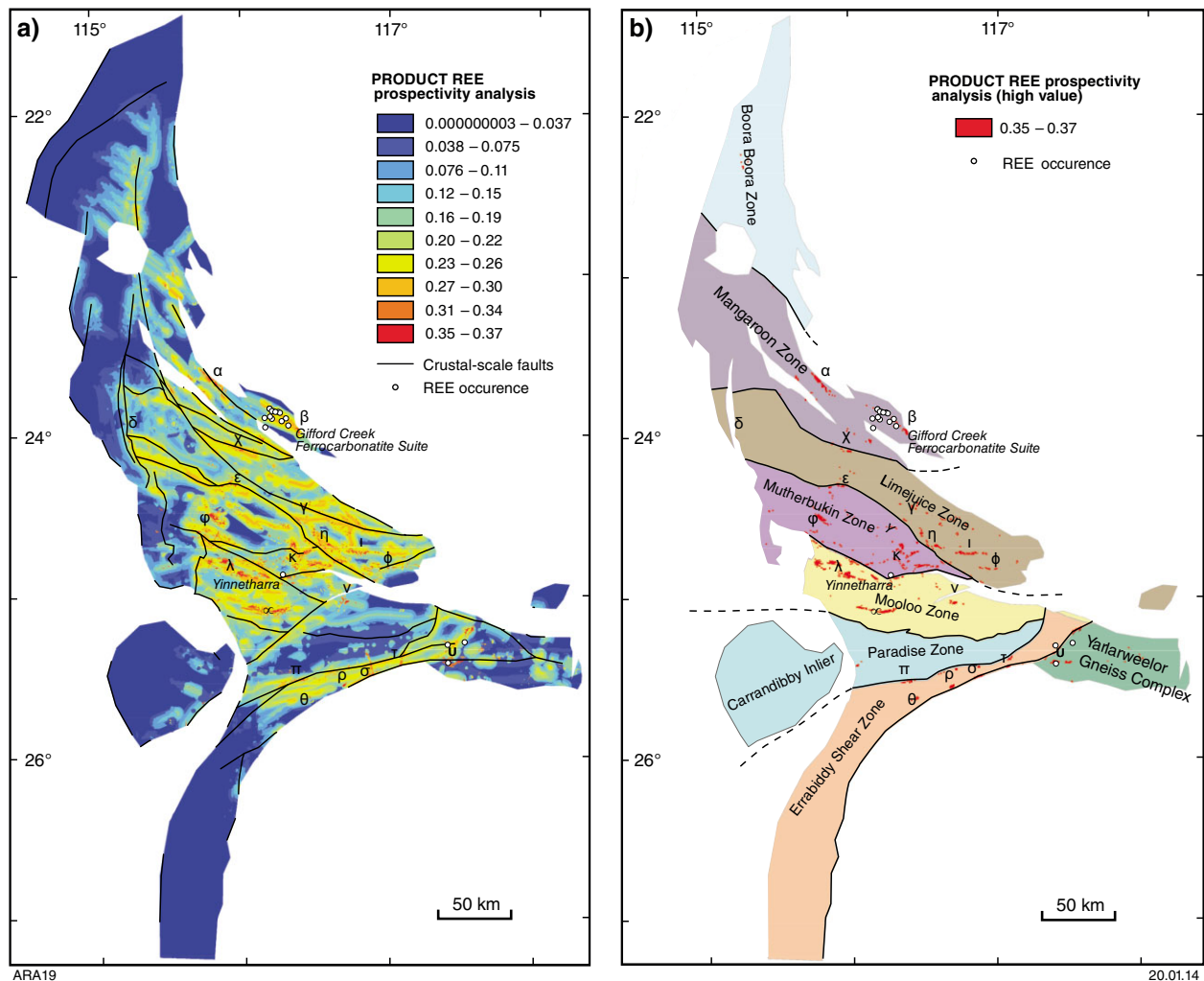


Figure 19. (a) Fuzzy prospectivity model for magmatic REE mineral system; (b) zone of high fuzzy value for the magmatic REE prospectivity analysis over Gascoyne Province zones

The Glenburgh deposit, hosted by high-grade rafts of pelitic gneisses within granitic gneisses of the 2005–1970 Ma Dalgaringa Supersuite, confirms that the Gascoyne Province contains all the ingredients required to form gold deposits. Factors favourable for the formation of gold deposits are:

- granitic rocks as the main source of metals and fluids
- major fluid pathways that undergo repeated hydraulic opening
- intense zones of deformation in the vicinity of crustal-scale lineaments.

Details of the predictor maps used in the prospectivity analysis, along with their geological rationale are given in Appendix 2. The predictor maps are combined into a four-stage inference network (Fig. 20) to generate the final prospectivity map (Fig. 21).

Results of gold prospectivity analysis

A majority of the prospective targets for the intrusion-related gold (granite source included) fall in the Limejuice Zone (Fig. 21). Fifteen target zones are highlighted [α], [β], [χ], [δ], [ε], [γ], [η], [ι], [ϕ], [κ], [λ], [μ], [ν], [σ], and [π]. Their fuzzy PRODUCT value varies between 0.24 and 0.25. The Glenburgh prospect corresponds to target zone [ν] and its surrounding area with a fuzzy PRODUCT value varying from 0.21 to 0.25.

The results for orogenic gold prospectivity analysis, where resolved (Fig. 22), are very similar to the results from intrusion-related gold prospectivity analysis (Fig. 21). The prospective clusters from the orogenic gold prospectivity analysis have fuzzy PRODUCT values varying between 0.47 and 0.51.

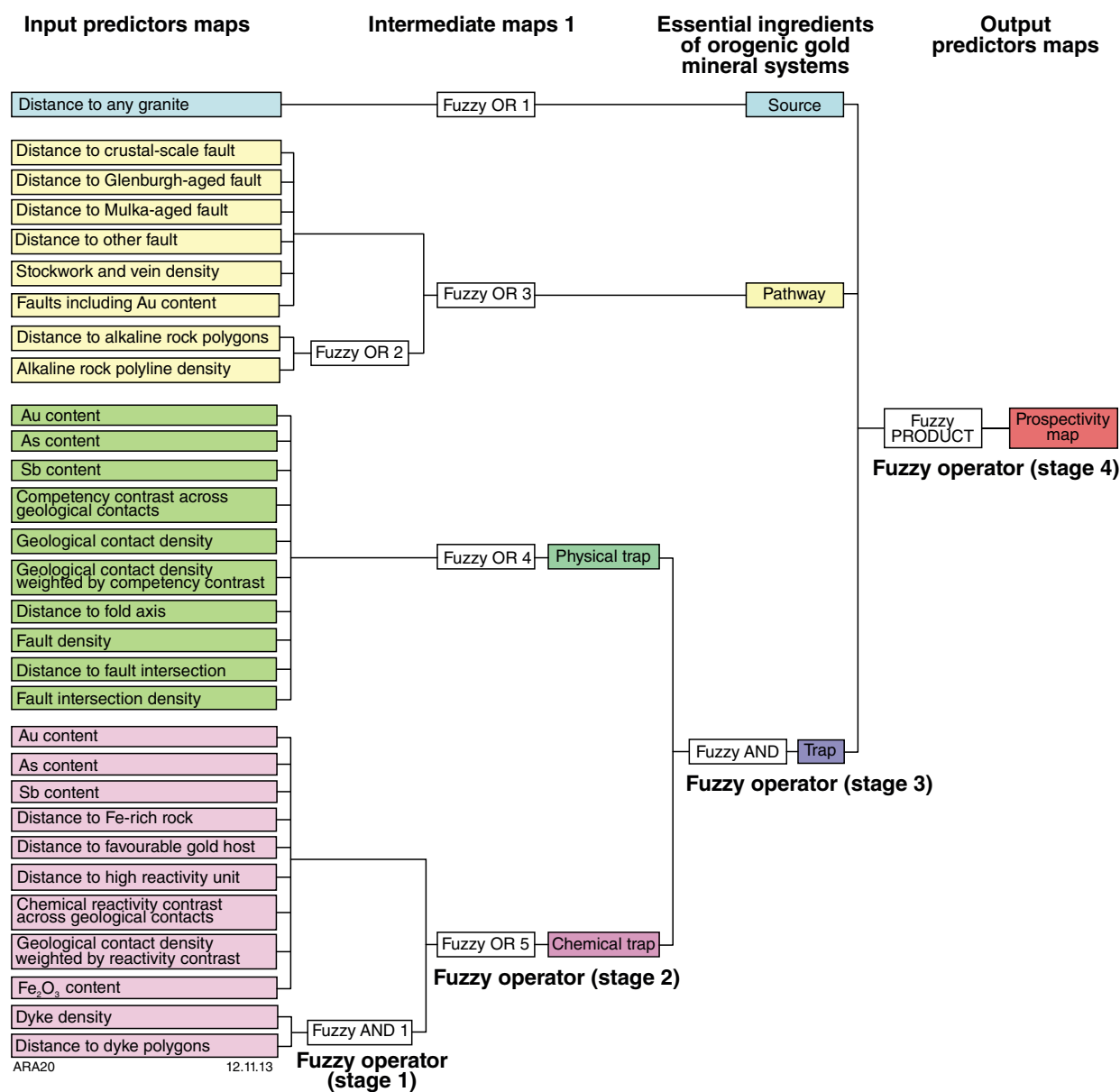


Figure 20. Multi-stage fuzzy inference network used for combining fuzzy gold predictor maps

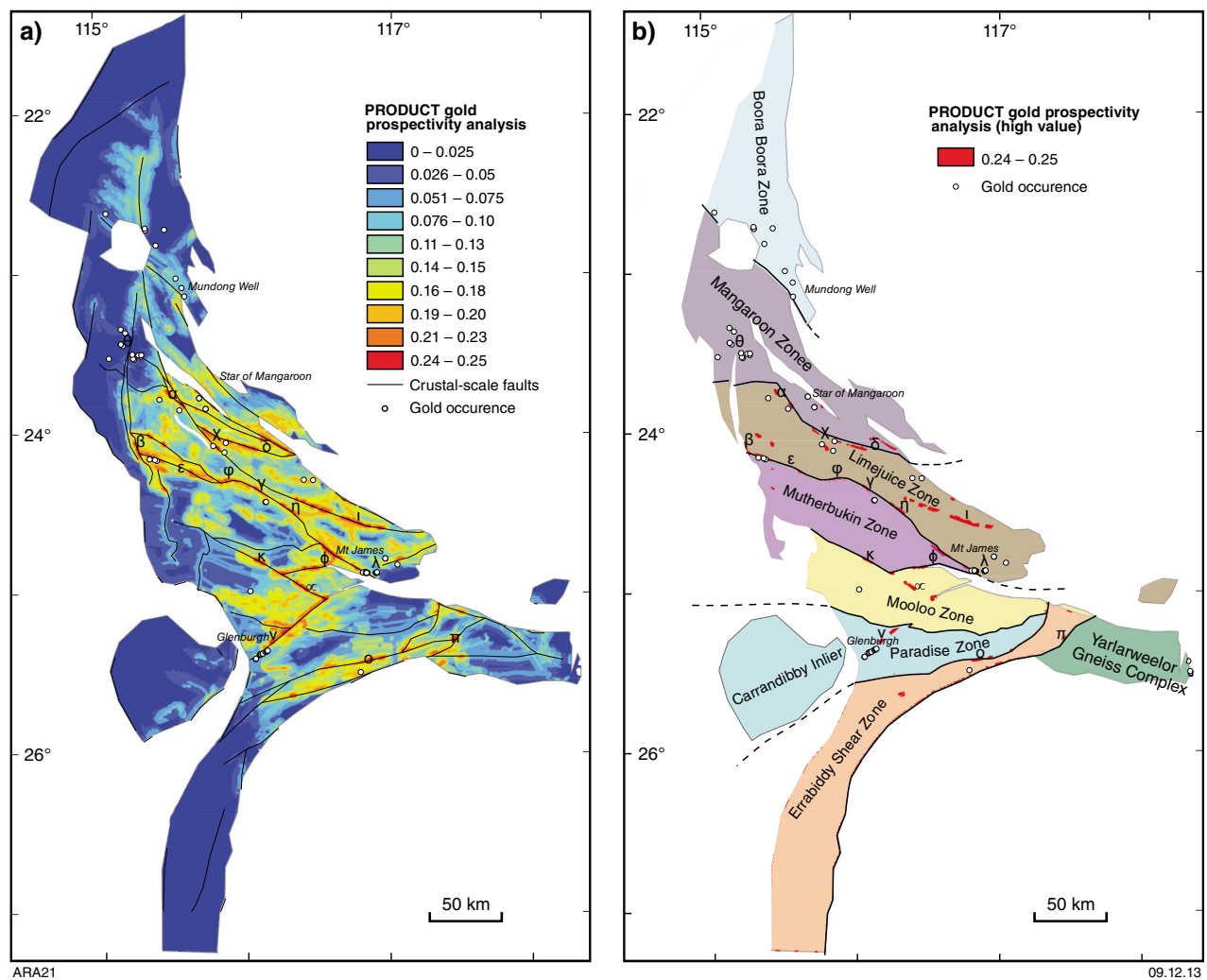


Figure 21. (a) Fuzzy prospectivity model for the intrusion-related gold mineral system; (b) zone of high fuzzy value for the intrusion-related gold prospectivity analysis over Gascoyne Province zones

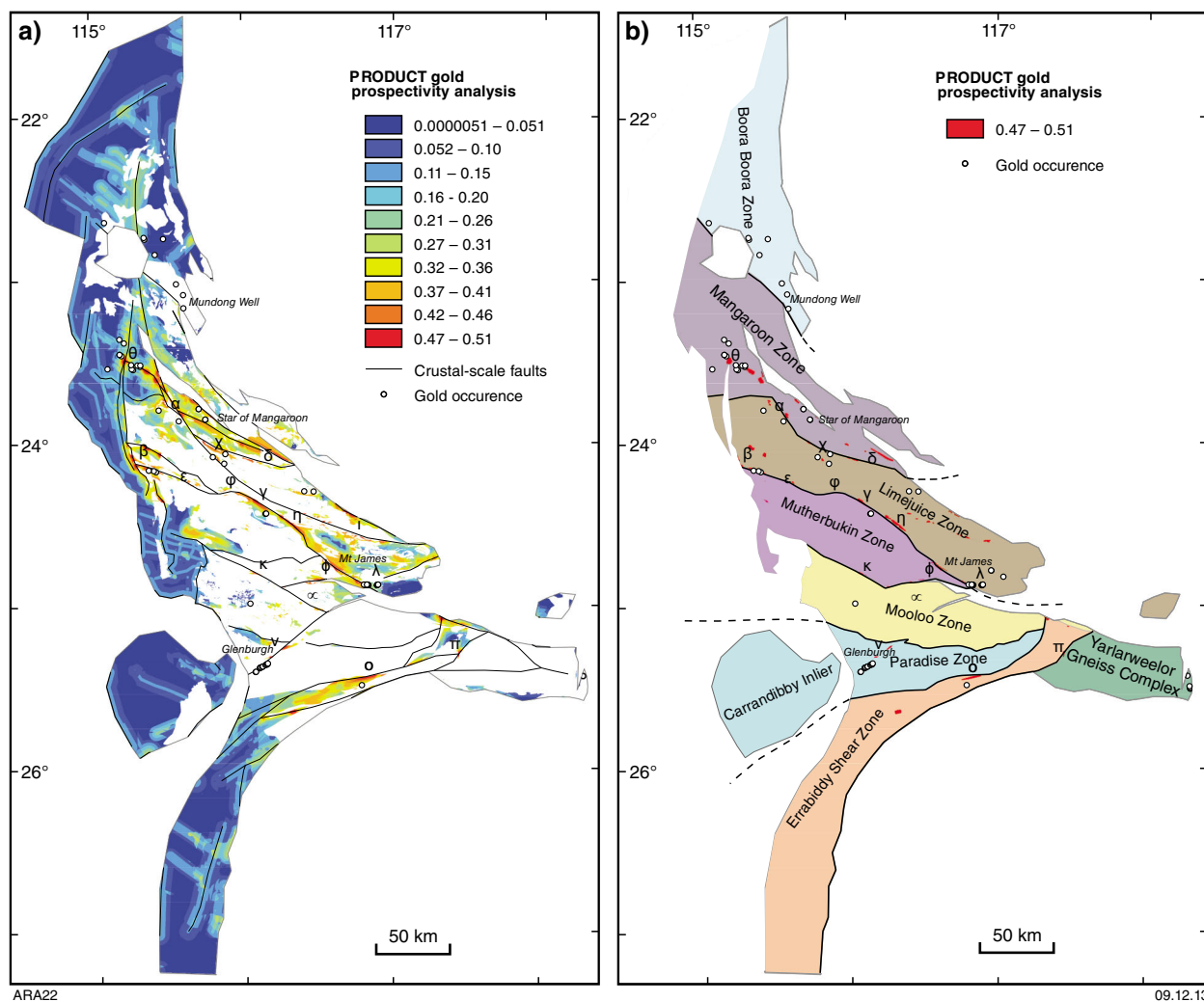


Figure 22. (a) Fuzzy prospectivity model for the orogenic gold mineral system, disregarding granitic rocks as a source predictor; (b) zone of high fuzzy value for the orogenic gold prospectivity analysis over Gascoyne Province zones

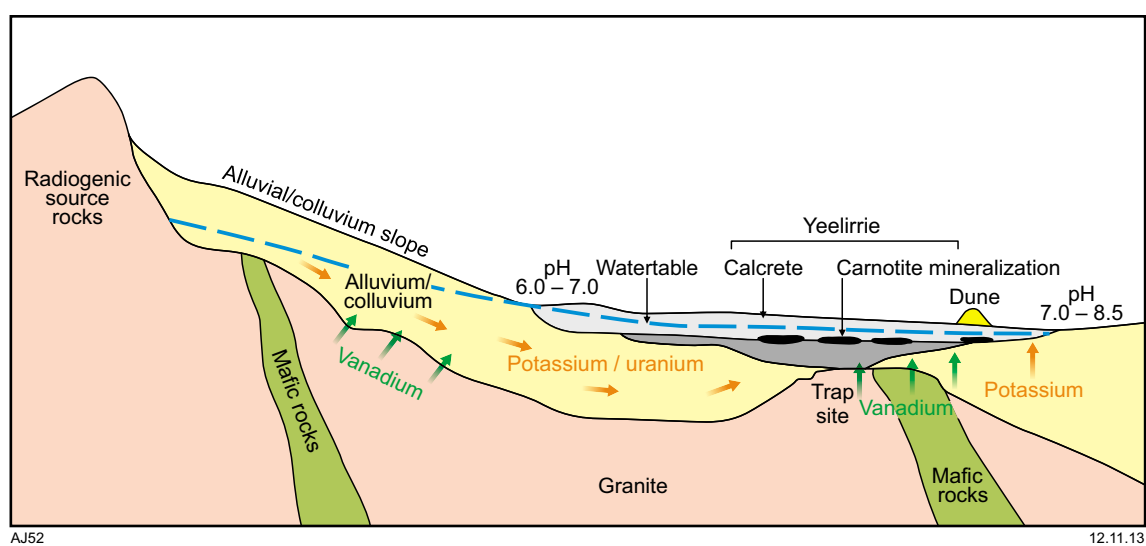


Figure 23. Model depicting the setting and processes involved in the formation of carnotite deposits in calcretized channels (Carlisle, 1983)

In the orogenic gold prospectivity analysis, areas [γ], [η], [ι], and [κ] in the Limejuice Zone are highlighted as very prospective, but they are less prospective for intrusion-related gold analysis. Target zone [θ], in the Mangaroon Zone is very prospective for intrusion-related gold and corresponds to an area of known shows.

Surficial uranium mineral system

Uranium deposits have been classified historically into 14 categories on the basis of host rocks, structural setting, and mineralogy of the deposit (Dahlkamp, 1978; International Atomic Energy Agency, 2000; McKay and Miezitis, 2001). However, this scheme is not optimal for prospectivity analyses. Kreuzer et al. (2010) instead grouped different uranium deposit types into six system models: surficial, sedimentary, igneous-related, metamorphic/metasomatic, unconformity-related, and vein-related uranium systems. The grouping is based on similarities in genetic processes, environments of ore formation, and mineral system approach proxies mappable at the regional to continent scale.

Western Australia has total known resources of 188 kt of contained U_3O_8 , of which surficial uranium is the dominant deposit type. These deposits typically occur in young (Cenozoic), unconsolidated sediments and soils, although they also occur in peat bogs and karst caverns (Fig. 23; McKay and Miezitis, 2001). Uranium mineralization typically occurs as carnotite $K_2(UO_2)_2(VO_4)_2 \cdot 3H_2O$, commonly cemented by secondary minerals including calcite, gypsum, dolomite, ferric oxide, and halite. There are three types of surficial uranium deposits: fluvatile, lacustrine (or playa), and pedogenic. All of these usually form in regions where uranium-rich granitic rocks are weathered and leached in a semi-arid

to arid climate by both surficial and underground water (Fig. 23; Carlisle, 1983). Western Australian examples occur in valley-fill sediments along Cenozoic drainage paleochannels (e.g. Yeelirrie) and in playa lake sediments (e.g. Lake Maitland). Associated vanadium is derived from mafic–ultramafic rocks.

There are no known surficial-hosted uranium deposits in the Gascoyne Province, but there are several prospects and occurrences. The Gascoyne Province contains all the ingredients required to form surficial uranium deposits, including (Kreuzer et al., 2010):

- an extensive paleodrainage system
- calcrete accumulations within and adjacent to drainage lines
- appropriate sources of uranium (felsic igneous rocks) and vanadium (mafic volcanics)
- arid climatic conditions.

Details of the predictor maps used in the prospectivity analysis, along with their geological rationale are given in Appendix 2. The predictor maps are combined into a four-stage inference network (Fig. 24) to generate the final prospectivity map (Figs 25 and 26).

Results of surficial uranium prospectivity analysis

Figures 25 and 26 illustrate potentially prospective areas for exploration in the whole Gascoyne Province and in the MOUNT PHILLIPS 1:250 000 map sheet area, respectively. Prospective zones with a PRODUCT fuzzy value varying from 0.14 to 0.23 are highlighted in the northern and central parts of the Gascoyne Province. All prospective

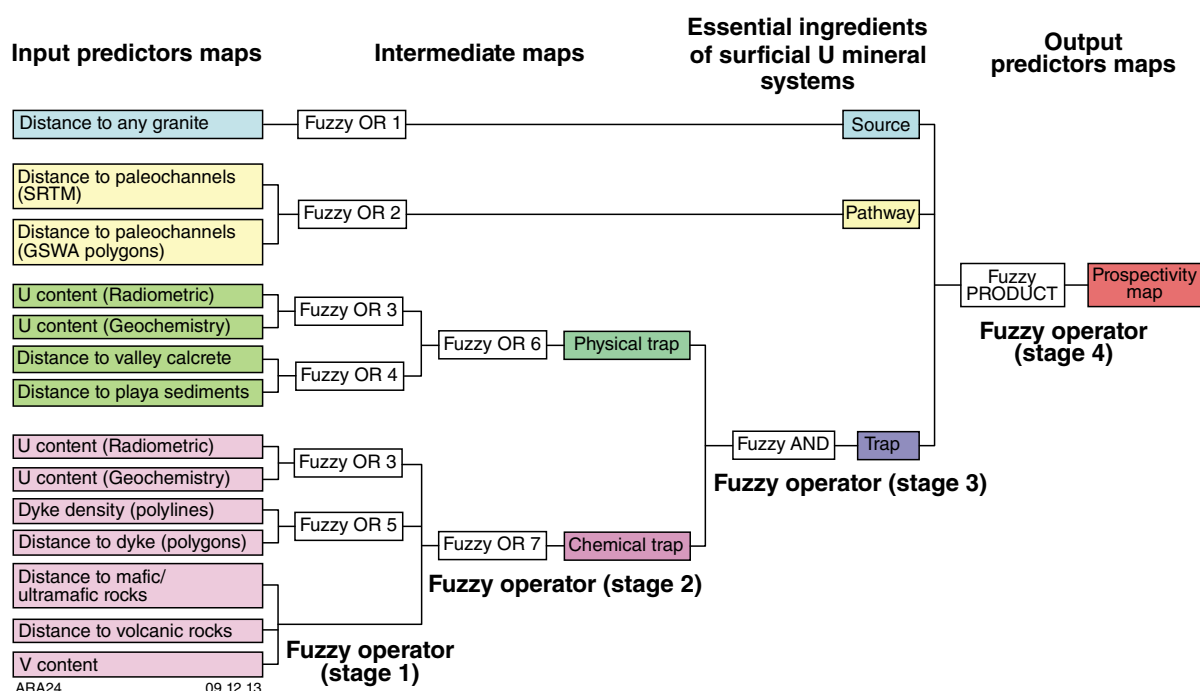


Figure 24. Multi-stage fuzzy inference network used for combining fuzzy surficial uranium predictor maps

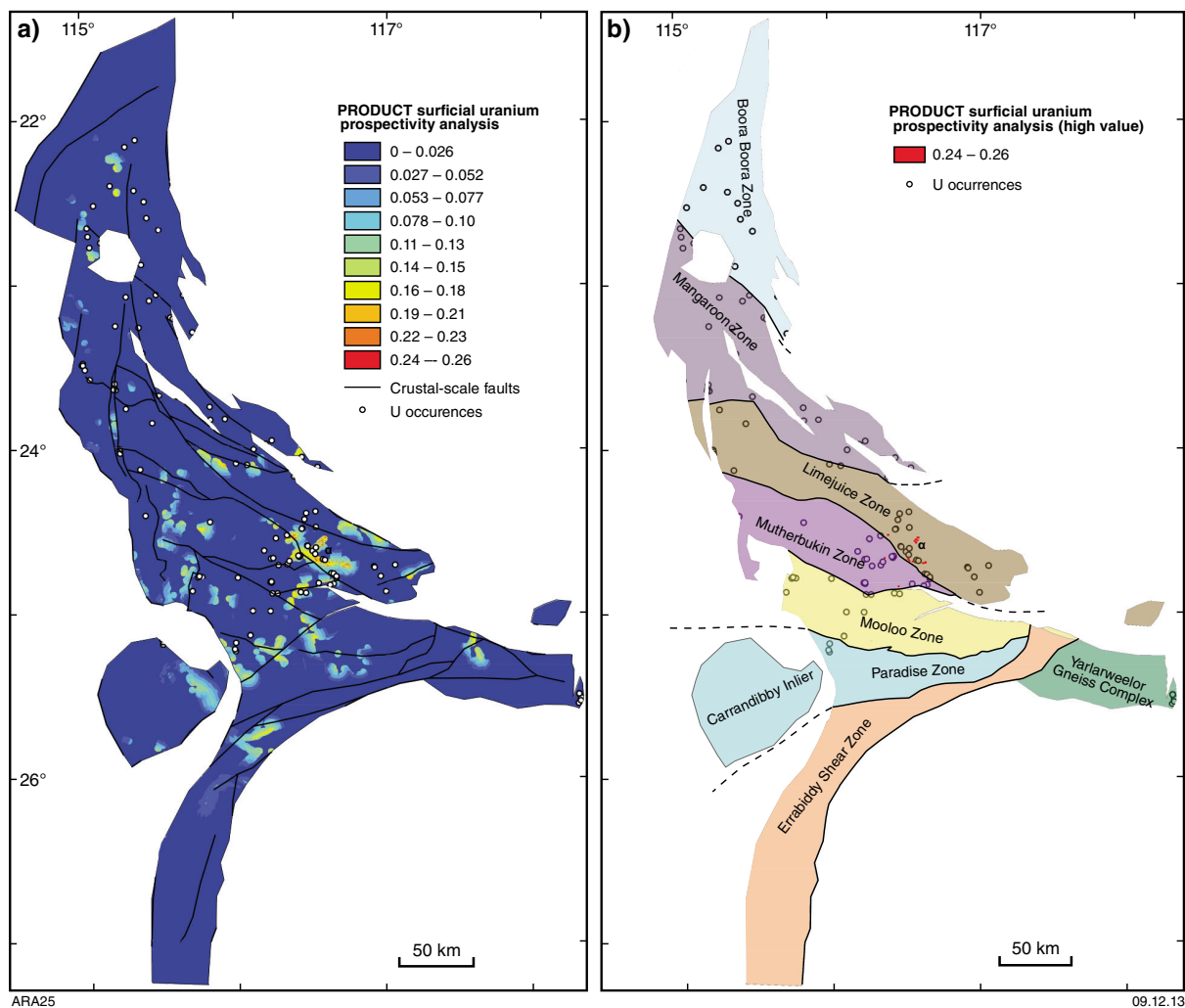


Figure 25. (a) Fuzzy prospectivity model for the surficial uranium mineral system; (b) zone of high fuzzy value for the surficial uranium prospectivity analysis over the Gascoyne Province zones

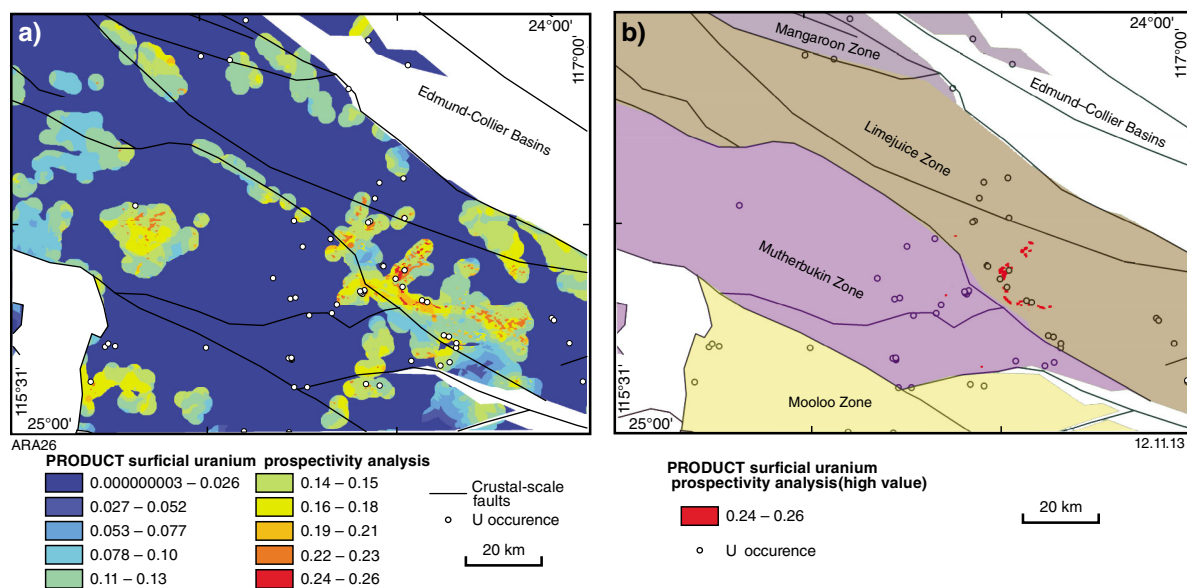


Figure 26. (a) Fuzzy prospectivity model for the surficial uranium mineral system within the MOUNT PHILLIPS 1:250 000 map sheet area; (b) zone of high fuzzy value for the surficial uranium prospectivity analysis over the Gascoyne Province zones within the MOUNT PHILLIPS map sheet area

zones are associated with granites and the presence of inferred or known paleochannels. There exists only one highly prospective area $[\alpha]$, with a PRODUCT fuzzy value varying from 0.24 to 0.26, located in the western part on the Limejuice Zone (Fig. 25). Locality $[\alpha]$ is close to granitic rocks, paleochannels, volcanic units, and calcrete. More details on the location of prospective zones are given in Figure 26, where paleochannels have been mapped in the field (GSWA, 2012) and incorporated during the analysis.

Porphyry base metal mineral system

Porphyry base metal (PBM) systems are defined as large volumes (10–100 km³) of hydrothermally altered rock centred on an intrusion (Sillitoe, 2010) and encompassing iron oxide–copper–gold (IOCG), skarn, and porphyry deposits. PBM deposits are arguably the most studied and potentially best known and understood ore deposit type, and their relationships with the skarn environment have been known for many years (Einaudi et al., 1981). Only recently, however, have the physico-chemical connections with the high- and intermediate-sulfidation epithermal environment within and around overlying lithocaps been clarified (Hedenquist et al., 2000).

Breccias, veins, disseminations and massive lenses with polymetallic enrichments are genetically associated with A-type to I-type granitic rocks, alkaline stocks, and crustal-scale fault zones (Fig. 27; Groves et al., 2010). PBM host lithologies and ages are non-diagnostic but their alteration zones are, with calcic–sodic regional alteration juxtaposed against potassic and iron oxide alteration. PBM systems are generated mainly in magmatic-arc (including back-arc) environments subjected to a spectrum of regional-scale stress regimes, apparently ranging from moderately extensional through oblique slip to contractional (Tosdal and Richard, 2001). Groves and Vielreicher (2001) suggested that most PBM deposits (especially the largest deposits, e.g. Carajás, Brazil and Olympic Dam, Australia) are located close to a craton margin or other major lithospheric boundary, where decompression melting of metasomatized mantle produces volatile-rich alkaline magmas rich in REE, phosphorous, and fluorine, and other incompatible elements such as sulfur, copper, and gold.

The presence of the Mount James, Glenburgh, Minnie Springs and Mundong Well prospects highlights the potential for PBM mineralization in the Gascoyne Province. The province contains all the ingredients required to form polymetallic PBM deposits:

- mafic rocks and granites as the main metal source
- crustal-scale structures that would permit fluid migration
- sites where basinal brines could be trapped beneath regional seals
- the presence of skarn potentially indicative of hydrothermal alteration.

Details of the predictor maps used in the prospectivity analysis, along with their geological rationale are given in Appendix 2. The predictor maps are combined into a four-stage inference network (Fig. 28) to generate the final prospectivity map (Fig. 29).

Results of PBM prospectivity analysis

The final prospectivity map identifies 12 target zones (Fig. 29) marked as $[\alpha]$, $[\beta]$, $[\chi]$, $[\delta]$, $[\varepsilon]$, $[\phi]$, $[\gamma]$, $[\eta]$, $[\iota]$, $[\varphi]$, $[\kappa]$, and $[\lambda]$. Their fuzzy PRODUCT value varies between 0.39 and 0.42. The known copper–gold PBM deposits or occurrences Minnie Springs, Mt James, Glenburgh, and Mundong Well correspond to high fuzzy PRODUCT values of 0.22 – 0.38. Those fuzzy values are not the highest, meaning that other highly prospective areas are still to be explored in the EDMUND, MOUNT PHILLIPS, GLENBURGH, and ROBINSON RANGE 1:250 000 map sheet areas. The Limejuice, Mutherbukin, and Mooloo Zones are the most prospective domains.

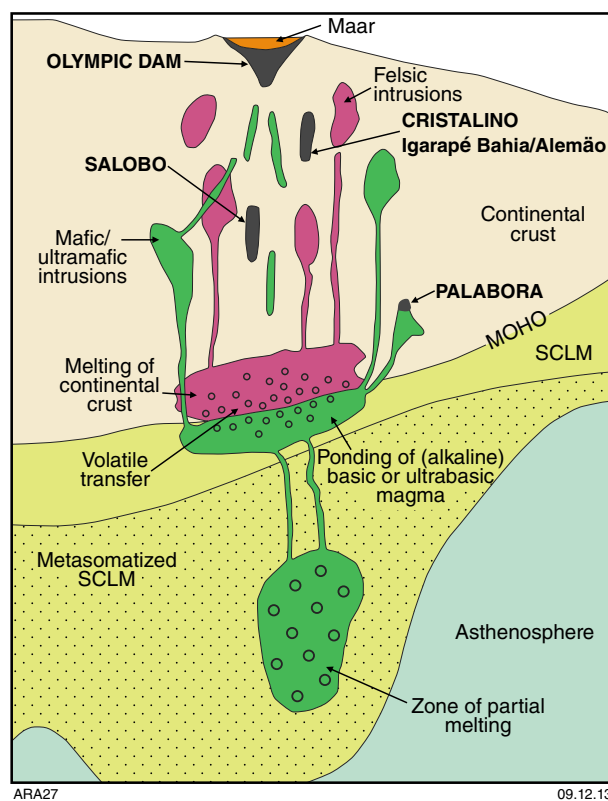


Figure 27. Schematic diagram showing model for genesis of PBM deposits. Small degrees of partial melting of metasomatized Sub-Continental Lithospheric Mantle (SCLM) produces basic and ultrabasic melts, probably of alkaline affinity and enriched in volatiles, Cu, and Au. This melt ponds at the crust–lithosphere boundary and causes partial melting of the continental crust to produce felsic melts. Volatiles and metals transfer across the melt boundary. Felsic magmas ascend to produce felsic plutons, allowing higher density basic or ultrabasic magmas to follow, producing mafic–ultramafic intrusions in the same district. Deep volatile exsolution produces giant breccia pipes with silicate rocks replaced by iron oxides, followed by Cu, Au, U, and other enriched elements (Groves et al., 2010).

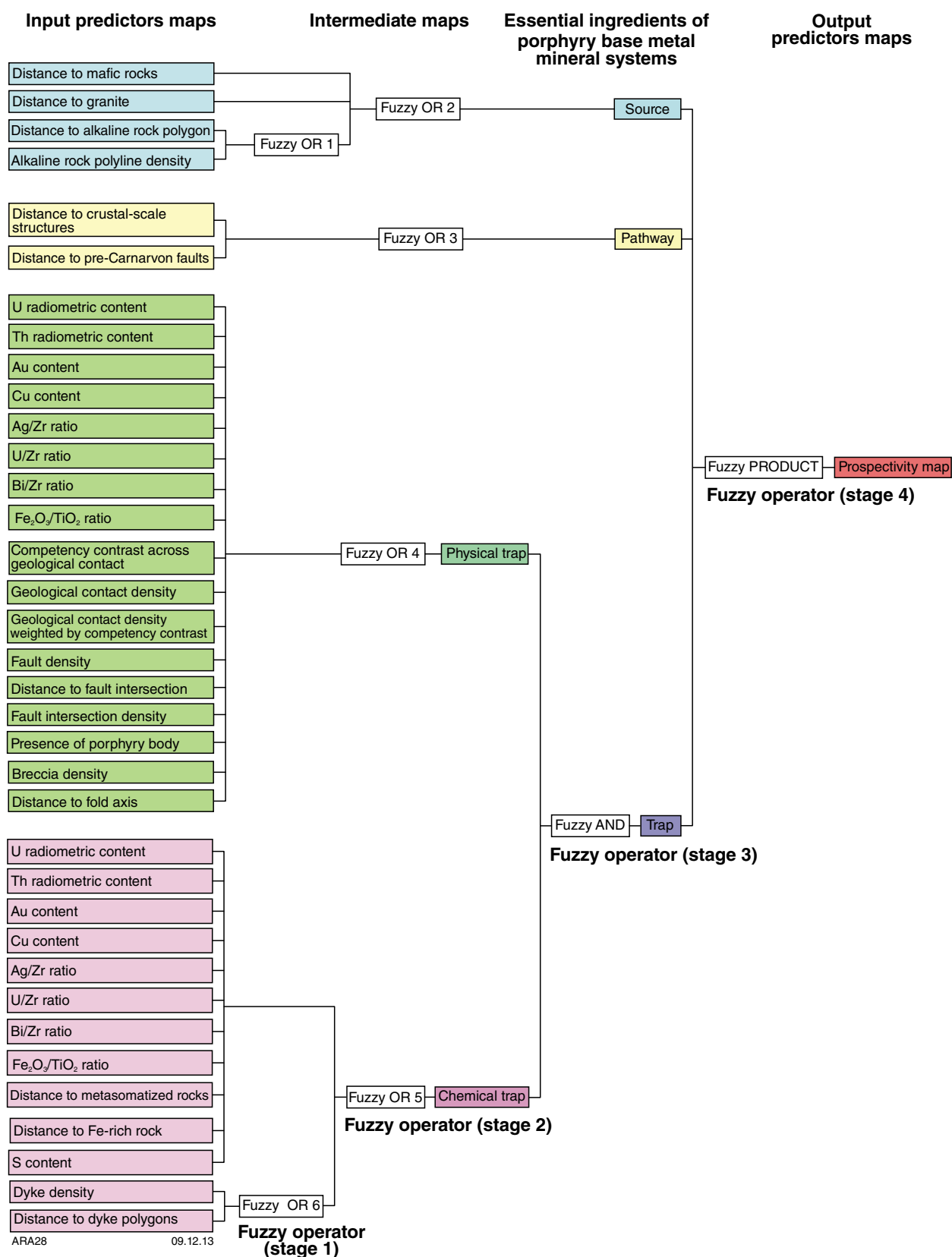


Figure 28. Multi-stage fuzzy inference network used for combining fuzzy PBM predictor maps

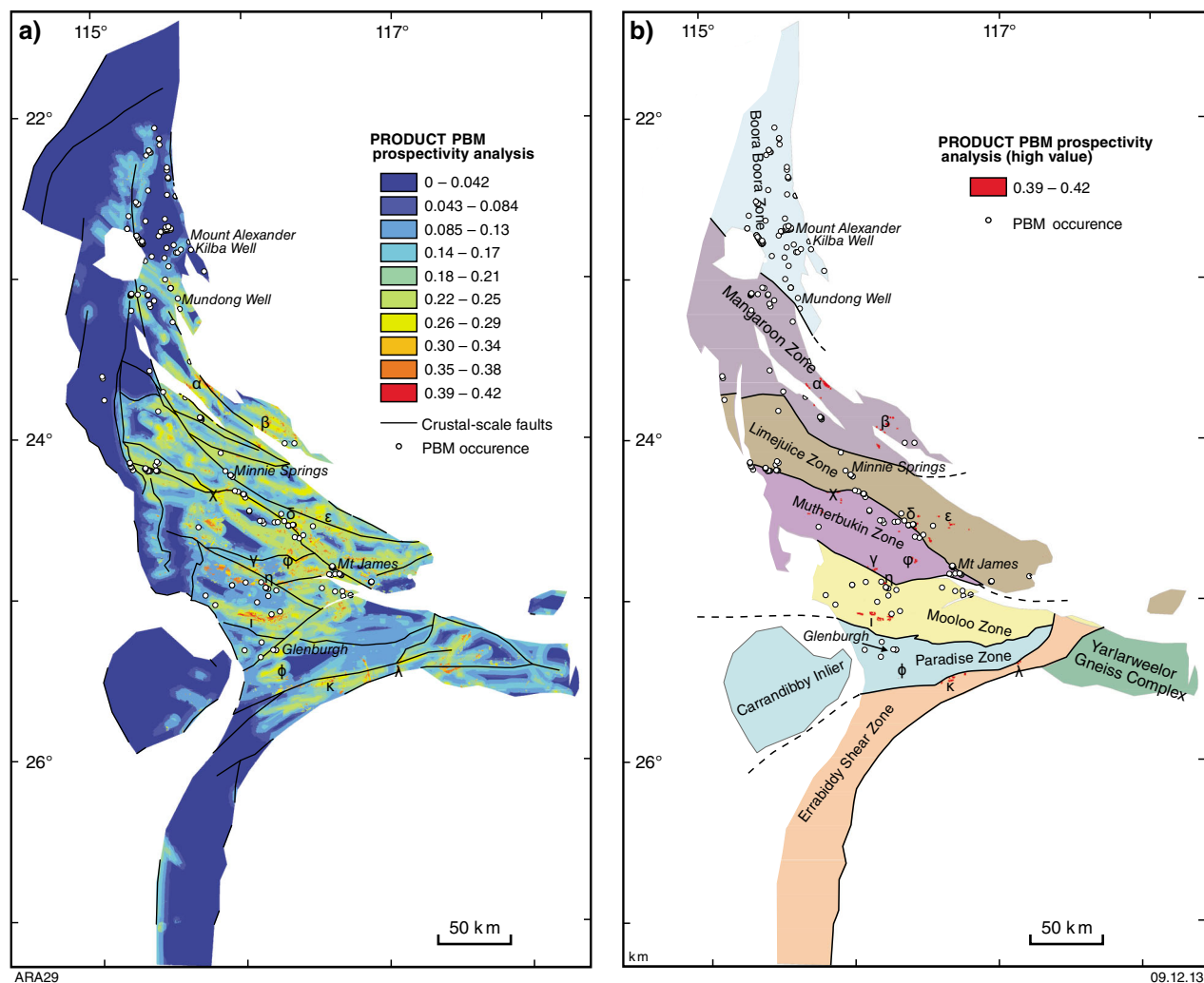


Figure 29. (a) Fuzzy prospectivity model for the PBM mineral system; (b) zone of high fuzzy value for the PBM prospectivity analysis over the Gascoyne Province zones

Granite-hosted tin–tungsten mineral system

Tin deposits that contain subordinate tungsten have been reviewed by Heinrich (1990), whereas deposits in which tungsten is the dominant metal with tin as the next most abundant metal have been reviewed by Wood and Samson (2000). Most tin–tungsten (\pm molybdenum) deposits are spatially associated with granitic magmatism (Ferguson and Bateman, 1912; Eugster, 1985). Mineralization is typically situated toward the apical regions of granitic cupolas within pegmatites, quartz veins, stockworks, or as disseminations (Lehmann, 1990).

Most of Australia's historical tin and tungsten production has been from pipes and skarns associated with tungsten–molybdenum-bearing post-orogenic, subduction-related granites (Solomon et al., 1994). The nature and timing of Sn–W mineralization suggests a complex magmatic–

hydrothermal continuum during the mineralizing process (Landis and Rye, 1974; Heinrich, 1990; Roberts et al., 1998). In general, these deposits have multiple stages of mineralization (Solomon et al., 1994).

There are currently no known Sn–W deposits in the Gascoyne Province, although at Nardoo Hill (Fig. 31), contact metamorphosed sediments host scheelite within the crustal-scale Chalba Shear Zone. This scheelite unit is prospective for tungsten (Mincor Resources NL, 2006). At Hectors Bore, a marble unit of the 2240–2125 Ma Moogie Metamorphics hosts syngenetic tungsten mineralization (Hassan, 2006). The province contains the ingredients required to form Sn–W deposits:

- highly fractionated granitic rocks as a source
- deep-penetrating structures that permit fluid migration
- rocks with very high chemical reactivity, such as skarns and dolomites.

Details of the predictor maps used in the prospectivity analysis, along with their geological rationale are given in Appendix 2. The predictor maps are combined into a three-stage inference network (Fig. 30) to generate the final prospectivity map (Fig. 31).

Results of granite-hosted tin–tungsten prospectivity analysis

The final prospectivity map (Fig. 31) identifies eight high-prospectivity areas for granite-hosted tin–tungsten (marked by $[\alpha]$, $[\beta]$, $[\chi]$, $[\delta]$, $[\varepsilon]$, $[\phi]$, $[\gamma]$, and $[\eta]$). Their fuzzy PRODUCT varies from 0.26 to 0.28. Known Sn–W occurrences coincide with areas of high fuzzy PRODUCT value (0.18 – 0.25). The Nardoo Well occurrences fall into a fuzzy PRODUCT value of 0.23 to 0.25. The results highlight several highly prospective areas that have not yet been explored. The western part of Limejuice Zone appears to be the most prospective zone.

Discussion

Tectonic summary

Our structural interpretation of the Gascoyne Province records a tectonic evolution extending from the Neoproterozoic to the Paleozoic. Within this period, there have been two major collisional events, the Ophthalmian and Glenburgh Orogenies, during which the Glenburgh Terrane, the Pilbara Craton, and the Yilgarn Craton were

assembled to form the West Australian Craton. The major structures related to these assembly events have shaped the architecture of the province (Johnson et al., 2011a, 2013). The preserved record, however, is dominated by intraplate reactivation of pre-existing architecture. The major fault zones are all multiply reactivated, and each can be associated with several tectonic events. Towards the centre of the province, the age of the youngest event preserved is progressively younger (Fig. 32).

The 2005–1950 Ma Glenburgh Orogeny is limited in extent to the southern Gascoyne Province, and is most strongly developed within the Paradise Zone, where it is the dominant event, although it also significantly affected the Narryer Terrane and the Yarlalweelor Gneiss Complex, and the Mooloo Zone (Fig. 32a cf. Fig. 2). The northern limit of this event is poorly defined, as younger rocks become dominant. Observed structures trend broadly east-northeast and define compressive deformation associated with the collision of the Glenburgh Terrane and Narryer Terrane.

The 1820–1770 Ma Capricorn Orogeny is the first event to be recognized province wide, and is the most widely observed event within the province (Fig. 32b). It is especially well developed (or preserved) at the margins of the Paradise Zone, i.e. in the Errabiddy Shear Zone, where it is defined by intense, northeasterly oriented fabrics, and in the southern Mooloo Zone, where it is defined by southeasterly oriented fabrics. In the Mutherbuckin Zone, there is no evidence of Capricorn Orogeny structures; however, this is more likely a result of the intensity of subsequent events rather than an absence of the effects of the Capricorn Orogeny. Significant Capricorn Orogeny-

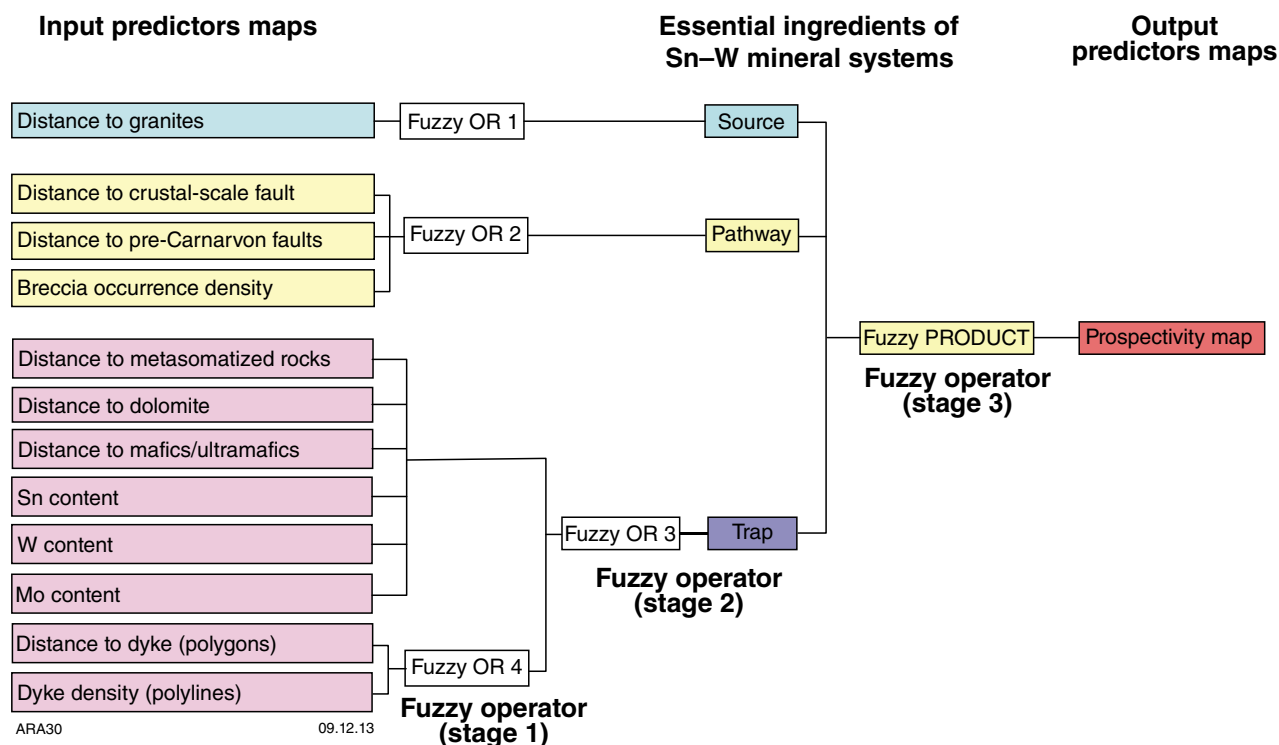


Figure 30. Multi-stage fuzzy inference network used for combining fuzzy Sn–W predictor maps

age structures are preserved in the Boora Boora Zone, where the Capricorn Orogeny generated the dominant north-trending fabric.

The 1680–1620 Ma Mangaroon Orogeny dominantly affected the northern part of the Province, north of the Chalba and Mt Clere faults (Fig. 32c cf. Fig. 2). In this zone, it is characterized by extensive felsic magmatism of the Durlacher Supersuite and structures that trend east-southeast to southeast. The Limejuice Zone is located approximately in the centre of the Mangaroon Orogeny, but is dominated by the Minnie Creek batholith. Moreover, the Limejuice Zone shows little evidence for Mangaroon-age deformation compared to the adjacent zones, although without significant exposures of units of suitable age, the minimum ages of deformation events are poorly constrained.

The Mangaroon Orogeny was followed by deposition of the 1620–1465 Ma Edmund Group, which was subsequently intruded by the c. 1465 Ma Narimbunna Dolerite at. Although

these rocks are prominently folded, they are generally nonmetamorphosed. Subsequent tectonic events, the 1385–1170 Ma Mutherbukin Tectonic Event and the 1030–955 Ma Edmundian Orogeny, cannot be separated on the basis of relative age, except in the northern Mutherbukin Zone, where the 995–940 Ma Thirty Three Supersuite was intruded as part of the Edmundian Orogeny. Mutherbukin and Edmundian Orogeny structures are focused in the Mutherbukin Zone (Fig. 32c), although they extend into the Mooloo Zone, and are also common in the Limejuice and Mangaroon Zones. Of all the major tectonic events, this event has the narrowest footprint and is also located most centrally.

Following the Edmundian Orogeny, the province was intruded by mafic dykes of the c. 755 Ma Mundine Well Dolerite Suite, and many of the major fault zones were reactivated during the c. 570 Ma Mulka Tectonic Event (Sheppard et al., 2010b). The initiation of the Carnarvon Basin during the Paleozoic has also exerted a minor influence on the westernmost parts of the province (Fig. 32d).

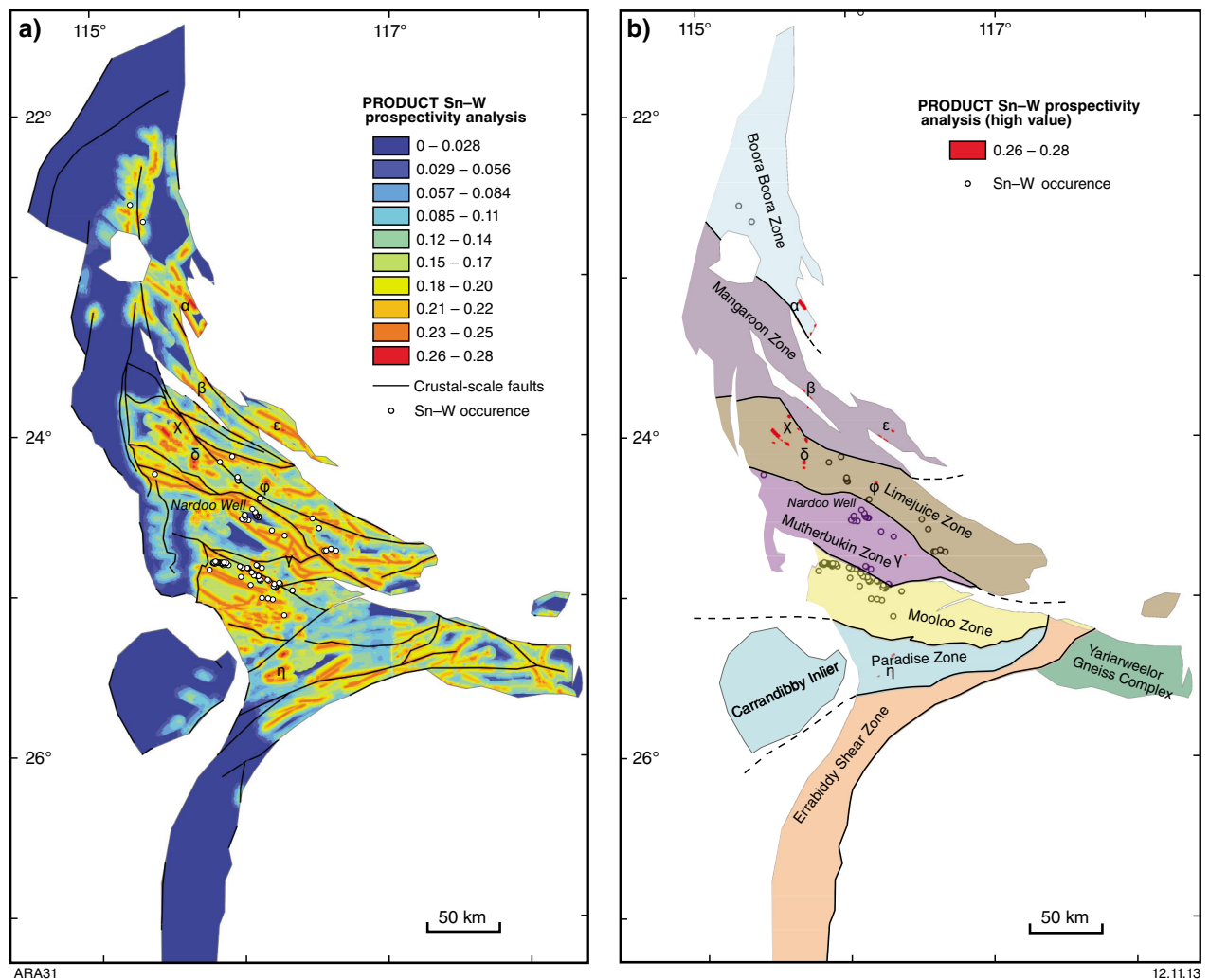


Figure 31. (a) Fuzzy prospectivity model for the Sn-W mineral system; (b) zone of high fuzzy value for the Sn-W prospectivity analysis over the analysed area with even data coverage

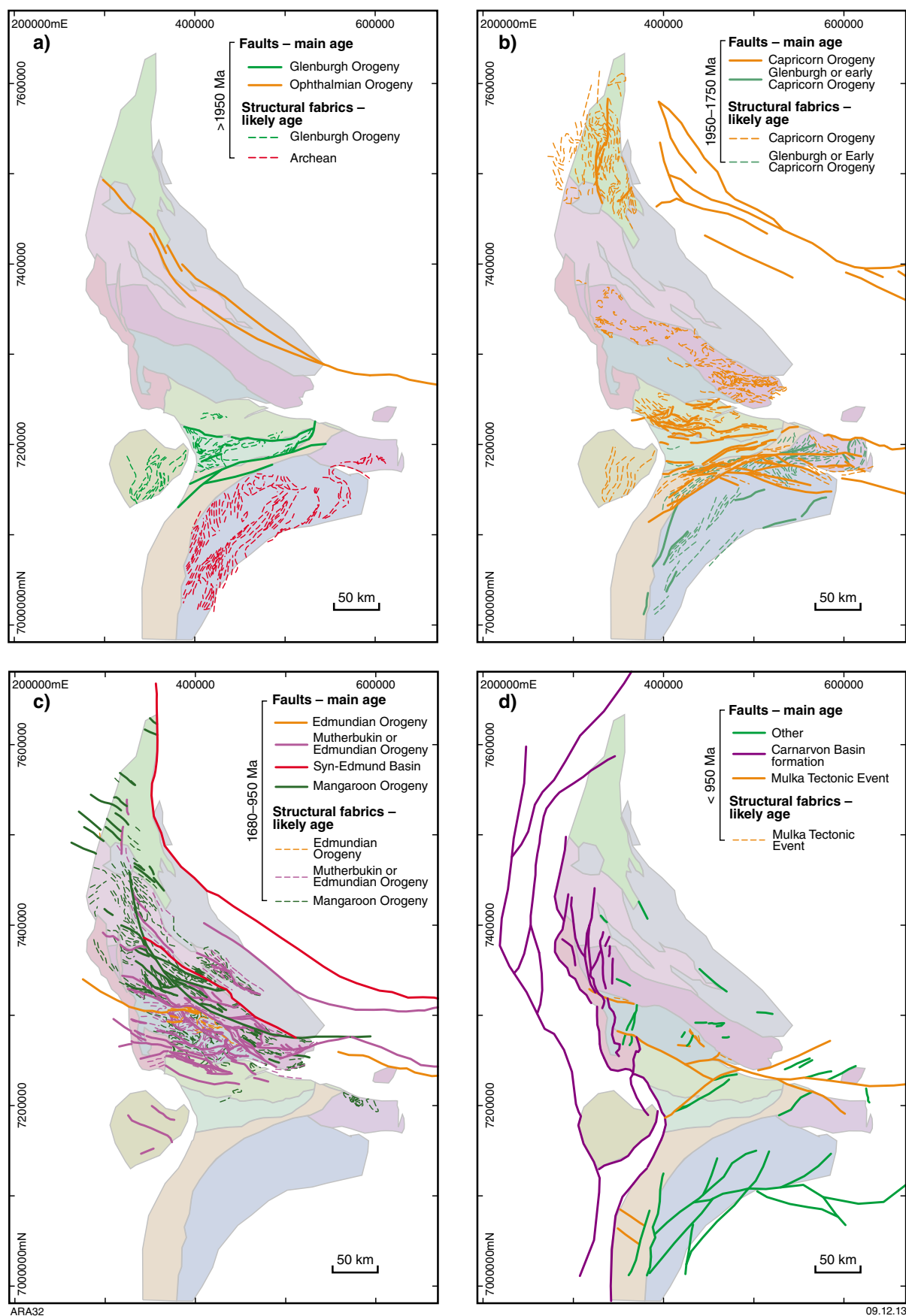


Figure 32. Structural overview of the Gascoyne Province. Faults have mostly been reactivated several times, and are coloured according to the most prominent event in their activation history. Fabrics are not considered reactivated, and are coloured according to overprinting relationships with geological units. Note the decrease in preserved event age towards the centre of the province (Mutherbukin Zone).

Inward-stepping intraplate orogenesis

One aspect of the Gascoyne Province that has become clear with this work is that, after the two collisional events, each of which primarily affected the respective northern and southern margins of the Glenburgh Terrane, the intraplate orogenic events show a narrowing in their extent towards the centre of the province (Fig. 32). The Capricorn Orogeny had a very widespread influence, affecting all zones of the Gascoyne Province and extending into the Yilgarn Craton. Although there is currently little evidence that the Capricorn Orogeny affected the Mutherbukin and Mangaroon Zones, this is most likely a result of the extensive reworking and magmatism these zones have experienced during later deformation, overprinting any record of earlier events (Sheppard et al., 2010b).

The Mangaroon Orogeny was focused within the Mangaroon Zone, but was also very significant within the Mutherbukin Zone, and involved widespread magmatism throughout much of the province, including the Yarlalweelor Gneiss Complex and the Boora Boora Zone. Interestingly, the Limejuice Zone lies in the centre of the recognized boundaries of this event, and yet preserves little evidence for either magmatism or metamorphism during the Mangaroon Orogeny, although some deformation is inferred. Despite being composed of older 1820–1775 Ma Moorarie Supersuite rocks, it has significantly lower metamorphic grade than the adjacent Mutherbukin and Mangaroon Zones. If the Mangaroon Orogeny is extensional, as indicated by low-pressure, high-temperature metamorphism and a lack of compressional structures (Sheppard et al., 2005), one interpretation is that the Minnie Creek batholith was sufficiently rigid and thick that it formed an uplifted basement high during the Mangaroon Orogeny.

In the basement rocks, the influence of the Mutherbukin Tectonic Event and Edmundian Orogeny is more confined still. These events are dominantly focused around the Mutherbukin Zone, and those parts of the Mooloo and Limejuice Zones nearest to their boundaries with the Mutherbukin Zone.

This inward-stepping intraplate orogenesis is somewhat unusual; however, a compelling explanation is that, through time, the exterior parts of the province became cratonized as the lithosphere cooled and thickened. This lithospheric architecture can lead to the channelling of magmatism and also the focusing of deformation within relatively narrow zones. From an exploration perspective, this means that the central parts of the province (and their extensions beneath the Edmund and Collier Basins) have the greatest potential for long-lived, multiply activated fault zones that might have focused fluid flow.

Lower-crustal structure of the Gascoyne Province

The lower-crustal structure of the Gascoyne Province preserves a few interesting features. Moho geometry

(based on the seismic compilation of Kennett et al., 2011) shows a general eastwards deepening, from ~30 km to ~40 km. This likely relates to crustal thinning to the west as a result of Gondwana breakup. Superimposed on this is a northwest–southeasterly trending pattern characterized by thicker crust beneath the Paradise Zone and the Mooloo Zone (40–45 km), thinner crust beneath the Mutherbukin, Limejuice, and Boora Boora Zones (35–40 km), and thicker crust again beneath the Edmund Basin (~42 km). The Pilbara and Yilgarn Cratons have relatively thin crust, with the Moho at ~35 km depth.

The east–west Moho gradient is directly reflected in the gravity field; however, the thick crust of the Paradise and Mooloo Zones is located beneath a mid-wavelength gravity high, indicating that the crust must be dense (see Aitken et al., 2012). There is little evidence that the upper-crustal rocks are any denser within these zones, and so the lower crust must be either denser, or perhaps thicker, beneath these zones. The Capricorn seismic transect identified the MacAdam Seismic Province (Johnson et al., 2011a, 2013), a region of distinctively reduced seismic reflectivity in the lower crust. We show in our modelling that, following the seismically defined geometry of this seismic province, a fit to the gravity data can be achieved with a density for the MacAdam Seismic Province of 3000–3300 kg/m³. With small geometrical changes and reasonable changes to upper-crustal densities, this density could be ± 100 kg/m³, but still denser than typical lower crust. The geological nature of this package of extremely dense lower-crustal rocks is unclear; however, it does not occur north of the Lyons River Fault, and is not observed beneath the Yilgarn Craton. This indicates that it is a pre-amalgamation feature of the Glenburgh Terrane. Elsewhere, the lower crust is of relatively similar density (2900 kg/m³) and thickness, although some minor variations are observed.

Crustal structure and mineral prospectivity

Large-scale crustal structure has been recognized as a key control on many styles of mineralization (e.g. Bierlein et al., 2006), although ore deposit genesis also relies on many other factors, most of which operate at smaller scales. GIS-based mineral systems analysis applied at the province scale, with high resolution, allows the influence of crustal architecture to be applied within a more holistic framework to predict prospectivity at smaller scales. Our analysis for the Gascoyne Province shows the importance of crustal structure for each deposit type, except surficial uranium.

For REEs, prospectivity is focused within a triangular central zone defined by the Deadman Fault to the southeast, and the Ti Tree Shear Zone and Edmund Fault to the north (Fig. 19 cf. Fig. 1). The Gifford Creek Ferrocarnatite Suite lies in a separate region, also showing high prospectivity, and there is a third area along the Errabiddy Shear Zone. For orogenic gold, the results clearly show high prospectivity along the major fault zones, most notably the Ti Tree and Chalba Shear Zones, and the Deadman and Minga Bar Faults; although again,

the Errabiddy Shear Zone is a separate zone of elevated prospectivity (Figs 21 and 22 cf. Fig. 1). PBM prospectivity is more diffuse, and generally has lower peaks than the above systems. Nevertheless, concentrations are found in broad zones around the Deadman Fault, Ti Tree Shear Zone, and Errabiddy Shear Zone (Fig. 29 cf. Fig. 1). Finally, tin–tungsten granite prospectivity is not focused onto the major faults, but is generally enhanced along smaller structures within the Mooloo, Mutherbukin, and Limejuice Zones (Fig. 31 cf. Fig. 1).

These results indicate that prospectivity within the Gascoyne Province is focused towards the central parts of the province, in particular the Mooloo Zone northwest of the Deadman Fault, the Mutherbukin Zone, and the southern Limejuice Zone. According to our structural interpretations, these central regions have been subjected to a greater degree of intraplate reworking as the intraplate orogenic activity has stepped inwards through time, and hence may have greater potential for multiple ore-concentrating events. In all prospectivity analyses presented here, the northern and southern regions of the province are less prospective, perhaps representing a lesser degree of reactivation. The Errabiddy Shear Zone is, for most mineralization types, more prospective than the adjacent areas, but less so than the central region. With the exception of clustered PBM occurrences around Mt Alexander and Kirba Well (Fig. 31 cf. Fig. 1), the distribution of mineralization around the province echoes the trends revealed in the prospectivity analysis.

Conclusions

A structural interpretation, based on aeromagnetic images and gravity and magnetic inversions, has outlined the relative tectonic evolution of the Gascoyne Province. Each zone of the province shows a different sequence and style of structural events. Following the two main continent collisions responsible for the assembly of the West Australian Craton (the 2215–2145 Ma Ophthalmian Orogeny and the 2005–1950 Ma Glenburgh Orogeny), the province was subject to punctuated intracratonic reworking. Structural analyses presented here, demonstrate the inward-stepping nature of this orogenic reworking. The 3D inversion models show that the major tectonometamorphic zones of the province represent distinct crustal boundaries, the orientations of which have controlled the location and style of tectonic reworking.

Mineral prospectivity of the province was investigated using a mineral systems approach. The results demonstrate that rare earth element, gold, tin–tungsten, and base metal mineralization are more prospective closer to the major zone-bounding faults, implying a link between deep, mantle-tapping crustal structures, punctuated intracontinental reworking, and near-surface mineralization.

Appendix 1: Geophysical analysis methods

Interpretational confidence estimation

The reliability of the features interpreted in this Report depends on many factors, including interpreter biases and experience, but also, fundamentally, the degree to which the available data permits detailed tectonostratigraphic interpretations. As part of this work, we prepared a map of the influence of data richness, considered a proxy for interpretational uncertainty, to differentiate areas of relative data richness from areas of relative data poverty. This provides a guide to the reliability of the interpretation, and hence, the reliability of any analyses that are based in part upon it.

We followed the method of Aitken et al. (2013a), who combined a series of measures to estimate interpretational confidence for the west Musgrave Province. These included: 1) the abundance of outcrop and the quality of mapping that was applied to that outcrop, 2) the strength of gradients in the geophysical data, and the influence of structural complexity, and 3) gridding errors and the effect of anisotropic data collection on the resolution of gradients in the geophysical data.

Geological constraint

The first of the confidence measures was defined using a kernel density function applied to a rasterized geological map where, instead of lithology, an outcrop quality factor (OQF) was assigned. High OQFs indicate that high quality geological information was available for that outcrop, and that the outcrop's geology is relevant to the geology of interest.

For the Capricorn Orogen, we assigned OQF on the basis of: 1) the scale of available mapping, and 2) the age of the outcropping rocks. Given that the geology of interest is largely Proterozoic, we assign Proterozoic rocks the greatest influence (10), whereas Archean rocks (8) and Phanerozoic rocks (6) have reduced significance. We superimposed on this the difference between recent 1:100 000 scale mapping and older 1:250 000 scale mapping, and assigned outcrops in the areas mapped at 1:250 000 a value equal to one third of the OQF for outcrops mapped at 1:100 000 scale.

This OQF map was then regionally averaged using a kernel density function with a search radius of 5 km. Essentially, for each data point, this function generates a 'bell curve' with maximum amplitude (equal to the OQF) over the point, and zero amplitude beyond the search radius. At each point, the resulting function is the summation of the amplitude of every bell curve that overlaps that point. The resulting map (Fig. 1.1) shows high geological constraint through much of the central Capricorn Orogen, and is dominated by the outcrop

density, and by the difference between the scales of mapping. The age of outcropping rocks exerts a minor influence on OQF that is largely overridden by the above factors.

Data Interpretability

Potential field data are essential as these datasets primarily drive the interpretation. To define this, we followed Aitken et al. (2013a) and used the combined strength of a number of gradient/edge filters as well as the level of directional content in automatically picked features. We applied this analysis to both aeromagnetic and gravity data.

For gradient analysis we used the following filters: total horizontal gradient (Blakely and Simpson, 1986); standard deviation of texture (Holden et al., 2008); TDX (Cooper and Cowan, 2006); phase congruency (Holden et al., 2012). We combined these using a weighted sum of the normalized grids. In doing this summation, we considered the degree to which interpretation was amplitude independent, either through the use of filters (e.g. tilt derivative) or through nonlinear or spatially variable colour stretches. For the aeromagnetic data we used a ratio of 2:1 in favour of amplitude dependent filters (horizontal gradient and texture) over the amplitude independent filters (TDX and phase congruency) (Fig. 1.2). For the gravity data we used a ratio of 2:1 in favour of the amplitude independent measures (Fig. 1.3). These maps show a much more consistent image of uncertainty, due to the more regular coverage of geophysical data. However, magnetic data show some characteristic features including high feature strength in the Narryer Terrane and Paradise, Mooloo, and Mutherbukin zones, and less in the Errabiddy Shear Zone and beneath the Edmund and Collier Basins (Fig. 2).

A further measure of data interpretability is the level of structural complexity in the data. We used the level of directional content in the data as a proxy for structural complexity, as poly-directional data are typically more difficult to interpret than mono-directional or non-directional data. To compute this, we used the orientation entropy filter (Holden et al., 2012), applied to automatically picked linear features. We used eight orientation bins, permitting the separation of, for example, a feature trending north-northeast from a feature trending northeast. For aeromagnetic data, we used a sample window size of 5 x 5 km, which optimizes the trade-off between capturing detail and eliminating sensitivity to the abundance of features (Fig. 1.4). This filter shows low orientation entropy in the Carnarvon Basin, and slightly reduced orientation entropy in the Errabiddy Shear Zone, Edmund and Collier Basins (Fig. 2), and magnetic quiet zones. The gravity feature detection returned too few features for a meaningful characterization.

Data processing or collection errors

Finally, we considered the influence that an imperfect data distribution has on our ability to define geophysical anomalies correctly. For aeromagnetic data, based on the experience in the west Musgrave Province, data collection errors and gridding errors are negligible at this scale, and we excluded them from this analysis. For gravity, we considered the errors likely to result from gridding of imperfectly spaced data. We defined this from the statistical error returned during kriging (Fig. 1.5).

Gravity data used during this study were gridded at 2 km cell size, matching the highest resolution data collected. For spherical-cap Bouguer anomaly data gridded at 2 km cell size, kriging errors can be very high (as much as 4.4 mGal), reflecting the fact that data are in places quite sparse compared to the level of geological detail they are detecting. However, the central region is covered by a recent, closely spaced gravity grid (2 km grid), and errors here are significantly less (0–2 mGal).

Overall data richness map

We combined the above measures into an overall data richness map (Fig. 3 in main body of text) using a simple weighted summation of the individual grids (Equation 1). This process involved matching the relevant weighting factors to fit the interpreter's perception of their influence on interpretational confidence. For this work, the highest weighting (0.55) was assigned to the aeromagnetic data because they were the primary dataset from which features were interpreted. Within the aeromagnetic dataset, feature strength received a high weighting (0.8), whereas structural complexity received a lower weighting (0.2). Geological knowledge is a crucial constraint on the interpretation of the tectonic significance of the aeromagnetic features, and this received a moderate weighting (0.25). Gravity data received a similar but lower weighting (0.20) as these had less influence on the interpretation, within which feature strength (0.8) dominates over gridding errors (0.2).

$$\begin{aligned} \text{Data richness} = & w_1 \times \text{GC} + \\ & w_2 \times (\text{sw}_1 \times \text{MFS} + \text{sw}_2 \times (1 - \text{MSC})) + \\ & w_3 \times (\text{sw}_1 \times \text{GFS} + \text{sw}_2 \times (1 - \text{GGE})) \end{aligned} \quad \text{Equation 1}$$

where GC – geological complexity; MFS – magnetic feature strength; MSC – magnetic structural complexity; GFS – gravity feature strength; GGE – gravity gridding error. w_1 to w_3 indicate the major weightings, and sw_1 and sw_2 denote minor weightings within categories.

Magnetic susceptibility and density measurement methods

Magnetic susceptibility measurements were made with a GMS-2 magnetic susceptibility meter, which has a sensitivity of 1×10^{-5} SI units. For each specimen, several measurements were made, taking care to sample different faces of the specimen and different orientations. The arithmetic mean of these individual measurements is

considered indicative of the overall magnetic susceptibility of the individual specimen.

Specific gravity was determined using the relation between the weight of the specimen in air (dry weight) and the weight of the specimen suspended in water (wet weight; Equation 2). Each specimen was weighed on a bench top balance to determine the dry weight, and wet weights were established by suspending the specimen in water using a simple apparatus. Care was taken to ensure that the volume of the apparatus immersed as a result of the addition of the specimen was minimal. Most specimens were crystalline metamorphic or igneous rocks with low porosity, and so it was deemed unnecessary to establish the difference between a water-saturated specimen and an unsaturated specimen.

$$\text{SG} = W_D / (W_D - W_W) \quad \text{Equation 2}$$

where SG = specific gravity, W_D = dry weight, W_W = wet weight

Analysis

For analysis (Fig. 12), the susceptibility and specific gravity data were divided into relevant lithological groups. Population sizes were generally too small to permit detailed analysis, but basic statistical analysis was performed. We also provide a qualitative interpretation of how variability might relate to lithology.

2D combined gravity and magnetic modelling methods

Magnetic data for modelling were sampled from a reduced-to-pole (RTP) magnetic grid derived by stitching together RTP grids of several individual surveys with flight line spacings of 200–400 m, and nominal flying heights of 80–100 m. Most were flown north–south, but some were flown east–west. There are few visible artefacts resulting from the stitching process (Fig. 2a), but longer wavelength trends may be misrepresented as a result of the detrending process associated with grid stitching. The magnetic grid was upward continued by 100 m and was sampled at 500 m spacing. Magnetic calculations in modelling used a sensor height of 200 m above a flat model (ground) surface. For gravity modelling, terrain-corrected, spherical-cap Bouguer anomaly data from Geoscience Australia's national database were gridded at 2000 m cell size (Fig. 2b). Terrain corrections were not available for profile 5, and were therefore not included. This grid was also sampled at 500 m spacing for modelling. Gravity calculations used in modelling used a sensor height of 1 m above the surface.

Forward modelling is an effective and fairly robust method when applied using geological and petrophysical constraints, as well as constraints from other geophysical studies. The method used here involved as a first step the construction of an interpreted geological cross section, with the upper crust constrained predominantly by geological observations at the surface, and the lower crust constrained by seismic information.

Geological cross sections were constructed using the distribution of lithologies in mapped outcrop (where available) and interpreted geology elsewhere. In addition, the initial crustal structure was constrained by the GSWA WAROX (field observations) database of structural measurements. Measurements used include primary structures (bedding and igneous layering) and secondary structures (cleavages or foliations, fold plunges, etc.). Although these data provide a useful guide to the geometry of the subsurface, they are prone to error for several reasons. Firstly, these measurements are rarely exactly on the profile, and are typically clustered in dense groups. The structural geometry must therefore be averaged and extrapolated. This is particularly important where the measurements indicate structure that is nearly parallel with the profile. Secondly, with the exception of bedding, the structural data in this database are not always explicitly linked to particular deformation events or larger-scale structures. Finally, the structures indicated by these structural observations do not necessarily correlate with the geophysically defined features. The structural measurements used are indicated on the profile figures (Figs 13–17) by tick marks above the interpreted geology.

The Gascoyne Province has been the subject of several seismic investigations, including a major crustal-scale seismic reflection profile (Johnson et al., 2011a, 2013), passive seismic studies (Clitheroe et al., 2000; Reading et al., 2012), and also MT studies (Selway et al., 2009; Johnson et al., 2011a), from which a broader understanding of crustal structure can be established. For our profiles, the geometry of the Moho was sampled from the continent-scale compilation of Kennett et al. (2011), which includes Moho picks from the seismic reflection profiles, as well as all passive seismic stations for which receiver function analyses have been conducted. Gravity inversion modelling indicates that the resulting model is

quite robust beneath the whole Gascoyne Province, with 2σ errors typically less than 2 km (Aitken et al., 2013b). Hence, the Moho was not significantly modified during modelling, except to image small-scale structural detail resolved in the seismic reflection profile. From the seismic reflection profile, we also established the crustal-scale shear zone architecture. This shear zone architecture was used as a direct constraint on our models at cross-over points between our profiles and the seismic profile, and was used as a conceptual constraint for modelling away from the seismic lines.

The starting models were populated with statistically acceptable petrophysical properties to achieve an approximate fit before starting the modelling of near-surface structure. Near-surface structure, i.e. the top few kilometres, is primarily defined by generating a fit to the magnetic data, although short-wavelength gravity anomalies were considered where they are preserved in the data. Once near-surface structure was defined, the deeper crust was modelled, with an emphasis on the fit to the gravity data.

Ultimately, the models generated using this method can be considered as geological models of crustal structure that satisfy both gravity and magnetic data. As such, the models may include features that are not required by the geophysical data, but are supported by geological inference, and serve to illustrate the likely geological scenario. For example, thin layers were generally continued to depths beyond the limit of geophysical sensitivity on the basis that they are part of a conformable package of rocks. Furthermore, the petrophysical contrast between the different units is typically low, and lower than the variability within the units. Hence geological boundaries are not necessarily associated with strong geophysical anomalies, and vice versa.

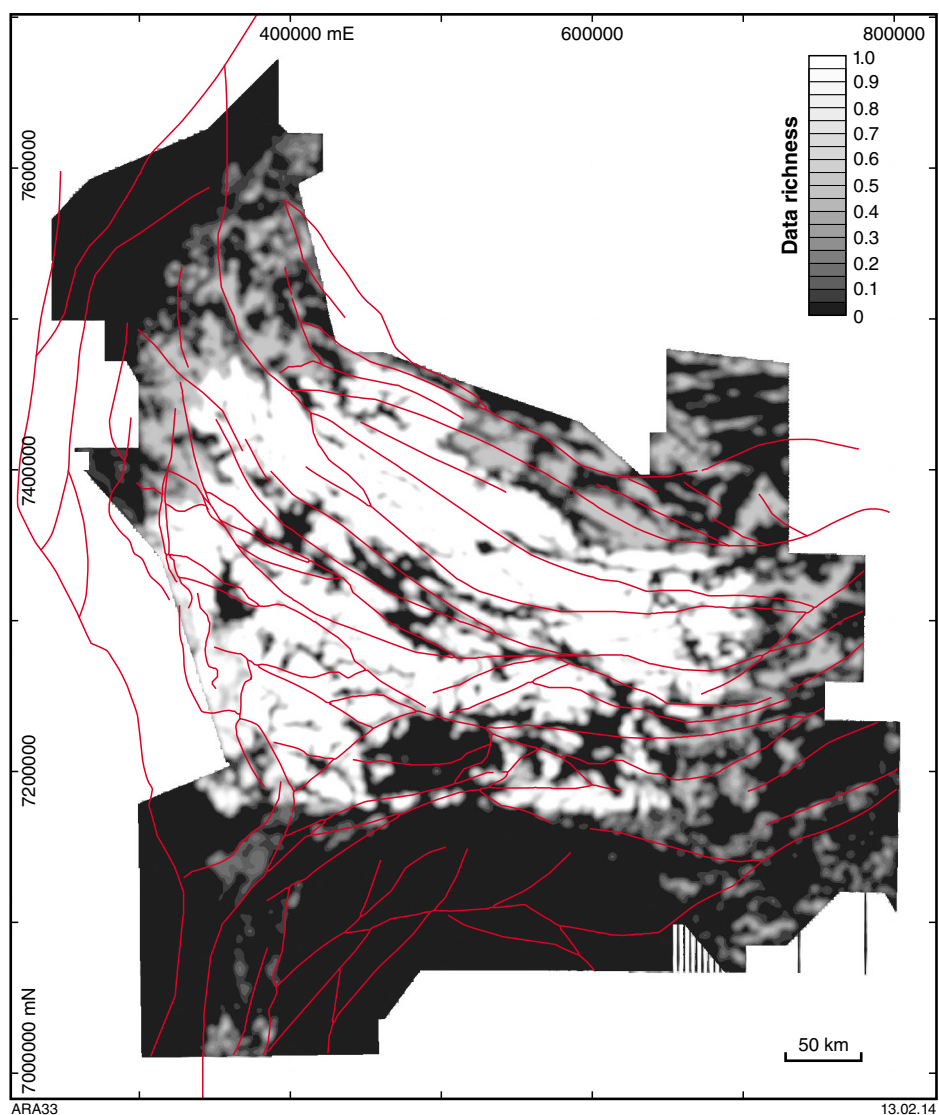


Figure 1.1. Normalized geological constraint, computed with a kernel density function of search radius 5 km. Red lines are crustal-scale faults

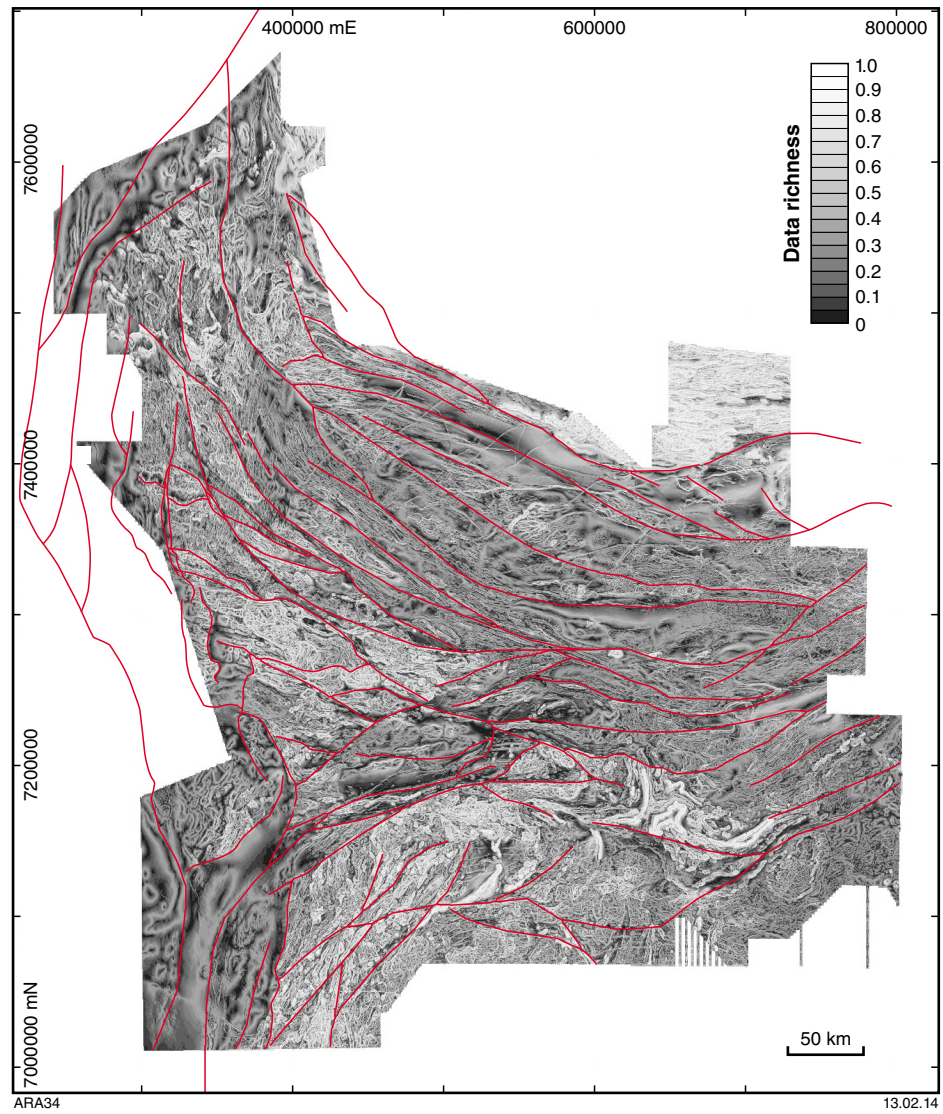


Figure 1.2. Normalized magnetic feature strength. Amplitude dependent measures (Texture, Horizontal gradient) have twice the influence of amplitude independent (TDX, Phase Congruency) measures. Red lines are crustal-scale faults

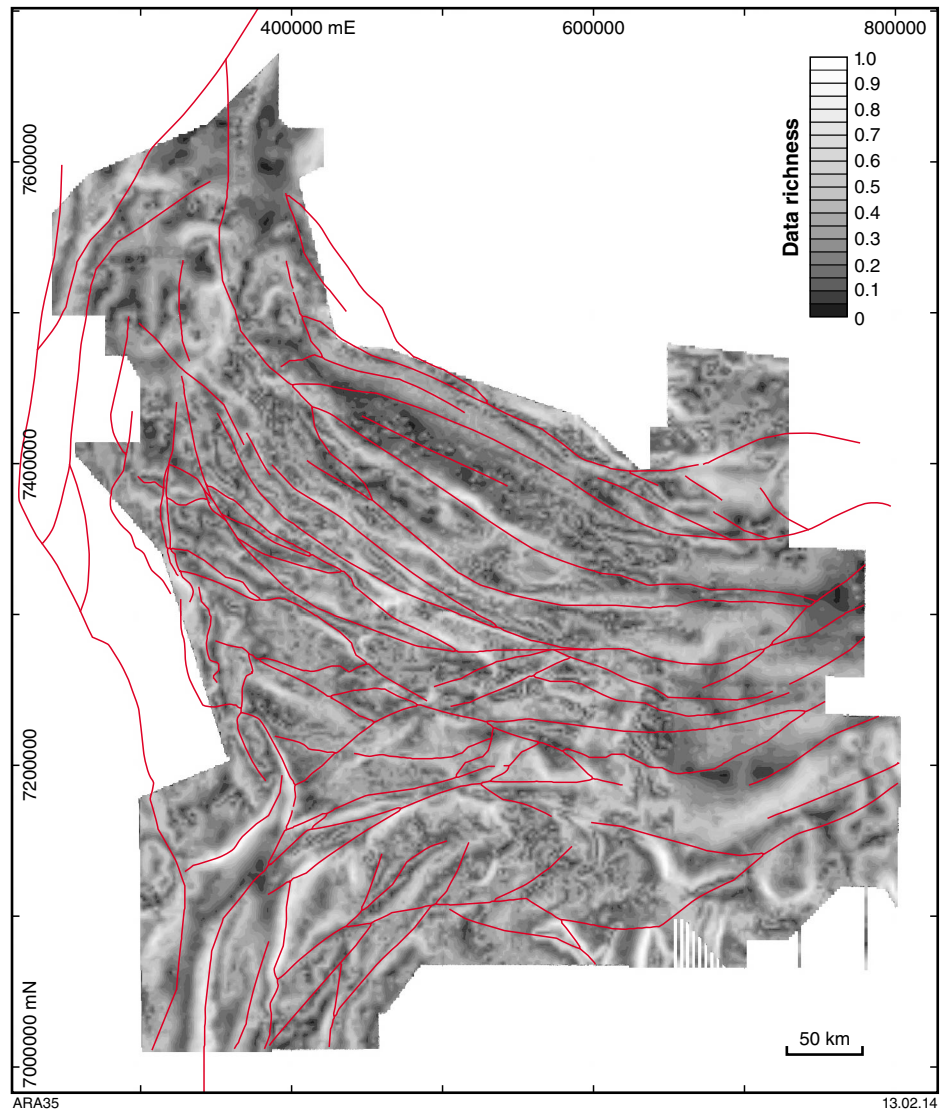


Figure 1.3. Normalized gravity feature strength. Amplitude independent measures have twice the influence of amplitude dependent measures. Red lines are crustal-scale faults

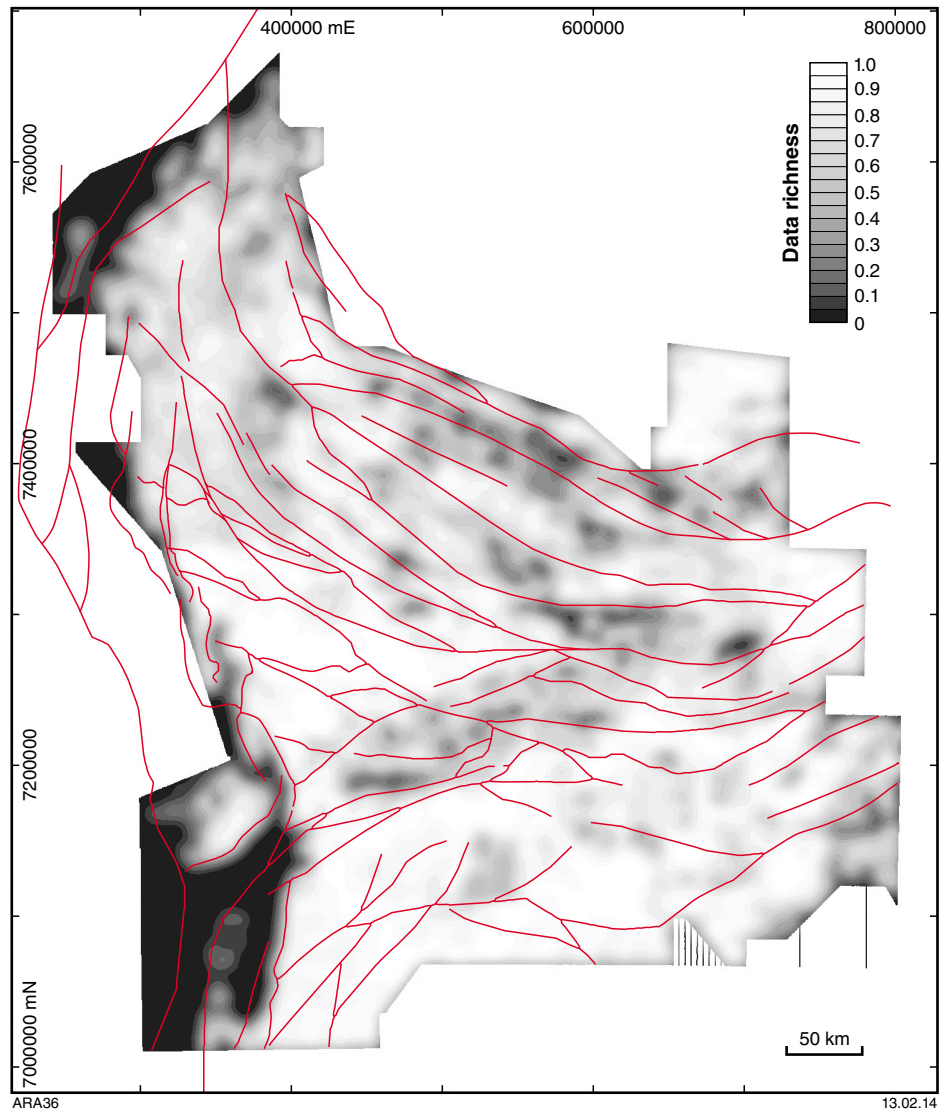


Figure 1.4. Normalized structural complexity (orientation entropy) of aeromagnetic data. Red lines are crustal-scale faults

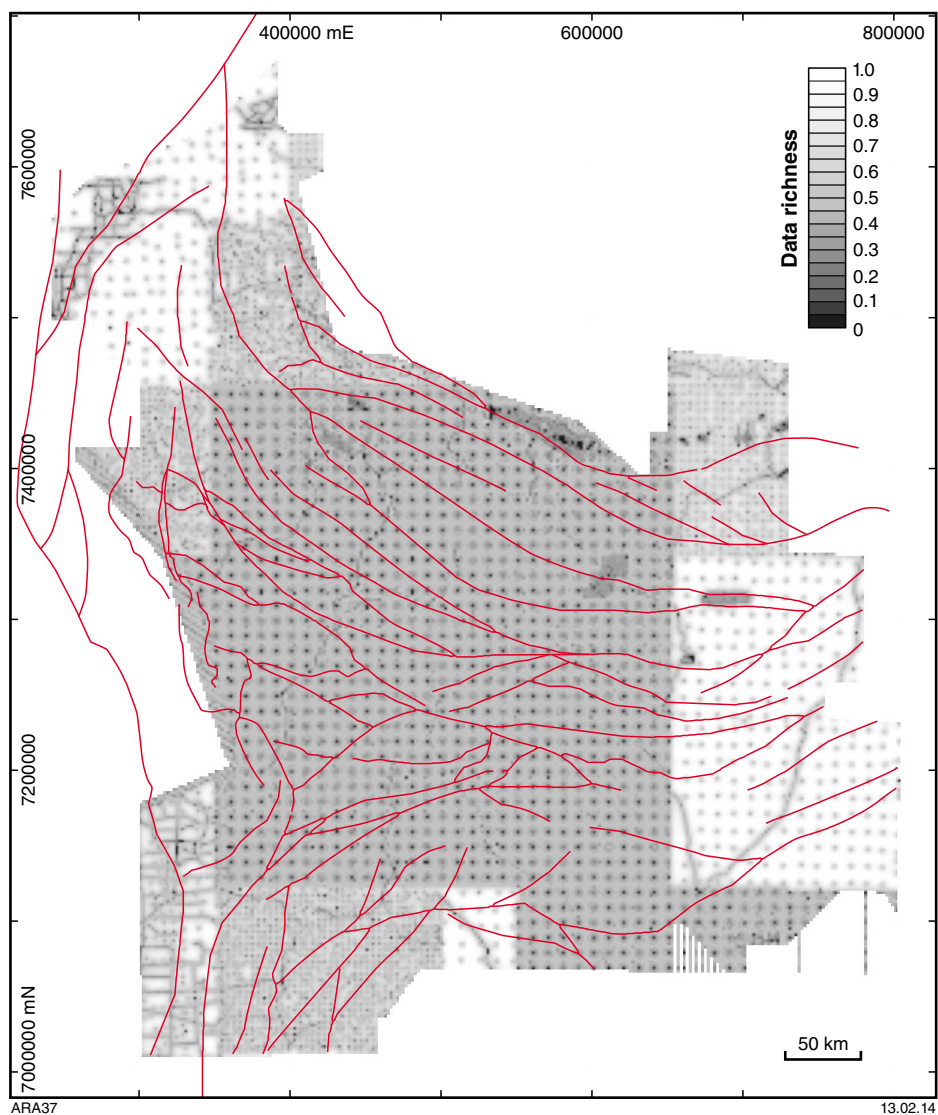


Figure 1.5. Normalized gravity data gridding error. Red lines are crustal-scale faults

Appendix 2: Fuzzy-logic mineral prospectivity

Detailed description of methods

Fuzzy logic is a knowledge-driven approach for prospectivity mapping that relies on expert opinion for choosing the input predictor maps and their associated weightings. The user assigns values between 0.001 and 10 for the map weight, class-weight and confidence factor, with values closer to zero representing a poor predictor for the style of mineralization being investigated or high uncertainty, and values closer to 10 representing a good predictor or low uncertainty. These three factors are multiplied together for each predictor map and normalized to a range between 0.001 and 1 to give a fuzzy value. The resulting fuzzy value maps are then combined using a fuzzy method appropriate to the mineral system (e.g. Fig. 18).

The fuzzy membership (or map weight) is the fundamental means to assess uncertainty in the fuzzy-logic method. The fuzzy membership defines how each point in the input space is mapped to a given set. Membership value (or degree of membership) is usually a real number between 0 (non-membership) and 1 (full membership).

A generalized fuzzy model for mineral prospectivity mapping can be defined as follows. If X is a set of n predictor maps X_i ($i=1$ to n) with r patterns (or classes) denoted generically by x_{ij} ($j=1$ to r), then n fuzzy sets \tilde{A}_i in X , containing ‘favourable indicators for the targeted mineral deposit type’, can be defined as follows (Porwal et al., 2003):

$$\tilde{A}_i = (x_{ij}, \mu_{\tilde{A}_i}) | x_{ij} \in X_i \quad \text{Equation 3}$$

where $\mu_{\tilde{A}_i}$ is the membership function for estimating the fuzzy value of x_{ij} in the fuzzy set \tilde{A}_i . The fuzzy-membership function can be linear, Gaussian, or any other appropriate function. In the present study, we used the following linear function:

$$\mu_{\tilde{A}_i} = \frac{m_i \times w_j \times cf_i}{1000} \quad \text{Equation 4}$$

where m_i is the map weight, w_j is the class-weight and cf_i is the confidence factor.

Map weights correspond to the importance of the prospective feature, and confidence factors relate to how reliable the data are as indicators of a chosen prospectivity factor. Map weights are subjectively assigned a value between 0.001 and 10 (10 being the most prospective) based on expert knowledge.

Class-weights correspond to the proximity function to the prospective feature. These are also subjectively assigned values between 0.001 and 10 (10 being the most prospective); however, the classes that are less

likely to have a relation to mineralization are assigned very low class-weights. These can be close to zero, but never actually zero, as there is still an unknown potential relation. For example, the proximity function may comprise a buffer zone which represents the maximum distance to the feature for it to be indicative of prospectivity. Areas beyond the buffer zone are assigned a class-weight of 0.001. In the analysis, zero values are not assigned because these values, when transmitted through the fuzzy inference network, could result in some areas being apparently entirely unprospective, even if they contained several other highly favourable indicators.

Confidence factors are assigned subjectively based on the perceived reliability of the data and their ability to accurately define the feature of interest. The perception of reliability is generally low when it is necessary to interpolate sparse datasets.

Fuzzy modelling is implemented in the following steps: 1) assigning map weights, class-weights, and confidence factors, and estimating fuzzy values for the fuzzy predictor maps; 2) combining the fuzzy predictor maps using an appropriate fuzzy inference network to derive the fuzzy prospectivity map (Joly et al., 2012).

Assigning map weights, class-weights and confidence factors

An understanding of the different mineral systems and the geological characteristics and history of the Gascoyne Province (Table 1) were used to assign the map weights and class-weights to the different fuzzy predictor maps. The fuzzy values for the predictor maps were estimated from the map weights, class-weights and confidence factor using equation 4.

The use of subjectively derived fuzzy-membership layers is a useful way of incorporating geological knowledge into GIS-based automated methods but does have three main drawbacks. Firstly, there is a loss of information when changing raw data values to fuzzy-membership values because a range of raw data values must be mapped to a single fuzzy-membership value (in this case, a map weight). Secondly, the fuzzy-membership values are usually applied according to the degree to which parameter values conform to a model of deposit formation, which itself may be flawed. Finally, the assignment of fuzzy-membership values is highly subjective and strongly reflects the operator’s personal bias (e.g. D’Ercole et al., 2000). Although spatial analysis can provide a basis for estimating the fuzzy-membership values — for example, the use by Knox-Robinson and Wyborn (1997) of statistically determined fuzzy-membership values — subjective judgement is used to determine the structure of the fuzzy inference net and to select the fuzzy operators used to combine the GIS layers.

Igneous and metamorphic-related REE mineral systems (carbonatite, pegmatite, veins)

Predictor maps

Source

In the Gascoyne Province, REE occurrences are hosted in granitic pegmatites and carbonatite complexes (Witt, 1990; Flint and Abeyasinghe, 2000). Pegmatites generally form by fractional crystallization of a granitic-type melt. It has, however, also been proposed that granitic-type melt can be formed by direct anatexis of rocks with the appropriate composition (Černý, 1991a,b). Based on petrogenetic considerations, three families of pegmatites are distinguished (Černý and Ercit, 2005): the NYF family with progressive accumulation of niobium, yttrium, and fluorine; the LCT family marked by prominent accumulation of lithium, cesium, and tantalum; and the mixed NYF + LCT family. As any type of REE pegmatites are considered to be of interest, all granitic rocks are considered as a REE source.

Alkaline igneous rocks form from cooling of magmas derived by small degrees of partial melting of rocks in the Earth's mantle. The resulting alkaline magmas are rare and significantly enriched in REE. The mineral deposits associated with these rocks are quite diverse and problematic to classify, in that the distinctive features of these deposits and their rarity can yield categories that have only one or a few known examples. In the Gascoyne Province, carbonatite sills, ferro-carbonatite-magnetite dykes, and iron oxide veins (ironstones) host REE mineralization (Pearson, 1996; Pearson and Taylor, 1996; Pearson et al., 1996; Pirajno and González-Álvarez, 2013). These are the only alkaline igneous rocks identified in the studied area.

We produced three predictor maps based on pegmatite and alkaline igneous rock source recognition: 1) a map of distance to any granite (Fig. 2.1); 2) a map of distance to alkaline igneous rocks (Fig. 2.2); 3) a map of the density of alkaline igneous rocks (Fig. 2.3). Alkaline igneous rocks in the database (GSWA, 2012) are delineated either as polylines or as polygons. We derived the density map from the polylines by measuring the density of all line features per square kilometre. Class-weights were defined by buffering the maps of distance to carbonatite and granite, with 5 km and 25 km wide zones around features, respectively. Within these buffered zones, class-weight reduces linearly from 10 to 0.001 with increasing distance. Those three maps are assigned a high map weight of 8 because they conceptually are the best representation of REE source. The confidence factor for these predictor maps was 8.

Pathways

Mineral exploration companies have long recognized the empirical relationship between ore deposits and major,

potentially mantle-tapping structures and fault corridors (Groves et al., 1998; Sillitoe, 2000; Grauch et al., 2003). Such structures are likely to provide pathways for fluids and play a major role in focusing mineralized fluids into the upper crust. Essentially, these zones represent trans-lithospheric columns of low strength and high permeability (Cox et al., 2001). We used the distance to crustal-scale faults determined from the structural analysis as the criterion for mineralization related to pathways (Fig. 2.4). Class-weight was defined by, placing a 10 km wide buffer zone around the faults, within which class-weight reduced linearly from 10 to 0.001 with increasing distance. A map weight of 9 was assigned since such faults are considered to be essential components of the mineral system that promote crustal contamination. The confidence factor for this predictor map was 8.5.

The Proterozoic Gifford Creek Ferrocarbonatite Suite is a high-level alkaline complex. U–Th–Pb SHRIMP monazite age data constrains carbonatite magmatism to c. 1300 Ma; i.e. during the Mutherbukin Tectonic Event (Johnson, 2013).

In the Nardoo Hills area, monazite from a rare-element pegmatite (sample UWA 117154; Trautman, 1992) was dated using the SHRIMP U–Th–Pb system and provided a weighted mean $^{207}\text{Pb}/^{206}\text{Pb}$ age of 954 ± 12 Ma (Sheppard et al., 2007). Thus, REE pegmatite emplacement occurred during the Edmundian Orogeny (Pearson et al., 1996; Davies, 1998; Foley, 2008; Sheppard et al., 2010b).

Since structures associated with the Edmundian and Mutherbukin events are coeval with the alkaline complex and pegmatite emplacement, respectively, they are also potentially critical pathways for transporting REE mineralizing fluids. Therefore, we produced a predictor map of distance to either Edmundian or Mutherbukin structures with a 5 km buffer zone and with a high map weight score of 9 (Table 2.1, Fig. 2.5). The confidence factor for this predictor map was 8.5.

Pre-Mutherbukin structures are important as they are commonly reactivated structures that could tap crustal fluid and a possible unexposed alkaline intrusive body. On this basis, we produced a predictor map of distance to pre-Mutherbukin structures with a 5 km buffer (Fig. 2.6, map weight = 8, confidence factor = 8.5). Post-Edmundian structures could remobilize REE-rich sills (Pearson et al., 1996), or could be reactivated older structures, hence are also potential predictors. Again, a 'distance to' map was produced with a 5 km buffer width. This predictor map was given a map weight of 7 and a confidence weight of 8.5 (Fig. 2.7).

The last type of indicator for REE fluid flow is the occurrence of breccias. These rocks are evidence of fluid circulation and hydraulic fracturing. Thus, areas with more breccias, stockwork, and veins are more likely to be areas where mineralized fluids circulated. We attributed a map weight of 8 to the 'breccia density' map that is derived by mapping the density of breccias, stockwork, and veins in areas of one square kilometre (Fig. 2.8). Confidence weight is 7.

Traps

Deposition of metals is triggered by chemical and physical processes that alter the make-up of melts or fluids migrating through trap zones. Fluids in the trap can concentrate their solutes and form deposits.

REE metamorphic and igneous rocks are enriched in uranium and thorium. Therefore, both elements are potential indicators of REE trapping, for which both a physical and chemical traps are required (Fig. 18). Radiometric data are the best available predictor for uranium and thorium content, provided that occurrences are very close to the surface. We generated the radiometric-Th and radiometric-U content map for surface deposits using all such data above the threshold ζ (with $\zeta = x(\log [U]) + 2\sigma(\log [U])$, Figs 2.9 and 2.10). A map weight of 8 and a confidence factor of 9 is assigned to both maps.

The lithium (Li), tantalum (Ta), cesium (Cs), niobium (Nb), yttrium (Y), fluorine (F), and beryllium (Be) contents of rocks are the most direct evidence of LCT-type and NYF-type pegmatite chemical and physical traps. We used the concentrations of these elements in GSWA and Geoscience Australia geochemical databases to create the predictor maps. A map weight of 8 and a confidence factor of 7 was assigned to each (Figs 2.11 – 2.17). These chemical abundances are considered to be a direct indicator of the likelihood that trapping has occurred, which requires both a physical and chemical trap. Hence, they are included in both the physical and chemical components of the trap calculations.

Physical traps

Favourable REE traps are physical traps (e.g. brittle–ductile shear zones, stockwork, breccias) where mineralizing fluid flow was focused in the presence of a favourable geochemical environment (Groves et al., 1998; Hagemann and Cassidy, 2000). Such throttles may include breaches (e.g. through impermeable stratigraphy) or localized damage zones on regional faults. Contacts between geological units with a high competency contrast are considered particularly favourable trap sites. We have created a predictor map by assigning to each generalized lithological unit a (relative) rheology value (Fig. 2.18), then attributed each geological contact with the difference in the rheology between units on each side. The ‘competency contrast across geological contact’ map (Fig. 2.19) was derived by allocating to each unit cell the value of the rheology difference of the nearest contact, up to a maximum distance of 1 km. We assigned this a map weight of 8 and a confidence factor of 7.

Higher geological contact densities imply increased probability of competency differences, and hence increased fault/fracture densities and space for trapping metal. Therefore, we derived a ‘geological contact density’ map by mapping the density of geological contacts in areas of one square kilometre (Fig. 2.20) and attributing with a map weight of 7 and a confidence factor of 7.

We also created a ‘geological contact density weighted by competency contrast’ map to capture the competency

contrast at some contact (Fig. 2.21). This map was derived by mapping the geological contact densities per square kilometre weighted by competency contrast and was given a higher map weight of 9. Confidence factor remains at 7.

The most favourable REE traps occur in brittle–ductile shear zones (Long et al., 2010). Maps of fault occurrence density (Fig. 2.22), the distance to fault intersections, buffered to 5 km (Fig. 2.23), and fault intersection density (Fig. 2.24) are proxies for structural complexity, hence likely sites of fluid focusing. Fold axes are conceptually good traps for hydrothermal fluids, hence a predictor map of distance to fold axes (Fig. 2.25) was created, again buffered to 5 km. These four factors are probably less important than the geological contact density weighted by competency contrast map and were assigned map weights of 7.5 or 8 (Table 2.1), but they have higher confidence factors (9).

Pegmatites are recognized as REE physical traps (Partington et al., 1995; Černý and Ercit, 2005). Two predictor maps were generated: 1) a distance to pegmatite (Fig. 2.26) which was buffered to 5 km to derive the class-weight; 2) a pegmatite density map (Fig. 2.27). These were each assigned a map weight of 8 and confidence factors of 6 and 8, respectively.

Finally, stockworks and veins are known to contain REE (Long et al., 2010). The predictor map of veins and stockwork density (Fig. 2.28) was generated by mapping the veins and stockwork per square kilometre, and assigned a map weight of 8 and a confidence factor of 7.

Chemical traps

Cooling and fractionation of pegmatite is important for a good REE chemical trap. Pegmatites are formed at pressures (4 to 1.5 kbar) generally similar to the pressures at which the host rocks of upper-greenschist to lower-amphibolite facies metamorphism are formed. Under these conditions, pegmatites are well preserved (Černý, 1991a,b; Černý and Ercit, 2005). In addition, metasomatic rocks are a good chemical trap as the anatexis process allows good preservation of REE-bearing rocks. The anatexis of Proterozoic volcano-sedimentary sequences preserve REE pegmatites well (Černý and Ercit, 2005).

To image these two processes, two predictor maps were created. The distance to medium/high-grade metamorphic facies rocks (Fig. 2.29) acts as a proxy for the first. The distance to anatectized Proterozoic volcano-sedimentary sequences (Fig. 2.30) acts as a proxy for the second. Each has a 5 km buffer zone, and these were each assigned map weights of 8 and confidence factors of 7 and 6, respectively.

Fuzzy model

Combining fuzzy-membership values

The map weights and confidence factors for each of the 30 predictor maps used in this study, including the rationale for assigning these values, are shown in Table 2.1.

Fuzzy predictor maps were combined using a four-stage inference network (Fig. 18). In the source component, fuzzy predictor maps for distance to alkaline igneous rocks (GIS polygons) and alkaline igneous rock density (GIS polylines) were firstly combined using the fuzzy OR operator to create a fuzzy alkaline igneous rock predictor map. The fuzzy OR is used because both maps represent the same proxy but do not indicate the same location. For the same reason, when determining the physical trap component, the two predictor maps distance to pegmatite (GIS polygons) and pegmatite density (GIS polylines) were merged using the fuzzy OR operator.

Next, a single fuzzy predictor map for each critical component of the REE mineral system (source, pathway, chemical trap, physical trap) was generated using the fuzzy OR operator. This operator was selected because the presence of any of the predictor maps is sufficient to infer the presence of the respective component. The fuzzy predictor maps for physical trap and chemical trap, in a third stage, were then combined to derive a single predictor map for traps using the fuzzy AND operator. The fuzzy AND operator was selected because both the physical trap sites and the conducive geochemical environment are necessary for precipitation of REE from the mineralization fluids. Finally, the three fuzzy predictor maps for source, pathway, and traps were combined using the fuzzy PRODUCT operator to create the output fuzzy prospectivity maps shown in Figure 19.

Orogenic and intrusive gold mineral system

Predictor maps

In the following subsections, details of the fuzzy predictor maps generated for the gold prospectivity analysis is given along with their geological rationale (Table 2.2). The predictor maps were combined in a four-stage inference network (Fig. 20) to generate the final prospectivity maps (Figs. 21 and 22).

Source

Gold-bearing hydrothermal fluids in the case of intrusion-related gold systems are typically derived from granitic intrusions; hence, gold mineralization is most likely in the vicinity of granitic bodies, with the probability of mineralization decreasing with the increasing distance from the granitic rocks (Fig. 2.1). We assigned a map weight of 7 (Table 2.2) and a confidence factor of 7, and used a 25 km buffer.

For orogenic gold systems, the metal and fluids are generally considered to be related to regional metamorphism and to have no direct genetic relation to granitic intrusions. To reflect the controversy regarding the importance of granitic rocks in deposit genesis, we ran a separate fuzzy analysis disregarding the source component altogether, and excluding areas with granite at the surface.

Pathways

Transport of large quantities of ore components from source to trap regions can only occur and be sustained where fluids have access to permeable pathways. These conduits are commonly active faults or shear zones. However, permeability can be rapidly destroyed by fracture sealing during mineral deposition. Hence, deformation must be on-going for structures to be continuously or repeatedly active and to maintain their effectiveness for passing the enormous volumes of fluid and metals required to produce a sizeable gold deposit (Kreuzer et al., 2008). Gold is leached from crustal rocks and deposited by large-scale hydrothermal systems involving extensive plumbing systems at, or above, the brittle–ductile transition (Groves and Phillips, 1987; Groves, 1993; Groves et al., 1998; Phillips and Powell, 2009). Faults and shear zones are therefore the most likely critical pathways for mineralizing fluids and crustal-scale examples are probably the most important (McCuaig et al., 2010; Joly et al., 2012). We therefore use the map for distance to crustal-scale fault (Fig. 2.4) and assign a map weight of 9 and a confidence factor of 8.5. In this case a buffer of 10 km was used to create the predictor map.

The primarily base metal Glenburgh deposit is intimately associated with Paleoproterozoic magmatic-arc rocks, the Dalgaringa Arc, which formed along the southern margin of the Glenburgh Terrane during the Glenburgh Orogeny (Occhipinti et al., 2004; Sheppard et al., 2004). Subsequent greenschist facies alteration has remobilized the primary deposit into shear zones of Mulka Tectonic Event age (Dynasty Metal Australia Ltd, 2011; Energy Desert, 2011; Johnson et al., 2011a). The recognition of ore mobilization along the Glenburgh and Mulka structures implies that they are the most likely critical pathways for mineralizing fluids. Therefore, a predictor map was created for each, showing distance to faults of these ages with a 5 km wide buffer. These are assigned to a high map weight of 9, and a confidence factor of 8.5 (Glenburgh) or 9 (Mulka) (Figs 2.31, 2.32).

Any faults predating the Glenburgh deposit could be reactivated and any younger faults could have remobilized gold, so these faults are potentially significant. For this reason, all other faults were combined into a single map, with 5 km buffer zones (Fig. 2.33). A relatively low map weight of 7.5 was used, to reflect a lower perceived prospectivity compared to Glenburgh and Mulka event structures. Confidence factor was 8.5.

Gold content around these faults is a key predictor of prospectivity. Across the province, surface gold concentrations from GSWA geochemical data vary between 0.001 and 0.73 ppm. Each fault was buffered to 5 km and the median gold value in each buffer was extracted and attributed to the buffer (Fig. 2.34). The result is a derivative predictor map which combines proximity to all faults and gold assay, and hence is a very reliable indicator of pathways. We assign a map weight of 9. Confidence factor is quite low, 6, due to uncertainty as to whether gold content is correctly assigned to structures, given the uneven density of geochemistry data points.

There is growing evidence to link alkaline rocks to a previously melt-metasomatized mantle source. Therefore, alkaline rocks could indicate the presence of trans-lithospheric faults (Mutschler and Mooney, 1993). Hence, we used the predictor maps alkaline rock density and distance to alkaline/carbonatite rock (Figs 2.2 and 2.3) and assigned map weight of 8 and confidence factors of 8 to each.

Areas (116.5°E, 24.4°S) of mineralized quartz veins were identified during 2010 in the Gascoyne Province (Gascoyne Resources Limited, 2012). A quartz vein system has returned values up to 7.8 g/t Au along a strike length of 350 m. Hydrothermal breccias, stockwork, and veins indicate fluid pathways (Fig. 2.28). We used the density of these features, and attributed a map weight of 8 and a confidence factor of 7.

Traps

Trapping is required to concentrate the metal via some physical, chemical or geological mechanism to a level that forms mineable ore.

Gold (Au), arsenic (As), and antimony (Sb) concentrations are potential indicators of the presence of gold even if the concentration is relatively low and localized over the whole area (Phillips and Groves, 1983), and the concentrations of these may be used as both chemical and physical trap predictor maps (Figs 2.35 – 2.37). The gold prospectivity map is a direct indicator of gold content, and hence was assigned a map weight of 9. Arsenic and Sb sulfide mineral occurrences are often associated with gold mineralization (Cline, 2001), therefore As and Sb are possible indicators of gold mineralization, and we attributed to these maps a weight of 7. Confidence factors of 7 were assigned to these predictor maps due to uncertainties related to interpolation of a non-ideal sample distribution.

Physical traps

Trap zones (i.e. effective melt or fluid channels) focus mineralized fluid migration. A trap needs to be sufficiently wide to accommodate large amounts of metal but narrow enough to efficiently focus melt or fluid migration during protracted or brief and repetitive events of energy and mass flux. We used the six predictor maps previously used for the REE analysis: competency contrast across geological contacts (Fig. 2.19), geological contact density (Fig. 2.20), geological contact density weighted by competency (Fig. 2.21), fault density (Fig. 2.22), distance to fault intersection (Fig. 2.23), fault intersection density (Fig. 2.24), and distance to a fold axis (Fig. 2.25). Map weights were between 7.5 and 9, and confidence factors were between 7 and 9 (Table 2.2).

Chemical traps

Gold deposition can occur due to changes in physical conditions, abrupt changes in chemical gradient, phase separation, and/or fluid mixing. Dramatic reduction in fluid pressure can induce chemical changes that can, in turn, trigger gold precipitation (McCuaig and Kerrich, 1998).

Gold deposition can occur in fluid–wallrock reactions where iron-rich minerals in the wallrocks react with gold-sulfide complexes in the fluids, resulting in desulfidation of the fluids and breakdown of gold-sulfide complexes (Phillips and Groves, 1983; Groves et al., 1998; Mikucki, 1998; Hagemann and Cassidy, 2000). Therefore, we created a map showing the distance to iron-rich rocks — e.g. the presence of magnetite, hematite, banded iron-formation (Fig. 2.38) — using the interpreted bedrock geological map (GSWA, 2012). A 5 km buffer zone was used and we assigned a map weight of 9 and a confidence factor of 7.

The Camel Hills and Leake Springs Formations and the Gifford Creek Ferrocarbonatite Suite (GSWA, 2012) constitute locations where there is high lithological diversity (and hence rheological contrast), and high reactivity due to iron-rich rocks. We created a predictor map of the distance to these favourable gold host units with a 5 km buffer, and assigned a map weight of 9 and a confidence factor of 7 (Fig. 2.39).

Rocks with a high Fe/(Mg+Fe+Ca) ratio are more prone to sulfidation reactions. We allocated each generalized lithology a (relative) chemical reactivity value that is estimated based on the sulfidation index given by the ratio $\text{Fe}^{2+}/(\text{Fe}_{\text{total}} + \text{Ca}^{2+} + \text{Mg}^{2+})$ (Fig. 2.13; Groves, 1993). Units with a sulfidation index of 4 and 5 are selected to generate a predictor map of with a 5 km wide buffer around these units (Fig. 2.40). Sulfidation is an important process in gold mineralization, hence we assigned the highest map weight (9) to the reactivity map. Confidence factor is 7.

In addition, we created a map of chemical reactivity contrast across geological contacts (Fig. 2.41) by using the generalized lithology allocated with the chemical reactivity value (Fig. 2.13). Each contact is then attributed with the difference in chemical reactivity between the lithological units on each side of the contact. A map of reactivity contrast is derived by allocating to each unit cell the value of the chemical reactivity difference from the nearest contact, up to a maximum distance of 1 km.

A map of geological contact density weighted by reactivity contrast was derived using the values in the chart shown in Figure 2.13, then mapping geological contact densities per square kilometre, weighted by reactivity contrast (Fig. 2.42). Chemical reactivity contrast across geological contacts and reactivity contrast only show chemical contrast, hence we assigned this map, a map weight of 7 (Table 2.2). Confidence factor is 7 for each of these.

Dykes are conceptually prospective hosts for gold because of their (relatively) high iron content, and hence reactivity. We generated two predictor maps, a dyke density map using the GIS polylines (Fig. 2.43 and the distance to dykes using the GIS polygons (Fig. 2.44; GSWA, 2012). We allocated a map weight of 9 to these predictor maps.

Finally, Fe_2O_3 content is a good proxy for areas prone to desulfidation (map weight = 8) and the breakdown of gold complexes due to fluid–wallrock reactions. We include a map of this based on the Geoscience Australia (GA) and GSWA geochemical databases (Fig. 2.45).

Fuzzy model

Combining fuzzy-membership values

Fuzzy predictor maps were combined using a four-stage inference network (Fig. 20). First, fuzzy predictor maps for distance to dyke and dyke density, as well as distance to alkaline rock and alkaline rock density, were merged using the fuzzy AND operator to produce single fuzzy dyke and alkaline rocks predictor maps. Fuzzy predictor maps for pathway, and chemical and physical traps were combined using the fuzzy OR operator to create a fuzzy predictor map for each critical component of the gold mineral system. This operator was selected because the presence of favourable conditions in any of the predictor maps is sufficient to infer the presence of the respective component. The fuzzy predictor maps for physical trap and chemical trap were combined to derive a single predictor map for traps using the fuzzy AND operator. The fuzzy AND operator was selected because both the physical trap sites and the conducive geochemical environment are necessary for precipitation of gold from the mineralization fluids. Finally, the three fuzzy predictor maps for source, pathway, and traps were combined using the fuzzy PRODUCT operator to create the output fuzzy prospectivity maps for intrusion-related gold (Fig. 21).

The orogenic gold model assumes that proximity to granitic rocks (source) is not a critical input for a camp-scale prospectivity analysis. A second inference network was then applied to assess orogenic gold prospectivity by disregarding the source component (proximity to granitic rocks) and deriving the prospectivity map based only on pathway and trap (Fig. 22). The area where granitic rocks are present at the surface was excluded from this analysis.

Surficial uranium mineral system

Predictor maps

A four-stage inference network (Fig. 24) was used to estimate prospectivity for surficial uranium. The geological basis for the source, pathway, and trap components of the MSA follows.

Source

A nearby source enriched in uranium may, or may not, be necessary to form surficial uranium deposits. Uranium is highly soluble under oxidizing conditions and insoluble under reducing conditions, meaning that it is highly mobile in the near-surface environment and may be concentrated extremely efficiently even though the source may be low in uranium. Nevertheless, the presence of uranium-rich granitic rocks is considered to be an advantageous component of the mineral system. Therefore, we used 'distance to granitic rocks of any age' as a spatial proxy for source (Fig. 2.1, map weight = 8, confidence factor = 8). A 25 km buffer was applied.

Pathways

Oxidized groundwater is the primary medium for uranium transportation in solution. Groundwater is drawn to the surface by evaporation in fluvial (paleochannel valleys) and playa systems. Paleochannels are the main pathways for groundwater flow.

The Gascoyne Province has experienced no known major tectonic event during the Cenozoic. The present-day drainage system essentially follows ancient drainage and may be used as a proxy for the presence of paleochannels. We therefore mapped the distance to third-order and higher level present-day drainage systems using Shuttle Radar Topography Mission (SRTM) topographic data and a drainage-tracing algorithm. Possible minor shifts in the drainage network were accommodated by establishing a 10 km wide zone around the drainage system (Fig. 2.46). This predictor map is assigned a map weight of 9 and a confidence factor of 7. In addition, paleochannels were mapped in the field on the MOUNT PHILLIPS 1:250 000 map; we used the field-delineated contour with a 10 km buffer zone (GSWA, 2012). This predictor map (Fig. 2.47) was assigned a map weight of 9 and a confidence factor of 6.

Traps

Radiometric data are the best available predictor for uranium content, provided that occurrences are very close to the surface. We used the radiometric-U content map for surface deposits (Fig. 2.9). We also used U content extracted from the GSWA geochemistry database (GSWA, 2011) and GA Ozchem database (Champion D. C. et al, 2007) to generate the predictor maps for both chemical and physical trap components (Fig. 2.48). Map weight is 8 in both cases and confidence factor is 9 for the radiometric map and 7 for the GSWA geochemistry map. This reflects the sub-optimal distribution of geochemistry data points.

Physical traps

Valley calcrete and playa sediments provide a favourable environment for carnotite deposition. The predictor map of valley calcrete (Fig. 2.49) was derived from the surface geological data for calcrete provided by GSWA (2012), with a 1 km buffer. The playa sediment map (Fig. 2.50) was derived from surface geological data (GSWA, 2012), with a 1 km buffer. The permeability of coarse-grained calcrete is normally greater than the permeability of playa sediment. Highly permeable rock provides the most favourable host rocks for large, relatively high-grade surficial uranium deposits. A map weight of 8 was therefore given to the map of valley calcrete (confidence factor = 8), and a map weight of 7 (confidence factor = 8) was attributed to the playa sediment map.

Chemical traps

Uranium precipitation is a reduction–oxidation process that involves U fixation by vanadium. We therefore created a 'V content' predictor map (Fig. 2.51). Vanadium

can equally well be provided by mafic and ultramafic rocks, dykes, and volcanic units. Hence, distance to mafic/ultramafic rocks, dyke density, distance to dykes, and distance to other volcanic units can also be used as chemical trap maps (Figs 2.52, 2.43, 2.44, and 2.53 respectively). Five-kilometre buffers were applied to the distance-based maps.

We assigned all the chemical trap predictor maps a map weight of 8, except for the volcanic units, which we assigned a map weight of 7.5 because these may contain felsic rocks that are less chemically reactive. Confidence factors are 8 for all but the vanadium content, which is 7 due to interpolation uncertainties.

Fuzzy model

Combining fuzzy-membership values

Table 2.3 summarizes the map weights and confidence factors, and the rationale for assigning these values for each of the predictor maps used in this study.

Two types of uranium prospectivity analyses were run: one focused on the whole Gascoyne Province, and one on the MOUNT PHILLIPS 1:250 000 map sheet area, where additional paleochannel mapping has been conducted (GSWA, 2012). Uneven data coverage in the geochemical datasets leads to boundary and radial flaring effects related to the lack of data at map edges or related to interpolation.

A four-stage inference network was designed to combine the fuzzy predictor maps (Fig. 24). In the physical trap component, U-content maps from the geochemistry data and radiometric data were firstly combined using the fuzzy OR, so as to include any high uranium contents. The predictor maps for valley calcrete and playa sediment were also combined using the fuzzy OR. In the chemical trap component, the dyke density and distance to dyke maps were combined using the fuzzy OR because both do not represent the same attribute. All elements for the chemical traps and physical traps were then combined using fuzzy OR, because the presence of any one of the elements is sufficient. A combined physical and chemical trap map was generated using the fuzzy AND operator because both types of trap sites are necessary for precipitation of uranium from oxidized waters.

The pathway component was analysed differently in the MOUNT PHILLIPS area and the regional analysis. For the MOUNT PHILLIPS area, both paleochannel predictor maps were merged using the fuzzy OR, as paleochannels are represented in two different ways: distance to polygons, and polylines derived from the SRTM. For the regional analysis, only the paleochannel polylines from SRTM were considered. The 'distance to granites' map was used directly as the predictor map for source. Finally, the three fuzzy predictor maps for source, pathway, and traps were combined using the fuzzy PRODUCT operator to derive the output fuzzy prospectivity maps (Figs 25 and 26).

Porphyry base metal mineral system

Predictor maps

In the following sub-sections, details on the fuzzy predictor maps generated for the porphyry base metal (PBM) prospectivity analysis are given, together with their geological rationale (Table 2.4). The predictor maps were combined into a four-stage inference network (Fig. 28) to generate the final prospectivity map (Fig. 29).

Source

Porphyry base metal systems are initiated by injection of oxidized magma saturated with S-rich and metal-rich, aqueous fluids from cupolas on the tops of the subjacent parental plutons. Hydrothermal activity associated with these magmas produces deposits with an element association compatible with their source, including variable combinations of Au, Co, Cu, F, Fe, LREE, Ni, P, Pd, P, Th, and U (Mathur et al., 2002). Mafic intrusions are the most likely to be donors of Cu (Johnson and Cross, 1995); hence, we generated a distance to mafic rocks predictor map using a 10 km wide zone around those units extracted from the interpreted bedrock geological map (GSWA, 2012), and assigned a map weight of 9 and a confidence factor of 7 (Fig. 2.54).

The sources of metals in PBM deposits are variously inferred to have been primitive calc-alkaline arc magmas (Sillitoe, 2003), I-type or A-type granitoids in debated intracratonic or distal arc settings in Australia and North America (Pollard et al., 1998), or carbonatite to strongly alkaline magmas (Groves and Vielreicher, 2001).

A- and I-type granites are considered critical for PBM deposit formation (map weight = 9, Table 2.4), although in some cases the deposits can be spatially separated from such magmas (e.g. Olympic Dam deposit). Consequently, a lack of surface expression of magmatism does not necessarily translate into unfavourable conditions for PBM mineralization. In the Gascoyne Province, the Thirty Three Supersuite granites are A-type (potassium-rich) granites, whereas the Dalgaringa and Moorarie Supersuite granites are I-type (sodium-rich). The Moorarie Supersuite is both oxidized and fractionated, and is associated with a few small Au and Cu prospects (e.g. Minnie Springs) in the southeast.

The lack of distinction between A- and I-type granites in the Gascoyne Province mapping means we consider all granites collectively (Fig. 2.1). We have generated a predictor map with a 10 km wide buffer around granitic intrusions, and assigned a map weight of 9 and a confidence factor of 6, reflecting the lack of discrimination between granite types.

PBM systems may be spatially associated with alkaline rocks that involve very reactive fluids associated with short-lived magmatism (Sillitoe, 1973; Mark et al., 2000).

Alkaline rocks are indicative of metasomatized mantle lithosphere (Mathur et al., 2002). Two predictor maps were created: distance to alkaline rocks (Fig. 2.2) and alkaline/carbonatite rock occurrence density (Fig. 2.3) are used with a map weight of 8. This is slightly lower than the other predictor maps to reflect the less common relationship with PBM deposits (Sillitoe, 2010). Confidence factors are 8 for these maps.

Pathways

Extensional and transtensional faults can channel hot, deep-seated fluids upwards and cold surface waters downward, allowing fluid mixing, large-scale alteration, and mineralization. The depth at which fluid and metal recharge and discharge take place will influence the resulting alteration and mineralization patterns. In a general sense, all faults before the Carnarvon event can be prospective within this scenario, although crustal-scale faults are required as fluid conduits in a PBM system. Also, Cu–Pb–Mo prospects at Minnie Springs are located within a corridor defined by the crustal-scale Ti Tree Shear Zone, which affects granitic rocks of the Minnie Creek batholith by remobilizing PBM (Pirajno et al., 2008). We have created two predictor maps: distance to crustal-scale faults (Fig. 2.4) with a 10 km buffer applied, and distance to pre-Carnarvon structures with a 5 km wide buffer zone (Fig. 2.55). We allocated both maps a weight of 9, and confidence factors of 8.5 and 9, respectively.

Traps

Gold and Cu contents are the most direct geochemical evidence of PBM physical and chemical traps (Hitzman and Valenta, 2005). The Au and Cu contents were used to create predictor maps with a map weight of 9 and a confidence factor of 7 (Figs 2.35 and 2.56, respectively).

PBM deposits are enriched in Th and U. Radiometric data is the best available predictor for uranium and thorium content, provided that occurrences are very close to the surface. We used the radiometric-U and radiometric-Th content maps (Figs 2.9 and 2.10), with map weights and confidence factors of 9.

PBM polymetallic enrichments contain other very mobile but economically less significant elements such as Ag, U, Fe, and Bi. We normalized these data against either Zr or Ti content (which are immobile) to evaluate mass transfer processes (following Stanley and Madeisky, 1994). High Fe_2O_3 and TiO_2 values are due mainly to the presence of magnetite and titanite, respectively (Williams et al., 2005). High Ag/Zr, U/Zr, Bi/Zr and $\text{Fe}_2\text{O}_3/\text{TiO}_2$ ratios are likely to indicate PBM-type traps and we used these to create the predictor maps comprising Figures 2.57 to 2.60, assigning a map weight of 8 and a confidence factor of 7 to each.

Physical traps

PBM deposits commonly form within intense zones of deformation in the vicinity of crustal-scale lineaments (Groves and Vielreicher, 2001; Sillitoe, 2010). Structural and stratigraphic controls are pronounced, and PBM deposits are characteristically associated with fault intersections, shear zones, lithological contacts, or

breccia bodies. Therefore, we used the six predictor maps previously used in the orogenic gold system: competency contrast across geological contact (Fig. 2.19); geological contact density (Fig. 2.20); geological contact density weighted by competency (Fig. 2.21); fault density (Fig. 2.22); distance to fault intersection (Fig. 2.23); fault intersection density (Fig. 2.24); distance to fold axes (Fig. 2.25). We applied the same map weights as in orogenic gold for the same reasons.

PBM deposits are commonly, but not exclusively, contained within large pipe-like breccia bodies with radii varying 1000–10 000 m, that contain sulfur-poor assemblages enriched in incompatible elements. For example, the Olympic Dam PBM deposit (Australia) is hosted within a 5 x 7 km, funnel-shaped, hematite-rich hydrothermal breccia (Reeve et al., 1990). Breccias are therefore considered as potential physical traps. We attributed the breccia density map a weight of 8 and a confidence factor of 8 (Fig. 2.8).

These breccia bodies are an essential physical trap (map weight = 9) and hydrothermal alteration associated with PBM-style mineralization will then typically comprise concentric zones surrounding a roughly circular body. The breccia and proximal alteration zone are commonly associated with positive magnetic anomalies, whereas the outer alteration zones are much less magnetic. The location of possible hydrothermal alteration systems were interpreted from GSWA magnetic datasets (GSWA, 2012) using the CET Porphyry Analysis system (Holden et al., 2011). The algorithm only detects features of a given size range with circular to elliptical cross sections in plan. It will therefore only detect potential porphyry bodies that are close to vertical and will not differentiate them from other types of circular features. We attempted some discrimination by limiting radii values to between 1000 m and 10 000 m and radial symmetry thresholds to 500 m, ensuring that only features with the strongest response pass the screening. We also established an exclusion radius of 500 m to constrain the minimum allowable distance between detected features. The resulting predictor map ‘porphyry body’ is illustrated in Fig. 2.61.

Chemical traps

Skarn-type PBM deposits occur as disseminations or irregular zones in granulite and gneissic marbles or calcareous schists (Boyle, 1982). In many parts of the Grenville Province of Ontario, skarn-type deposits occur in skarn and metamorphic pyroxenites and amphibolites (Boyle, 1982). Scheelite-bearing skarns in the northwestern Gascoyne Province were discussed in detail by Davies (1998) and reviewed by Pirajno (2004). These skarn deposits (Mount Alexander and Kilba Well, Fig. 1), are developed in calcite–tremolite–chlorite marble at the contact with monzogranite and granodiorite intrusions. The skarns, associated with greisen and sericitic alteration of the intrusions, show well-developed mineralogical zoning. Skarns in the Gascoyne Province were queried using GSWA (2012) to create a predictor map of ‘distance to metasomatized rock’ using a 5 km wide buffer zone. To this map we assigned a map weight of 8 and a confidence factor of 7 (Fig. 2.62).

A sulfur source is required for precipitation of Cu, and this may be the critical factor for economically important accumulations of PBM, regardless of the source of fluids and metals (Williams et al., 2005). We therefore created a 'S (sulphur) content' predictor map from the geochemical databases, and assigned a map weight of 8 (Fig. 2.63) and a confidence factor of 7.

Overprinting of the PBM host rocks by extensive hydrothermal iron oxide alteration is characterized by iron oxides, sericite, and silica. Consequently, we used the predictor map distance to iron-rich rocks (including presence of magnetite and hematite) as the criterion for mineralization related to pathways. A buffer of 5 km was applied (Fig. 2.38), and a map weight of 8 and a confidence factor of 7 were used.

Metal associations in PBM deposits are influenced by circulation of magmatic or hydrothermal fluids with resultant fluid – host rock exchange reactions (Groves et al., 2010). A dyke can then conceptually be a prospective host for PBM mineralization because of its high chemical reactivity and its interaction with the country rocks. As with previous examples, dyke density and distance to dyke maps were used (map weight = 8, confidence factor = 8; Figs 2.43 and 2.44).

Fuzzy model

Combining fuzzy-membership values

The map weights, and the confidence factors for each of the predictor maps used in this study, including the rationale for assigning these values, are shown in Table 2.4.

We used a four-stage inference network to combine the predictor maps (Fig. 28). Dyke density and distance to dyke maps were combined using the fuzzy OR, and alkaline rock density and distance to alkaline rocks were also combined using fuzzy OR. We used the fuzzy OR because both maps do not represent the same attribute. Next, the sets of chemical and physical traps were each combined using the fuzzy OR. The resultants were combined using the fuzzy AND to generate an overall traps map. Maps for the source and pathway components were derived from their predictor maps using the fuzzy OR. Finally, the respective predictor maps of the three key components of the PBM mineral system — source, pathways, and traps — were combined using the fuzzy PRODUCT operator to derive the fuzzy prospectivity map for PBM deposits in the Gascoyne Province (Fig. 29).

Granite-hosted tin–tungsten mineral system

Predictor maps

A three-stage inference network (Fig. 30) was used to estimate Sn–W(–Mo) prospectivity. The geological basis for the source, pathway, and trap components of the MSA is described below.

Source

Scheelite-bearing skarns in the Gascoyne Province are associated with highly differentiated and weakly peraluminous granitic rocks (Davies, 1998). The available geochemical database does not allow sufficient categorization, and so we used all granites and applied a confidence factor of 6 to reflect this uncertainty. We created a distance to granite map (Fig. 2.1) by extracting all granites and buffering them with a distance to 10 km. We assigned this map a map weight of 9 to reflect the fundamental role of granites in deposit formation.

Pathways

Major fluid pathways that are likely to focus Sn–W-enriched fluid will be those that undergo repeated hydraulic opening (Lehmann, 1990). Crustal-scale features (Fig. 2.4) are important fluid conduits (McCuaig et al., 2010; Joly et al., 2012), as is shown at Nardoo Well, where tungsten skarns are hosted within the Chalba Shear Zone. Therefore, we assigned this factor a map weight of 9 and a confidence factor of 8.5. The influence of these faults was buffered to 10 km.

All pre-Carnarvon structures in the Gascoyne Province could be significant pathways for metal transport or could have created suitable geometries potentially inducing flow of mineralizing fluids (Fig. 2.55). This predictor map was buffered to 5 km, and assigned a map weight of 9 and a confidence factor of 9.

Hydrothermal breccias also provide a useful predictor map because they are good evidence for fluid conduits. Breccia occurrence density was used to represent these (Fig. 2.8). Map weight was assigned as 9 while confidence factor was 8.

Traps

Tin, tungsten, and molybdenum contents are proxies for granite-related Sn–W deposits and were considered as chemical and physical traps (Figs 2.64, 2.65, and 2.66, respectively). Sn, W and Mo are considered together because they are found together in tin–tungsten granite occurrences. We assigned a map weight of 9 to both Sn and W, whereas we used a map weight of 8 for Mo because this is not a direct proxy for Sn–W mineralization. Confidence factors for each of these were set at 7.

Physical traps

Most tin and tungsten deposits occur in the apical regions of granitic cupolas, because this is where exsolved magmatic fluids have evolved, been focused, and/or ponded (Lehmann, 1990). The most prospective granites should be either shallowly buried or, if exposed, have preserved roof zones. However, there is a lack of petrophysical contrast with the country rocks which prevents geophysical data from mapping their distribution, and limits their usefulness in the prospectivity analysis. Therefore, no physical trap was considered in this analysis.

Chemical traps

Tin–tungsten mineralization is related to post-magmatic alteration contact between intrusive felsic bodies and the country bedrock. Formation of skarns or greisens, or alteration mineralogy with abundant albite and tourmaline, are the most common manifestations of alteration associated with Sn, W, and Mo (Thompson et al., 1999), and hence are proxies for chemical traps. Alteration is not adequately described in the available database to create a predictor map. However, skarns are significant potential host rocks for Sn–W mineralization (e.g. Red Dome, Queensland (Thompson et al., 1999); Mount Bischoff, Tasmania (Solomon et al., 1994)). Dolomites and mafic or ultramafic igneous rocks are particularly amenable to formation of skarns, and albite and tourmaline mineralization (e.g. Lucky Draw, New South Wales). Furthermore, the tungsten at Nardoo Hill in the Gascoyne Province occurs within scheelite in contact-metamorphosed sedimentary rocks, mainly as vesuvianite skarns and para-amphibolites. We therefore used the distance to metasomatized rocks and the distance to dolomites as predictor maps (Figs 2.62, 2.67), with a 5 km wide buffer zone (GSWA, 2012). Relevant occurrences of mafic and ultramafic rocks were extracted and buffered to 5 km (Fig. 2.52); these include peridotite, harzburgite, pyroxenite, dunite, basalt, gabbro, troctolite, gabbro-norite, dolerite, and amphibolite. The skarn and dolomite predictor maps were assigned map weights of 9, whereas a map weight of 8 was assigned to mafic and ultramafic rocks, which that are amenable to skarn alteration, but not to the same extent as dolomite. Confidence factors of 6 were assigned for the metasomatized rocks and dolomite predictor maps, whereas mafic rocks were assigned a confidence factor of 8.

Sn–W deposits can have a close relationship with sills and dykes due to the chemical reactivity of the latter (e.g. Red Dome, Kidston in Queensland). We therefore also used the distance to dyke and dyke density maps as an indication of possible chemical trapping (Figs 2.43 and 2.44), and assigned a map weight of 8 to these to reflect their lower importance than metasomatized rocks and dolomites. Confidence factor for these predictor maps was 8.

Fuzzy model

Combining fuzzy-membership values

The map weights and the confidence factors for each of the 12 predictor maps used in this study, including the rationale for assigning these values, are shown in Table 2.5. A three-stage inference network was used to combine the predictor maps (Fig. 30). We first combined the distance to dyke and dyke density maps using the fuzzy OR. We then combined the respective predictor maps for the source, pathway, and trap components of the Sn–W mineral system, also using the fuzzy OR, because the presence of any one of the predictor maps is sufficient to infer the presence of the respective component. We then combined these three maps using the fuzzy PRODUCT operator to derive the fuzzy prospectivity map for Sn–W deposits in the Gascoyne Province (Fig. 31).

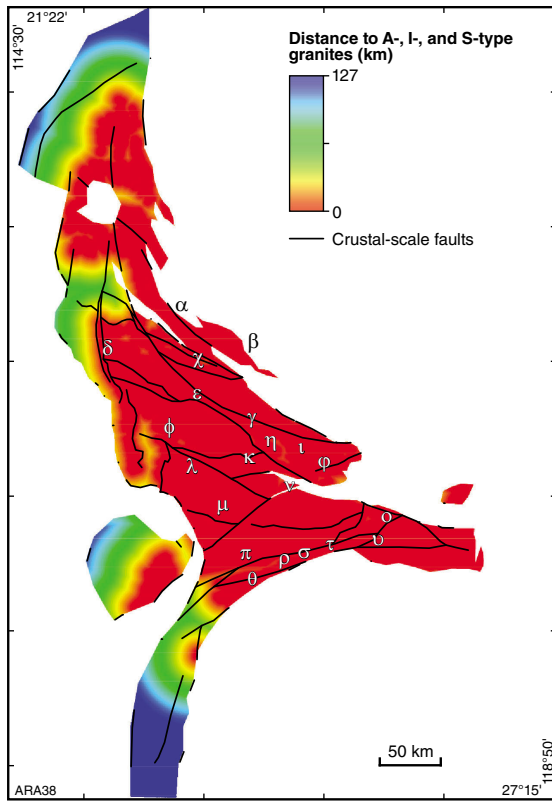


Figure 2.1. Predictor map for REE, gold source, PBM and Sn-W: proximity to A-, I- and S- type granite (up to 25 km). Greek letters correspond to the REE prospective zone (Fig. 19).

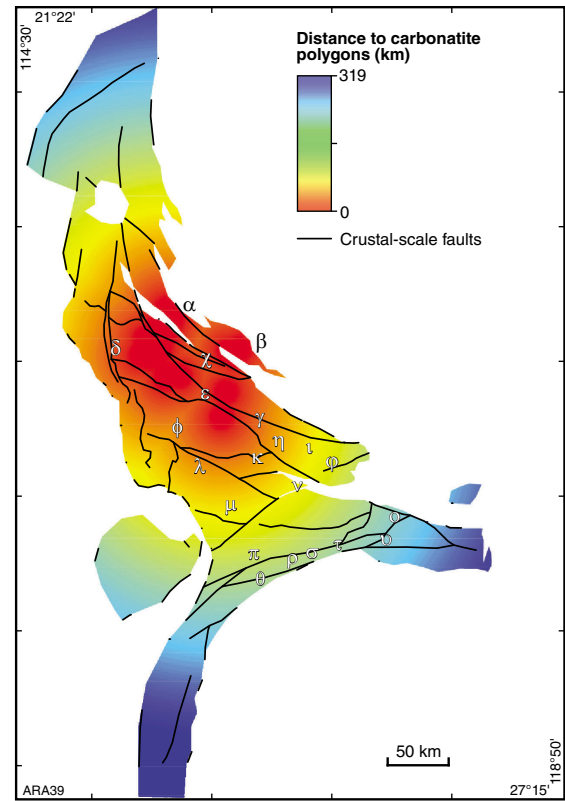


Figure 2.2. Predictor map for REE source and gold pathway: proximity to alkaline igneous rocks (from GIS-type polygon). Greek letters correspond to the REE prospective zone (Fig. 19).

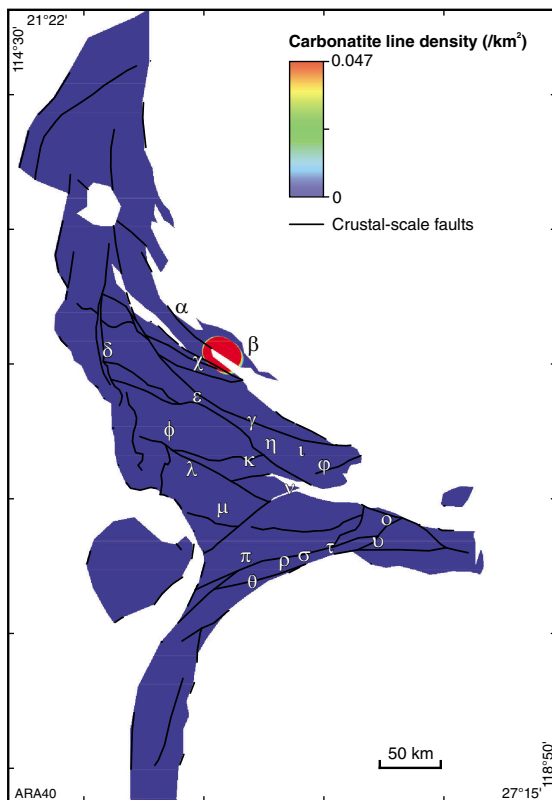


Figure 2.3. Predictor map for REE source and gold pathway: alkaline igneous rock density (from GIS-type polyline). Greek letters correspond to the REE prospective zone (Fig. 19).

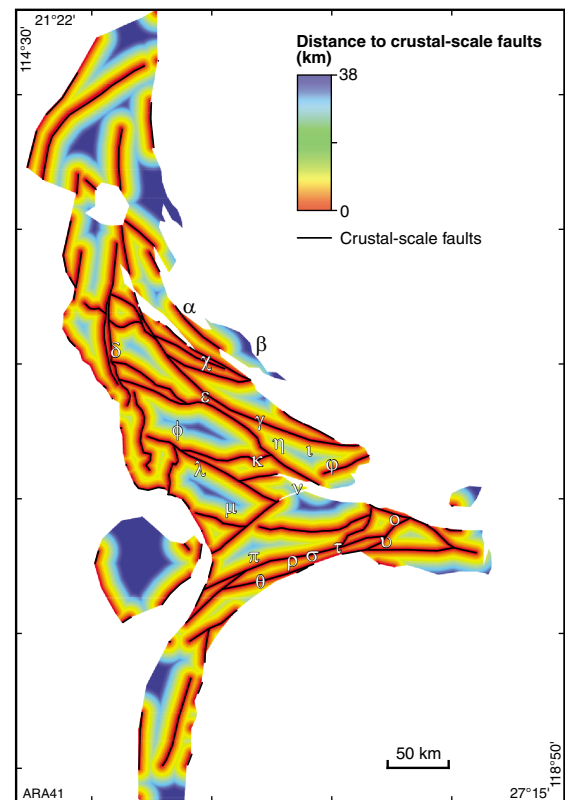


Figure 2.4. Predictor map for REE, gold, PBM and Sn-W pathway: distance to crustal-scale faults. Greek letters correspond to the REE prospective zone (Fig. 19).

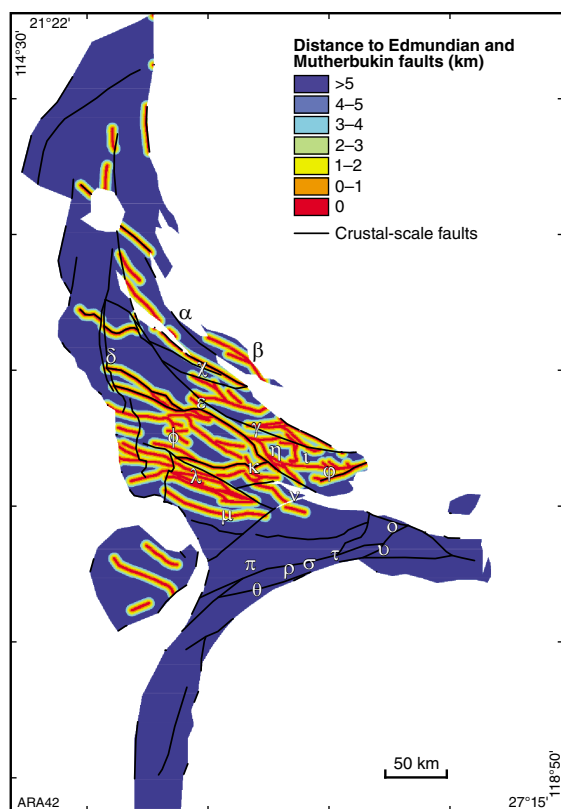


Figure 2.5. Predictor map for REE pathway: distance to Edmundian and Mutherbukin faults. Greek letters correspond to the REE prospective zone (Fig. 19).

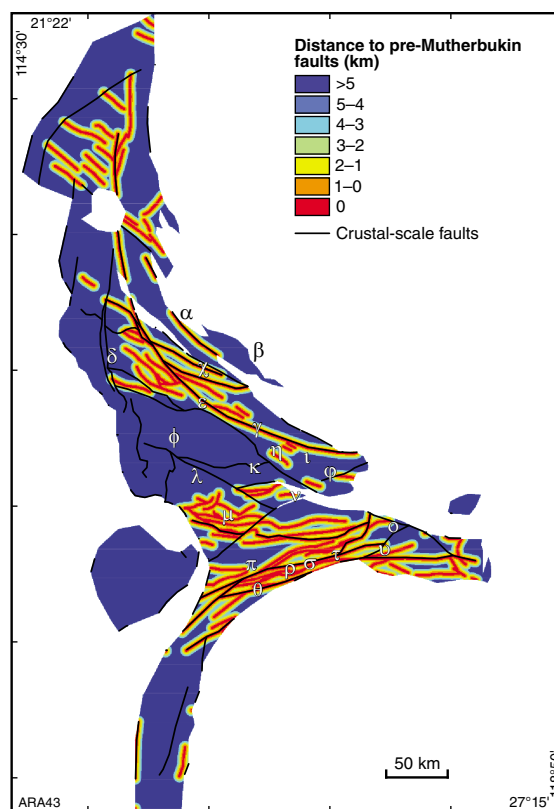


Figure 2.6. Predictor map for REE pathway: distance to pre-Mutherbukin faults. Greek letters correspond to the REE prospective zone (Fig. 19).

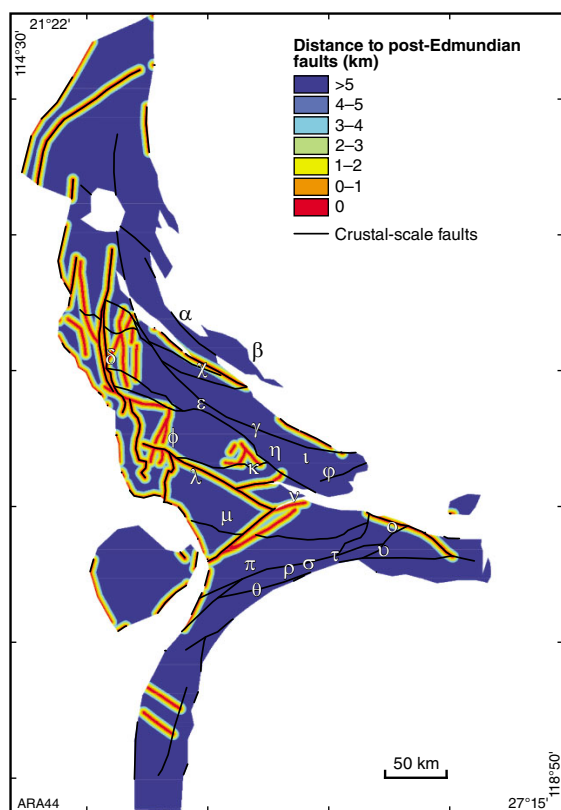


Figure 2.7. Predictor map for REE pathway: distance to post-Edmundian fault. Greek letters correspond to the REE prospective zone (Fig. 19).

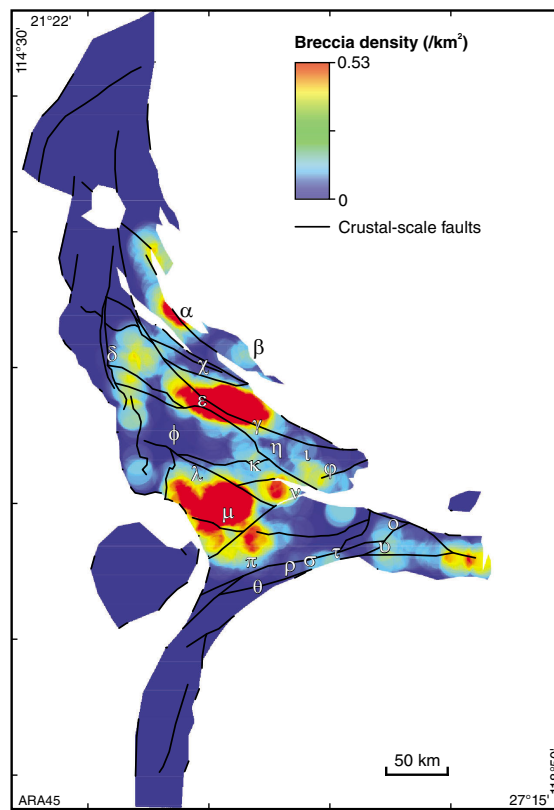


Figure 2.8. Predictor map for REE, gold and Sn-W pathways and PBM physical trap: breccia density. Greek letters correspond to the REE prospective zone (Fig. 19).

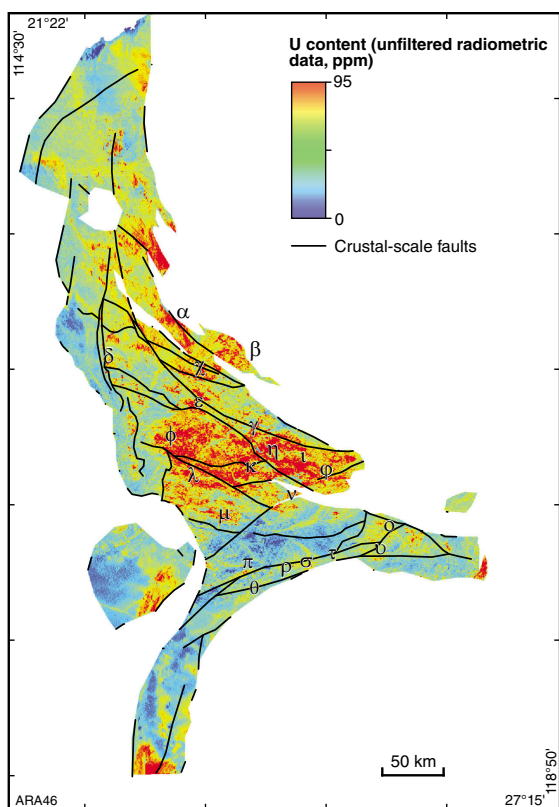


Figure 2.9. Predictor map for REE and surficial uranium trap: radiometric uranium content (ppm). Greek letters correspond to the REE prospective zone (Fig. 19).

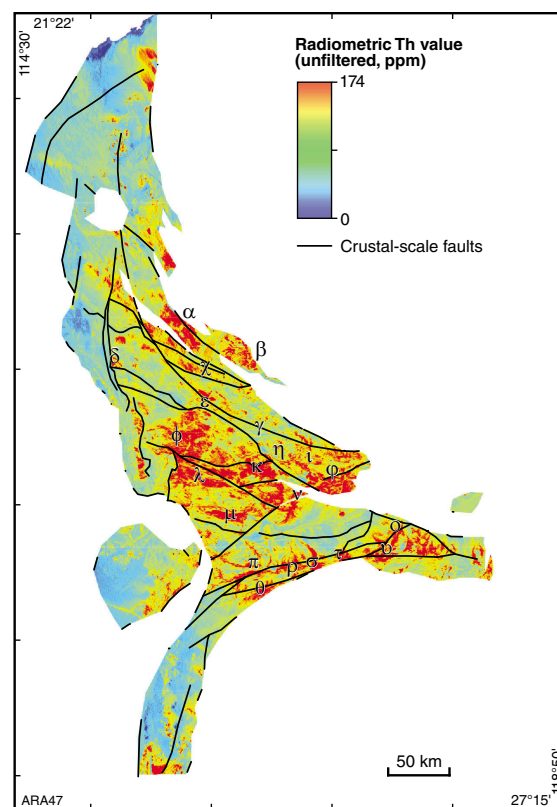


Figure 2.10. Predictor map for REE and PBM trap: radiometric thorium content (ppm). Greek letters correspond to the REE prospective zone (Fig. 19).

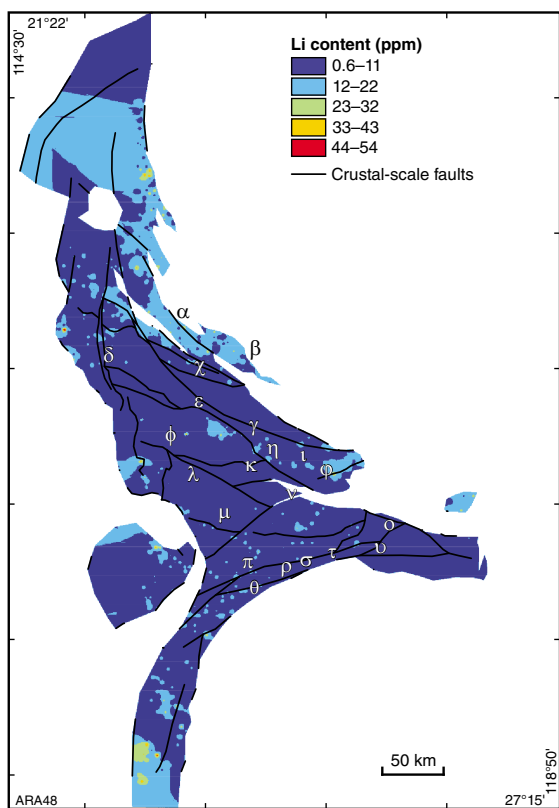


Figure 2.11. Predictor map for REE trap: lithium content (ppm). Greek letters correspond to the REE prospective zone (Fig. 19).

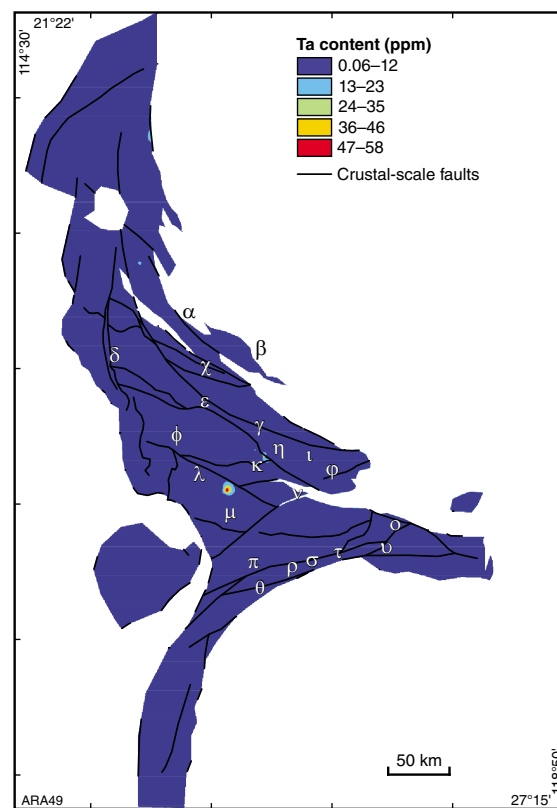


Figure 2.12. Predictor map for REE trap: tantalum content (ppm). Greek letters correspond to the REE prospective zone (Fig. 19).

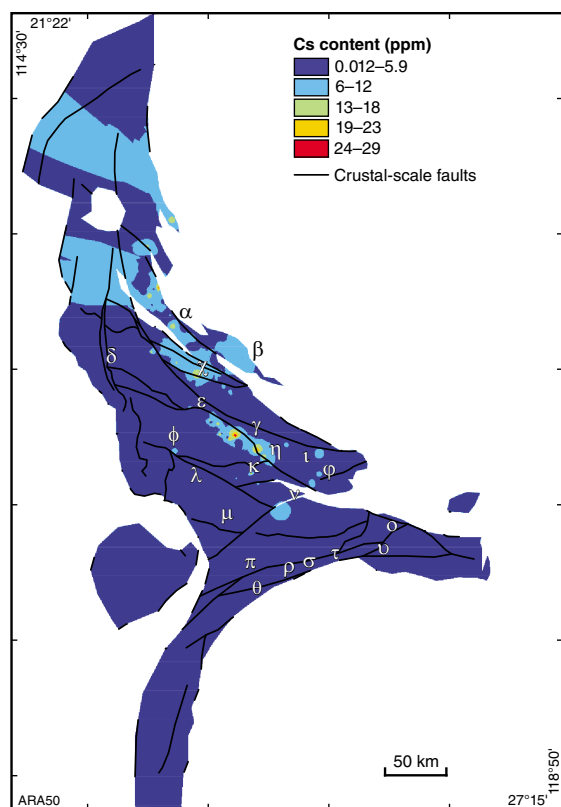


Figure 2.13. Predictor map for REE trap: cesium content (ppm). Greek letters correspond to the REE prospective zone (Fig. 19).

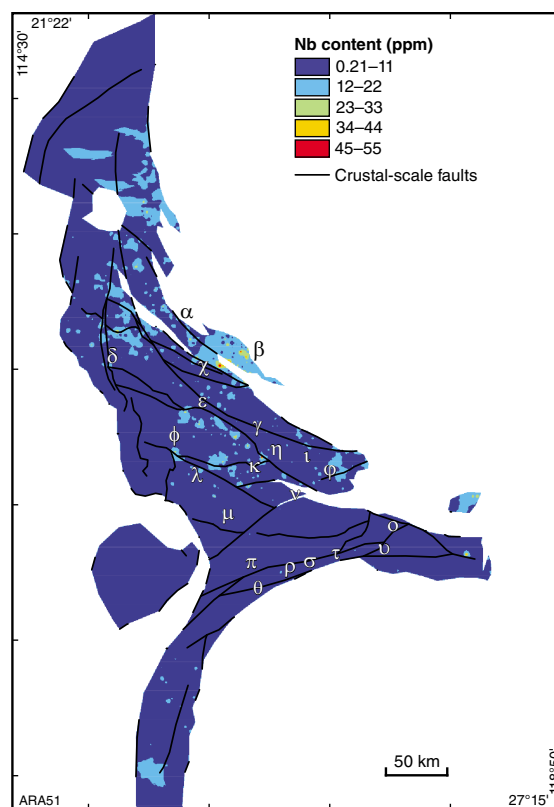


Figure 2.14. Predictor map for REE trap: niobium content (ppm). Greek letters correspond to the REE prospective zone (Fig. 19).

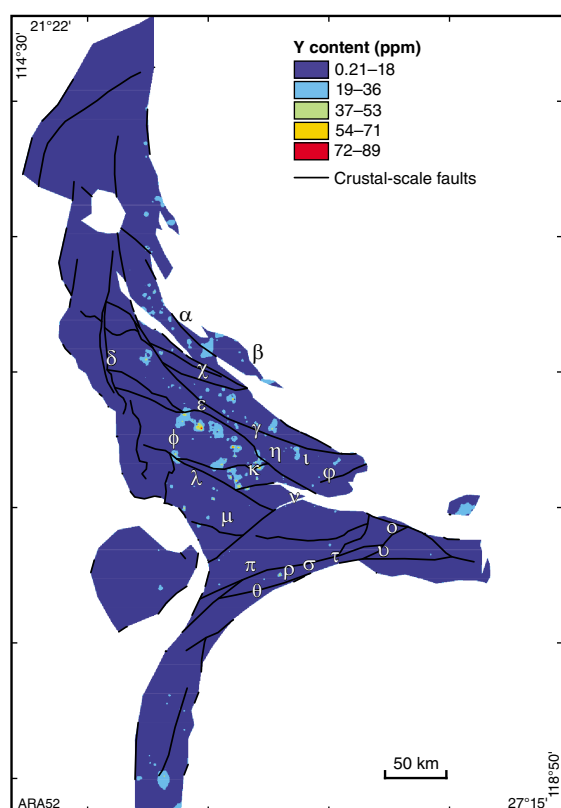


Figure 2.15. Predictor map for REE trap: yttrium content (ppm). Greek letters correspond to the REE prospective zone (Fig. 19).

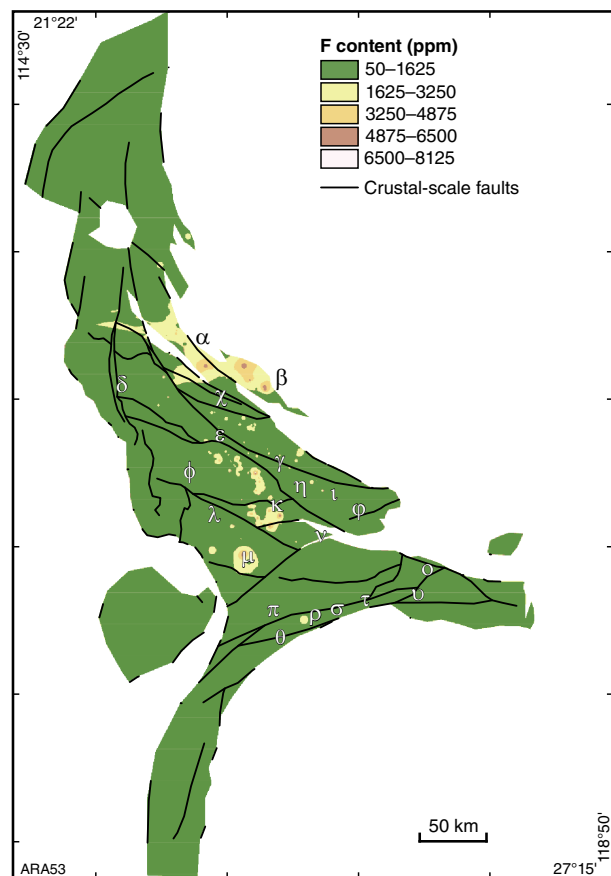


Figure 2.16. Predictor map for REE trap: fluorine content (ppm). Greek letters correspond to the REE prospective zone (Fig. 19).

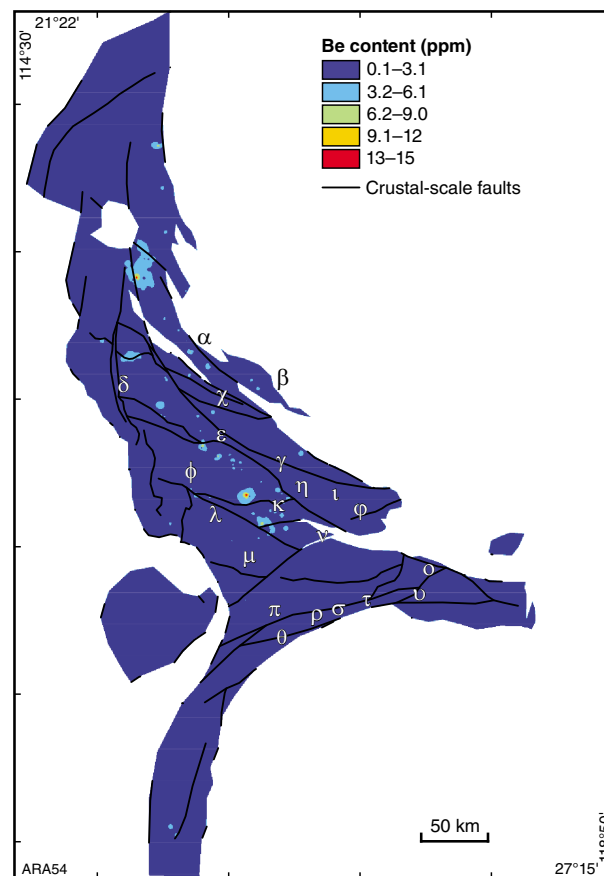


Figure 2.17. Predictor map for REE trap: beryllium content (ppm). Greek letters correspond to the REE prospective zone (Fig. 19).

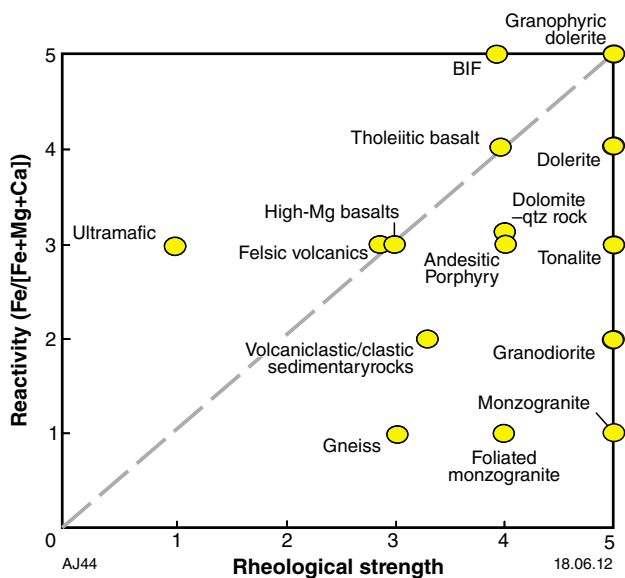


Figure 2.18. Relative chemical reactivity and rheological strengths for selected rocks (from Brown, 2002).

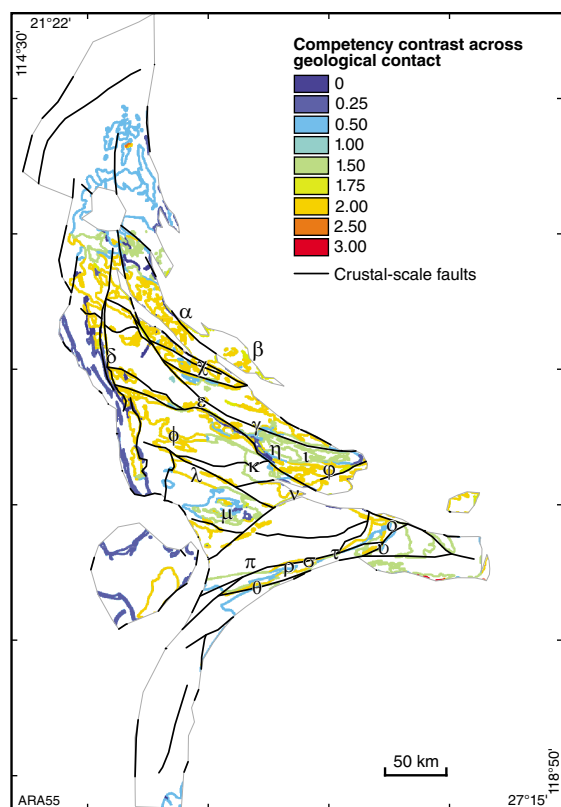


Figure 2.19. Predictor map for REE, gold and PBM physical trap: competency contrast across geological contact. Greek letters correspond to the REE prospective zone (Fig. 19).

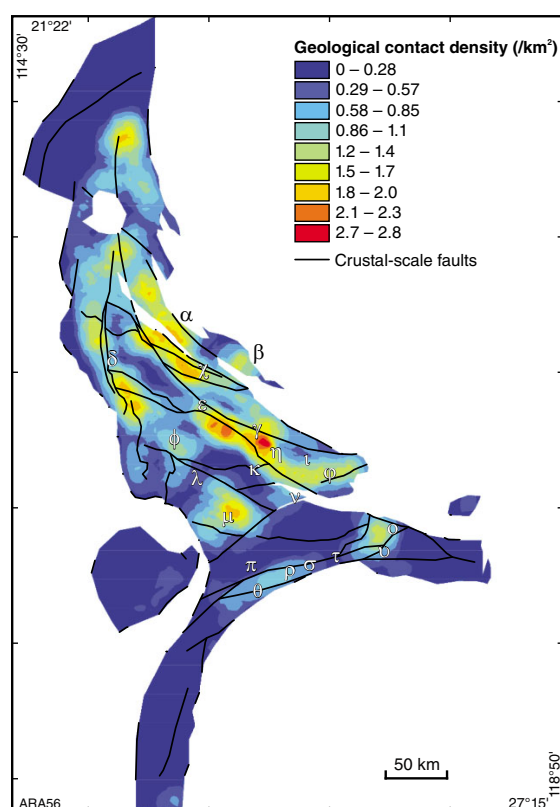


Figure 2.20. Predictor map for REE, gold and PBM physical trap: geological contact density map. Greek letters correspond to the REE prospective zone (Fig. 19).

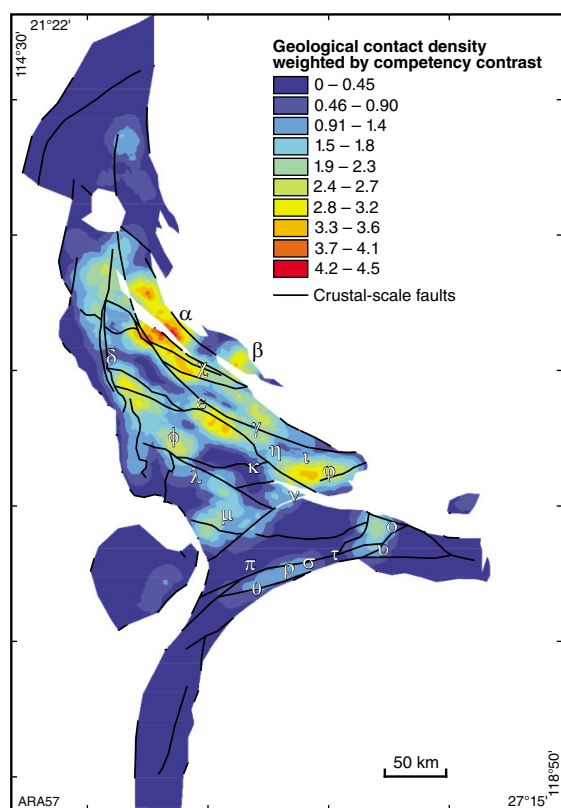


Figure 2.21. Predictor map for REE, gold and PBM physical trap: geological contact density weighted by competency contrast map. Greek letters correspond to the REE prospective zone (Fig. 19).

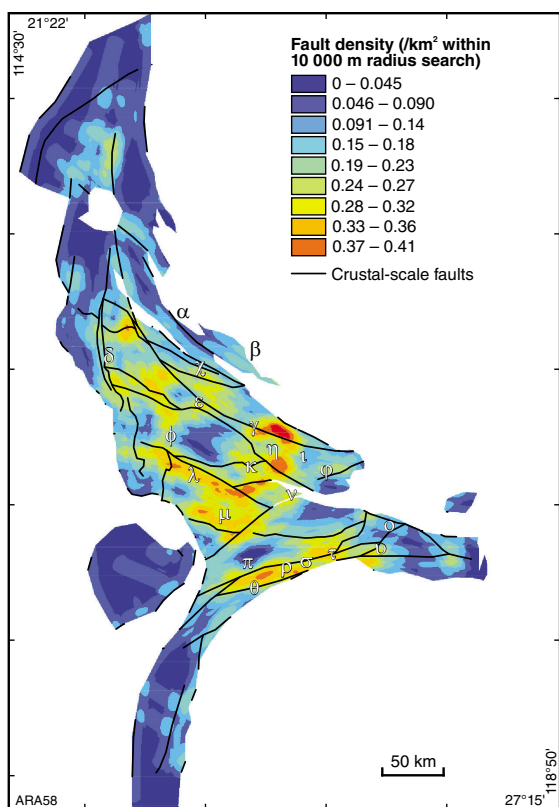


Figure 2.22. Predictor map for REE, gold and PBM physical trap: fault density map. Greek letters correspond to the REE prospective zone (Fig. 19).

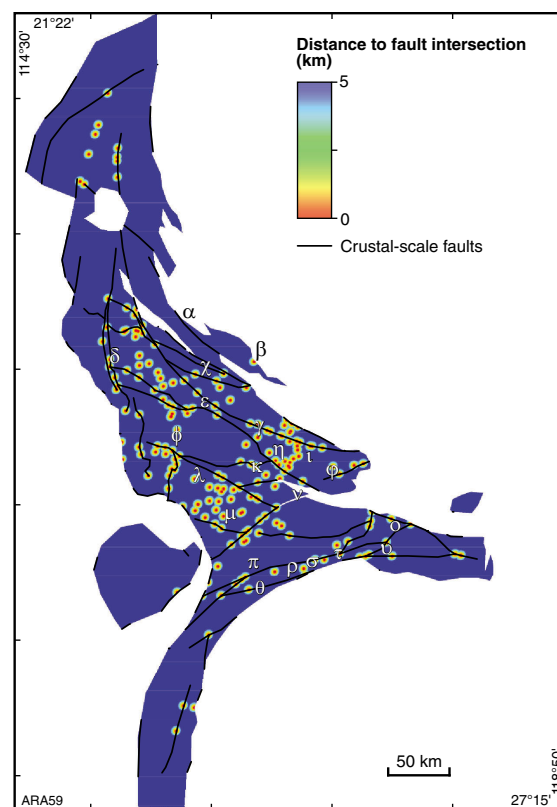


Figure 2.23. Predictor map for REE, gold and PBM physical trap: fault intersection map. Greek letters correspond to the REE prospective zone (Fig. 19).

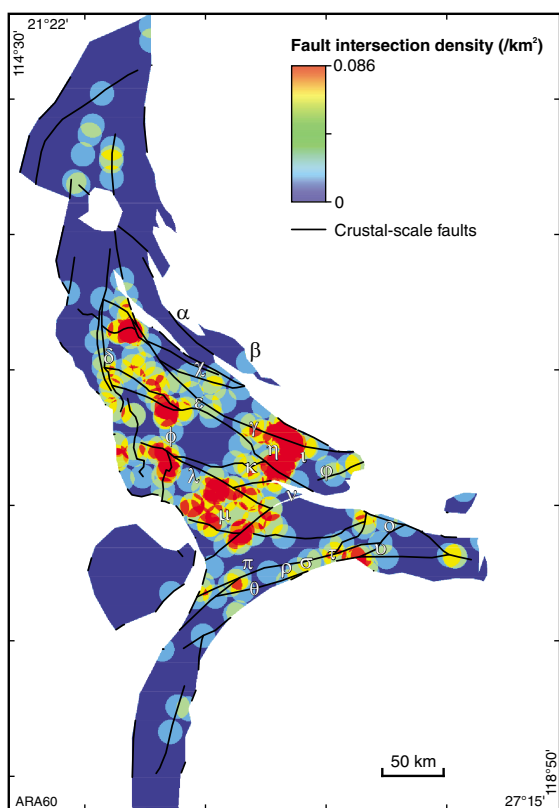


Figure 2.24. Predictor map for REE, gold and PBM physical trap: fault intersection density map. Greek letters correspond to the REE prospective zone (Fig. 19).

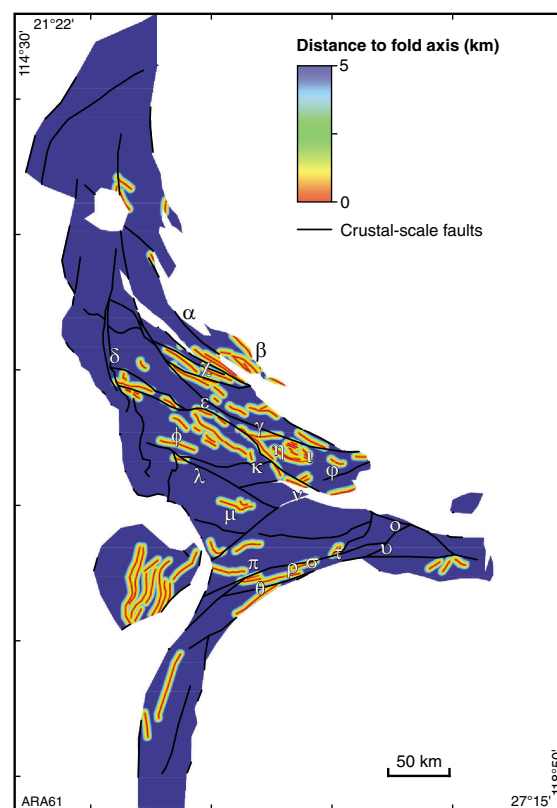


Figure 2.25. Predictor map for REE, gold and PBM physical trap: proximity to fold map. Greek letters correspond to the REE prospective zone (Fig. 19).

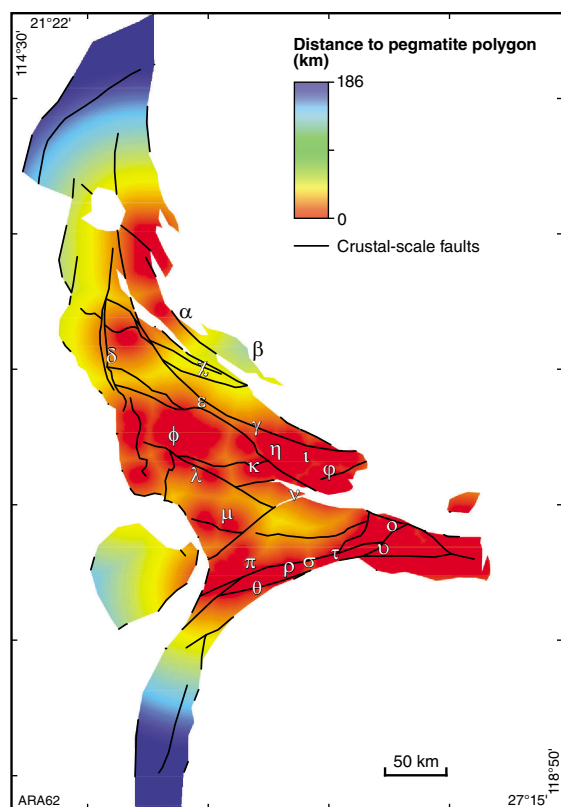


Figure 2.26. Predictor map for REE physical trap: proximity to pegmatite map (from GIS-type polygons; GSWA, 2012).

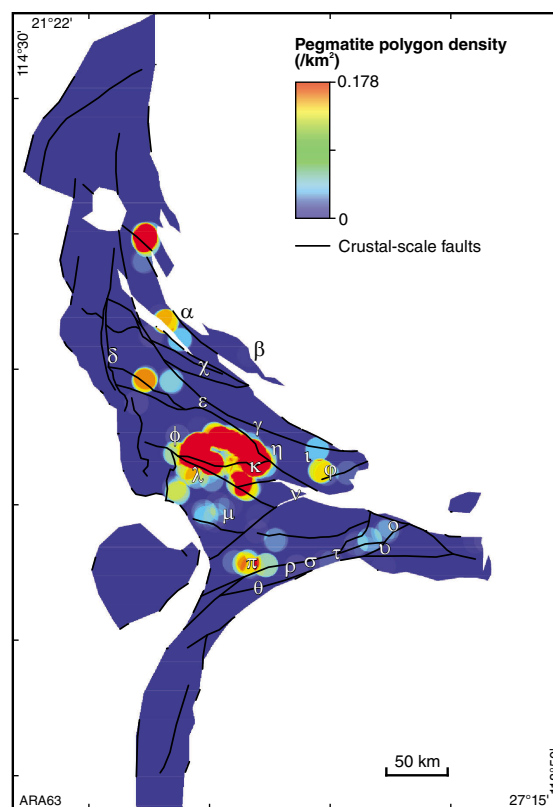


Figure 2.27. Predictor map for REE physical trap: pegmatite density map (from GIS-type polylines; GSWA, 2012).

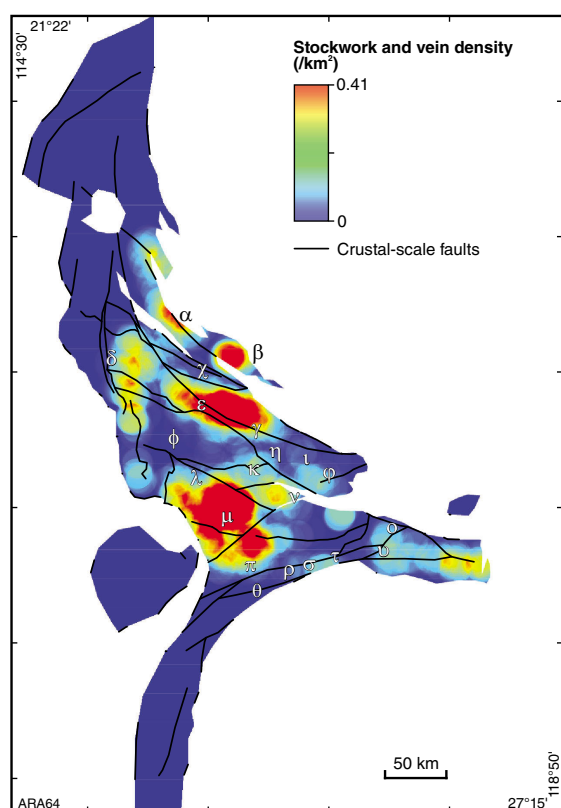


Figure 2.28. Predictor map for REE physical trap: stockwork and vein density map. Greek letters correspond to the REE prospective zone (Fig. 19).

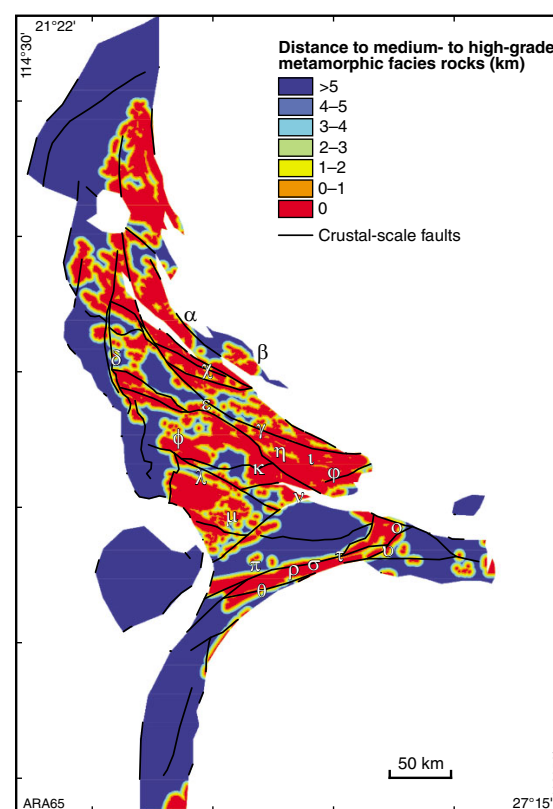


Figure 2.29. Predictor map for REE chemical trap: proximity to medium- to high-grade metamorphic facies and metasomatism. Greek letters correspond to the REE prospective zone (Fig. 19).

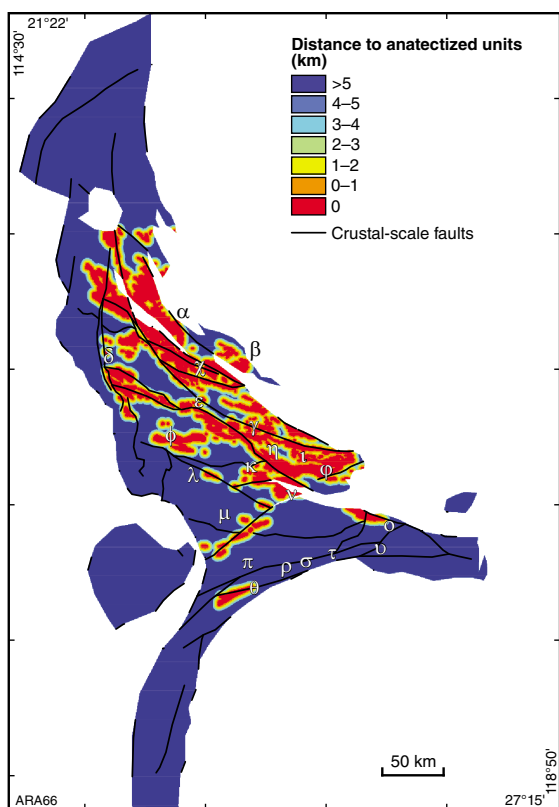


Figure 2.30 Predictor map for REE chemical trap: proximity to anatectized rocks. Greek letters correspond to the REE prospective zone (Fig. 19).

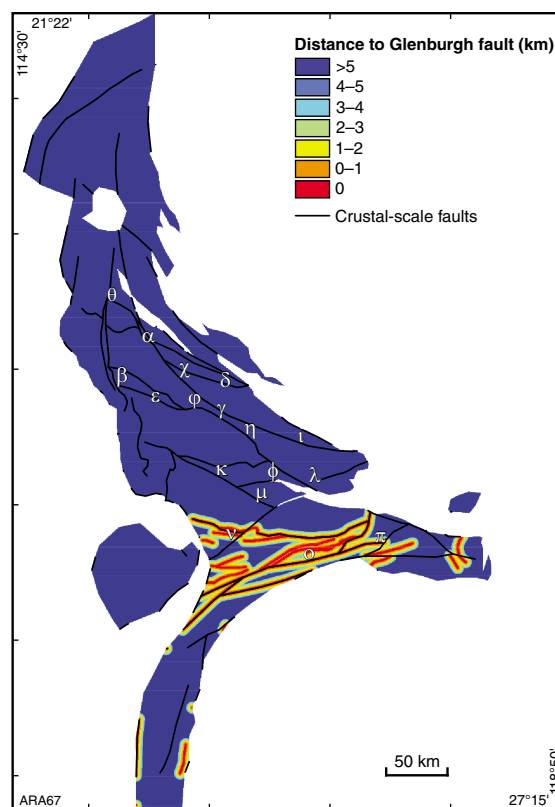


Figure 2.31. Predictor map for gold source: distance to Glenburgh fault. Greek letters correspond to the gold prospective zone (Fig. 21).

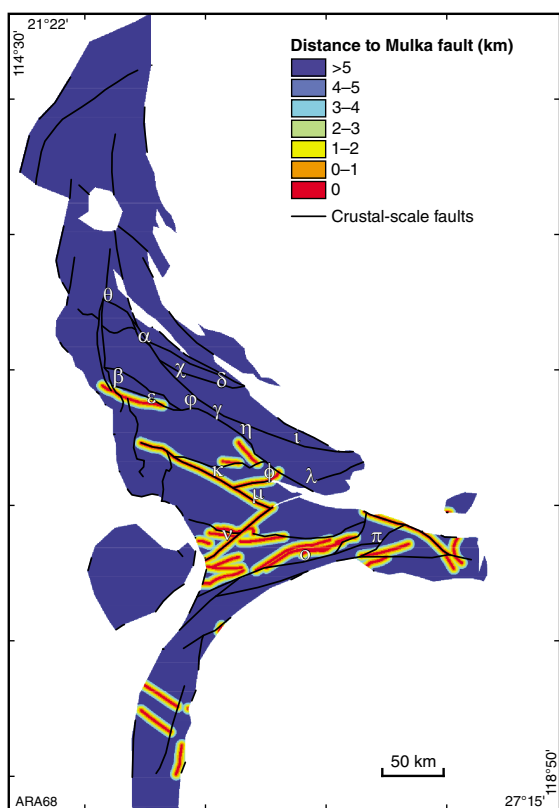


Figure 2.32. Predictor map for gold pathway: distance to Mulka fault. Greek letters correspond to the gold prospective zone (Fig. 21).

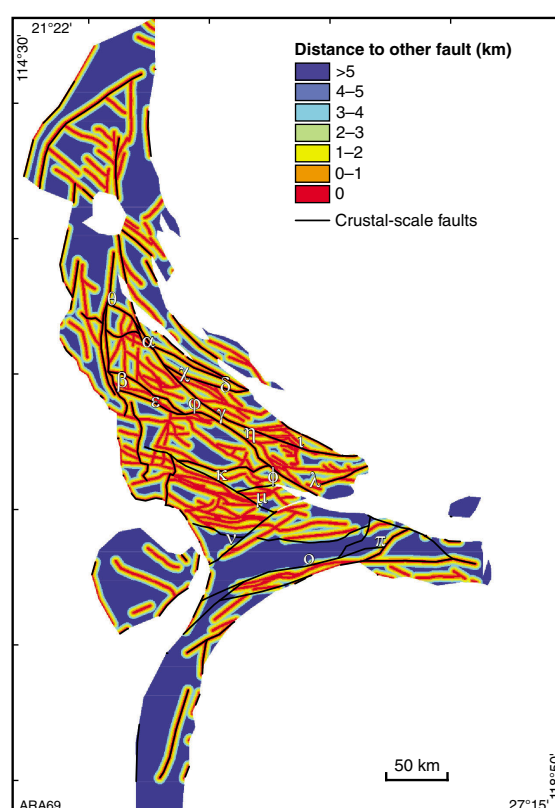


Figure 2.33. Predictor map for gold pathway: distance to faults (no Glenburgh or Mulka structures). Greek letters correspond to the gold prospective zone (Fig. 21).

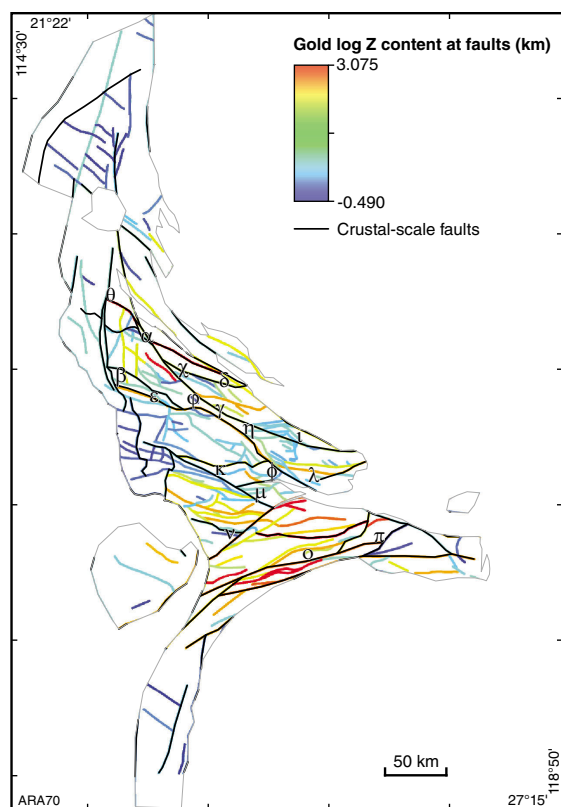


Figure 2.34. Predictor map for gold pathways: gold contents over all faults. Zones shown in red indicate areas very close to faults that are linked to high gold contents; zones shown in blue correspond to the contrary.

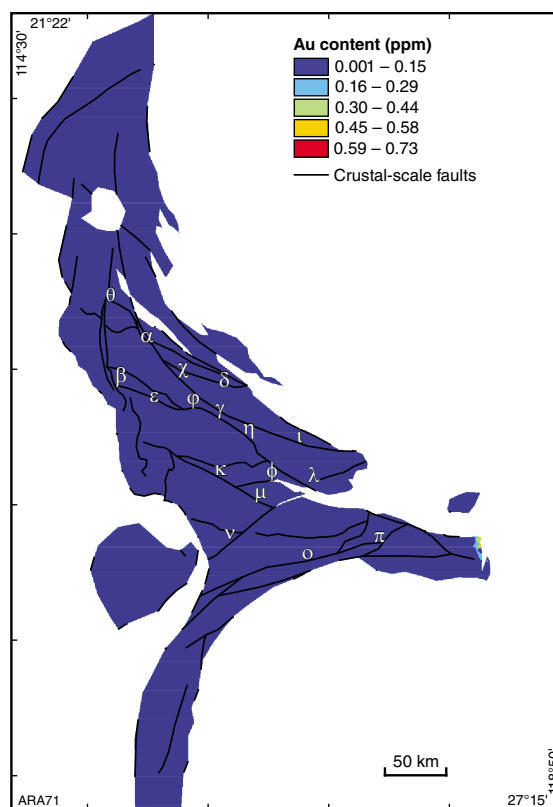


Figure 2.35. Predictor map for gold and PBM: gold content map (ppm). Greek letters correspond to the gold prospective zone (Fig. 21).

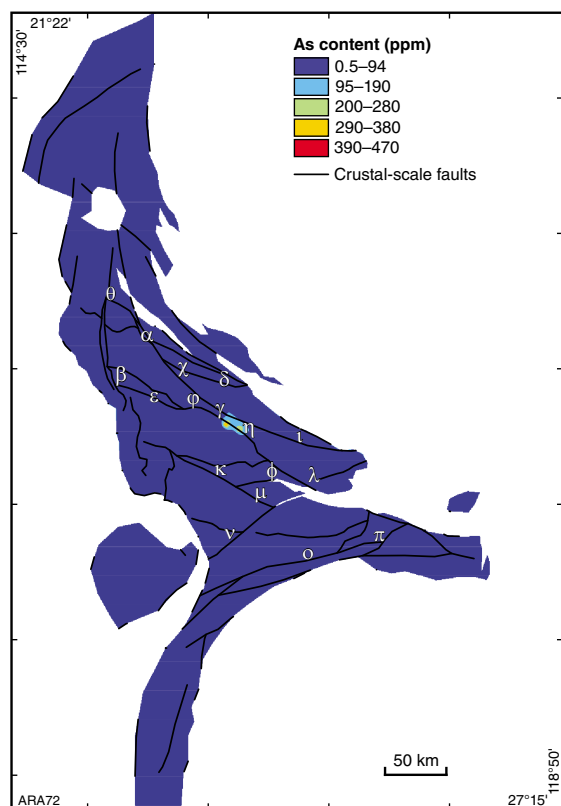


Figure 2.36. Predictor map for gold trap: arsenic content map (ppm). Greek letters correspond to the gold prospective zone (Fig. 21).

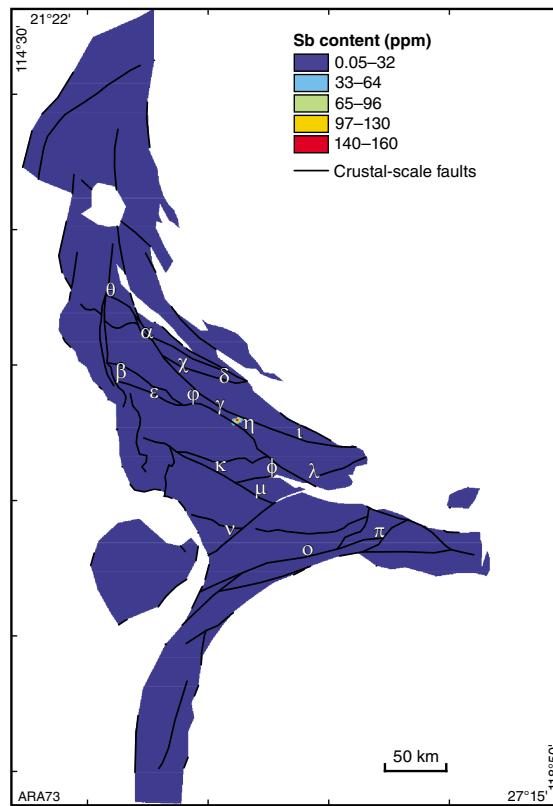


Figure 2.37. Predictor map for gold trap: antimony content map (ppm). Greek letters correspond to the gold prospective zone (Fig. 21).

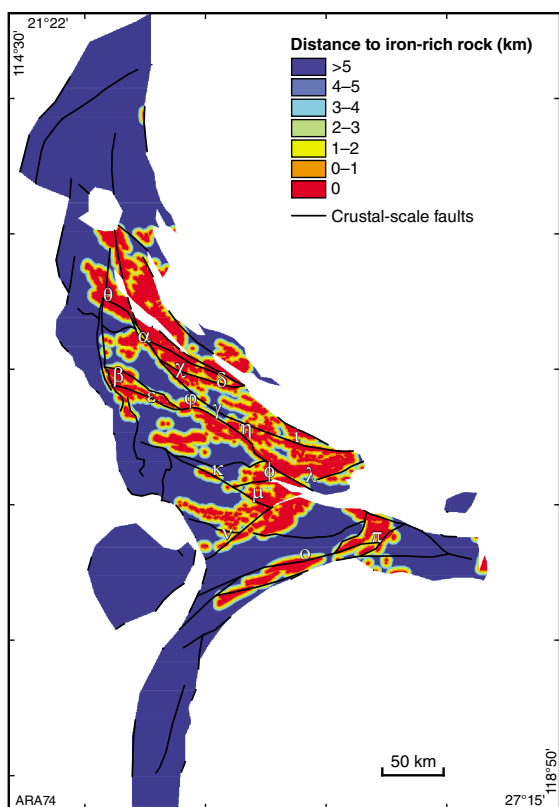


Figure 2.38. Predictor map for gold, PBM chemical trap: presence of Fe-rich rocks. Greek letters correspond to the gold prospective zone (Fig. 21).

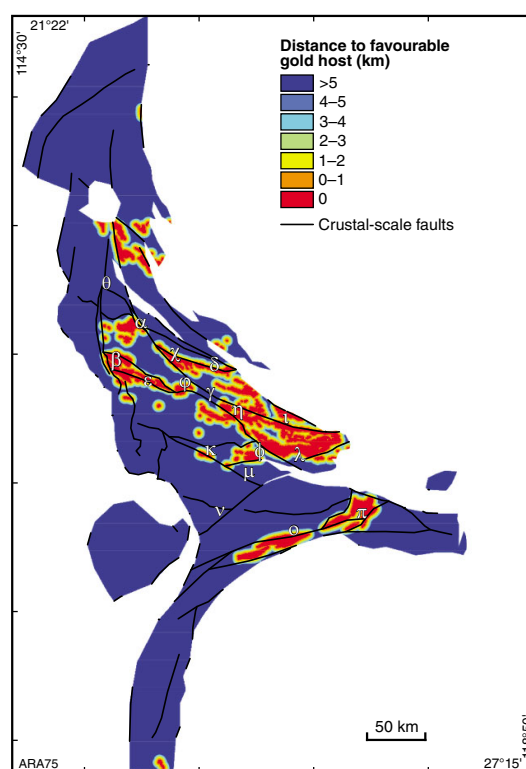


Figure 2.39. Predictor map for gold and PBM chemical trap: presence of gold host unit (felsic volcanic formation like the Camel Hills and Leake Spring Metamorphics and the Gifford Creek Ferrocarnatite Suite (GSWA, 2012). Greek letters correspond to the gold prospective zone (Fig. 21).

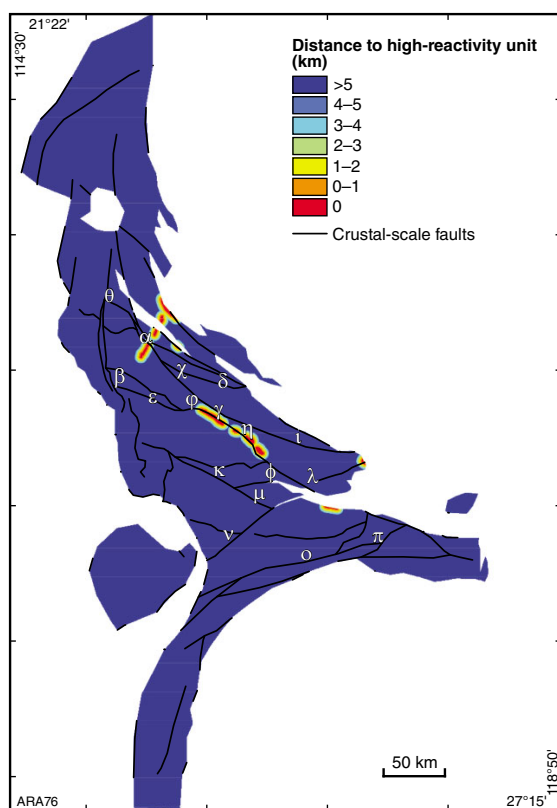


Figure 2.40. Predictor map for gold, PBM chemical trap: chemical reactivity. Greek letters correspond to the gold prospective zone (Fig. 21).

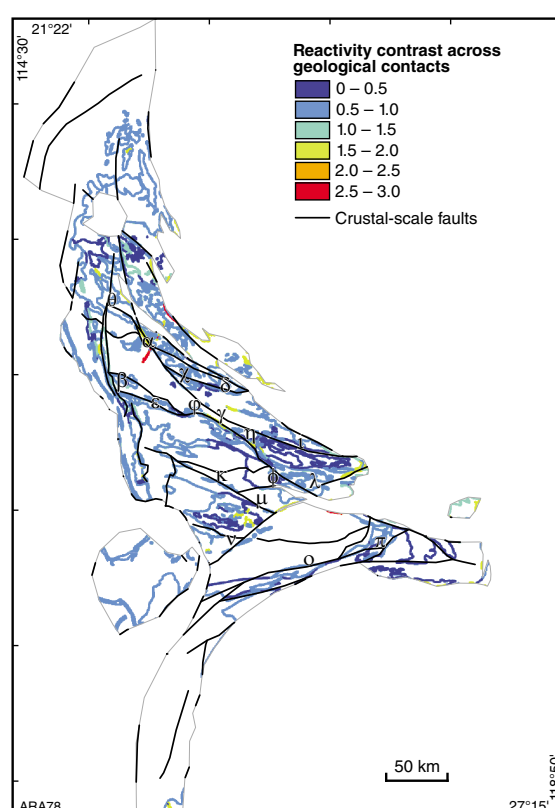


Figure 2.41. Predictor map for gold, PBM chemical trap: reactivity contrast across geological contacts. Greek letters correspond to the gold prospective zone (Fig. 21).

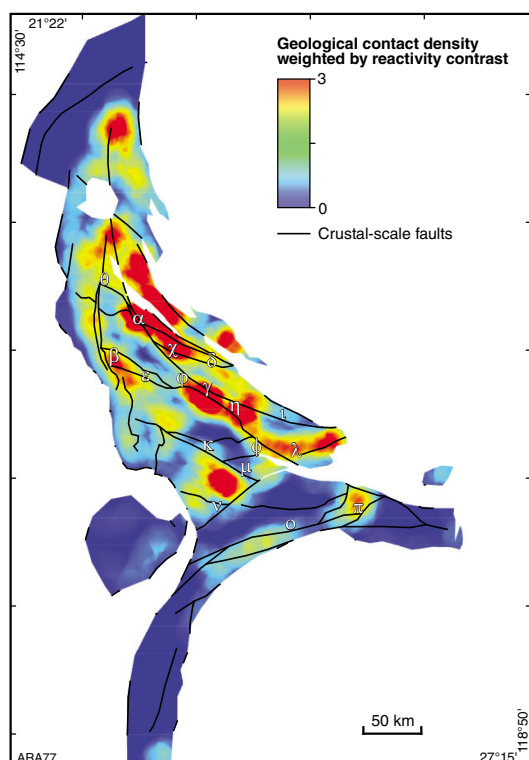


Figure 2.42. Predictor map for gold, PBM chemical trap: geological contact density weighted by reactivity contrast. Red indicates areas with the most intense competency chemical contrast weighted by geological contact; blue correspond to the contrary. Greek letters correspond to the gold prospective zone (Fig. 21).

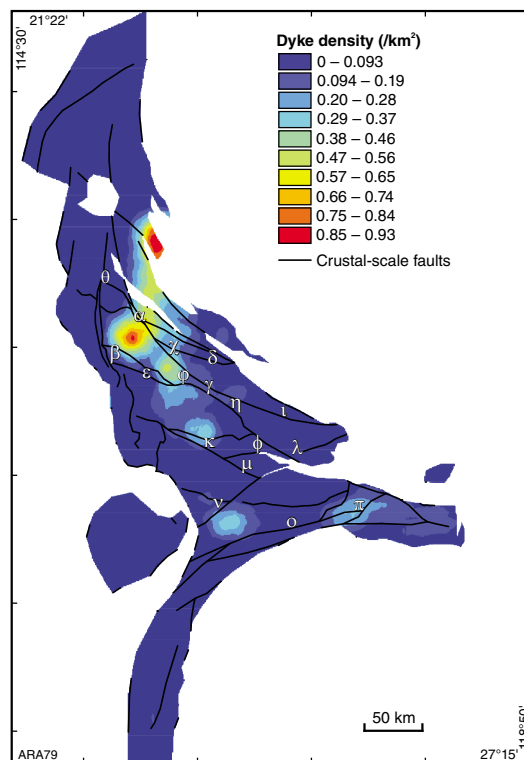


Figure 2.43. Predictor map for gold, PBM, Sn-W and surficial uranium chemical trap: dyke density map (using GIS polylines, GSWA, 2012). Greek letters correspond to the gold prospective zone (Fig. 21).

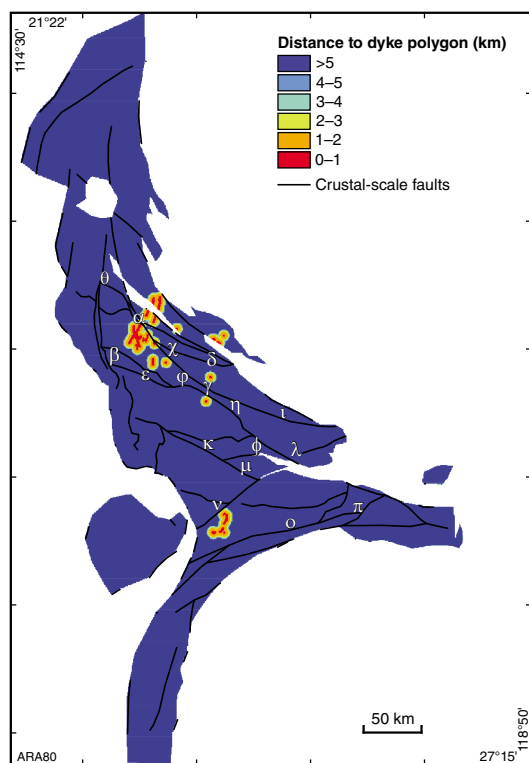


Figure 2.44. Predictor map for gold, PBM, Sn-W and surficial uranium chemical trap: distance to dykes with a 5 km buffer zone (using GIS polygons, GSWA, 2012). Greek letters correspond to the gold prospective zone (Fig. 21).

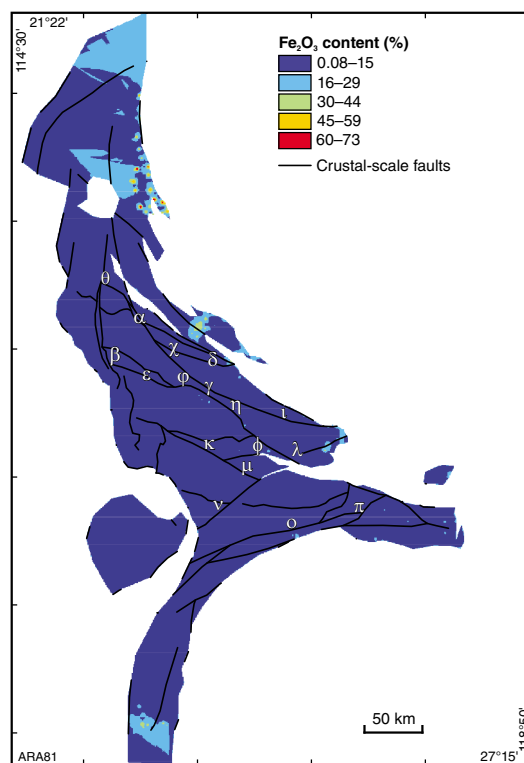


Figure 2.45. Predictor map for gold chemical trap: Fe_2O_3 content. Greek letters correspond to the gold prospective zone (Fig. 21).

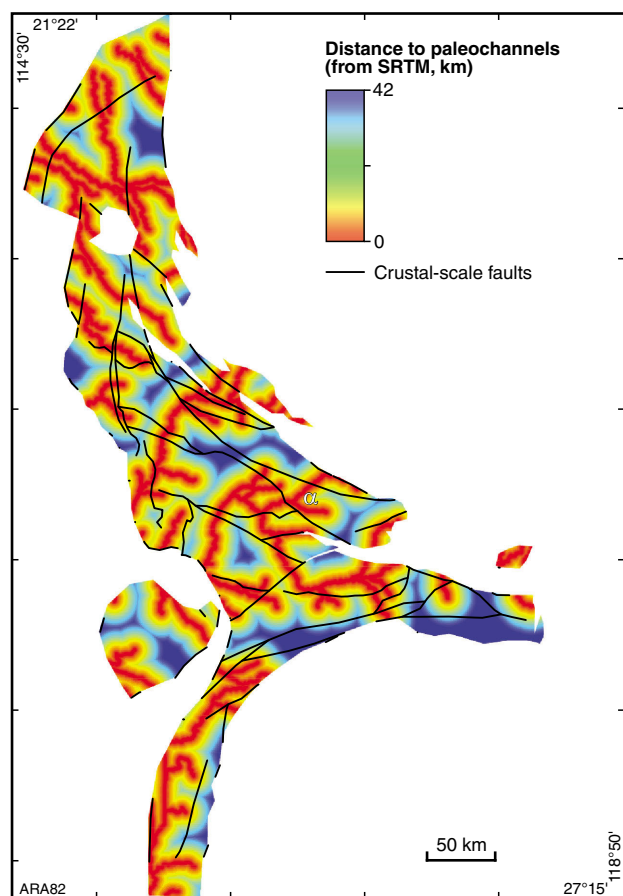


Figure 2.46. Predictor map for surficial uranium pathway: proximity to paleochannels (using SRTM data). Greek letters correspond to the surficial uranium prospective zone (Fig. 25).

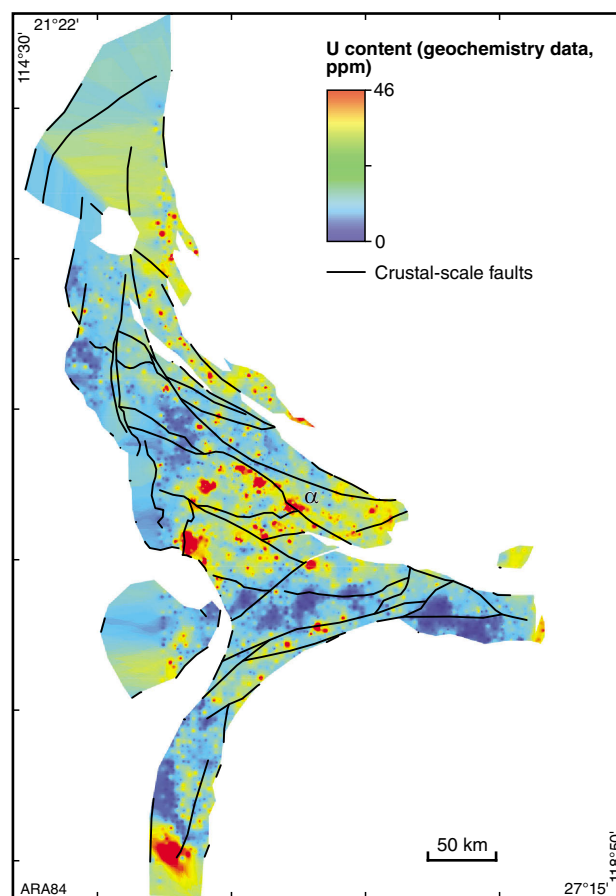


Figure 2.48. Predictor map for surficial uranium trap: U content map (ppm, from geochemistry data). Greek letters correspond to the surficial uranium prospective zone (Fig. 25).

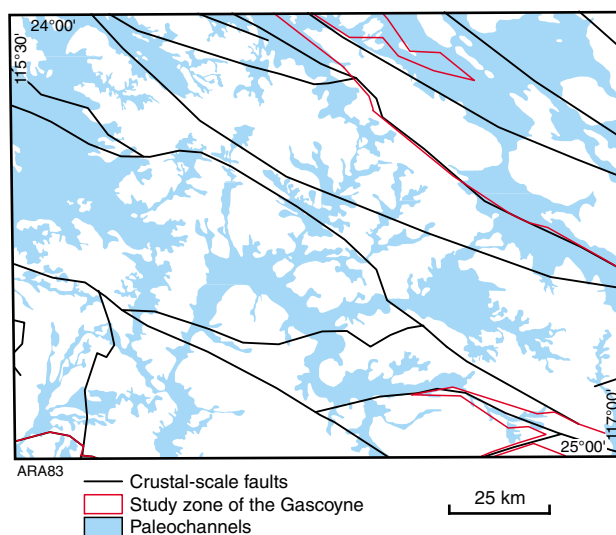


Figure 2.47. Predictor map for surficial uranium pathway: occurrence of paleochannels, MOUNT PHILLIPS 1:250 000 map (using polygons from Krapf, 2012). Greek letters correspond to the surficial uranium prospective zone (Fig. 26).

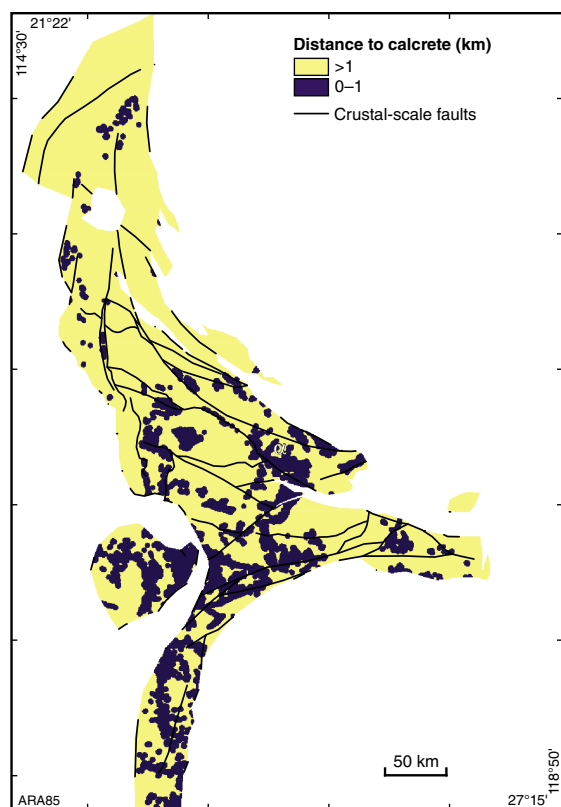


Figure 2.49. Predictor map for surficial uranium physical trap: valley calcrete map. Greek letters correspond to the surficial uranium prospective zone (Fig. 25).



Figure 2.50. Predictor map for surficial uranium physical trap: proximity to playa sediments map. Greek letters correspond to the surficial uranium prospective zone (Fig. 25).

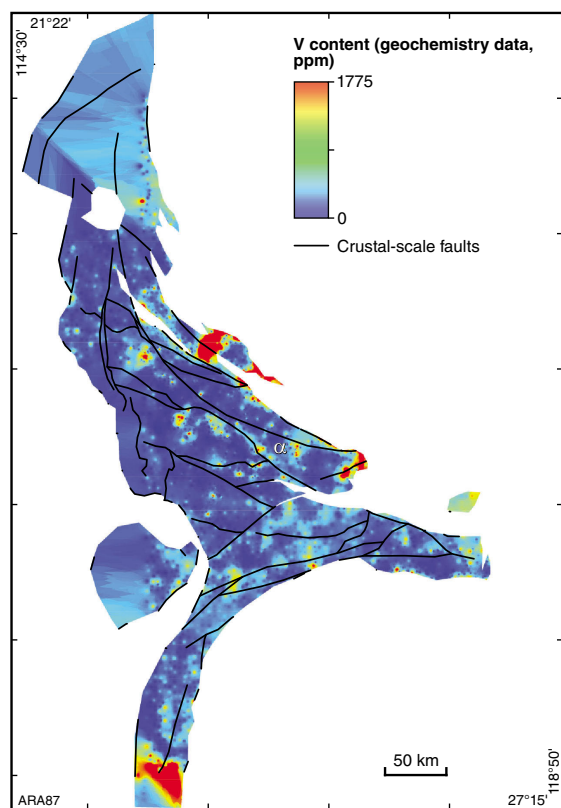


Figure 2.51. Predictor map for surficial uranium chemical trap: V content map (ppm). Greek letters correspond to the surficial uranium prospective zone (Fig. 25).

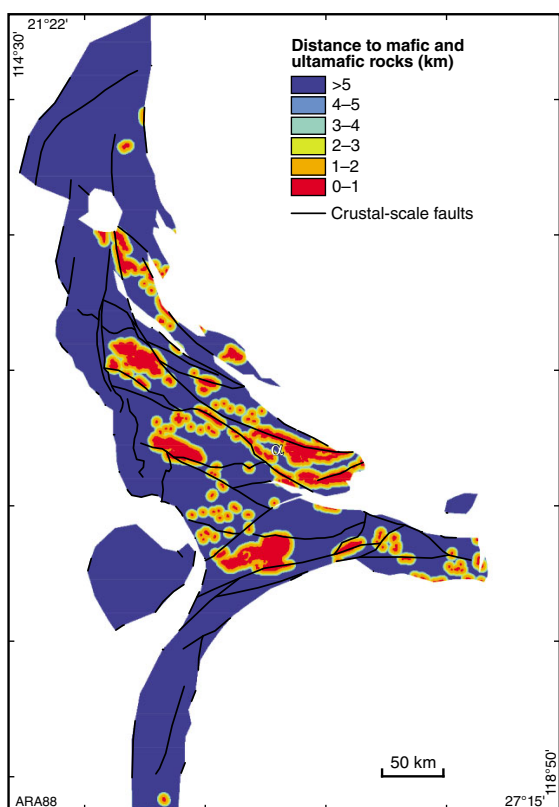


Figure 2.52. Predictor map for surficial uranium and Sn-W chemical trap: distance to mafic and ultramafic rocks. Greek letters correspond to the surficial uranium prospective zone (Fig. 25).

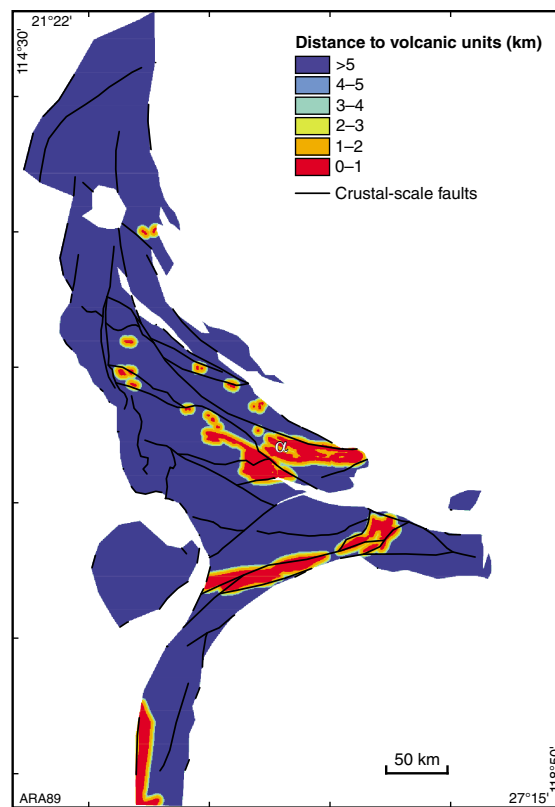


Figure 2.53. Predictor map for surficial uranium chemical trap: distance to volcanic units. Greek letters correspond to the surficial uranium prospective zone (Fig. 25).

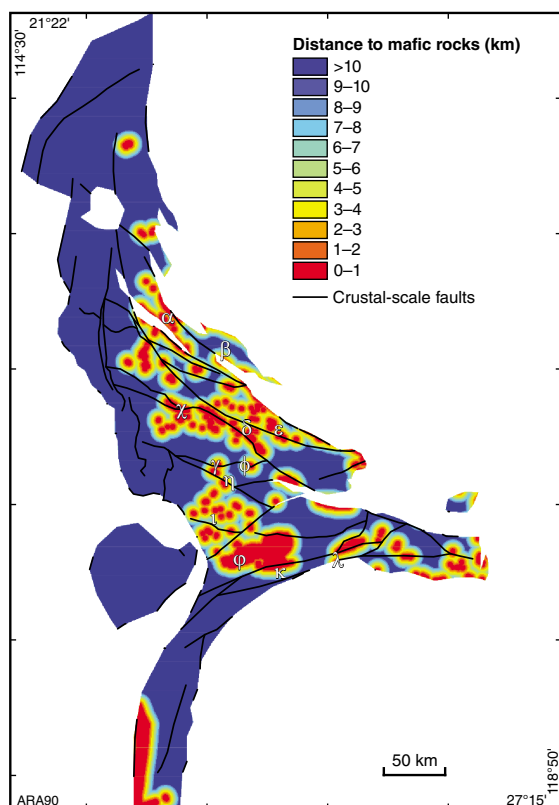


Figure 2.54. Predictor map for PBM source: distance to mafic rocks. Greek letters correspond to the PBM prospective zone (Fig. 29).

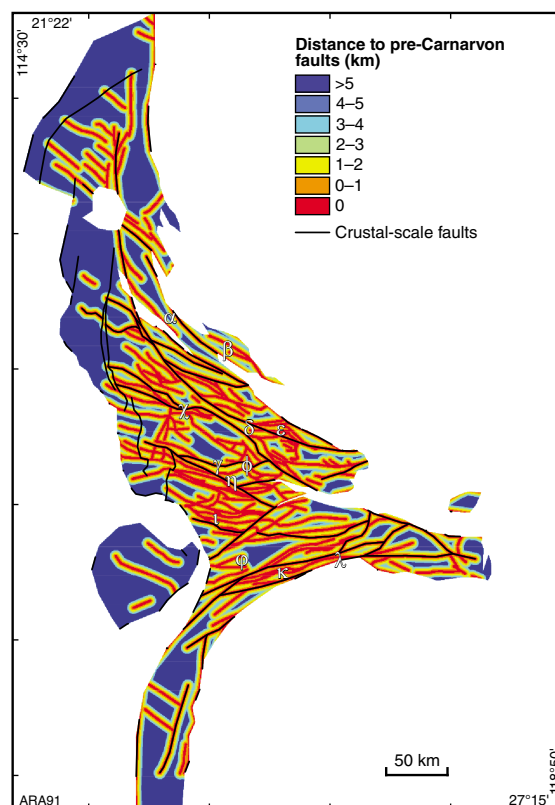


Figure 2.55. Predictor map for PBM pathway: distance to pre-Carnarvon faults. Greek letters correspond to the PBM prospective zone (Fig. 29).

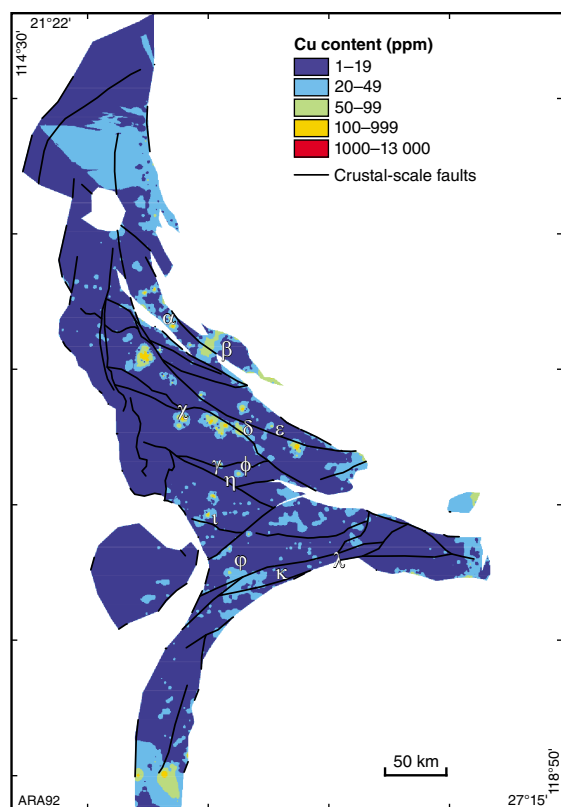


Figure 2.56. Predictor map for PBM trap: Cu content map (ppm). Greek letters correspond to the PBM prospective zone (Fig. 29).

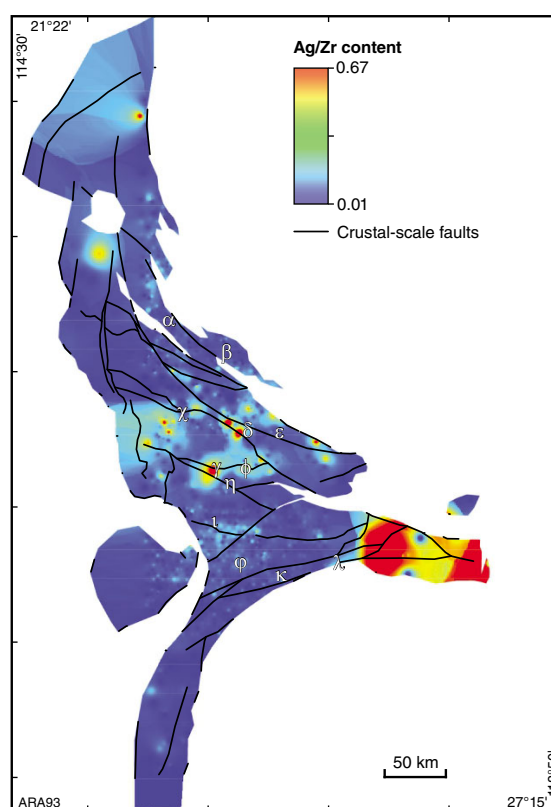


Figure 2.57. Predictor map for PBM trap: Ag/Zr ratio map. Greek letters correspond to the PBM prospective zone (Fig. 29).

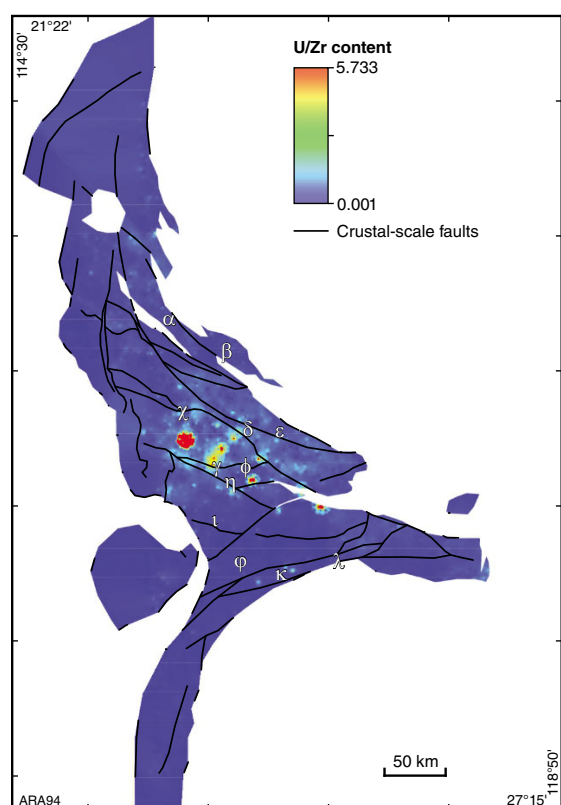


Figure 2.58. Predictor map for PBM trap: U/Zr ratio map. Greek letters correspond to the PBM prospective zone (Fig. 29).

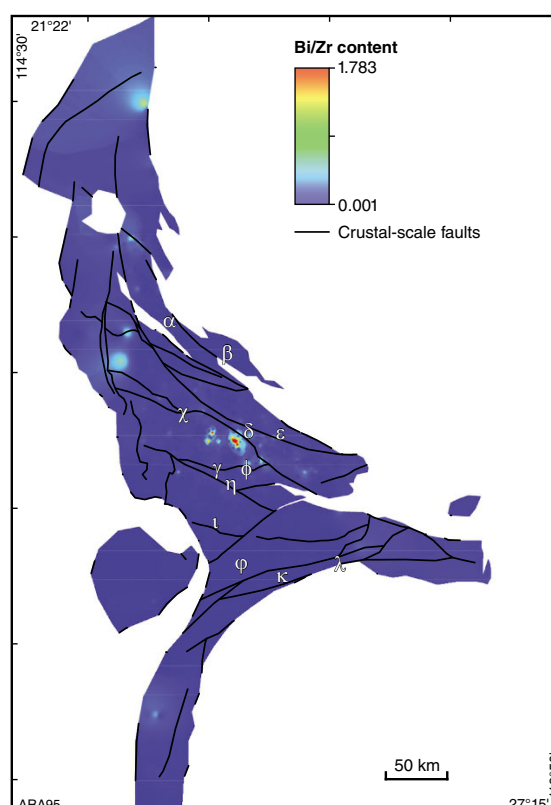


Figure 2.59. Predictor map for PBM trap: Bi/Zr ratio map. Greek letters correspond to the PBM prospective zone (Fig. 29).

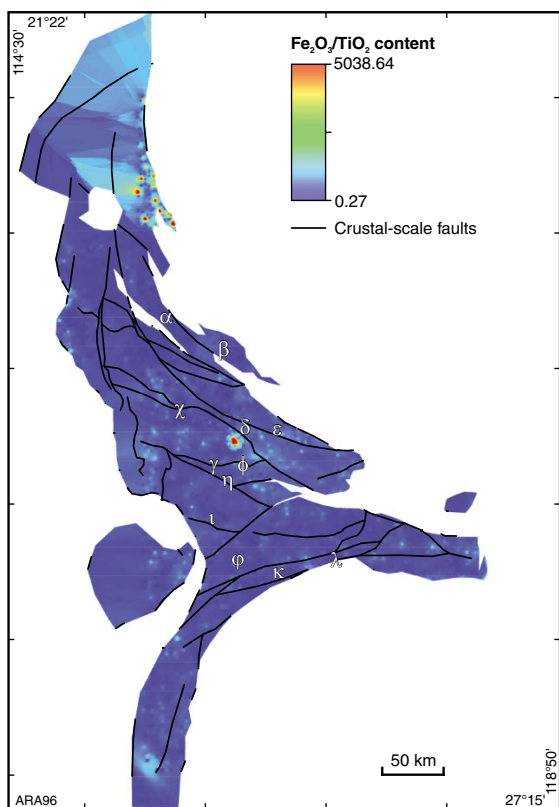


Figure 2.60. Predictor map for PBM trap: $\text{Fe}_2\text{O}_3/\text{TiO}_2$ ratio map. Greek letters correspond to the PBM prospective zone (Fig. 29).

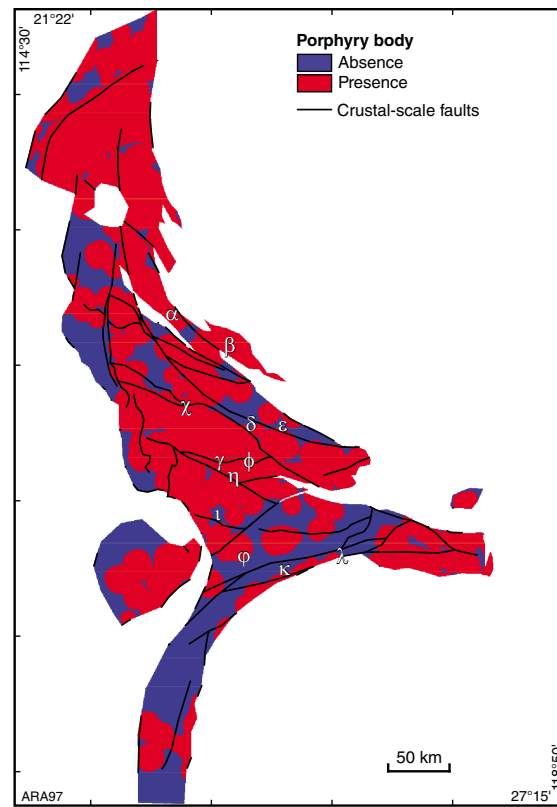


Figure 2.61. Predictor map for PBM physical trap: occurrence of porphyry body. Greek letters correspond to the PBM prospective zone (Fig. 29).

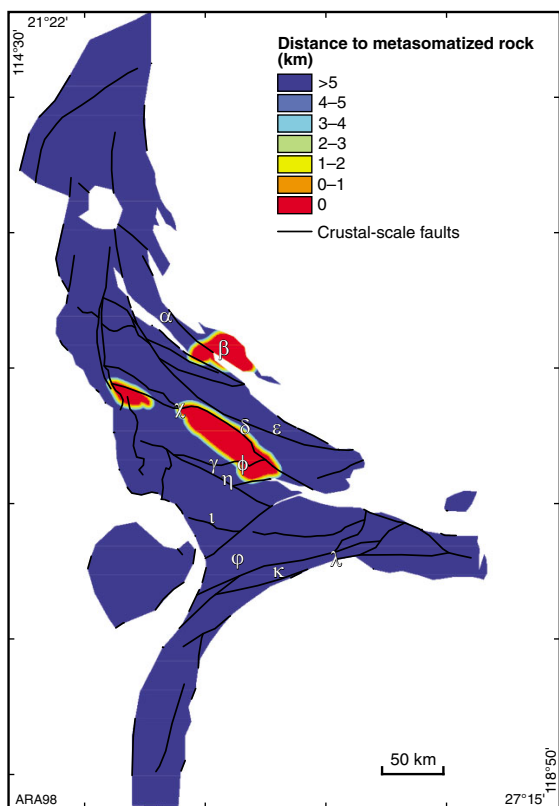


Figure 2.62. Predictor map for PBM and Sn-W chemical trap: distance to skarn/metamorphism. Greek letters correspond to the PBM prospective zone (Fig. 29).

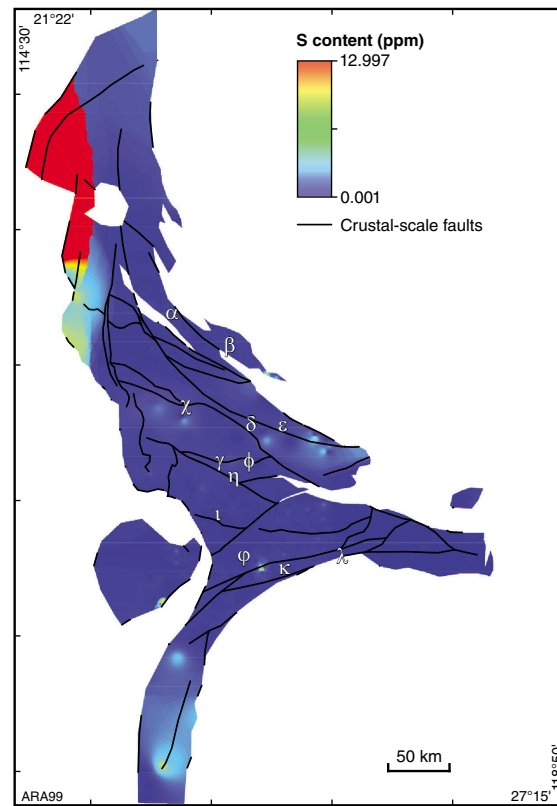


Figure 2.63. Predictor map for PBM chemical trap: S content map (ppm). Greek letters correspond to the PBM prospective zone (Fig. 29).

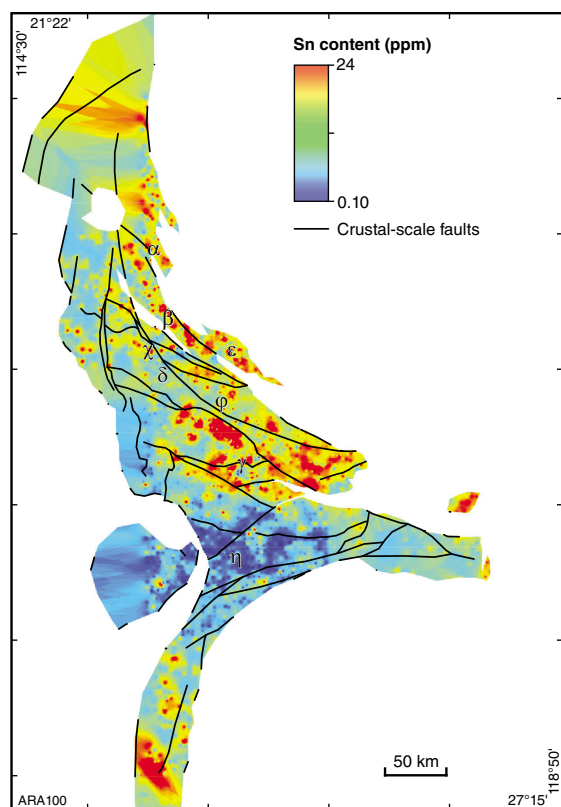


Figure 2.64. Predictor map for Sn–W chemical trap: Sn content map (ppm). Greek letters correspond to the Sn–W prospective zone (Fig. 31).

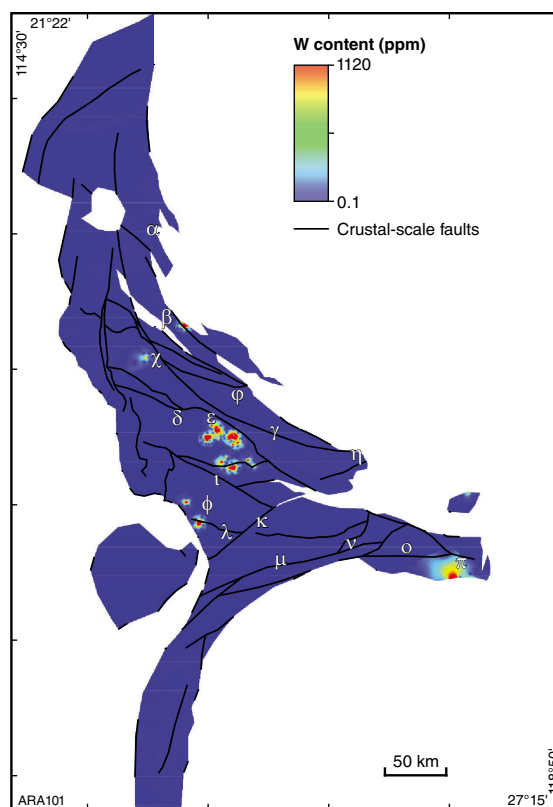


Figure 2.65. Predictor map for Sn–W trap: W content map (ppm). Greek letters correspond to the Sn–W prospective zone (Fig. 31).

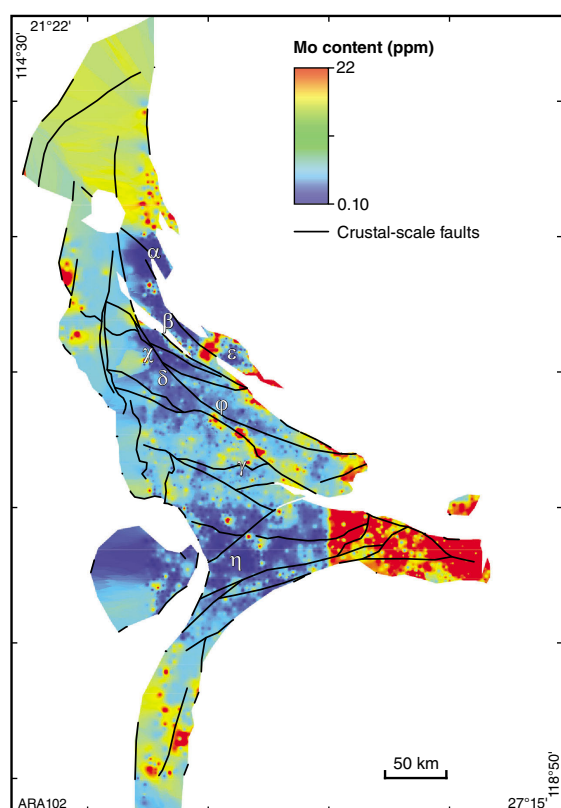


Figure 2.66. Predictor map for Sn–W chemical trap: Mo content map (ppm). Greek letters correspond to the Sn–W prospective zone (Fig. 31).

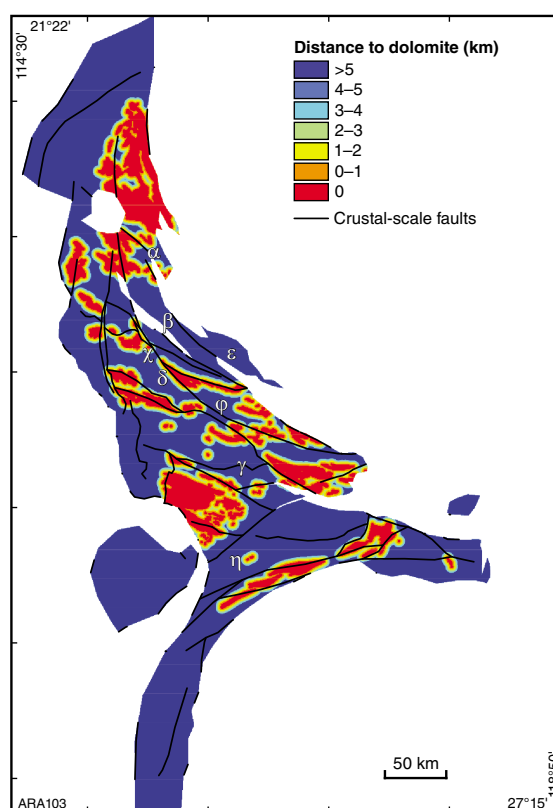


Figure 2.67. Predictor map for Sn–W chemical trap: distance to dolomite. Greek letters correspond to the Sn–W prospective zone (Fig. 31).

References

- Agterberg, FP 1989, Systematic approach to dealing with uncertainty of geoscience information, *in* Application of Computers and Operations in the Mineral Industry *edited by* A Weiss: Colorado Society of Mining Engineers; 21st APCOM Symposium, Las Vegas, February 1989, p. 165–178.
- Agterberg, FP and Bonham-Carter, GF 1990, Deriving weights of evidence from geoscience contour maps for the prediction of discrete events, *in* Applications of Computers and Mathematics in the Mineral Industries: Technical University of Berlin; 22nd APCOM Symposium, Berlin, Germany, 17 September 1990, p. 381–395.
- Aitken, ARA and Betts, PG 2009, Multi-scale integrated structural and aeromagnetic analysis to guide tectonic models: an example from the eastern Musgrave Province, central Australia: *Tectonophysics*, v. 476, no. 3–4, p. 418–435.
- Aitken, ARA, Holden, E-J and Dentith, MC 2013a, Semiautomated quantification of the influence of data richness on confidence in the geologic interpretation of aeromagnetic maps: *Geophysics*, v. 78, no. 2, p. J1–J13, doi:10.1190/geo2012-0033.1.
- Aitken, ARA, Salmon, ML and Kennett, BLN 2013b, Australia's Moho: a test of the usefulness of gravity modelling for the determination of Moho depth: *Tectonophysics*, v. 609, p. 468–479.
- An, P, Moon, WM and Rencz, AN 1991, Application of fuzzy set theory to integrated mineral exploration: *Canadian Journal of Exploration Geophysics*, v. 27, p. 1–11.
- Bierlein, FP, Groves, DI, Goldfarb, RJ and Dube, B 2006, Lithospheric controls on the formation of provinces hosting giant orogenic gold deposits: *Mineralium Deposita*, v. 40, p. 874–886.
- Blake, TS 1993, Late Archaean crustal extension, sedimentary basin formation, flood basalt volcanism, and continental rifting. The Nullagine and Mount Joep Supersequences, Western Australia: *Precambrian Research*, v. 60, p. 185–241.
- Blake, TS 2001, Cyclic continental mafic tuff and flood basalt volcanism in the Late Archaean Nullagine and Mount Joep Supersequences in the eastern Pilbara, Western Australia: *Precambrian Research*, v. 107, p. 139–177.
- Blake, TS and Barley, ME 1992, Tectonic evolution of the Late Archaean to Early Proterozoic Mount Bruce megasequence set, Western Australia: *Tectonics*, v. 11, p. 1415–1425.
- Blake, TS, Buick, R, Brown, SJA and Barley, ME 2004, Geochronology of a Late Archaean flood basalt province in the Pilbara Craton, Australia: constraints on basin evolution, volcanic and sedimentary accumulation, and continental drift rates: *Precambrian Research*, v. 133, no. 3–4, p. 143–173, doi:10.1016/j.precamres.2004.03.012.
- Blakely, RJ and Simpson, RW 1986, Approximating edges of source bodies from magnetic or gravity anomalies: *Geophysics*, v. 51, p. 1494–1498.
- Blockley, JG 1971, The lead, zinc and silver deposits of Western Australia: *Geological Survey of Western Australia, Mineral Resources Bulletin* 9, 234p.
- Bodorkos, S and Wingate, MTD 2007, The contribution of geochronology to GSWA's mapping programs: current perspectives and future directions, *in* GSWA 2007 extended abstracts: promoting the prospectivity of Western Australia: *Geological Survey of Western Australia, Record* 2007/2, p. 10–11.
- Bonham-Carter, GF 1994, *Geographic Information Systems for geoscientists: modelling with GIS*: Pergamon Press, Elsevier B.V., Amsterdam, The Netherlands, 416p.
- Bonham-Carter, GF and Agterberg, FP 1990, Application of a microcomputer-based geographic information system to mineral-potential mapping, *in* Microcomputer-based Applications in Geology *edited by* JT Hanley and DF Merriam: Pergamon Press, New York, US, p. 49–74.
- Boyle, RW 1982, *Geochemical prospecting for thorium and uranium deposits*: Elsevier Scientific Publishing, New York, US, 498p.
- Brown, W 2002, *Artificial Neural Networks: a new method for mineral-prospectivity mapping*: The University of Western Australia, Perth, Western Australia, PhD thesis (unpublished).
- Carlisle, D 1983, Concentration of uranium and vanadium in calcrete and gypcrete, *in* *Residual Deposits* edited by RCL Wilson: Geological Society, London, UK, Special Publication 11, p. 185–195.
- Carranza, EJM 2008, *Geochemical anomaly and mineral prospectivity mapping in GIS*: Elsevier B.V., The Netherlands, 368p.
- Carranza, EJM and Hale, M 2001, Geologically constrained fuzzy mapping of gold mineralization potential, Baguio District, Philippines: *Natural Resources Research*, v. 10, no. 2, p. 125–136.
- Carter, JD 1984, Mortimer Hills pegmatite uranium prospect: a Rossing-type uranium deposit in the Gascoyne Province, *in* *Professional papers for 1982*: Geological Survey of Western Australia, Report 12, p. 27–31.
- Cassidy, KF, Champion, DC, Krapež, B, Barley, ME, Brown, SJA, Blewett, RS, Groenewald, PB and Tyler, IM 2006, A revised geological framework for the Yilgarn Craton, Western Australia: *Geological Survey of Western Australia, Record* 2006/8, 8p.
- Cawood, PA and Tyler, IM 2004, Assembling and reactivating the Proterozoic Capricorn Orogen: lithotectonic elements, orogenies, and significance: *Precambrian Research*, v. 128, p. 201–218.
- Černý, P 1991a, Rare-element granitic pegmatites. Part I: anatomy and internal evolution of pegmatite deposits: *Geoscience Canada*, v. 18, p. 49–67.
- Černý, P 1991b, Rare-element granitic pegmatites. Part II: regional to global environments and petrogenesis: *Geoscience Canada*, v. 18, p. 68–81.
- Černý, P and Ercit, TS 2005, The classification of granitic pegmatites revisited: *Canadian Mineralogist*, v. 43, p. 2005–2006.
- Champion, DC, Budd, AR and Wyborn, LAI 2007, OZCHEM National whole rock geochemistry database (digital data repository): *Geoscience Australia, Canberra, ACT*, viewed December 2013, <<http://www.ga.gov.au/meta/ANZCW0703011055.html>>.
- Cheng, Q 2007, Mapping singularities with stream sediment geochemical data for prediction of undiscovered mineral deposits in Gejiu, Yunnan Province, China: *Ore Geology Reviews*, v. 32, p. 314–324.
- Cline, JS 2001, Timing of gold and arsenic sulfide mineral deposition at the Getchell carlin-type gold deposit, North-Central Nevada: *Economic Geology*, v. 96, p. 75–89.
- Clitheroe, G, Gudmundsson, O and Kennett, BLN 2000, The crustal thickness of Australia: *Journal of Geophysical Research*, v. 105, p. 13697–13713.
- Compston, W and Pidgeon, RT 1986, Jack Hills, evidence of more very old detrital zircons in Western Australia: *Nature*, v. 321, p. 766–769.
- Cooper, GRJ and Cowan, DR 2006, Enhancing potential field data using filters based on the local phase: *Computers and Geosciences*, v. 32, p. 1585–1591.
- Cox, SF, Knackstedt, MA and Braun, J 2001, Principles of structural control on permeability and fluid flow in hydrothermal systems: *Reviews in Economic Geology*, v. 14, p. 1–24.
- Cutten, HN, Thorne, AM and Johnson, SP 2011, Geology of the Edmund and Collier Groups, *in* *Capricorn Orogen seismic and magnetotelluric (MT) workshop 2011: extended abstracts* *edited by* SP Johnson, AM Thorne and IM Tyler: *Geological Survey of Western Australia, Record* 2011/25, p. 41–48.
- D'Ercole, C, Groves, DI and Knox-Robinson, CM 2000, Using fuzzy logic in a geographic information system environment to enhance conceptually based prospectivity analysis of Mississippi Valley-type mineralisation: *Australian Journal of Earth Sciences*, v. 47, no. 5, p. 913–927.

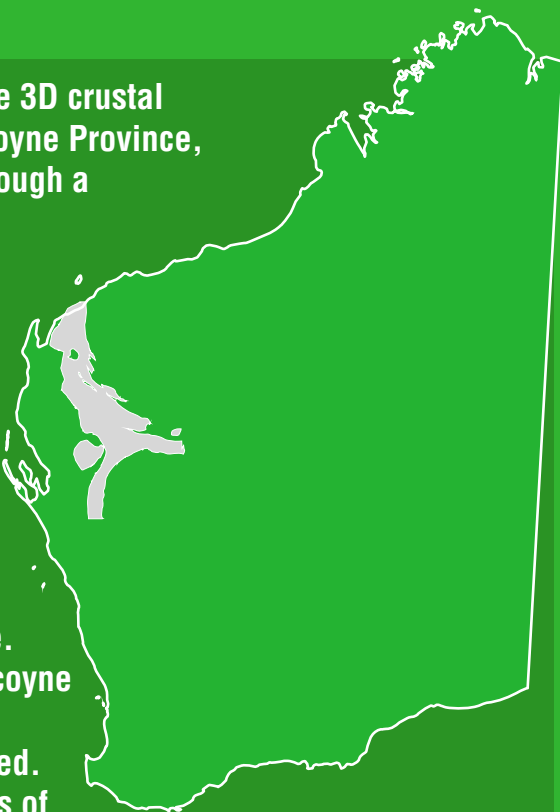
- Dahlkamp, FJ 1978, Classification of uranium deposits: *Mineralium Deposita*, v. 13, p. 83–104.
- Davies, BM 1998, Proterozoic zoned tungsten-bearing skarns and associated intrusives of the northwest Gascoyne Complex, Western Australia: Geological Survey of Western Australia, Report 53, 54p.
- Desert Mines and Minerals 2011, Camel Hills Joint Venture Update: Desert Mines and Minerals, Belmont, WA, viewed 5 December 2013, 4p. <<http://www.asx.com.au/asxpdf/20110919/pdf/4214xkv399gm5q.pdf>>.
- Dynasty Resources Limited 2013, Hector Bore: Dynasty Resources Limited, West Perth, WA, viewed 5 December 2013, 1p. <<http://www.dynastymetals.com.au/projects/uranium-and-base-metals/western-australia-projects/hector-bore.html>>.
- Einaudi, MT, Meinert, LD and Newberry, RJ 1981, Skarn deposits, *in* Seventy-fifth Anniversary Volume, 1906–1980 *edited by* BJ Skinner: Economic Geology Publishing Co., p. 317–391.
- Equus Ltd 1999, Quarterly report for the period ending 31 March 1999: Report to Australian Securities Exchange (ASX), 31 March 1999.
- Eugster, HP 1985, Granites and hydrothermal ore-deposits: a geochemical framework: *Mineralogical Magazine*, v. 49, p. 7–23.
- Ferguson, HG and Bateman, AM 1912, Geologic features of tin deposits: *Economic Geology*, v. 7, p. 209–262.
- Ferguson, KM 1999, Lead, zinc and silver deposits of Western Australia: Geological Survey of Western Australia, Mineral Resources Bulletin 15, 314p.
- Fetherston, JM 2004, Tantalum in Western Australia: Geological Survey of Western Australia, Mineral Resources Bulletin 22, 162p.
- Flint, DJ and Abeysinghe, PB 2000, Geology and mineral resources of the Gascoyne Region: Geological Survey of Western Australia, Record 2000/7, 29p.
- Foley, SF 2008, Rejuvenation and erosion of the cratonic lithosphere: *Nature Geoscience*, v. 1, p. 503–510.
- Froude, CF, Ireland, TR, Kinny, PD, Williams, IS, Compston, W, Williams, IR and Myers, JS 1983, Ion-microprobe identification of 4100–4200 Myr old terrestrial zircons: *Nature*, v. 304, p. 616–618.
- Gascoyne Resources Limited 2012, Glenburgh gold resource increases to 1.04 Moz: Report to Australian Securities Exchange (ASX), 2 October 2012, 7p.
- Geological Survey of Western Australia 2011, WACHEM: State geochemistry database: Geological Survey of Western Australia, viewed December 2011, <<http://www.dmp.wa.gov.au/datacentre>>.
- Geological Survey of Western Australia 2012, Western Capricorn Orogen, 2011 update: Geological Survey of Western Australia, 1:100 000 Geological Information Series.
- Goodwin, JA 2011, Potential-field interpretation of the Capricorn Orogen, Western Australia: worms, forward modelling, and 3D inversion, *in* Capricorn Orogen seismic and magnetotelluric (MT) workshop 2011: extended abstracts *edited by* SP Johnson, AM Thorne and IM Tyler: Geological Survey of Western Australia, Record 2011/25, p. 61–74.
- Grauch, VJS, Rodriguez, BD, Bankey, V and Wooden, JL 2003, Evidence for a Battle Mountain-Eureka crustal fault zone, north-central Nevada, and its relation to Neoproterozoic-Early Paleozoic continental break: *Journal of the Geophysical Research B: Solid Earth*, v. 108, no. 3, p. 3–15.
- Groves, DI, Bierlein, FP, Meinert, LD and Hitzman, MW 2010, Iron Oxide Copper-Gold (IOCG) Deposits through Earth History: Implications for Origin, Lithospheric Setting, and Distinction from Other Epigenetic Iron Oxide Deposits: *Economic Geology*, v. 105, no. 3, p. 641–654.
- Groves, DI, Goldfarb, RJ, Gebre-Mariam, M, Hagemann, SG and Robert, F 1998, Orogenic gold deposits: a proposed classification in the context of their crustal distribution and relationship to other gold deposit types: *Ore Geology Reviews*, v. 13, no. 1–5, p. 7–27.
- Groves, DI and Phillips, GN 1987, The genesis and tectonic controls on Archean lode gold deposits of the Western Australian shield: a metamorphic-replacement model: *Ore Geology Reviews*, v. 2, p. 287–322.
- Groves, DI and Vielreicher, NM 2001, The Phalabowra (Palabora) carbonatite-hosted magnetite–copper sulfide deposit, South Africa: an end-member of the iron oxide copper–gold–rare earth element deposit group?: *Mineralium Deposita*, v. 36, p. 189–194.
- Hagemann, SG and Cassidy, KF 2000, Archean lode gold deposits, *in* Gold in 2000 *edited by* SG Hagemann and PE Brown: Reviews in Economic Geology 13, p. 9–68.
- Hardy, A 1992, The structural and metamorphic setting of the Yinnetharra pegmatites in the Nardoo Hill area, Gascoyne Complex, Western Australia: The University of Western Australia, Perth, Western Australia, BSc (Hons) thesis (unpublished).
- Hart, CJR 2007, Reduced intrusion-related gold systems, *in* Mineral deposits of Canada: a synthesis of major deposit types, district metallogeny, the evolution of geological provinces, and exploration methods *edited by* WD Goodfellow: Geological Association of Canada, Mineral Deposits Division, Special Publication 5, p. 95–112.
- Hassan, LY 2006, Potential for major deposits - a new look at mineralization in the Gascoyne, *in* GSWA 2006 extended abstracts: promoting the prospectivity of Western Australia: Geological Survey of Western Australia, Record 2006/3, p. 13–14.
- Hedenquist, JW, Arribas, A and Gonzalez-Urien, E 2000, Exploration for epithermal gold deposits: *Reviews in Economic Geology*, v. 13, p. 245–278.
- Heinrich, CA 1990, The chemistry of hydrothermal tin(-tungsten) ore deposition: *Economic Geology*, v. 85, p. 457–481.
- Hitzman, MW and Valenta, RK 2005, Uranium in iron oxide–copper–gold (IOCG) systems: *Economic Geology*, v. 100, p. 1657–1661.
- Hocking, RM, Williams, SJ, Moore, PS, Denman, PD, Lavingar, IH and Van De Graaff, WJE 1983, Explanatory notes on the Kennedy Range 1:250 000 geological sheet, Western Australia: Geological Survey of Western Australia, Record 1983/5, 55p.
- Holden, E-J, Dentith, MC and Kovesi, P 2008, Towards the automated analysis of regional aeromagnetic data to identify regions prospective for gold deposits: *Computers and Geosciences*, v. 34, p. 1505–1513.
- Holden, E-J, Fu, SC, Kovesi, P, Dentith, MC, Bourne, B and Hope, M 2011, Automatic identification of responses from porphyry intrusive systems within magnetic data using image analysis: *Journal of Applied Geophysics*, v. 74, p. 255–262.
- Holden, E-J, Wong, JC, Kovesi, P, Wedge, D, Dentith, MC and Bagas, L 2012, Identifying structural complexity in aeromagnetic data: an image analysis approach to greenfields gold exploration: *Ore Geology Reviews*, v. 46, p. 47–59.
- Hronsky, JMA and Groves, DI 2008, Science of targeting: definition, strategies, targeting and performance measurement: *Australian Journal of Earth Sciences*, v. 55, p. 3–12.
- International Atomic Energy Agency 2000, Methods of exploitation of different types of uranium deposits: International Atomic Energy Agency, Vienna, Austria, 75p.
- Johnson, JP and Cross, KC 1995, U-Pb geochronological constraints on the genesis of the Olympic Dam Cu–U–Au–Ag deposit, South Australia: *Economic Geology*, v. 90, p. 1046–1063.
- Johnson, SP 2013, The birth of supercontinents and the Proterozoic assembly of Western Australia: Geological Survey of Western Australia, Perth, Western Australia, 78p.

- Johnson, SP, Sheppard, S, Rasmussen, B, Wingate, MTD, Kirkland, CL, Muhling, JR, Fletcher, IR and Belousova, E 2010, The Glenburgh Orogeny as a record of Paleoproterozoic continent–continent collision: Geological Survey of Western Australia, Record 2010/5, 54p.
- Johnson, SP, Thorne, AM and Tyler, IM (editors) 2011a, Capricorn Orogen seismic and magnetotelluric (MT) workshop 2011: extended abstracts: Geological Survey of Western Australia, Record 2011/25, 120p.
- Johnson, SP, Sheppard, S, Rasmussen, B, Wingate, MTD, Kirkland, CL, Muhling, JR, Fletcher, IR and Belousova, EA 2011b, Two collisions, two sutures: punctuated pre-1950 Ma assembly of the West Australian Craton during the Ophthalmanian and Glenburgh Orogenies: Precambrian Research, v. 189, no. 3–4, p. 239–262, doi: 10.1016/j.precamres.2011.07.011.
- Johnson, SP, Sheppard, S, Thorne, AM, Rasmussen, B, Fletcher, IR, Wingate, MTD and Cutten, HN 2011c, The role of the 1280–1250 Ma Matherbukin Tectonic Event in shaping the crustal architecture and mineralization history of the Capricorn Orogen, in GSWA 2011 extended abstracts: promoting the prospectivity of Western Australia: Geological Survey of Western Australia, Record 2011/2, p. 1–3.
- Johnson, SP, Sheppard, S, Wingate, MTD, Kirkland, CL and Belousova, EA 2011d, Temporal and hafnium isotopic evolution of the Glenburgh Terrane basement: an exotic crustal fragment in the Capricorn Orogen: Geological Survey of Western Australia, Report 110, 27p.
- Johnson, SP, Thorne, AM, Tyler, IM, Korsch, RJ, Kennett, BLN, Cutten, HN, Goodwin, J, Blay, OA, Blewett, RS, Joly, A, Dentith, MC, Aitken, ARA, Holzschuh, J, Salmon, M, Reading, A, Heinson, G, Boren, G, Ross, J, Costelloe, RD and Fomin, T 2013, Crustal architecture of the Capricorn Orogen, Western Australia and associated metallogeny: Australian Journal of Earth Sciences, v. 60, no. 6–7, p. 681–705, doi:10.1080/08120099.2013.826735.
- Joly, A, Aitken, ARA, Dentith, M, Porwal, AK and Smithies, RH in press, Mineral prospectivity analysis of the West Musgrave Province: Geological Survey of Western Australia, Report 117.
- Joly, A, Porwal, A and McCuaig, TC 2012, Exploration targeting for orogenic gold deposits in the Granites–Tanami Orogen: Mineral system analysis, targeting model and prospectivity analysis: Ore Geology Reviews, v. 48, p. 349–383.
- Kemp, AIS, Wilde, SA, Hawkesworth, CJ, Coath, CD, Nemchin, AA, Pidgeon, RT, Vervoort, JD and DuFrane, SA 2010, Hadean crustal evolution revisited: new constraints from Pb–Hf isotope systematics of the Jack Hills zircons: Earth and Planetary Science Letters, v. 296, p. 45–56.
- Kennett, BLN, Salmon, M, Saygin, E and AusMoho Working Group 2011, AusMoho: the variation of Moho depth in Australia: Geophysical Journal International, v. 187, no. 2, p. 946–958, doi:10.1111/j.1365-246X.2011.05194.x.
- Kinny, PD, Williams, IS, Froude, DO, Ireland, TR and Compston, W 1988, Early Archaean zircon ages from orthogneisses and anorthositic at Mount Narryer, Western Australia: Precambrian Research, v. 38, p. 325–341.
- Knox-Robinson, CM 2000, Vectorial fuzzy logic: a novel technique for enhanced mineral prospectivity mapping, with reference to the orogenic gold mineralisation potential of the Kalgoorlie Terrane, Western Australia: Australian Journal of Earth Sciences, v. 47, p. 929–941.
- Knox-Robinson, CM and Wyborn, LAI 1997, Towards a holistic exploration strategy: using Geographic Information Systems as a tool to enhance exploration: Australian Journal of Earth Sciences, v. 44, no. 4, p. 453–463.
- Kogarko, LN, Kononova, VA, Orlova, MP and Woolley, AR 1995, Alkaline rocks and carbonatites of the world – Part Two: Former USSR: Chapman & Hall, London, UK, 226p.
- Krapf, CBE 2012, New insights into the regolith of parts of the Gascoyne region: Geological Survey of Western Australia, Record 2011/22, 54p.
- Kreuzer, OP, Etheridge, MA, Guj, P, McMahon, ME and Holden, DJ 2008, Linking mineral deposit models to quantitative risk analysis and decision-making in exploration: Economic Geology, v. 103, no. 4, p. 829–850, doi:10.2113/gsecongeo.103.4.829.
- Kreuzer, OP, Markwitz, V, Porwal, AK and McCuaig, TC 2010, A continent-wide study of Australia's uranium potential: Part I: GIS-assisted manual prospectivity analysis: Ore Geology Reviews, v. 38, no. 4, p. 334–366.
- Landis, GP and Rye, RO 1974, Geologic, fluid inclusion, and stable isotope studies of the Pasto Buena tungsten-base metal ore deposit, Northern Peru: Economic Geology, v. 69, no. 7, p. 1025–1059, doi:10.2113/gsecongeo.69.7.1025.
- Lang, JR and Baker, T 2001, Intrusion-related gold systems: the present level of understanding: Mineralium Deposita, v. 36, no. 6, p. 477–489.
- Lehmann, B 1990, Metallogeny of tin: Springer Berlin Heidelberg, New York, US, 212p.
- Long, KR, Van Gosen, BS, Foley, NK and Cordier, D 2010, The principal rare Earth elements deposits of the United States – a summary of domestic deposits and a global perspective: US Geological Survey Scientific Investigations Report 2010-5220: US Geological Survey, 96p.
- Mark, G, Oliver, NHS, Williams, PJ, Valenta, RK and Crookes, RA 2000, The evolution of the Ernest Henry Fe-Oxide–(Cu–Au) hydrothermal system, in A Global Perspective edited by TM Porter: PGC Publishing, Adelaide, SA, p. 123–136.
- Martin, DM and Morris, PA 2010, Tectonic setting and regional implications of ca. 2.2 Ga mafic magmatism in the southern Hamersley Province, Western Australia: Australian Journal of Earth Sciences, v. 57, p. 911–931.
- Martin, DM and Thorne, AM 2004, Tectonic setting and basin evolution of the Bangemall Supergroup in the northwestern Capricorn Orogen: Precambrian Research, v. 128, p. 385–409.
- Martin, DM, Sheppard, S and Thorne, AM 2005, Geology of the Maroonah, Ullawarra, Capricorn, Mangaroo, Edmund, and Elliott Creek 1:100 000 sheets: Geological Survey of Western Australia, 1:100 000 Geological Series Explanatory Notes, 65p.
- Martin, DM, Sircombe, KN, Thorne, AM, Cawood, PA and Nemchin, AA 2008, Provenance history of the Bangemall Supergroup and implications for the Mesoproterozoic paleogeography of the West Australian Craton, in Assembling Australia: Proterozoic building of a continent edited by PA Cawood and RJ Korsch: Precambrian Research v. 166, no. 1–4, p. 93–110.
- Mathur, R, Marschik, R, Ruiz, J, Munizaga, F, Leveille, RA and Martin, W 2002, Age of mineralization of the Candelaria Fe oxide Cu–Au deposit and the origin of the Chilean iron belt, based on Re–Os isotopes: Economic Geology, v. 97, p. 59–71.
- McCuaig, TC, Beresford, S and Hronsky, J 2010, Translating the mineral systems approach into an effective exploration targeting system: Ore Geology Reviews, v. 38, p. 128–138.
- McCuaig, TC and Hronsky, JM 2000, The current status and future of the interface between the exploration industry and economic geology research: Reviews in Economic Geology, v. 13, p. 553–559.
- McCuaig, TC and Kerrich, R 1998, P–T–t–deformation–fluid characteristics of lode gold deposits: evidence from alteration systematics: Ore Geology Reviews, v. 12, no. 6, p. 381–453.
- McKay, AD and Miezeitis, Y 2001, Australia's uranium resources, geology and development of deposits: Australian Geological Survey Organisation – Geoscience Australia, Mineral Resource Report 1, 184p.
- Meissner, R 1989, Rupture, creep, lamellae and crocodiles: happenings in the continental crust: Terra Nova, v. 1, no. 1, p. 17–28.

- Mikucki, EJ 1998, Hydrothermal transport and depositional processes in Archean lode-gold systems: a review: *Ore Geology Reviews*, v. 13, no. 1–5, p. 307–321.
- Mincor Resources NL 2006, High-grade mineralisation confirmed at Gascoyne Tungsten Project, Media Release 26 June 2006.
- Mutschler, FE and Mooney, TC 1993, Precious metal deposits related to alkaline igneous rocks — provisional classification, grade-tonnage data, and exploration frontiers, in *Mineral deposit modeling edited by RV Kirkham, WD Sinclair, RI Thorpe and JM Duke*: Geological Association of Canada, Special Paper 40, p. 479–520.
- Myers, JS 1988, Early Archean Narryer Gneiss Complex, Yilgarn Craton, Western Australia: *Precambrian Research*, v. 38, p. 279–307.
- Nelson, DR 1996, 105007: leucocratic orthogneiss, Churla Well; *Geochronology Record 12*: Geological Survey of Western Australia, 4p.
- Nelson, DR 1999, 142914: porphyritic biotite–hornblende monzogranite, Bulladger Bore; *Geochronology Record 339*: Geological Survey of Western Australia, 4p.
- Occhipinti, SA, Sheppard, S, Passchier, C, Tyler, IM and Nelson, DR 2004, Palaeoproterozoic crustal accretion and collision in the southern Capricorn Orogen: the Glenburgh Orogeny: *Precambrian Research*, v. 128, p. 237–255.
- Partington, GA, McNaughton, NJ and Williams, IS 1995, A review of the geology, mineralization, and geochronology of the Greenbushes Pegmatite, Western Australia: *Economic Geology*, v. 90, p. 616–635.
- Pearson, JM 1996, Alkaline rocks of the Gifford Creek Complex, Gascoyne Province, Western Australia — their petrogenetic and tectonic significance: University of Western Australia, Perth, Western Australia, PhD thesis (unpublished), 286p.
- Pearson, JM and Taylor, WR 1996, Mineralogy and geochemistry of fenitized alkaline ultrabasic sills of the Gifford Creek Complex, Gascoyne Province, Western Australia: *The Canadian Mineralogist*, v. 34, no. 2, p. 201–219.
- Pearson, JM, Taylor, WR and Barley, ME 1996, Geology of the alkaline Gifford Creek Complex, Gascoyne Complex, Western Australia: *Australian Journal of Earth Sciences*, v. 43, no. 3, p. 299–309.
- Phillips, GN and Groves, DI 1983, The nature of Archaean gold-bearing fluids as deduced from gold deposits of Western Australia: *Journal of the Geological Society of Australia*, v. 30, no. 1, p. 25–39.
- Phillips, GN and Powell, R 2010, Formation of gold deposits: a metamorphic devolatilization model: *Journal of Metamorphic Geology*, v. 28, p. 689–718.
- Pirajno, F 2004, Metallogeny in the Capricorn Orogen, Western Australia: *Precambrian Research*, v. 128, p. 411–439.
- Pirajno, F and González-Álvarez, I 2013, The ironstone veins of the Gifford Creek ferrocarbonatite complex, Gascoyne Province: *Geological Survey of Western Australia, Record 2013/12*, 19p.
- Pirajno, F, Sheppard, S, Groenewald, PB and Johnson, SP 2008, Mineral systems in the Gascoyne Complex, Western Australia, in *GSWA 2008 extended abstracts: promoting the prospectivity of Western Australia*: Geological Survey of Western Australia, Record 2008/2, p. 4–7.
- Pollard, PJ, Mark, G and Mitchell, LC 1998, Geochemistry of post-1540 Ma granites in the Cloncurry district, Northwest Queensland: *Economic Geology*, v. 93, p. 1330–1344.
- Porwal, A, Carranza, EJM and Hale, M 2003, Knowledge-driven and data-driven fuzzy models for predictive mineral potential mapping: *Natural Resources Research*, v. 12, no. 1, p. 1–25.
- Porwal, AK and Kreuzer, OP 2010, Introduction to the Special Issue: Mineral prospectivity analysis and quantitative resource estimation: *Ore Geology Reviews*, v. 38, no. 3, p. 121–127.
- Rasmussen, B, Fletcher, IR, Muhling, JR and Wilde, SA 2010, In situ U–Th–Pb geochronology of monazite and xenotime from the Jack Hills belt: implications for the age of deposition and metamorphism of Hadean zircons: *Precambrian Research*, v. 180, no. 1–2, p. 26–46.
- Reading, AM, Tkalcic, H, Kennett, BLN, Johnson, SP and Sheppard, S 2012, Seismic structure of the crust and uppermost mantle of the Capricorn and Paterson Orogens and adjacent cratons, Western Australia, from passive seismic transects: *Precambrian Research*, v. 196–197, p. 295–308, doi: 10.1016/j.precamres.2011.07.001.
- Reeve, JS, Cross, KC, Smith, RN and Oreskes, N 1990, The Olympic Dam copper–uranium–gold–silver deposit, South Australia, in *Geology and mineral deposits of Australia and Papua New Guinea edited by F Hughes*: Australasian Institute of Mining and Metallurgy, Monograph 14, p. 1009–1035.
- Roberts, S, Sanderson, DJ and Gumiel, P 1998, Fractal analysis of Sn–W mineralization from central Iberia; insights into the role of fracture connectivity in the formation of an ore deposit: *Economic Geology*, v. 98, no. 3, p. 360–365.
- Selway, K, Sheppard, S, Thorne, AM, Johnson, SP and Groenewald, PB 2009, Identifying the lithospheric structure of a Precambrian orogen using magnetotellurics: the Capricorn Orogen, Western Australia: *Precambrian Research*, v. 168, p. 185–196.
- Sheppard, S, Bodorkos, S, Johnson, SP, Wingate, MTD and Kirkland, CL 2010a, The Paleoproterozoic Capricorn Orogeny: intracontinental reworking not continent–continent collision: *Geological Survey of Western Australia, Report 108*, 33p.
- Sheppard, S, Johnson, SP, Wingate, MTD, Kirkland, CL and Pirajno, F 2010b, Explanatory Notes for the Gascoyne Province: *Geological Survey of Western Australia, Perth, Western Australia*, 336p.
- Sheppard, S, Occhipinti, SA and Nelson, DR 2005, Intracontinental reworking in the Capricorn Orogen, Western Australia: the 1680–1620 Ma Mangaroon Orogeny: *Australian Journal of Earth Sciences*, v. 52, p. 443–460.
- Sheppard, S, Occhipinti, SA and Tyler, IM 2003, The relationship between tectonism and composition of granitoid magmas, Yarlalweelor Gneiss Complex, Western Australia: *Lithos*, v. 66, p. 133–154.
- Sheppard, S, Occhipinti, SA and Tyler, IM 2004, A 2005–1970 Ma Andean-type batholith in the southern Gascoyne Complex, Western Australia: *Precambrian Research*, v. 128 (Assembling the Palaeoproterozoic Capricorn Orogen), p. 257–277.
- Sheppard, S, Rasmussen, B, Muhling, JR, Farrell, TR and Fletcher, IR 2007, Grenvillian-aged orogenesis in the Palaeoproterozoic Gascoyne Complex, Western Australia: 1030–950 Ma reworking of the Proterozoic Capricorn Orogen: *Journal of Metamorphic Geology*, v. 25, p. 477–494.
- Sillitoe, RH 1973, The tops and bottoms of porphyry copper deposits: *Economic Geology*, v. 68, p. 799–815.
- Sillitoe, RH 2000, Gold-rich porphyry deposits: descriptive and genetic models and their role in exploration and discovery: *Society of Economic Geologists Reviews*, v. 13, p. 315–345.
- Sillitoe, RH 2003, Iron oxide–copper–gold deposits: An Andean view: *Mineralium Deposita*, v. 38, p. 787–812.
- Sillitoe, RH 2010, Porphyry copper systems: *Economic Geology*, v. 105, p. 3–41.
- Singer, DA and Kouza, R 1999, A comparison of the weights-of-evidence method and probabilistic neural networks: *Natural Resources Research*, v. 8, no. 4, p. 287–298.
- Soloman, M, Groves, DI and Jaques, AL 1994, The geology and origin of Australia's mineral deposits: Oxford University Press, 1002p.

- Spaggiari, CV 2007, Structural and lithological evolution of the Jack Hills greenstone belt, Narryer Terrane, Yilgarn Craton, Western Australia: Geological Survey of Western Australia, Record 2007/3, 49p.
- Sullivan, MP 1996, Annual report on Gascoyne Joint Venture Project covering E09/531, E09/648, E09/649, E09/679, E09/716, E09/719 and E09/734; Equatorial Mining NL: Geological Survey of Western Australia, Statutory mineral exploration report, A47150.
- Sweetapple, MT 2000, Characteristics of Sn-Ta-Be-Li industrial mineral deposits of the Archaean Pilbara Craton, Western Australia: AGSO Record 2000/044, Canberra, 54p.
- Sweetapple, MT and Collins, PLF 2002, Genetic framework for the classification and distribution of Archean rare metal pegmatites in the North Pilbara Craton, Western Australia: Economic Geology, v. 97, p. 873–895.
- Thompson, JFH, Stilltoe, RH, Baker, T, Lang, JR and Mortensen, JK 1999, Intrusion-related gold deposits associated with tungsten–tin provinces: Mineralium Deposita, v. 34, no. 4, p. 323–334.
- Thorne, AM, Johnson, SP, Tyler, IM, Cutten, HN and Blay, OA 2011, Geology of the northern Capricorn Orogen, in Capricorn Orogen seismic and magnetotelluric (MT) workshop 2011: extended abstracts edited by SP Johnson, AM Thorne and IM Tyler: Geological Survey of Western Australia, Record 2011/25, p. 7–18.
- Thorne, AM and Seymour, DB 1991, Geology of the Ashburton Basin, Western Australia: Geological Survey of Western Australia, Bulletin 139, 141p.
- Thorne, AM and Trendall, AF 2001, Geology of the Fortescue Group, Pilbara Craton, Western Australia: Geological Survey of Western Australia, Bulletin 144, 249p.
- Tosdal, RM and Richard, JP 2001, Magmatic and structural controls on the development of porphyry Cu \pm Mo \pm Au deposits: Reviews in Economic Geology, v. 14, p. 157–181.
- Trautman, RL 1992, The mineralogy of the rare-element pegmatites of the Yinnetharra pegmatite belt, Gascoyne Province, Western Australia: The University of Western Australia, Perth, Western Australia, BSc (Hons) thesis (unpublished).
- Tyler, IM and Thorne, AM 1990, The northern margin of the Capricorn Orogen, Western Australia — an example of an early Proterozoic collision zone: Journal of Structural Geology, v. 12, p. 685–701.
- Van Kranendonk, MJ, Smithies, RH, Hickman, AH and Champion, DC 2007, Review: secular tectonic evolution of Archean continental crust: interplay between horizontal and vertical processes in the formation of the Pilbara Craton, Australia: Terra Nova, v. 19, no. 1, p. 1–38.
- Wilde, SA, Valley, JW, Peck, WH and Graham, CM 2001, Evidence from detrital zircons for the existence of continental crust and oceans on the Earth 4.4 Gyr ago: Nature, v. 409, p. 175–178.
- Williams, PJ, Barton, MD, Johnson, DA, Fontbot, L, de Haller, A, Mark, G, Oliver, NHS and Marschik, R 2005, Iron oxide copper–gold deposits: Geology, space-time distribution, and possible modes of origin: Economic Geology (100th Anniversary Volume), p. 371–405.
- Wingate, MTD and Kirkland, CL 2011, Introduction to geochronology information released in 2011: Geological Survey of Western Australia, 5p.
- Witt, WK 1990, Mineral resources — pegmatite metals, in Geology and mineral resources of Western Australia: Geological Survey of Western Australia, Memoir 3, p. 709–715.
- Wood, SA and Samson, IM 2000, The hydrothermal geochemistry of tungsten in granitoid environments: I. Relative solubilities of ferberite and scheelite as a function of T, P, pH and mNaCl: Economic Geology, v. 95, p. 143–182.
- Woolley, AR 1987, Alkaline rocks and carbonatites of the world, Part 1: North and South America: British Museum of Natural History, London, UK, 216p.
- Woolley, AR 2013, Alkaline rocks and carbonatites of the world, Part 3: Africa: The Geological Society Publishing House, Bath, UK, 372p.
- Wyborn, LAI, Heinrich, CA and Jaques, AL 1994, Australian Proterozoic mineral systems: essential ingredients and mappable criteria, in Australian mining looks north — the challenges and choices edited by PC Hallenstein: Australian Institute of Mining and Metallurgy; 1994 AusIMM Annual Conference, Darwin, Northern Territory, 5 August 1994, p. 109–115.
- Zhongxin, Y, Ge, B, Chenyu, W, Zhongqin, Z and Xianjiang, Y 1992, Geological features and genesis of the Bayan Obo REE ore deposit, Inner Mongolia, China: Applied Geochemistry, v. 7, p. 429–442.

This report focuses on better understanding the 3D crustal structure and geological evolution of the Gascoyne Province, as well as the prospectivity of the province through a mineral-systems based prospectivity analysis. Inverse gravity and magnetic modelling of five sections across the province produced an architecture similar to that defined by the Capricorn Orogen deep crustal seismic survey. Structural interpretation of aeromagnetic data shows that, during intracontinental reactivation, there is a general tendency for the tectonic events to become geographically narrower over time, which may represent the influence of a cooling (cratonizing) lithosphere. Based on the review of the geology of the Gascoyne Province, and on our understanding of mineral systems, a prospectivity analysis was conducted. This approach considered the potential sources of metals, fluid pathways to transport those metals, and the physical and chemical traps to precipitate them. Although the results are influenced by imperfect data distributions, as well as inferences made about the local geology and the way these mineral deposits form, a relative prospectivity map was generated for each of the chosen deposit types. In general, these maps showed a strong control by crustal structure on deposit location, and that the central part of the Gascoyne Province is generally more prospective than the east, north, and south, perhaps reflecting a greater degree of intraplate reworking.



Further details of geological products and maps produced by the Geological Survey of Western Australia are available from:

Information Centre
Department of Mines and Petroleum
100 Plain Street
EAST PERTH WA 6004
Phone: (08) 9222 3459 Fax: (08) 9222 3444
www.dmp.wa.gov.au/GSWApublications